Erbacher, J., Mosher, D.C., Malone, M.J., et al., 2004
*Proceedings of the Ocean Drilling Program, Initial Reports* Volume 207

# 6. Site 1259[1]

Shipboard Scientific Party[2]

## BACKGROUND AND OBJECTIVES

Site 1259 is located in a water depth of 2354 meters below sea level (mbsl) on the gently dipping (~1°) north-facing slope of Demerara Rise, which is ~380 km north of Suriname (see Fig. F1, p. 5, in Shipboard Scientific Party ["Site Survey and Underway Geophysics"], this volume). The site is located on a ridge of Paleogene sediments subcropping near the seafloor and is the second shallowest of all sites forming the intended paleoceanographic depth transect across Demerara Rise. The major objectives were the following:

1. Core and log a Paleogene–Albian section to evaluate paleoceanographic and paleoclimatic changes, with emphasis on major and abrupt events during this interval that include the Eocene/Oligocene [E/O] and Paleocene/Eocene [P/E] boundaries and Cretaceous oceanic anoxic events [OAEs]).
2. Reconstruct the history of the opening of the Equatorial Atlantic Gateway by obtaining benthic foraminifer proxy data. These data will help to understand changes in bottom water circulation over Demerara Rise during the gradual opening of the seaway.
3. Recover continuous and expanded sediment records of the Paleogene and Cretaceous in order to reconstruct short- and long-term changes in greenhouse forcing.

### Seismic Stratigraphy

The seismic stratigraphy established for Demerara Rise, including Horizons "A," "B," "B′," and "C," has been correlated proximally to Site 1259 with line GeoB219 (Fig. F1); the closest of the three holes drilled at this site is 170 m from this line. Industry line C2206a crosses the site

F1. Seismic lines GeoB219 and GeoB220, p. 39.

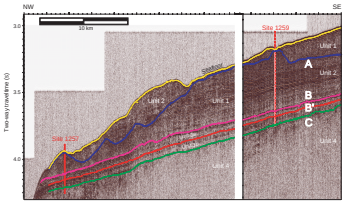


[1]Examples of how to reference the whole or part of this volume.
[2]Shipboard Scientific Party addresses.

orthogonal to line GeoB219 (Fig. F2). Lines GeoB219 and GeoB220 form a single northeast-trending strike line that ties Sites 1257 and 1259 (Fig. F1).

Reflector A, representing the top of a presumably early Miocene erosional unconformity, outcrops at the seafloor on the nearest seismic line. The Miocene section recovered in the core is probably not present at the extrapolated site position on the seismic line. Adjacent to the site position, however, seismic Unit 1, which lies above Reflector A, appears transparent and incoherent in seismic profile. It is variable in thickness but in general thickens in the upslope (southerly) direction.

At Site 1259 and between Reflectors A and B, seismic Unit 2 is 465 ms thick (~405 m using laboratory measured velocity information). The topmost sequence (180 ms [~130 m]) in this seismic unit consists of incoherent reflections that are not transparent as in Unit 1. The equivalent stratigraphic succession, 10- to 15-km upslope, consists of parallel high-amplitude reflections that terminate abruptly. Sediments composing this seismic facies at the drill site location likely have undergone some degree of mass flow displacement that disrupts reflector coherency.

Below 130 m, Unit 2 is represented by a 120-m-thick sequence of high-amplitude parallel coherent reflections followed by low-amplitude coherent reflections down to Reflector B at 463 ms subbottom (442 meters below seafloor [mbsf]). Seismic Unit 2 dips (~0.6°) to the north, slightly less than the seafloor dip. The parallel coherent reflections are occasionally separated by thin (15–20 m thick) horizons of low amplitude and poor coherency. They tend to pinch out up- and downslope. This echo character likely represents pelagic deposition with rare interbedded mass flow deposits. The high-amplitude sequence probably represents a different lithology than the underlying low-amplitude facies. This entire sequence of parallel reflections does not continue downslope to Site 1257 but appears eroded and composed of slope-failure sediment.

Reflector B is a high-amplitude laterally coherent double-wavelet reflection that correlates with the approximate position of the Cretaceous/Tertiary (K/T) boundary at previous sites. It laterally correlates to Site 1257 from Site 1259. Seismic Unit 3, between Reflectors B (462 ms subbottom [~400 mbsf]) and C (571 ms subbottom [~505 mbsf]) is a ~105-m-thick flat-lying sequence that dips <1° to the north. The upper part of this unit between Reflectors B and B′ is called Subunit 3a. It is acoustically incoherent and relatively transparent, extending from ~400 to 445 mbsf (462–503 ms subbottom). The basal part of Unit 3 is Subunit 3b, which lies between Horizons B′ and C (503–571 ms subbottom [~445–505 mbsf]). It is defined on the basis of a series of strong parallel coherent reflections that are laterally contiguous for several kilometers. At the base of Subunit 3b, just above Reflector C, is an incoherent low-amplitude reflection event that may represent another interbedded mass flow deposit.

Horizon C forms a regional unconformity that separates the Upper Cretaceous black shales and younger sediments from Albian and older synrift sediments (seismic Unit 4). At Site 1259, Reflector C is an angular unconformity, with underlying reflections cropping against it at relatively shallow angles (~2°) as they appear on the strike line GeoB219. On the industry seismic line C2206a, which intersects the site in a dip profile (northeast), these low-angle reflections are not resolved and the underlying sequence appears locally conformable (i.e., a disconformity).

F2. Seismic reflection lines C2206a and GeoB219, p. 40.

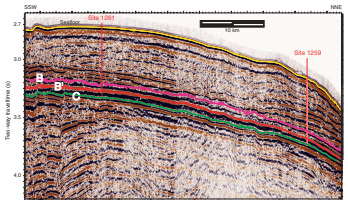

# OPERATIONS

## Transit from Site 1258 to Site 1259

The 32.6-nmi transit to Site 1259 was made in 4 hr at an average speed of 8.15 kt. As the ship settled on the site's coordinates, a positioning beacon was launched at 1208 hr on 1 February 2003, initiating operations at Site 1259.

## Hole 1259A

The same rotary core barrel (RCB) bottom-hole assembly used at the previous sites was deployed, tagging the seafloor at 2365.0 meters below rig floor (mbrf) (2353.8 mbsl). Hole 1259A was spudded at 1830 hr on 1 February and RCB cored from 0 to 391.1 mbsf. Poor recovery in Cores 41R and 42R and elevated pump pressures suggested an obstructed bit. The bit deplugger was dropped two times before pump pressures indicated the bit was clear. Coring resumed in Hole 1259A to 558.8 mbsf, recovering a total of 60 cores (average recovery = 66.6%) (Table T1). With the depth objective achieved, the hole was filled with sepiolite mud and the drill string was retracted. While pulling out of the hole, 20,000–30,000 lb of drag was noted, mostly in the upper section of the hole, probably the result of caving Neogene foraminifer sands. The bit cleared the rig floor at 0300 hr on 4 February, ending Hole 1259A. Continued operations at Site 1259 were postponed because a nonaccident-related medical evacuation of one of the ship's crew was required. After retraction of the thrusters and hydrophones and retrieval of the beacon, the ship departed for Barbados for the evacuation that was to be followed by operations at Site 1260 before returning to Site 1259.

T1. Coring summary, p. 78.

## Hole 1259B

We departed the Site 1260 operational area and returned to Site 1259, offsetting 130 m northeast of Hole 1259A. Hole 1259B was spudded at 0830 hr on 13 February, and we recovered an RCB core (Core 1R) at 0–9.6 mbsf. The hole was washed from 9.6 to 305.0 mbsf, cored from 305.0 to 381.9 mbsf, washed from 381.9 to 420.5 mbsf, and cored from 420.5 to 556.2 mbsf (average recovery = 69.2% in the cored intervals) (Table T1). With the depth objective achieved, the hole was displaced with 150 bbl of sepiolite mud for abandonment. The bit was pulled clear of the seafloor at 2135 hr on 14 February, ending operations in Hole 1259B.

## Hole 1259C

The ship was offset 60 m southwest of Hole 1259B (i.e., back toward Hole 1259A), and Hole 1259C was spudded at 2300 hr on 14 February. The hole was drilled from 0 to 308 mbsf, RCB cored from 308.0 to 373.3 mbsf, drilled from 373.3 to 436.0 mbsf, RCB cored from 436.0 to 445.6 mbsf, drilled from 445.6 to 480.0 mbsf, and RCB cored from 480.0 to 553.7 mbsf (recovery = 80.0% in the cored intervals) (Table T1). With the science objectives achieved, the hole was displaced with 172 bbl of sepiolite mud for abandonment. The bit was pulled clear of the rotary table at 1315 hr on 16 February, officially ending Hole 1259C.

# LITHOSTRATIGRAPHY

Site 1259 represents one of the shallower sites (current water depth = ~2354 mbsl) of the Leg 207 Demerera Rise transect. The sediments recovered at Site 1259 range in age from early Miocene–Cenomanian (see "Biostratigraphy," p. 11) and include records of several critical events, including those at the P/E and K/T boundaries. Hole 1259A was cored continuously to 559 mbsf and spot cored in Holes 1259B and 1259C to recover duplicate or triplicate copies of these critical time intervals and a complete record of the Upper Cretaceous (Cenomanian–Santonian) black shale interval.

Five lithostratigraphic units were recognized at Site 1259 (Fig. F3; Table T2). The oldest unit recovered (Unit V) consists of gray quartzose sandstone and dark-colored silty claystone and calcareous siltstone to sandstone. The superjacent unit (Unit IV) is predominantly composed of submillimeter-scale laminated calcareous claystones rich in organic matter and laminated limestones. The three youngest lithostratigraphic units (Units I–III) recovered at this site contain pelagic sediments. They are composed of calcareous chalks, with various amounts of clay and siliceous microfossils. These pelagic sediments are moderately to pervasively bioturbated

The lithostratigraphic units recognized at this site generally parallel those reported during Leg 207 for Sites 1257, 1258, 1260, and 1261, as well as those for Site 144 (Hayes, Pimm, et al., 1972), but include a >60-m-thick sequence of lower Miocene pelagic oozes and chalks (Unit I and Subunit IIA) that was not recovered elsewhere. The quartz sandstone encountered in Unit V at Site 1259 is petrographically similar to the sandstone recovered at Sites 1258, 1260, and 1261, but the silty claystones and calcareous siltstones in Unit V were only recovered at Site 1259.

F3. Carbonate and TOC content, p. 41.

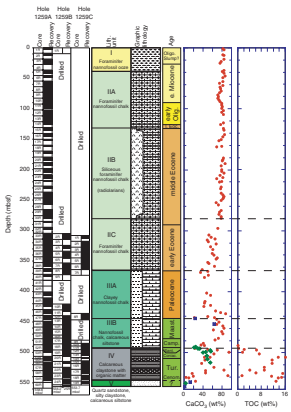


T2. Summary of units and subunits, p. 81.

## Lithostratigraphic Units

### Unit I

Interval: 207-1259A-1R-1, 0 cm, through 5R-2, 0 cm
Depth: 0.00–37.90 mbsf
Thickness: 37.90 m
Age: middle Miocene–early Oligocene
Lithology: foraminifer nannofossil ooze

Unit I consists of a foraminifer nannofossil ooze that exhibits a homogeneous texture and pale yellow color. It contains rare black mottles but discrete traces are rare to absent. Calcareous nannofossils are the dominant sediment component (up to 75%) and planktonic foraminifers constitute 25%–30% of the sediment. Clay, opaque minerals, quartz, and fragments of siliceous microfossils were observed as minor constituents in smear slides. The base of Unit I is placed at a distinct lithologic change from foraminifer nannofossil ooze to foraminifer nannofossil chalk. Unit I includes a major stratigraphic age inversion, with sediments of Oligocene age on top of lower Miocene strata, indicating a slump deposit or other type of slope failure.

## Unit II

Intervals: 207-1259A-5R-2, 0 cm, through 39R-5, 140 cm; 207-1259B-2R-1, 0 cm, through 8R-4, 106 cm; and 207-1259C-1R-1, 0 cm, through 7R-2, 120 cm
Depths: Hole 1259A: 37.90–368.25 mbsf; Hole 1259B: 305.00–368.26 mbsf; and Hole 1259C: 308.00–366.55 mbsf
Thickness: 330.35 m (Hole 1259A)
Age: early Miocene–early Eocene
Lithology: foraminifer nannofossil chalk

Unit II consists of light greenish gray to greenish gray foraminifer nannofossil chalk, foraminifer nannofossil chalk with radiolarians, and nannofossil chalk with foraminifers, containing 50%–80% carbonate in dominant lithologies (Fig. **F3**). *Zoophycos* and *Planolites* trace fossils are common, and *Chondrites* are present but less common. The unit is divided into three subunits based on the relative abundance of radiolarians and foraminifers. Subunits IIA and IIB both have a significant foraminifer component (20%–50%), with Subunit IIB distinguished from Subunit IIA on the basis of its higher siliceous microfossil content (15%–30% radiolarians and siliceous fragments). Foraminifer abundance declines in Subunit IIC to values of ~10%–20%. The upper contact of Unit II is placed at a distinct lithologic change from nannofossil ooze to nannofossil chalk, whereas the lower unit boundary contact corresponds to an equally prominent, but more gradual, downhole increase in clay content. The lower boundary corresponds to the biostratigraphically recognized P/E boundary (see **"Biostratigraphy,"** p. 11) and is expressed as a significant drop in carbonate content and a distinct clay layer.

### *Subunit IIA*

Interval: 207-1259A 5R-2, 0 cm, through 15R-1, 0 cm
Depth: 37.90–130.90 mbsf
Thickness: 93.00 m
Age: early Miocene–late Eocene
Lithology: foraminifer nannofossil chalk

Subunit IIA is composed of carbonate-rich (80 wt%) (nannofossils and foraminifers) pelagic sediments with trace amounts (<5%) of clay, zeolite, and diagenetic calcite. Black mottles and streaks are found occasionally throughout the subunit and are often concentrated in burrows (*Chondrites* and *Zoophycos* trace fossils). The sediments typically range from homogeneous to slightly burrow mottled.

The top of this subunit is placed at a distinct lithologic change from nannofossil ooze to nannofossil chalk at 37.90 mbsf (Hole 1259A). Below this transition, sediments exhibit light–dark color cycles. These cycles occur to varying extents throughout Subunit IIA. The color cycles are expressed as a progression from light greenish gray chalk to 20-cm-thick bands of greenish gray chalk followed by greenish gray chalk with common bioturbation. There is a gradual change to lighter values between Sections 207-1259A-10R-5 and 10R-6 that coincides with the Oligocene/Miocene boundary (see **"Biostratigraphy,"** p. 11). The base of Subunit IIA is placed at a marked increase in abundance of radiolarians from absent or trace amounts to abundances of 15%–25%.

### *Subunit IIB*

Interval: 207-1259A-15R-1, 0 cm, through 31R-1, 0 cm
Depth: 130.90–285.10 mbsf

Thickness: 154.20 m
Age: late Eocene–middle Eocene
Lithology: foraminifer nannofossil chalk with radiolarians

Subunit IIB consists of light greenish gray foraminifer nannofossil chalk with radiolarians (Fig. **F4A**). The chalk contains abundant foraminifers (15%–30%) but is distinguished from the overlying and underlying lithostratigraphic Subunits IIA and IIC by high abundances of siliceous microfossils. Radiolarian contents range from 5% to 10% at the top (Core 207-1259A-15R) and base (Core 30R) of the subunit and reach peak levels (25%–30%) in Cores 18R through 20R. This subunit is mottled and is moderately to heavily bioturbated. Discrete trace fossils include *Zoophycos, Chondrites,* and *Planolites*. Distinct light–dark color cycles can be recognized in the lowermost cores (Cores 207-1259A-27R through 30R).

### *Subunit IIC*

Intervals: 207-1259A-31R-1, 0 cm, through 39R-5, 140 cm; 207-1259B-2R-1, 0 cm, through 8R-4, 106 cm; and 207-1259C-1R-1, 0 cm, through 7R-2, 120 cm
Depths: Hole 1259A: 285.10–368.25 mbsf; Hole 1259B: 305.00–368.26 mbsf; and Hole 1259C: 308.00–366.55
Thickness: 83.15 m (Hole 1259A)
Age: middle Eocene–early Eocene (P/E boundary at base)
Lithology: foraminifer nannofossil chalk and nannofossil chalk with foraminifers

Subunit IIC consists of light greenish gray nannofossil chalk with foraminifers and clay, with carbonate contents of ~60 wt% (Fig. **F4B**). Calcareous nannofossils represent the major calcareous component (>50%), and planktonic foraminifers compose an additional 10%–35%. Bioturbation is pervasive to moderate, with white and greenish gray mottles and burrows. Discrete *Planolites* and *Zoophycos* trace fossils are common.

A distinct pattern of cyclic variations of lighter- and darker-colored sediment is observed throughout Subunit IIC. Intervals of light greenish gray sediment alternate at decimeter intervals with either greenish gray, yellowish brown, or pale olive-colored sediments. From smear slide analyses, it appears that the dark intervals have higher clay contents, whereas light intervals are rich in zeolite and calcite.

The upper boundary of this subunit is placed at the last consistent downcore occurrence of radiolarians. The transition between lithologies characteristic of Units II (relatively carbonate rich) and III (relatively clay rich) is gradual, but the base of Unit II is placed at the P/E boundary, a recognizable interval that can be correlated among holes and sites (Fig. **F5**). The P/E boundary is associated with a clay-rich layer in Holes 1259B and 1259C (see **"Biostratigraphy,"** p. 11) (Fig. **F5B**); the lack of a similar clay layer in Hole 1259A is attributed to drilling disturbance. Magnetic susceptibility records display a very prominent signal at this level in all three holes.

## Unit III

Intervals: 207-1259A-39R-5, 140 cm, through 52R-5, 13 cm; 207-1259B-8R-4, 106 cm, through 18R-7, 53 cm; and 207-1259C-7R-2, 120 cm, through 11R-3, 50 cm

**F4.** Representative lithologies, Units I and II, p. 42.

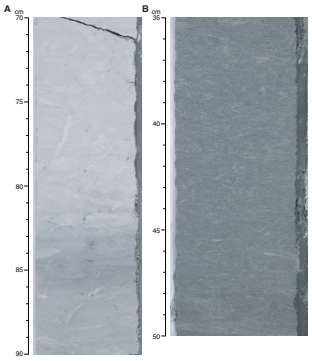

**F5.** Boundary between Units II and III, p. 43.

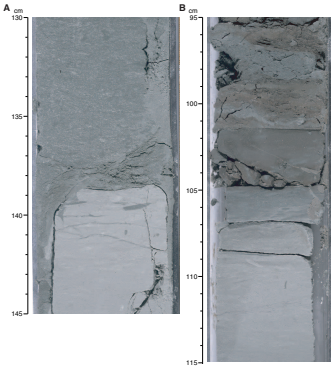

Depths: Hole 1259A: 368.25–492.96 mbsf; Hole 1259B: 368.26–494.52 mbsf; and Hole 1259C: 366.55–492.43 mbsf
Thickness: 126.26 m (Hole 1259B)
Age: late Paleocene–Campanian
Lithologies: clayey nannofossil chalk

Unit III is composed of nannofossil chalk, calcareous siltstone, clayey nannofossil chalk, and glauconitic claystone with nannofossils. Planktonic foraminifers, calcite debris (both biogenic and diagenetic), and zeolites are minor to major constituents in parts of the unit. Carbonate contents are generally <60 wt%. Dominant colors are shades of greenish gray, although reddish brown hues are prominent for several meters above and, to a lesser extent, below the K/T boundary. Subtle to distinct color cyclicity on a decimeter scale between light and darker intervals is observed throughout this unit. Unit III is subdivided into two subunits based on differences in the abundance of foraminifers and clay content. This unit also contains the K/T boundary interval, including an apparent ejecta layer recovered in all three holes (Fig. **F6B**).

The sediment in Unit III has a higher clay content than Unit II, but the transition is gradational. The contact is placed at the P/E boundary. Unit III is distinguished from the underlying Unit IV by its pervasively bioturbated fabric and low organic matter content. The base of Unit III is placed at a distinct color change from green glauconite-rich claystone to dark gray claystone with organic matter. This contact is sharp in Hole 1259C (Fig. **F7B**) but appears gradational in Holes 1259A and 1259B because of pervasive bioturbation of green glauconitic claystone into the dark gray claystone (Fig. **F7A**).

### *Subunit IIIA*

Intervals: 207-1259A-39R-5, 140 cm, through 47R-3, 75 cm; 207-1259B-8R-4, 106 cm, through 13R-1, 48 cm; and 207-1259C-7R-2, 120 cm, through 8R-5, 98 cm
Depths: Hole 1259A: 368.25–442.33 mbsf; Hole 1259B: 368.26–445.18 mbsf; and Hole 1259C: 366.55–442.47 mbsf
Thickness: 76.92 m (Hole 1259B)
Age: late Paleocene
Lithology: clayey nannofossil chalk and nannofossil chalk with clay

Subunit IIIA is a clayey nannofossil chalk to a nannofossil chalk with clay. It is distinguished from Unit II and Subunit IIB by its relatively high clay content (with the contact placed at the P/E and K/T boundaries, respectively). Discrete *Zoophycos, Chondrites,* and *Planolites* burrows are common, and this subunit is pervasively bioturbated (Fig. **F6A**). Trace amounts of pyrite and occasional pyrite nodules are present in all cores.

Subunit IIIA displays subtle to distinct alternations between lighter- and darker-colored clayey nannofossil chalk on 30-cm-scale intervals throughout. Colors are dominantly shades of greenish gray but become olive to reddish brown in the lower portions of the subunit.

The lower boundary of Subunit IIIA is the base of the K/T spherule layer. The spherule layer is overlain by an interval of greenish gray clay grading upward into light greenish gray calcareous clay that grades into the reddish brown cyclic interval mentioned above. The spherule bed is graded and is in sharp contact with a 1-mm thin white layer (Fig. **F6B**). The spherule bed is 1.5–1.9 cm thick and varies in color from black to white into light greenish gray and dark green.

**F6.** K/T boundary ejecta layer, p. 44.

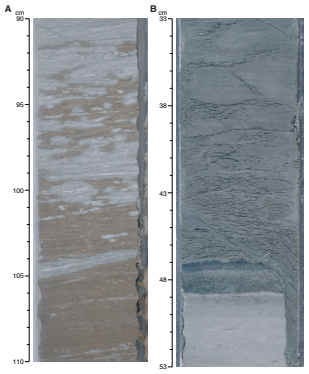

**F7.** Boundary between Units III and IV, p. 46.

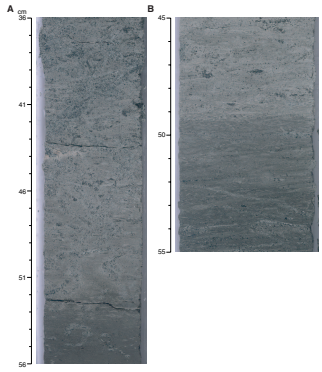

### *Subunit IIIB*

Intervals: 207-1259A-47R-3, 75 cm, through 52R-5, 13 cm; 207-1259B-13R-1, 48 cm, through 18R-7, 53 cm; and 207-1259C-8R-5, 98 cm, through 11R-3, 50 cm
Depths: Hole 1259A: 442.33–492.96 mbsf; Hole 1259B: 445.18–494.52 mbsf; and Hole 1259C: 442.47–492.43 mbsf
Thickness: 50.63 m (Hole 1259A)
Age: late Maastrichtian–Campanian
Lithology: nannofossil chalk with clay and calcareous debris, calcareous siltstone, and glauconitic claystone

Subunit IIIB is dominantly a nannofossil chalk with varying amounts of nannofossils, calcareous debris, and clay. This subunit displays very distinct rhythmic alternations between light greenish gray and greenish gray colors at 5- to 20-cm-thick intervals. The lighter intervals have a higher percentage of nannofossils and foraminifers, whereas the darker intervals have a higher clay content. Bioturbation is moderate to pervasive with distinct black *Zoophycos* and *Chondrites* burrows (Fig. **F8**). Pyrite, barite, and marcasite increase in abundance downhole. Glauconite is present in the lower portion of the subunit (clayey chalk and claystone), and a greenish color marks the lowermost part of Subunit IIIB (Table **T2;** Fig. **F8B, F8C**). The top of this glauconite-rich interval can be correlated among the three holes (see also **"Physical Properties,"** p. 33, and **"Composite Depths,"** p. 25).

The boundary between Subunits IIIB and IIIA is placed at the base of the K/T boundary ejecta layer (Fig. **F6B**), but the lithologic transition between the subunits is gradational. On the other hand, a distinct color and lithologic change defines the boundary between Subunit IIIB (greenish gray to olive-gray clayey chalk and claystone) and Unit IV (black laminated calcareous claystone with organic matter) (Fig. **F7**).

**F8.** Sedimentary structures in Subunit IIIB, p. 47.

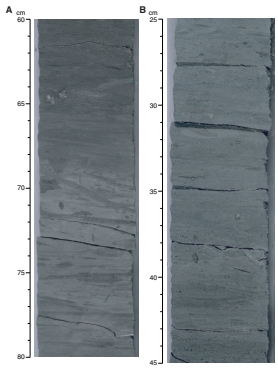

## Unit IV

Intervals: 207-1259A-52R-5, 13 cm, through 60R-1, 0 cm; 207-1259B-18R-7, 53 cm, through 24R-4, 42 cm; and 207-1259C-11R-3, 50 cm, through 19R-1, 0 cm
Depths: Hole 1259A: 492.96–549.10 mbsf; Hole 1259B: 494.52–548.52 mbsf; and Hole 1259C: 492.43–547.10 mbsf
Thickness: 56.14 m (Hole 1259A)
Age: Santonian–Cenomanian
Lithology: laminated calcareous claystone with organic matter, clayey chalk, and limestone

Unit IV primarily consists of dark olive-gray to black, submillimeter-scale laminated calcareous claystone with organic matter (black shale) and clayey chalk and limestone with organic matter (Fig. **F9**). The upper contact of Unit IV lies below a distinct lithologic transition from the glauconite-rich greenish to olive-gray sediment of lower Unit III to olive-gray and black calcareous claystone with organic matter. The lower part of this transition is heavily mixed by bioturbation and includes some discrete large burrows (Fig. **F7A**). The lower boundary of Unit IV is defined by the first occurrence of dark greenish gray to gray, medium-grained quartz sandstone (quartz arenite) (Holes 1259A and 1259C) and dark gray calcareous siltstone and silty clay intercalations (Hole 1259B).

The uppermost part of Unit IV at Site 1259 contains a massive dark gray to black bioturbated claystone with organic matter, which is Santo-

**F9.** Typical lithologies in Unit IV, p. 49.

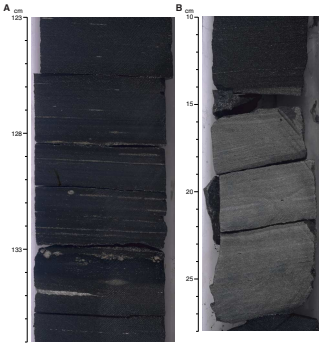

nian in age (Table T2). The remainder of Unit IV shows well-developed submillimeter-scale laminations and has a strong petroliferous odor. Contacts between the major lithologies in the unit are gradational over a centimeter to decimeter scale and form the rhythmic light–dark color variations that are typical for Unit IV.

Carbonate content is highly variable and ranges as high as ~95 wt% in individual carbonate-rich layers and as low as ~5 wt% in black claystones (Fig. F3). The lighter intervals have higher carbonate content largely due to a higher abundance of diagenetic calcite (see Fig. F9B). Other carbonate constituents include nannofossils (concentrated in fecal pellets), foraminifers, and shell fragments. Total organic carbon (TOC) values range from ~5 to 16 wt%, with one sample as high as 29 wt%. Rock-Eval analyses indicate Type II kerogen, which is consistent with a marine origin of the organic matter. The organic matter is clearly visible in thin sections. Fish scales and bone fragments (francolite) and amorphous to cryptocrystalline phosphatic nodules (collophane) up to 2 cm in diameter are common throughout, either parallel to bedding or concentrated in thin gravity deposits and can be seen as white to light brown blebs and streaks on core surfaces. A distinct feature in the black claystone are white millimeter-scale calcite stringers composed entirely of foraminifers filled with sparry calcite. A distinct minor lithology in Unit IV is a calcite cemented, unsorted glauconitic claystone, with phosphatic nodules, fish remains, and shells (Table T2; Figs. F15, F31). A similar lithology was found in Unit IV at Sites 1258 and 1260.

### Unit V

Intervals: 207-1259A-60R-1, 0 cm, through 60R-1, 140 cm; 207-1259B-24R-4, 42 cm, through 25R-CC, 10 cm; and 207-1259C-19R-1, 0 cm, through 19R-4, 87 cm
Depth: Hole 1259A: 549.10–550.50 mbsf; Hole 1259B: 548.52–556.01 mbsf; and Hole 1259C: 547.10–551.39 mbsf
Thickness: 7.49 m (Hole 1259B)
Age: unknown
Lithology: quartz sandstone, silty claystone, and calcareous siltstone

Unit V is composed of quartz sandstone, calcareous siltstone, and silty claystone. The top of the unit is placed at the first downhole occurrence of a dark greenish gray to gray, medium-grained quartz sandstone (quartz arenite). Sand grains are angular to subrounded and are cemented by calcite. The sandstone contains minor amounts of glauconite, pyrite, and bioclastics (echinoid fragments, bivalves, gastropods, and large agglutinated benthic foraminifers). No sedimentary structures were observed. The sandstone is 1.40 m thick in Hole 1259A, <5 cm thick in Hole 1259C, and was not recovered in Hole 1259B. At the base of the sandstone in Holes 1259A and 1259C is a sharp transition to very dark gray and brownish calcareous siltstones and silty claystones (Fig. F10). These siltstones and silty claystones contain "tepee-structures" and apparent tempestites, as well as strongly bioturbated intervals. The burrows are filled with quartz silt.

F10. Typical lithology and sedimentary structures, Unit V, p. 51.

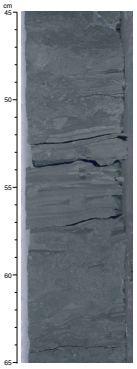

## Summary

The oldest interval recovered at Site 1259 is a unit dominated by interbedded dark gray and brownish calcareous siltstones and silty clay-

stones, as well as gray, medium-grained sandstone (Unit V) of unknown age. The lithology shows strongly bioturbated intervals and is characterized by tepee-structures and apparent tempestites. These observations suggest deposition in a shallow-marine environment, possibly including tidal flats.

Cenomanian–Santonian sediments are dominated by laminated calcareous claystones and laminated chalks/limestones of Unit IV. Organic carbon concentrations in Unit IV reach 29 wt%, with the organic matter of marine origin. High productivity and low bottom water oxygen levels resulted in the preservation of large volumes of organic and phosphatic matter in the sediments. Zeolites (clinoptilolite) and rare radiolarians suggest siliceous microfossils were a common component of Unit IV sediment. Carbonate values are highly variable (5–95 wt%) and reflect diagenetic dissolution and precipitation of calcite. Macrofossils occur frequently (mainly fish fragments and inoceramids) in the black claystones, but trace fossils are absent. The lack of bioturbation, the relatively high TOC content, and common phosphoritic layers suggest a deposition in a restricted, probably shallow, but fully marine environment.

The nonlaminated, unsorted glauconitic claystone intercalated with the TOC-rich claystones in Unit IV is interpreted as a storm deposit. If correct, this interpretation limits water depths at this site to less than storm wave base. Alternatively, a period of very slow sedimentation and slightly higher oxygen levels could allow for the bioturbation and concentration of glauconite and phophatic material. The bioturbated claystone with organic matter in the uppermost part of Unit IV may represent slightly more oxygenized conditions at the seafloor, allowing bioturbation and preventing laminae preservation during part of the Santonian.

Open marine conditions and oxic bottom waters were established by the early Campanian, as indicated by the bioturbated pelagic marls of Unit III. Variations in sedimentary fabric and minor sedimentary components in the pelagic sediments in Units III–I suggest that conditions at the seafloor and/or overlying water column fluctuated substantially during the latest Cretaceous and Paleogene interval.

The K/T boundary interval seems to be complete in all three holes at Site 1259. It consists of the uppermost Maastrichtian of Subunit IIIB, followed by a discrete graded spherule layer, and the basal Paleocene calcareous claystone of Subunit IIIA. The spherules are up to 2.5 mm in diameter, an exceptional size considering the distance to the proposed location of impact.

The P/E boundary seems to be relatively complete in Holes 1259B and 1259C, whereas its recovery was incomplete in Hole 1259A. The most extensive record appears to be the 50-cm-thick greenish and reddish brown clay layer in Hole 1259B (see **"Biostratigraphy,"** p. 11). The lack of carbonate in this layer is consistent with sedimentary changes expected across the P/E boundary.

Similar to other Leg 207 sites, gravity flow deposits and temporal gaps are common in the uppermost pelagic record at Site 1259. The inversion of ages in Unit I (Hole 1259A), where ~20 m of Oligocene sediment overlies lower Miocene oozes, is most probably due to mass-failure displacement or faulting. Several hiatuses were recognized in Hole 1259A, with the most prominent ones occurring in the pelagic chalks of Unit IIA, at the transition between the clayey chalks and claystones of Units III, and in Unit IV (see **"Sedimentation Rates,"** p. 27).

## BIOSTRATIGRAPHY

The three holes at Site 1259 recovered sediments of early Miocene to Cenomanian age. The lowermost cores yielded marginal marine to nonmarine sediments of presumable Cenomanian or Albian age. The marine succession contains calcareous nannofossils, planktonic foraminifers, and radiolarians in varying abundances and states of preservation, depending on lithology and sediment induration. The shipboard examination of these microfossil groups from core catcher samples was supplemented by additional samples from in the cores. The biostratigraphic data permitted zonal or stage assignments to be made for the entire sequence. Datum levels are summarized in Figure **F11** and in Tables **T3, T4, T5, T6, T7, T8,** and **T9.**

A 26-m-thick nannofossil foraminiferal ooze (Cores 207-1259A-1R to 3R [upper part of lithostratigraphic Unit I]) at the top of the section has been attributed an early Oligocene age, reflecting a major slump or another type of redeposited sediment. This unit overlies a 342-m-thick, partly siliceous foraminiferal nannofossil ooze to chalk (Sample 207-1259A-4R-1, 0 cm, to 39R-5, 55 cm [lithostratigraphic Subunits IIA–IIC]) of early Miocene–earliest Eocene age, including the E/O boundary. Based on biostratigraphic data, two hiatuses were recognized in this interval: (1) the early Oligocene/early Miocene hiatus (Sections 207-1259A-10R-5 to 10R-6), with the late Oligocene being absent, and (2) the middle–late Eocene transition (Sections 207-1259A-15R-1 to 15R-2), with the proper boundary interval (planktonic foraminiferal Zone P15) missing. All microfossil groups studied are abundant and well preserved. An expanded section of 160 m of middle Eocene sediments was encountered.

The subsequent 75 m of clayey nannofossil chalk (Samples 207-1259A-39R-5, 55 cm, to 47R-3, 75 cm [lithostratigraphic Subunit IIIA]) is attributed to the Paleocene with a minor hiatus in its lower part, spanning parts of the early Paleocene (Core 207-1259A-46R). The P/E boundary is at 139 cm in Section 207-1259A-39R-5. At the base of the lowermost lowest Danian, a boundary clay and a spherule layer, which is believed to mark the base of the Tertiary, is developed. The K/T boundary sequence is considered to be complete or nearly complete because all the lower Danian and upper Maastrichtian biozones are represented in all holes.

The 50 m of upper Maastrichtian to mid-Campanian nannofossil chalk (Samples 207-1259A-47R-3, 75 cm, to 52R-5, 13 cm [lithostratigraphic Subunit IIIB]) is similar to that of the Paleocene, with calcareous microfossils being relatively rare and moderately preserved. A condensed glauconite-rich interval (80 cm thick) was recovered in Section 207-1259A-52R-4. It separates the Maastrichtian/upper Campanian chalk facies (lithostratigraphic Unit IIIB) from the ~56 m of black shales in lithostratigraphic Unit IV. Detailed high-resolution analyses of calcareous microfossils identify early Campanian assemblages at the top, early Campanian–Santonian assemblages in the upper third, early Santonian–late Coniacian taxa in the middle part, and early Coniacian taxa in the lowermost part of Section 207-1259A-52R-6. Cores 207-1259A-53R to 54R-CC are early Coniacian in age. Calcareous microfossils are generally present throughout the black shale. Foraminifers are often poorly preserved and of low diversity in calcareous interbeds, but pristine ("glassy") preservation is regularly found in clay-rich intervals. Calcareous nannofossils and planktonic foraminifers of early Turonian age

**F11.** Planktonic foraminifer, calcareous nannofossil, and radiolarian biozonation, p. 52.

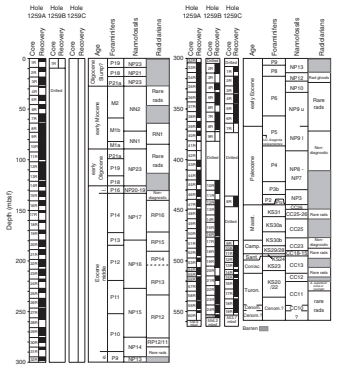

**T3.** Calcareous nannofossils, p. 82.

**T4.** Planktonic foraminifers, Hole 1259A, p. 83.

**T5.** Planktonic foraminifer datums, p. 84.

**T6.** Radiolarian datums, p. 85.

**T7.** Datum levels, ages, and preservation of samples, p. 86.

**T8.** Planktonic foraminifers, Hole 1259B, p. 87.

**T9.** Planktonic foraminifers, Hole 1259C, p. 89.

are present near the base of the black shale. Section 207-1259C-18R-5 contains nannofossils of mid- to late Cenomanian age. A sharp contact between the laminated black shale and quartz sandstone (lithostratigraphic Unit V) was recovered in Core 207-1259A-60R. The latter unit, of which 1.40 m was recovered, did not provide any calcareous microfossils and was not dated. A more variable lithology (silty claystones and shelly sandstones) was encountered in the bottom part of Holes 1259B and 1259C.

## Calcareous Nannofossils

As at the previous two sites, we recovered primarily Paleogene–mid-Cretaceous sediments from the three holes at Site 1259 that contain generally common to abundant calcareous nannofossils of moderate to good preservation. These allowed for zonal or stage assignments that are summarized in Figure **F11** and Tables **T3** and **T7.** Core catcher samples were examined for all holes and supplemented as necessary by samples in the cores for further refinement of the zonal assignments. These revealed major disconformities separating the following sedimentary packages:

1. Approximately 28 m of a winnowed lower Oligocene foraminiferal sand and nannofossil ooze with some Miocene contaminants, apparently representing a slump deposit resting disconformably on the subjacent unit;
2. Approximately 62 m of lower Miocene ooze of the same consistency, apparently in place, separated by another disconformity from the underlying unit;
3. A ~34-m lower Oligocene interval separated by a disconformity from 6 m of upper Eocene calcareous ooze. This unit in turn is separated by a disconformity from the underlying 300-m middle Eocene–Paleocene nannofossil chalks. A minor disconformity may be present in the lowermost Paleocene;
4. A 50-m Maastrichtian–late Campanian chalk beneath a complete K/T boundary; and
5. An early Campanian–Cenomanian black shale sequence, unconformably overlying an undated quartz-cemented sandstone/gray clay sequence at the base.

In the more detailed descriptions that follow, the assemblages and ages pertain to Hole 1258A core catchers unless noted otherwise.

The first core catcher in the Oligocene slump or otherwise reworked interval contains abundant well-preserved *Sphenolithus predistentus* and *Cyclicargolithus abisectus* but no *Sphenolithus distentus* and is assigned to the lower Zone NP23 (Zone CP17); discoasters are overgrown. The subjacent Sample 207-1259A-2-CC yielded well-preserved *Helicosphaera reticulata* and common *Reticulofenestra umbilica* and *Ericsonia formosa* and is assigned to Zone NP21, assuming the latter two index taxa are not reworked. The third core catcher, however, is assigned to the younger Zone NP23, indicating an inverted sequence; it also contained a specimen of *Coccolithus miopelagicus,* which is of early Miocene age.

Samples 207-1259A-4R-CC and 5R-CC contain *Sphenolithus belemnos* and *Triquetrorhabdulus carinatus* along with abundant *Hayaster perplexa,* indicating a zonal assignment of uppermost NN2 Zone or, alternatively, NN3 if the *T. carinatus* is reworked (an assignment to Zone CN2 of the Bukry and Okada zonal scheme avoids that potential problem). Sample

207-1259A-6R-CC contains abundant *H. perplexa* and several large *Discoaster druggii* (up to 19 µm), the nominate species of Zone NN2. Although the sometimes elusive *D. druggii* was not noted in Samples 207-1259A-7R-CC and 8R-CC, the latter contains abundant and well-preserved *T. carinatus,* the acme of which is encountered near the base of Zone NN2, indicating that level or slightly lower. *Sphenolithus disbelemnos* is very abundant in Sample 207-1259A-9R-CC, suggesting an assignment of uppermost Zone NN1; *Helicosphaera euphrates* is abundant.

Abundant *S. predistentus* and *C. abisectus* along with common *S. distentus* are noted in the section in Sample 207-1259A-10R-CC, this time in normal stratigraphic order, and are assigned to the lower Oligocene Zone NP23 (upper part) (Zone CP18 of the Bukry and Okada compilation). A disconformity representing the missing upper Oligocene must lie within that core or in the core break above. The next three cores downhole (Cores 207-1259A-11R to 13R) contain *S. predistentus* in the absence of *S. distentus, R. umbilica,* and *E. formosa,* and belong to the lower portion of Zone NP23 (Zone CP17). *Helicosphaera compacta* is abundant.

The E/O boundary lies at a sharp color change (disconformity) in Section 207-1259A-14R-4, 27.5 cm. *Lanternithus minutus* is abundant above and *Discoaster barbadiensis* and *D. saipanensis* below the break. Specimens of these two discoasters are reworked immediately above the disconformity. Sample 207-1259A-14R-CC contains very large *Cribrocentrum reticulatum* (up to 12.5 µm), which assigns the sample to Zone NP20–19 (CP15). Cores 207-1259A-15R and 16R contain *Dictyococcites bisectus* and both probably belong to the upper part of Zone N17. *Chiasmolithus grandis,* however, was not observed until Sample 207-1259A-17R-CC, which, in the absence of *D. bisectus,* belongs to the lower part of Zone NP17, as does Sample 207-1259A-18R-CC.

A few *Chiasmolithus solitus* in the subjacent Sample 207-1259A-19R-CC might be reworked, but these are common in Cores 207-1259A-20R to 24R, along with *R. umbilica,* and are assigned to the lower part of Zone NP16 (or Subzone CP13B). Zone NP15 is assigned to Cores 207-1259A-26R to 29R based primarily on the presence of *Chiasmolithus gigas,* whereas Zone NP14 is assigned Sample 207-1259A-31R-CC on basis of a few specimens identified as heavily overgrown *Discoaster sublodoensis*.

Preservation and numbers of coccoliths in general continue to deteriorate downsection, making it difficult to distinguish a few possible *Discoaster lodoensis* in Core 207-1259A-32R, which also contains common *Campylosphaera dela* (some with crossbar intact), but no *D. sublodoensis*. This and the subjacent core are assigned to Zone NP13. Zeolites in the latter obscure the nannofossils, a condition not uncommon in this portion of the lower Eocene and where it is easiest to search for zonal markers using cross-polarized rather than plane-transmitted or phase-contrast light.

Common *Tribrachiatus orthostylus,* if not reworked in Sample 207-1259A-34R-CC, denote Zone NP12. A pristine specimen of *Discoaster falcatus* in the sample is reworked, however. *Discoaster multiradiatus, D. diastypus,* numerous "glassy" and sometimes misshapen rhombs, plus heavily overgrown triangular forms are interpreted as representing the *Tribrachiatus bramlettei–Tribrachiatus contortus* evolutionary transition; hence, this core catcher is assigned to Zone NP10.

Opal-CT lepispheres constitute the background of the partially silicified Samples 207-1259A-36R-CC and 37-CC, again making cross-polarized light the most practical way to search for coccoliths. Abundant

*Zygrhablithus bijugatus, D. multiradiatus,* and somewhat misshapen "glassy" rhombs (interpreted as *Rhomboaster* spp.), however, indicate the upper part of Zone NP9. *Neochiastozygus junctus* is also abundant and continues, minus the rhombs but with occasional fasciculiths, down to the P/E boundary in Section 207-1259A-39R-3 or 39R-4. Below that level, fasciculiths replace *N. junctus* and *Z. bijugatus* in dominance and preservation improves considerably.

Sample 207-1259A-40R-CC yielded a variety of fasciculiths, *D. lenticularis,* and other characteristic Paleocene taxa such as *Neochiastozygus concinnus*. Zeolites are few in the subjacent clay-rich Sample 207-1259A-41R-CC, and preservation is quite good as indicated by pristine specimens of *Toweius eminens;* the sample belongs to the lower portion of Zone NP9. Helioliths are present in the subjacent core, and *Discoaster mohleri* persists downsection through an interval of nonrecovery (Core 207-1259A-42R) to Sample 207-1259A-43R-CC, which is assigned to the combined Zones NP7–NP8. The subjacent Sample 207-1259A-44R-CC contains common *Ellipsolithus macellus,* large *Cruiciplacolithus tenuis* (with well-developed "feet"), and common *Lopholithus nascens* but no helioliths. Below that, nannofossils are rare and poorly preserved in Sample 207-1259A-46R-CC, which yielded *C. tenuis* and possible *Chiasmolithus danicus* but no *E. macellus;* the sample was assigned to Zone NP3 of the Danian.

Immediately beneath the K/T boundary, *Micula prinsii* is present in Sample 207-1259A-47R-CC, which was assigned to Zone CC26. Its upper Maastrichtian ancestor, *Micula murus,* ranges downhole to Sample 207-1259A-49R-CC, which lies slightly below the lower CC26 zonal boundary. This species can be effectively substituted as the marker taxon for Zone CC26, as *Nephrolithus frequens* has hitherto not been observed in tropical latitudes.

In contrast to the expanded upper Maastrichtian section, the lower Maastrichtian is poorly represented if not absent entirely, as Core 207-1259A-50R is assigned to Zone CC25 and the subjacent core belongs to upper Zone CC23, based on the co-occurrence of *Uniplanarius trifidum* and *Uniplanarius sissinghii,* which top out at the Campanian/Maastrichtian boundary. This zone is traced downhole through Core 207-1259A-51R and into Sample 207-1259A-52R-3, 1 cm.

The transition into the black shales is well displayed in the photograph of Sections 207-1259B-18R-6 and 18R-7 (see **"Lithostratigraphy,"** p. 4) (Fig. **F7**). The normally greenish Campanian chalks have a dark gray color but with a greenish tinge at the base where glauconite appears. This glauconite-rich chalk continues downhole to the top of Section 207-1259B-18R-7, where Sample 18R-7, 20 cm, contains essentially the same upper Campanian nannofossil assemblage as above (*U. trifidum, U. sissinghii, Micula decussata,* and *Aspidolithus parcus constrictus,* etc., of Zone CC23).

Immediately beneath the green glauconitic chalk is a light yellowish to tan chalk separated from the chalk above by a heavily burrowed contact. Glauconite in this unit may have been introduced along with chalk from above by bioturbation; hence, care was taken to sample it where glauconite appeared to be absent. A "toothpick" sample 3 cm beneath the contact (Sample 207-1259B-18R-7, 27 cm) yielded common to abundant *M. decussata,* along with *Eiffellithus eximius, A. parcus constrictus* (two specimens), *Broinsonia enormis,* and *Zeugrhabdotus bicrescenticus* and a single but well-preserved specimen of the dissolution-resistant *Marthasterites furcatus*. This assemblage belongs to the lowermost

Campanian Zone CC18, which is bounded at the top by *M. furcatus* and at the base by *A. parcus*.

The lithology changes rather abruptly again in Section 207-1259B-18R-7 from the light tan to a darkish brown claystone at ~53 cm, again with a heavily bioturbated contact. A coherent sample 3 cm below the contact at 56 cm also contained a sparse nannoflora with *M. decussata, E. eximius,* and *B. enormis* in the absence of *A. parcus,* the age of which could range from CC17 to CC14; planktonic foraminifers suggest a Santonian age, which would constrain the age of the sample to Zones CC17–CC15 (or CC18–CC15 if *A. parcus* is present). Several of the nannofossil datums traditionally used to further subdivide this interval are the dissolution-susceptible holococcoliths that are largely absent in the Cretaceous of the Leg 207 drill sites, such as *Calculites obscurus* (base of CC17) and *Lucianorhabdus cayeuxii* (base of CC16), hence the lack of precision in delineating these zones. We suspect that much of the Santonian is missing and that the lithologic change in Sample 207-1259C-18R-7, 53 cm, represents another hiatus.

Closely spaced samples beginning with Sample 207-1259A-52R-6, 2 cm, through 52R-6, 104 cm, recovered a condensed sequence of Santonian age. Sample 207-1259A-52R-6, 110 cm, continuing through 52R-6, 124–138 cm, contains *E. eximius* in the absence of both *M. decussata* and *Lithastrinus septenarius* and in the presence of occasional *M. furcatus,* all of which were assigned to the lower Coniacian Zone CC13. *Marthasterites* is common to abundant in the core catcher, and its acme seems to be characteristic of selected samples in the lower Coniacian of the Leg 207 sites. Cores 207-1259A-53R and 54R are also assigned to Zone CC13, with three samples (Samples 207-1259A-53R-1, 50 cm; 5R-CC; and 54-CC) also containing *Quadrum gartneri*. Nannoliths in the latter samples are common to abundant and well preserved.

Sample 207-1259A-55R-CC yielded no *M. furcatus* but rather the exclusively Turonian taxon *Liliasterites angularis* in the presence of *E. eximius* and *Stoverius archylosus; Eprolithus eptapetalus* is rare. The sample, therefore, is assigned to the mid- to upper Turonian Zone CC12.

Nannoliths are rare but well preserved in Core 207-1259A-57R, which is rich in zeolites and opal-CT lepispheres. *Eiffellithus eximius* is absent, but the numbers of *E. eptapetalus* are proportionately greater relative to the previous core catcher. This acme continues into the subjacent core catcher, and both cores are assigned to the lower Turonian Zone CC11.

Sample 207-1259A-59R-CC was problematic, as the very dark black zeolitic shale yielded rare and poorly preserved coccoliths consisting mostly of *Eprolithus apertior, Eprolithus floralis, Zeugrhabdotus embergeri, Radiolithus planus,* and small prediscosphaerids with small round bases ~6.5 µm across. An examination of samples in the core revealed *L. angularis* and *Tranolithus orionatus* in Sample 207-1259A-59R-1, 138 cm, and common *Eprolithus octopetalus* in Sample 59R-1, 138 cm, which together still indicate a Turonian age. A sample (207-1259C-18R-5, 75 cm), however, was dated as mid- to late Cenomanian in age based on the only specimen of *Lithraphidites acutus* observed on board ship during this leg.

Core 207-1259A-60R recovered only a silica-cemented quartz sand with cement particles that appeared opalescent in phase-contrast light. The two lowest core catchers in Hole 1259B (from Cores 207-1259B-25R and 26R) were both barren of nannofossils, the latter being a gray mudstone with numerous scattered 5- to 10-µm highly birefringed rhombs (dolomite?).

## Planktonic Foraminifers

Planktonic foraminifer biostratigraphy at Site 1259 was based upon a combination of core catchers and samples taken from every section in Hole 1259A as well as from core catchers in Holes 1259B and 1259C. Zonal assignments are summarized in Figure F11 and Tables T4, T5, T8, and T9. Planktonic foraminifer Zones M2 (Miocene) through Zone KS20/KS22 (Turonian) were identified in Hole 1259A, along with significant breaks in the biozonation in the middle Oligocene–lowermost Miocene, the lower/middle Eocene boundary, and the upper Danian. Planktonic foraminifers were present in nearly all samples but varied widely in preservation and abundance. Preservation was best in clay-rich parts of the Turonian–Santonian sequence, although foraminifers were difficult to extract and clean in the black shales. Foraminifers in the light-colored bands of the black shales were frequently filled with calcite spar. Good preservation was found in the Miocene, Oligocene, and middle Eocene, whereas preservation was moderate or poor in the chalk of the lower Eocene, Paleocene, and Maastrichtian–Campanian sequences.

Sample 207-1259A-1R-1, 0–2 cm, contains a mixture of modern diatoms together with modern planktonic foraminifers such as *Orbulina universa, Globigerinoides sacculifer, Neogloboquadrina dutertrei,* and *Globigerinoides ruber.* The fine fraction (<150 µm) includes fragments of Oligocene foraminifers and pieces of manganese crust. Pleistocene sediments are only a few centimeters thick and were nearly entirely washed off the core top in Hole 1259A, whereas the core top was relatively well preserved in Hole 1259B.

Yellow calcareous ooze in Sample 207-1259A-1R-CC contains a diverse lower Oligocene foraminifer assemblage including common *Turborotalia ampliapertura, Turborotalia euapertura, Globoquadrina galavisi, Chiloguembelina cubensis,* and *Cassigerinella chipolensis,* representing Zone P19. In contrast, Sample 207-1259B-1R-CC contains markers for Oligocene Subzones P21b and P21a and Zones P20 and P19, together with Pleistocene foraminifers. Likewise, Samples 207-1259A-2R-CC and 3R-CC are also of Oligocene age but decrease in age downhole from Zone P18 to Subzone P21a, suggesting either massive contamination of the core catchers in the soupy foraminifer sands or massive reworking. Extensive reexamination of Sample 207-1259A-1R-CC did not reveal any reworked components.

The surficial Oligocene foraminifer sands are likely to represent a slump or reworking, since Samples 207-1259A-4R-CC to 9R-CC contain a succession of foraminifers representing lower Miocene foraminifer zones in stratigraphic order. Samples 207-1259A-4R-CC to 7R-2, 50–54 cm, contain a typical Zone M2 fauna with *Globoquadrina dehiscens, Globigerinoides primordius, Globoquadrina binaensis, Dentoglobigerina altispira,* and *Globigerinoides altiapertura*. The species *Globorotalia mayeri, Globigerinella obesa, Globigerina angulosuturalis,* and *Globoturborotalita woodi* are secondary components. A small four-chambered, heavily encrusted foraminifer resembling *Neogloboquadrina pachyderma* was found in most Miocene samples and has been provisionally called *Neogloboquadrina nympha* after the species described originally by Jenkins (1966) from the Southern Ocean.

Sample 207-1259A-7R-3, 50–54 cm, contains the highest record of *Fohsella kugleri* in Hole 1259A and marks the top of Subzone M1b. The base of this zone is marked by the first appearance of *G. dehiscens* in Sample 207-1259A-9R-7, 50–54 cm. Typical assemblages in Zone M1 in-

clude *G. mayeri, F. kugleri, Globoquadrina venezuelana, Globoquadrina praedehiscens,* and *G. altiapertura*. Subzone M1a, defined by the presence of *F. kugleri* in the absence of *G. dehiscens,* extends to Sample 207-1259A-10R-5, 50–54 cm.

A significant unconformity representing the upper Oligocene and possibly part of the basal Miocene occurs between Samples 207-1259A-10R-5, 50–54 cm, and 10R-6, 50–54 cm. Overlying sediments are assigned to Zone M1a based on the presence of the zone marker species *F. kugleri,* whereas sediments below the boundary contain abundant *C. cubensis, G. angulosuturalis,* and *C. chipolensis,* indicating lower Oligocene Zone P21a. Between Samples 207-1259A-11R-2, 50–54 cm, and 11R-3, 50–54 cm, the disappearance of *G. angulosuturalis* and the absence of *Turborotalia ampilapertura* suggests Zone P20. However, Sample 207-1259A-11R-5, 50–54 cm, contains *G. angulosuturalis,* suggesting that the sample is either contaminated with material reworked downhole or that the overlying sediments are incorrectly dated as Zone P21a. Zone P19 occurs between Samples 207-1259A-11R-CC and 13R-3, 50–54 cm, and is characterized by the occurrence of *Turborotalia ampilapertura, C. chipolensis, C. cubensis, Globoquadrina tripartita,* and *Globoquadrina globularis*. Finally, Zone P18, characterized by *Pseudohastigerina* spp., was found between Samples 207-1259A-13R-4, 50–54 cm, and 14R-3, 50–54 cm.

We have not observed large-scale inversions of zonal assignments as seen in the Oligocene at Site 1260. However, there are age reversals that raise a flag of caution about the continuity of the section. For example, *G. angulosuturalis,* the marker for Subzone P21a, is present in a few samples from both Zones P18 and P19, including Sample 207-1259A-13R-CC, where it is common. These occasional apparent age reversals at Site 1259 could be the result of downhole contamination, but at least some of the reversals occur in chalks that are not notably disturbed by rotary coring. The other possibility is that the whole section was extensively reworked during the late early Oligocene or perhaps prior to the deposition of Miocene sediments.

The contact between the Eocene and Oligocene occurs in Sample 207-1259A-14R-4, 28 cm. Zone P18 assemblages are juxtaposed with those of Zone P16 that contain *Turborotalia cunialensis, Hantkenina alabamensis, Turborotalia pomeroli,* and *Globoquadrina pseudovenezuelana*. In turn, Zone P16 assemblages are in contact with Zone P14 faunas between Samples 207-1259A-15R-1, 50–54 cm, and 15R-2, 50–54 cm. Typical species in Zone P14 include *Turborotalia cerroazulensis, Morozovella spinulosa, Morozovella lehneri, Planorotalites renzi, H. alabamensis,* and *Acarinina rohri*. Zone P14 can be traced as low as the interval between Samples 207-1259A-19R-2, 50–53 cm, and 19R-3, 50–53 cm.

The remainder of the middle Eocene is well represented in Hole 1259A and consists of an expanded and nearly continuous sequence of biozones and datum levels. Zone P13 is present between Samples 207-1259A-19R-3, 50–53 cm, and 20R-4, 50–54 cm. These samples show the evolution of *Orbulinoides beckmanni* from a taxon with three chambers in the last whorl that is similar to large *Globigerinatheka kugleri* or *Globigerinatheka euganea* to a fully spherical variety in which the final chamber constitutes half or more of the total shell. The lower limits of Zone P13 are defined by the first appearance of large globigerinathekids that resemble the holotype of *O. beckmanni*, a specimen that is similar to a large example of *G. kugleri* (see discussion of Zone P13 in **"Calcareous Nannofossils,"** p. 12, in the "Site 1260" chapter). Common species in Zone P13 are *Igorina broedermanni, M. spinulosa, T. pomeroli, M. lehneri,*

and *Acarinina bullbrooki*. Zone P12 ranges from Sample 207-1259A-20R-5, 50–53 cm, to 23R-CC, whereas Zone P11, whose top is defined by the last appearance of *Morozovella aragonensis,* extends between Samples 207-1259A-24R-1, 50–54 cm, and 27R-1, 50–54 cm. *Morozovella lehneri* and *M. aragonensis* are both present between Samples 207-1259A-24R-1, 50–54 cm, and 24R-CC. Finally, Zone P10 was identified between Samples 207-1259A-27R-2, 50–54 cm, and 30R-CC, with its top defined by the first appearance of *G. kugleri* and its base approximated by the first appearance of *Guembelitroides nuttali*. Typical species in Zone P10 include *M. aragonensis, Acarinina praetopilensis, Muricoglobigerina senni, Acarinina punctocarinata, A. bullbrooki,* and *P. renzi*.

The lower Eocene may contain hiatuses in Zones P9 and P7 because these zones are relatively thin at Site 1259. The lower boundary of Zone P9 is located between Samples 207-1259A-33R-1, 50–54 cm, and 33R-2, 50–54 cm, based upon the lowest occurrence of fragmentary remains of *Planorotalites palmerae*. Assemblages in Zone P9 contain large specimens of *Acarinina aspensis,* with six or more chambers in the last whorl, in addition to *A. praetopilensis, Pseudohastigerina micra, A. bullbrooki, I. broedermanni,* and *M. aragonensis*. Zone P8 is represented by an assemblage that includes large "*Globigerina*" *lozanoi, Acarinina pentacamerata, M. aragonensis, Acarinina quetra,* and *P. renzi* in the absence of both *P. palmerae* and *Morozovella formosa*. Samples 207-1259A-33R-6, 50–54 cm, to 33R-CC are assigned to Zone P8. Zone P7 is recognized by the presence of *M. formosa* together with *M. aragonensis* and was observed only in Sample 207-1259C-1R-CC. In as much as Zone P7 represents ~1.5 m.y. of geologic time, it is likely that there are either unrecognized hiatuses in the biozone or a highly condensed section. In contrast, Zone P6 is represented by an expanded section between Samples 207-1259A-34R-CC and 38R-4, 52–55 cm. The foraminifer fauna consists of *Acarinina soldadoensis, Morozovella subbotinae, M. aequa, Morozovella gracilis,* and *Acarinina wilcoxensis* (major elements) and *Pseudohastigerina* sp., *M. formosa, Morozovella lensiformis,* and *Morozovella marginodentata* (secondary elements). We did not subdivide Zone P6 using the first occurrence of *M. formosa* because of very poor preservation in Samples 207-1259A-35R-CC to 37R-CC.

The P/E boundary occurs in Cores 207-1259A-39R, 207-1259B-7R, and 207-1259C-7R based upon a clay-rich horizon and the appearance of a distinctive fauna of "excursion taxa" (Kelley et al., 1998) as well as *Chiloguembelina wilcoxensis, Pseudohastigerina* sp., and *I. broedermanni*. The top of Zone P5 is indicated by the extinction of *Morozovella velascoensis* and occurs between Samples 207-1259A-38R-3, 52–55 cm, and 38R-4, 49–52 cm. A core gap in Hole 1259A prevents the detailed identification of the base of Zone P5, which occurs somewhere between Samples 207-1259A-41R-CC and 43R-CC.

A set of four small (~5 $cm^3$) samples were taken in the ~80-cm interval above the base of the P/E boundary interval in Section 207-1259C-7R-2 to document the preservation and species composition of the foraminifer assemblage associated with the boundary. The base of the distinctive green clay horizon occurs at 120 cm in this section, and Samples 207-1259C-7R-2, 100–102 cm, 7R-2 108–110 cm, and 7R-2 115–117 cm, were barren of planktonic foraminifers, although all contained small numbers of benthic foraminifers and abundant but poorly preserved spumullarian radiolarians. Sample 207-1259C-7R-2, 70–72 cm, contains a moderately well preserved foraminifer assemblage with abundant *Morozovella allisonensis* and *A. soldadoensis* and rare *Acarinina africana, Acarinina sibaiyaensis, Subbotina patagonica,* and *Parasubbotina*

*varianta*. Three of these species, *M. allisonensis, A. africana,* and *A. sibaiyaensis,* are associated with P/E boundary sections in other tropical and subtropical sites (Central Pacific, Egypt, Spain, New Jersey, and the Blake Plateau) and are known as the excursion fauna because of their abundance and near restriction to the Paleocene/Eocene Thermal Maximum (PETM) (Kelly et al., 1998). An unusual element of these assemblages is *Parasubbotina paleocenica,* a clavate species that has previously been reported only from ODP Site 1220 in the equatorial Pacific and its type area in coastal Senegal. The West African and equatorial Pacific settings of these previous discoveries suggest that *P. paleocenica* is associated with upwelling conditions. Hence, we infer that the excursion fauna may also represent an expansion of relatively productive waters during the PETM.

All the Paleocene zones are represented at Site 1259. Zone P4 is present between Samples 207-1259A-43R-CC and 45R-1, 50–54 cm, based upon the presence of *Globanomalina pseudomenardii, Acarinina nitida,* and *Acarinina subspherica,* all of which make their appearance in this zone. Subzone P3b occurs between Samples 207-1259A-45R-2, 50–54 cm, and 45R-CC. Typical species in Subzone P3b include *M. velascoensis, Morozovella angulata, Morozovella pasionensis, Subbotina velascoensis, Subbotina triangularis,* and *Igorina albeari*—a fauna similar to that of Zone P4 but lacking *G. pseudomenardii* and the acarininids. We have not found markers for Subzone P3a in any hole at Site 1259, but Zone P2 is well represented between Samples 207-1257A-46R-CC and the top of Core 207-1259A-47R by a low diversity assemblage of *Praemurica inconstans, Praemurica uncinata, Morozovella praeangulata, Parasubbotina pseudobulloides,* and *Globanomalina compressa*. A sample per section in Core 207-1259B-12R reveals a Subzone P1b fauna in Sample 207-1259B-12R-2, 94–95 cm, with *Subbotina triloculinoides, Praemurica pseudoinconstans,* and *P. pseudobulloides,* a Subzone P1a assemblage in Sample 207-1259B-12R-3, 67–68 cm, with *Praemurica taurica* and *Eoglobigerina eobulloides,* and a Pα fauna with *Parvularugoglobigerina eugubina, Guembelitria cretacea,* and *Woodringina* sp. in Samples 207-1259B-12R-4, 53–54 cm, 12R-CC, and 13R-1, 24–25 cm. The spherule bed that is believed to mark the base of the Danian is in Section 207-1259B-13R-1, 49 cm.

The Maastrichtian occurs between Core 207-1259A-47R and 50R. Sample 207-1259C-8R-7, 66–68 cm, taken ~16 cm below the spherule bed, yielded a diverse assemblage of uppermost Maastrichtian foraminifers including *Abathomphalus mayaroensis* (marker species for Zone KS31) and *Plummerita hantkenoides,* a species known to appear shortly before the Cretaceous/Tertiary (K/T) boundary. At best, *P. hantkenoides* is a rare species in most open ocean sites but its presence in Site 1259 suggests the upper Masstrichtian preserves an unusually complete record of latest Cretaceous paleoclimate and evolution. The combination of cyclostratigraphy and magnetostratigraphy that seems likely to be available at Leg 207 sites should allow the range of *P. hantkenoides* to be determined precisely during postcruise studies. As at other Leg 207 sites, Zone KS31 is represented by rare to common *Rugoglobigerina rugosa, Globotruncanita stuarti, Pseudoguembelina costulata, Pseudotextularia elegans, Rugoglobigerina rotundata, Rosita contusa, Gansserina gansseri,* and *Globotruncana aegyptiaca*. Occasional specimens of *Globotruncanita calcarata* and *Globotruncanita subspinosa* are found in most Maastrichtian samples, suggesting regular reworking from the Campanian. Zone KS31 is present between the K/T boundary and Sample 207-1259A-48R-7, 50–54 cm. The presence of *R. contusa* in the absence of *A. mayaroensis* suggests that Subzone KS30a (the *R. contusa–R. fructicosa* Zone) is present in

Samples 207-1259A-48R-CC to 49R-CC. The absence of *R. contusa* in Samples 207-1259A-50R-1, 50–54 cm, to 50R-CC that still contain *G. gansseri* suggests Subzone KS30b, which spans the Campanian/Maastrichtian boundary.

Campanian foraminifer assemblages are poorly preserved and represented by only rare individuals. The *G. aegyptiaca* Zone (KS29) is represented in Sample 207-1259A-51R-CC by *Rugotruncana subcircumnodifer, Globotruncana lineana, Globotruncanella petaloidea,* and *G. aegyptiaca* along with an abundance of fish bones, glauconite pellets, and benthic foraminifers. Assemblages that may represent either Zone KS29 or KS28 are found in Samples 207-1259A-52R-3, 49–52 cm, and 52R-4, 123–126 cm, in a glauconite-rich horizon that overlies organic-rich claystones at the top of the black shale sequence. These samples contain a diverse but flattened foraminifer fauna with *Heterohelix globulosa, Globotruncanella havanensis, R. rugosa, R. subcircumnodifer, Gansserina wiedenmayeri, Globotruncanita stuartiformis,* and *Globotruncanita esnehensis*. Sample 207-1259A-52R-5, 26–28 cm, contains mostly benthic foraminifers and pyrite nodules but also *Globigerinelloides prairiehillensis* and *R. rugosa,* suggesting a Campanian age.

In contrast to the Campanian foraminifer assemblages in the glauconite-rich horizon, the underlying brown organic-rich claystones in Sample 207-1259A-52R-6, 111–113 cm, contain a distinctive and well-preserved Santonian assemblage with *Marginotruncana coronata, Dicarinella concavata, Rosita fornicata, Archaeoglobigerina blowi,* and *Dicarinella canaliculata* that in aggregate suggest Zone KS24. Coniacian foraminifers are found in Samples 207-1259A-52R-CC to 54R-CC and include both spar-filled and glassy empty-chambered foraminifers representing Zone KS23. Species in the Coniacian sequence include *Marginotruncana sinuosa, Marginotruncana schneegansi, Dicarinella imbricata, Dicarinella primitiva,* and *Whiteinella inornata*.

Turonian foraminifers were found starting in Sample 207-1259A-55R-1, 130–132 cm, to the lowest identifiable foraminifer assemblages in Sample 59R-CC. Species diversity is relatively high in the upper half of this sequence but decreases to only one or two species that are not diagnostic of either Turonian or Cenomanian age. The upper part of the Turonian includes an abundance of whiteinellids, such as *W. inornata* with weak imperforate bands, *Whiteinella archaeocretacea,* and *Whiteinella baltica,* along with the nearly ever-present *Hedbergella delrioensis*. *Dicarinella imbricata* and *D. canaliculata* are also present in many samples. The clavate species, *Hastigerinelloides watersi, Hastigerinelloides amabilis,* and *Hastigerinelloides alexanderi,* are rare components. There is low species diversity in foraminifer assemblages from Sample 207-1259A-58R-4, 42–45 cm, to 59R-CC and consists of little more than *H. globulosa, Heterohelix moremani, H. delrioensis, W. archaeocretacea,* and *W. baltica,* which could indicate either a Turonian (KS20/KS21) or latest Cenomanian (KS20) age. Foraminifers are often small (<180 µm) but are frequently preserved as glassy specimens with empty chambers in the clay-rich parts of the sequence. Foraminifers are entirely absent from Sample 207-1259A-59R-CC and are represented only by a few specimens of *H. moremani* in Sample 207-1259A-59R-CC, along with rare very well rounded quartz grains. The underlying quartz sandstone and claystone sequence in Samples 207-1259B-24R-CC and 25R-CC did not yield any foraminifers.

## Radiolarians

Radiolarians at Site 1259 were found in most of the cored material but were abundant and well preserved only in the middle Eocene. Core catcher samples were examined systematically from Hole 1259A, with an additional limited number of samples taken from Holes 1258B and 1258C.

The earliest Miocene Zone RN1 was identified in Samples 207-1259A-8R-CC and 9R-CC, based on the marker species for the base of the zone (*Cyrtocapsella tetrapera)* and *Calocycletta serrata,* which last occurred at the upper part of Zone RN1.

In the middle Eocene interval, the abundant occurrence of species *Podocyrtis goetheana* in Samples 207-1259A-17R-CC and 18R-CC marks the base of Zone RP16. This combination with the presence of species *Spongatractus pachystylus* (last occurrence [LO] at the top of Zone RP16) in Sample 207-1259A-16R-CC allows restriction of the age of Cores 207-1259A-18R through 16R solely to Zone RP16. *Podocyrtis chalara* is very abundant in Samples 207-1259A-19R-CC and 20R-CC, whereas *Podocyrtis mitra* is absent in the former sample but present, although very rare, in the latter. These samples are, therefore, situated above the base of the evolutionary transition from *P. mitra* to *P. chalara* (which defines the base of Zone RP15). *Sethochytris triconiscus* and abundant *P. mitra* in Sample 207-1259A-21R-CC allows its assignment to the upper part of Zone RP14. Therefore, the boundary between Zones RP15 and RP14 is placed in Core 207-1259A-21R. *Podocyrtis fasciolata* and *Podocyrtis trachodes* were observed in Sample 207-1259A-22R-CC, which can be therefore assigned to the lower part of Zone RP14 or the top of Zone RP13. Samples 207-1259A-23R-CC and 24R-CC are assigned to the upper part of Zone RP13 based on the occurrence of abundant *Podocyrtis ampla, Podocyrtis sinuosa*, and *Eusyringium fistuligerum.*

Sample 207-1259A-25R-CC contains both *Podocyrtis phyxis* and *P. ampla,* but the former is more abundant than the latter. It is, therefore, placed below the base of Zone RP13. As rare representatives of species *E. fistuligerum* are present in this sample, its age can be restricted to the top of Zone RP12. Therefore, the boundary between Zone RP12 and RP13 is placed in Core 207-1259A-25R.

Cores 207-1259A-25R down to 29R are assigned to Zone RP12 based on the presence of species *Thyrsocyrtis triacantha.* Sample 207-1259A-29R-CC contains both *T. triacantha* and its ancestor, *Thyrsocyrtis tensa*. As the former is more abundant than the latter, Sample 207-1259A-29R-CC can still be assigned to Zone RP12. Radiolarian preservation is moderate to poor in Sample 207-1259A-30R-CC and deteriorates further downhole. The co-occurrence of *Dictyoprora mongolfieri* and *Thyrsocyrtis robusta* suggests that it can be assigned to the lower part of Zone RP12 or RP11.

With respect to the Upper Cretaceous and, more particularly, the Campanian, Sample 207-1259A-51R-CC contains abundant radiolarian specimens (i.e., *Amphipyndax* sp. and *Dictyomitra* sp.) of moderate preservation that could not be identified at the species level. Sample 207-1259A-57R-CC contains moderately well preserved but rare radiolarians. The presence of *Acanthocircus hueyi* allows its assignment to the *Alievium superbum* Zone (lower Turonian or younger).

# PALEOMAGNETISM

Shipboard paleomagnetic measurements from the three holes at Site 1259 resolved numerous Campanian–lower Miocene magnetic polarity zones. Chrons C31r–C29r are tentatively assigned to the Maastrichtian succession, and Chrons C24r–18r of uppermost Paleocene to middle Eocene are well defined.

## Shipboard and Shore-Based Procedures and Data Filters

Details are given in "Paleomagnetism," p. 16, in the "Explanatory Notes" chapter of the standard shipboard analysis using the pass-through cryogenic magnetometer, of the filtering and polarity interpretation procedures of this shipboard data, and of the shore-based progressive demagnetization of discrete minicores. Shipboard measurements of natural remanent magnetization (NRM) and after 10- and 15-mT alternating-field (AF) demagnetization steps were made at 5-cm intervals on all archive halves longer than 15 cm from Cores 207-1259A-1R through 52R, 207-1259B-2R through 18R, and 207-1259C-1R through 17R. In general, the 10-mT step was effective in removing steep downward overprints induced by the drilling process, and the 15-mT step was usually needed to resolve trends toward negative inclination directions but also reduced the magnetic intensity of the majority of the sediment intervals to the background noise level of the cryogenic magnetometer. As at the other Leg 207 sites, we did not analyze the black shale cores rather than partially removing the magnetization of these sediments without obtaining any useful shipboard information. These black shale intervals typically display magnetizations near the background noise level of the shipboard cryogenic magnetometer and were deposited during the Long Cretaceous Normal Polarity Superchron C34n.

Shipboard identification of polarity zones through nearly half of the succession was not possible because of weak magnetization near the noise limit of the cryogenic magnetometer, secondary overprints associated with reddish coloration that could not be removed by shipboard AF demagnetization, and several intervals characterized by reduced core recovery. Therefore, oriented paleomagnetic cylinders were drill pressed at 3-m spacing from all Campanian–middle Eocene sediments from Hole 1259B and Campanian–Maastrichtian sediments from Hole 1259A for combined progressive AF and thermal demagnetization at the magnetic-shielded facility at the University of Munich, Germany. Additional postcruise sampling of sediments from Hole 1259A filled some of the gaps in recovery in Hole 1259B. The magnetic polarity of each minicore was interpreted from an examination of the movement of its magnetic vector during progressive demagnetization (see "Paleomagnetism," p. 16, in the "Explanatory Notes" chapter) (Table T10). These shore-based measurements enabled resolution of removed and characteristic components of magnetization and significantly modified the tentative shipboard polarity interpretations from all facies.

T10. Characteristic directions of minicores, p. 91.

## Paleomagnetic Behavior and Interpretations of Magnetostratigraphy

The generalized stratigraphy of sediment facies, biostratigraphic ages, and magnetization characteristics at Site 1259 from the shipboard pass-through cryogenic magnetometer are summarized in Figure F12. Intervals of greenish white to light gray chalk are characterized by very weak magnetization, and nearly half of the measurements after the 15-mT demagnetization step for such intervals were below the $3 \times 10^{-5}$ A/m background noise level of the magnetometer system. There was a general association of "expanded stratigraphic sections" (e.g., the Maastrichtian, middle Eocene, and upper Oligocene) with these low intensities of magnetization, which suggests a dilution of the magnetic minerals by enhanced biogenic input of carbonate and silica tests. Relatively compact intervals, such as upper Eocene and Campanian–Maastrichtian greenish gray chalks, had a much stronger magnetic intensity.

F12. Shipboard paleomagnetic data, p. 53.

### Lower Miocene

The 85-m-thick unit of yellowish to greenish foraminifer–sand facies of early Miocene age (Cores 207-1259A-1R to upper 10R) has moderately strong magnetic intensities, averaging ~$1 \times 10^{-4}$ A/m, with numerous normal and reversed polarity zones (Fig. F12). The green–yellow color transition at ~40 mbsf does not appear to affect the magnetic characteristics. The early Miocene, which spans ~5 m.y., encompasses ~12 pairs of magnetic reversals (see Fig. F5, p. 59, in the "Explanatory Notes" chapter). The only "fingerprint" in this polarity pattern is the relatively long normal polarity Chron C6n in the upper M2 foraminifer zone and the upper NN2/lower NN3 nannofossil zones, which we tentatively correlate to the normal polarity zone in Core 207-1259A-5R at this same biostratigraphic level. An assumption of relatively constant sedimentation rates implies that the two overlying polarity pairs in the resedimented foraminifer sand dominated by Oligocene microfossils could be Chrons C5E and C5D, but shipboard resolution of this interval was very poor. Chron C6C of predominant reversed polarity spans the Oligocene/Miocene boundary; therefore, the reversed polarity zone at this biostratigraphic position in Hole 1259A is tentatively assigned to this chron. Limited core recovery precludes establishing the lower Miocene polarity zone pattern, so other polarity chron assignments are not reliable.

### Oligocene

The 40-m-thick Oligocene unit of greenish white chalk has an average magnetization after 15-mT demagnetization of only $3 \times 10^{-5}$ A/m, which is the background noise level of the magnetometer. Less than 20% of the measurements provide useful polarity information, but the broad biostratigraphic constraints and limited intervals with adequate magnetization are consistent with a possible assignment of Chron C12–Chron C10r. These tentative polarity zone identifications would require future verification from paleomagnetic studies of discrete minicores. We did not attempt to resolve this magnetostratigraphy in our post-cruise program.

## Upper Eocene

A narrow 10-m-thick zone of greenish gray chalk from the upper Eocene (Priabonian stage) has a relatively strong magnetization (average = $2 \times 10^{-4}$ A/m after 15-mT demagnetization) and is characterized by normal polarity with a possible thin reversed polarity band near the base (Fig. F12). Progressive demagnetization of minicores verified the shipboard interpretation (Fig. F13). This polarity and the biostratigraphic constraints (foraminifer Zone P16) may indicate Chrons C15n and C15r.

## Lower–Middle Eocene

The upper portion of the middle Eocene greenish white chalk (foraminifer Zones P12–P14) has a moderate magnetic intensity that averaged $1 \times 10^{-4}$ A/m after 15 mT. The lower portion (foraminifer Zones P10 and P11) is very weakly magnetized (averaging $<5 \times 10^{-4}$ A/m) (Fig. F12). Progressive thermal demagnetization of minicores yielded well-defined polarity zones, which are constrained by the biostratigraphy and characteristic pattern to be Chrons C21n–C18r. Low core recovery and wide spacing of minicores in the uppermost portion (Cores 207-1259A-16R to 18R) precluded a reliable chron assignment.

The upper half of the lower Eocene strata (foraminifer Zones P6–P9) displays distinctive cycles of reddish brown to gray or dark to light green. In the cyclic unit of similar age at Site 1258, it appeared that hematite was both the source of the reddish coloration and the carrier of a normal polarity overprint that persisted during AF demagnetization. Progressive thermal demagnetization of minicores was effective in resolving polarity zones, and these are constrained by the biostratigraphy to be Chrons C23n–C22n.

There is a possible hiatus in sedimentation during the middle of the early Eocene that appears to encompass foraminifer Zone P7, nannofossil Zone NP11, and portions of adjacent zones. The polarity zone pattern is consistent with the associated absence of Chrons C24n and C23r.

The lower half of the lower Eocene succession is a weakly magnetized white chalk. This interval and the underlying uppermost Paleocene displays reversed polarity, which is consistent with Chron C24r at the Paleocene/Eocene boundary interval. This thick reversed polarity interval contains a thin band of normal polarity in Core 207-1259A-37R (Fig. F13). The biostratigraphic position of this normal polarity subzone in the lower part of foraminifer Zone P6 is similar to the age of thin normal polarity bands observed in the paleomagnetic results of Site 1258 (Fig. F13) and of possible normal polarity subzones in Chron C24r at Site 1051A (Ogg and Bardot, 2001). However, without declination control on the minicore paleomagnetic behaviors during demagnetization, the validity of any thin polarity band in ODP cores is uncertain. In summary, the lower–middle Eocene succession contains a nearly complete record of Chrons C24r–C18r.

## Paleocene

It was not possible to make unambiguous identification of polarity zones in the upper Paleocene gray chalk or lower Paleocene reddish brown chalk. If one assumes that the ~25-m interval of negligible recovery from Cores 207-1259A-40R to 42R, which were not cored in Holes

F13. Shore-based paleomagnetic data, p. 54.

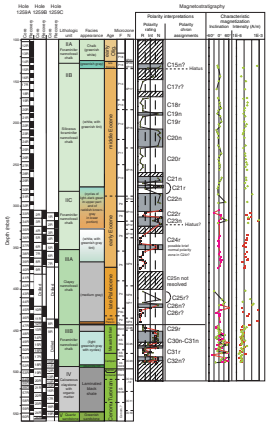

1259B or 1259C, contained the record of Chron C25n, then the underlying polarity pattern resolved from the minicores could be Chrons C26r–C25r. The relatively condensed reddish brown facies of the basal Paleocene (upper portion of Core 207-1259A-47R) carried a persistent normal polarity overprint that did not respond to AF demagnetization but was not sampled for postcruise analyses due to proximity to the K/T boundary.

### Campanian–Maastrichtian

The greenish gray chalk of Campanian–Maastrichtian age is characterized by light–dark cycles and was extensively sampled for postcruise paleomagnetic analyses with the goal of placing cyclostratigraphic constraints on the durations of the polarity chrons. This facies displayed weak intensity and susceptibility during shipboard measurements, and few pieces yielded magnetic intensities above the background noise of the magnetometer upon AF demagnetization (Fig. F12). Progressive thermal demagnetization of the suites of minicores from the duplicate intervals in Holes 1259A and 1259B yielded similar patterns of potential polarity interpretations (Fig. F13). Our tentative interpretation of the combined polarity pattern is a relatively expanded Chron C29r above a more compact record of Chrons C31r–C30n of the lower–middle Maastrichtian.

## COMPOSITE DEPTHS

Coring at Site 1259 extended to a total depth of 559 mbsf. Three discrete intervals were targeted for overlap and composite section construction: (1) the lower Eocene foraminifer nannofossil chalks of lithostratigraphic Subunit IIC (including the P/E boundary [~305–375 mcd]), (2) the Campanian–Maastrichtian nannofossil chalks and calcareous siltstones of lithostratigraphic Subunit IIIB (~440–505 mcd), and (3) the Cretaceous black shales (lithostratigraphic Unit IV—calcareous claystone with organic matter [~520–555 mcd]). Magnetic susceptibility and gamma ray attenuation (GRA) bulk density data were collected with the multisensor track (MST) at 2.5-cm intervals on all whole-core sections from Holes 1259A, 1259B, and 1259C. Natural gamma ray (NGR) data were collected at 7.5-cm intervals on all whole cores from Holes 1259A, 1259B, and 1259C. Noncontact resistivity (NCR) data were collected at 2.5-cm intervals on whole cores from Hole 1259A. No NCR data were collected from Holes 1259B and 1259C (see **"Physical Properties,"** p. 33, in the "Explanatory Notes" chapter for a discussion of problems associated with the calibration and accuracy of NCR data). Spectral reflectance data were collected at 2.5-cm intervals on all split cores. Magnetic susceptibility was the primary data set used to correlate between holes in the lower Eocene and the Campanian–Maastrichtian sections of Site 1259. Within the Cretaceous black shales, NGR and GRA bulk density data provided the most reliable core-to-core comparisons.

### Composite Section

The depth offsets that compose the composite section for Holes 1259A, 1259B, and 1259C are given in Table T11. In the lower Eocene and P/E boundary section (~305–375 mcd) and from the K/T boundary

T11. Composite depth offsets, p. 94.

to the top of the Cretaceous black shales (440–505 mcd), magnetic susceptibility is a sensitive indicator of the fluctuations in the carbonate/clay ratio in the calcareous chalks that compose these two intervals. These magnetic susceptibility data (Figs. F14, F15), combined with the good RCB recovery in all three holes, allowed the construction of a continuous composite section for both intervals. The quasiperiodic variability of the claystone and chalk/limestone composing the black shale unit resulted in strong signal-to-noise ratios in both the GRA bulk density and NGR data sets (Fig. F16). These data sets, combined with good RCB recovery over a significant portion of the black shale interval, allowed for the construction of a continuous composite section from ~520 to 555 mcd. Poor recovery from 495 to 520 mcd precluded the construction of a composite section in this upper interval of the Cretaceous black shales.

The composite depth scales constructed for each of these three intervals, however, cannot be tied to the intervals above and below because of gaps in the record resulting from poor recovery (e.g., the interval from 375 to 400 mcd). Thus, the absolute depth of these composite sections cannot be accurately determined. As at the other Leg 207 sites, these composite intervals "hang" in the composite depth scale linked only to correlative cores in other holes but not to the other discrete continuous intervals above or below.

The periodic variability in the lower Eocene and Campanian–Maastrichtian intervals at Site 1259 will provide a good basis for postcruise cyclostratigraphic studies. Age control is excellent, with well-defined paleomagnetic datums in both sections (e.g., Chrons C22n and C24 in the lower Eocene and Chrons C30n and C32n in the Campanian–Maastrichtian) (see "Paleomagnetism," p. 22). Preliminary investigation suggests the dominant periodicities of the magnetic susceptibility data are Milankovitch in nature.

## Splice Record

Following construction of the composite depth section at Site 1259, three discrete splice records were assembled for the aligned cores in the intervals 305–375, 440–505, and 520–555 mcd (Table T12; Figs. F14, F15, F16). Hole 1259A cores were used as the "backbone" for each splice, with cores from Holes 1259B and 1259C used to span gaps between cores in Hole 1259A. Figure F17 provides a qualitative estimate of the confidence of the core-to-core correlations and the resultant splices between cores in Holes 1259A, 1259B, and 1259C. When utilizing these splices as sampling guides, it is advisable to overlap a few decimeters from different holes to accommodate anticipated postcruise revisions to the composite depth scale. The reason for this approach is that distortion of the cored sequence can lead to stretching or compression of sedimentary features. Because much of the distortion occurs in individual cores on depth scales of <9 m, it was not possible to align every feature in the MST and color reflectance records. However, at crossover points along the splice, care was taken to align highly identifiable features from cores in each hole. Postcruise work will establish a detailed correlation between holes by establishing a revised meters composite depth (rmcd) scale that allows differential stretching and squeezing in cores.

F14. Magnetic susceptibility data, lower Eocene, p. 56.

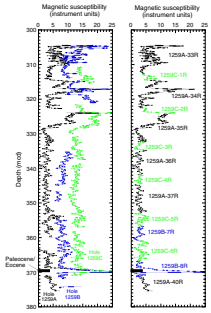

F15. Magnetic susceptibility data, Campanian–Maastrichtian, p. 57.

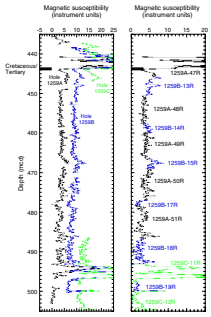

F16. GRA bulk density data, p. 58.

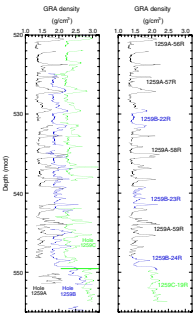

T12. Splice tie points, p. 95.

F17. Magnetic susceptibility data vs. composite depth, p. 59.

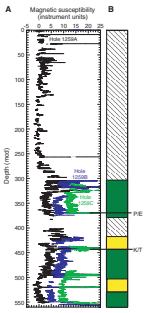

# SEDIMENTATION RATES

## Age-Depth Model

An age-depth model was established for Site 1259 by combining all available biostratigraphic and magnetostratigraphic datums from Hole 1259A (Fig. F18). The diagram was constructed by plotting highest and lowest possible ages for selected paleontological samples examined shipboard against the depth of those samples (Table T13). In addition, the age and depth of magnetic reversals recognized shipboard (Table T14) were also plotted.

The lower Miocene–Cenomanian section is punctuated by at least five unconformities or hiatuses and at least one condensed interval that spans the middle Campanian. Sedimentation rates ranged from 0.4 to 13 m/m.y. and are summarized in Table T15. The upper 50 m at Site 1259A is slumped Oligocene sediments sitting on lower Miocene sediments; this interval was not considered in sedimentation rate calculations.

F18. Age-depth plot, p. 60.

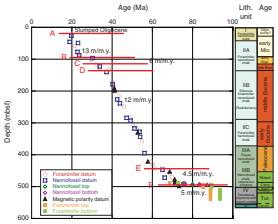


T13. Calcareous nannofossil and planktonic foraminiferal datums, p. 96.

T14. Magnetostratigraphic datums, p. 97.

T15. LSR and MAR, p. 98.

## Sedimentation Rates and Hiatuses

The lower Miocene nannofossil and foraminifer oozes accumulated at an average rate of 13 m/m.y. Calcareous microfossil datums indicate an unconformity (see letter B on Fig. F18) separating the lower Miocene and lower Oligocene. A 1.3-m.y. unconformity (see letter C on Fig. F18) is also recognized by nannofossil datums at the E/O boundary. The upper Eocene foraminifer-nannofossil chalks accumulated at a rate of 6 m/m.y. and are separated from the middle Eocene siliceous foraminifer-nannofossil chalks by an unconformity (see letter D on Fig. F18).

The longest interval of apparently continuous sedimentation is the middle Eocene–early Paleocene section of siliceous and foraminifer nannofossil chalks and clayey nannofossil chalks. Calcareous microfossil datums and paleomagnetic data indicate a relatively constant sedimentation rate of 12 m/m.y. through this interval. The absence of foraminiferal Zone P3a suggests an unconformity (see letter E on Fig. F18) in the basal upper Paleocene.

The Maastrichtian and upper Campanian clayey nannofossil chalks are characterized by relatively low accumulation rates of 4.5 m/m.y. A significant unconformity between the upper and lower Campanian (see letter F on Fig. F18) is indicated by calcareous nannofossil data. An expanded view of the lower Paleogene and Upper Cretaceous (Fig. F19) shows the condensed section found in dark brown clay-rich sediments deposited following the middle Campanian unconformity (see letter F on Fig. F18) in Sections 207-1259A-52R-5 and 52R-6. Calcareous nannofossil Zones CC18–CC15 are represented in Sections 207-1259A-52R-5 and 52R-6, indicating a minimum sedimentation rate of 0.4 m/m.y. for the earliest Campanian and Santonian.

F19. Expanded age-depth plot, p. 61.

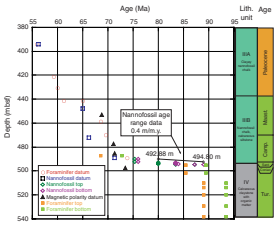


## Mass Accumulation Rates

Average mass accumulation rates (MARs) were calculated from linear sedimentation rates (LSRs) and averaged dry bulk density data. MARs were not calculated for Units IV and V because reliable dry bulk density data are not available for these units. MARs remove the influence of compaction on LSR calculation and give a better indication of the quantity of accumulating sediment. The lower Miocene had lower MAR

values (1.1 g/cm²/k.y.) but higher sedimentation rate (13 m/m.y.) than the middle Eocene (MAR = 1.4 g/cm²/k.y.; LSR = 12 m/m.y.), indicating possible burial compaction and infilling of pore space in the Eocene section. The MAR values (0.8 g/cm²/k.y.) found in the lower Paleocene–upper Campanian section are consistent with a shift to clay-rich deposition and lower carbonate percentages (see "Lithostratigraphy," p. 4).

MAR and carbonate MAR for the middle Eocene–upper Paleocene are shown in Figure F20. Carbonate MAR was calculated using percentage carbonate analyses that were taken within 4 cm of dry bulk density measurements. Significant gaps in the curve were filled by visual assessment of the locales of carbonate analyses and the nearest dry bulk density measurements with a separation not >30 cm between measurements. If no change in lithology or color was observed, then the data were used for the curve found in Figure F20. The 130- to 430-mbsf interval shows a slight increase in bulk MAR but relatively constant carbonate MAR. This trend is coincident with an increasing clay content downcore, suggesting a relatively constant carbonate production and changing terrigenous input.

F20. MAR and carbonate MAR, p. 62.

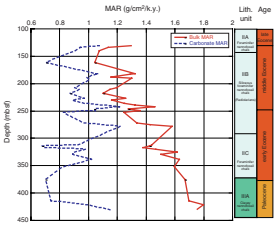


## ORGANIC GEOCHEMISTRY

Concentrations of inorganic carbon and TOC were determined on sediments from Holes 1259A, 1259B, and 1259C. Organic matter atomic carbon/nitrogen (C/N) ratios and Rock-Eval pyrolysis analyses were employed to assess the type of organic matter contained in the sediments. Routine monitoring of interstitial gas contents of Hole 1259A was performed for drilling safety, and the possiblity of microbial activity was evaluated from headspace gas contents of this hole.

### Inorganic and Organic Carbon Concentrations

Concentrations of inorganic carbon vary from 0.02 to 11.3 wt% at Site 1259 (Table T16). These concentrations are equivalent to 0.2–93.9 wt% sedimentary $CaCO_3$, assuming that all of the carbonate is calcite or aragonite. Carbonate concentrations in the five lithostratigraphic units (see "Lithostratigraphy," p. 4) generally become less with greater depth. However, the black shales that compose most of Unit IV still contain ~50 wt% carbonate, largely because calcite laminae were interspersed among the black shale laminae.

T16. TOC, inorganic carbon, and total nitrogen, p. 99.

Site 1259 sediments have a wide range of TOC concentrations. The sediments of Units I–III contain <0.8 wt% TOC (Table T16). In marked contrast, the black shales in Unit IV have TOC concentrations between 1.3 and an exceptionally high 29 wt% (Sample 207-1259B- 24R-3, 141–142 cm; C/N ratio = 41). The average TOC content for Unit IV is 9.3 wt%. One sample in Unit V (Sample 207-1259C-19R-3, 83–84 cm) has a TOC of 6 wt% and probably contains woody material; its high C/N ratio of 61 indicates its terrestrial origin. Otherwise, Unit V has low TOC values of <0.5 wt%.

### Organic Matter Source Characterization

Atomic $C_{organic}/N_{total}$ ratios were employed to help identify the origins of organic matter in Site 1259 sediments. C/N values in organic-lean Units I, II, and III are low, commonly below the range typical of fresh algal organic matter (4–8) (Meyers, 1997). These values are probably an

artifact of the low TOC concentrations combined with the tendency of clay minerals to absorb ammonium ions generated during degradation of organic matter (Müller, 1977).

The C/N ratios of the black shales in Unit IV average 29, which is a value typical of land-plant organic matter but also common to Cretaceous black shales (Meyers, 1997). A van Krevelen–type plot of hydrogen index (HI) and oxygen index (OI) values (Fig. F21) indicates that the black shales in Unit IV contain Type II (algal) organic matter. High HI and low $T_{max}$ values like those found in the black shales (Table T17) are characteristic of thermally immature, relatively well preserved marine organic matter (Espitalié et al., 1977; Peters, 1986). There are four data points in the van Krevelen plot that appear to be a mixture of Types II and III organic matter; $T_{max}$ values >400°C for three out of four of these samples confirm greater maturity that is most probably due to incorporation of some organic detrital matter in the black shales. The elevated C/N values that mimic those of land-derived organic matter are likely to be the result of partial alteration of marine organic matter. A probable scenario is that nitrogen-rich components are preferentially degraded during sinking of organic matter to the seafloor, thereby elevating the C/N ratio of the surviving organic matter (Twichell et al., 2002).

F21. Rock-Eval van Krevelen–type diagram, p. 63.

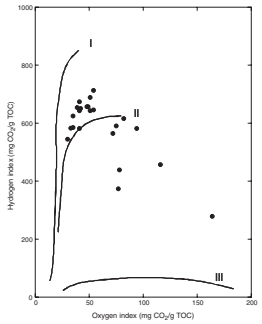


T17. Rock-Eval pyrolysis analyses, p. 102.

## Interstitial Gas Contents

Sediments at Site 1259 have low interstitial gas concentrations. Neither gas voids nor other evidence of gas release from cores was observed. A significant odor of hydrogen sulfide was noticeable in cores from the black shales (Unit IV; 493–563 mbsf), but the natural gas analyzer, which has a sensitivity of ~1 ppmv, did not detect this gas in headspace samples.

Headspace gas results from routine safety monitoring and the special microbial gas study are shown in Figure F22. The routine safety monitoring analyses show methane first appearing at 350 mbsf (bottom of Subunit IIC; foraminifer-nannofossil chalk) and concentrations steadily increasing to a maximum 76,400 ppmv at 545 mbsf (bottom of Unit IV; black shale) before falling to 2,300 ppmv in the last core (Unit V; quartz sandstone). Methane determined as part of the microbial gas study shows higher, though still small (3–50 ppmv), concentrations between 0 and 350 mbsf, then a rapid increase to 56,400 ppmv at the bottom of the black shales in Unit IV. The last core was not measured in the microbial gas study. The differences observed between the two experiments most likely reflects the different treatment of samples prior to analysis (see "Organic Geochemistry," p. 27, in the "Explanatory Notes" chapter). In both cases, however, high methane/ethane ($C_1/C_2$) ratios and the absence of significant amounts of $C_2$ and $C_3$ indicate that the methane is biogenic, rather than thermogenic, in origin (Table T18). A biogenic origin is also supported by the disappearance of interstitial sulfate at the same subbottom depth where methane concentrations begin to rise (see "Inorganic Geochemistry," p. 30); interstitial sulfate generally inhibits microbial methanogenesis (Claypool and Kvenvolden, 1983).

Interstitial gas concentrations and compositions were found to relate to lithology; concentrations increased abruptly and peaked in the black shales. The possible relation between sediment organic matter contents and gas concentrations was investigated by measuring the TOC concen-

F22. Headspace gas and microbial methane concentrations, p. 64.

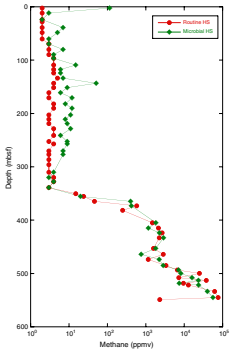


T18. Headspace analysis of gases, p. 103.

trations of the headspace sediment samples from Hole 1259A. A rough correspondence exists between higher TOC and larger gas concentrations (Fig. F23). Excursions from a simple linear relation suggest that organic matter quality, and not simply quantity, affect gas generation from the black shales. Moreover, dramatic changes in methane concentrations at lithologic boundaries (Fig. F22) suggest either that gas does not freely migrate from its origin in the black shales or that it migrates and is consumed/oxidized at the base of the sulfate reduction zone (see "Inorganic Geochemistry," p. 30).

F23. TOC and methane concentrations, p. 65.

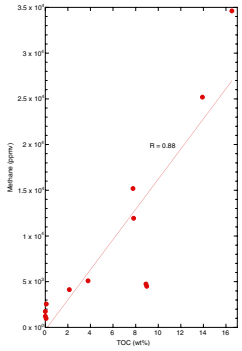


# INORGANIC GEOCHEMISTRY

We collected interstitial water from 32 samples at Site 1259, 28 from Hole 1259A (2.55–488.33 mbsf) and 4 from Hole 1259C (525.65–549.22 mbsf). One sample taken from Hole 1259B (interval 207-1259B-25R-1, 89.0–100.0 cm) is not considered in the following discussion, as interstitial water could not be retrieved. The samples from both holes were taken to constitute a single depth profile. However, slight differences in lithology may cause minor breaks in concentration-depth gradients of some chemical parameters. Chemical constituents were determined according to the procedure outlined in "Inorganic Geochemistry," p. 31, in the "Explanatory Notes" chapter. Alkalinity was not determined in three samples because of low yields of interstitial water. Results of the chemical analyses are presented in Table T19.

T19. Pore water chemical analyses, p. 104.

## Black Shales as a Diagenesis Bioreactor

Interstitial water chemistry at Site 1259 is dominated by the black shales and associated organic matter–rich sediments of Santonian–Cenomanian age (lithostratigraphic Unit IV [~493–549 mbsf]). The downhole pore water concentration profile of sulfate at Site 1259 approaches zero slightly above the top of Unit IV (see Fig. F24F), suggesting that this organic matter–rich unit provides a suitable substrate for ongoing microbial activity at depth. The pore water sulfate gradient from the base of Unit III to the sediment/water interface is essentially linear, suggesting that sulfate reduction is of minor importance at shallower depth intervals. We assume that methane diffusing upward from the black shales may provide the source for metabolic activity, possibly anaerobic methane oxidation (Borowski et al., 1999; Boetius et al., 2000). In contrast to the situation at nearby Site 1257, the smell of hydrogen sulfide was not noticeable within or above the black shales. It is possible that the intense pyritization observed in Unit III sediments is triggered by hydrogen sulfide production and immediate trapping in this zone. In particular, the Paleocene section (Subunit IIIA) is clay rich and therefore iron rich. This assumption is further supported by high dissolved iron concentrations further upward (Fig. F24O), with maximum values >100 µM in the chalky Subunits IIA–IIC. Even though chalks are generally iron poor, the absence of trace quantities of hydrogen sulfide may explain the high values.

The reducing character of the sedimentary column is also seen in slightly elevated Mn concentrations (Fig. F24P). Nevertheless, only very low concentrations (<1 µM) are attained in Unit IV. Presumably these sediments lost most of their Mn during or shortly after they were deposited, an interpretation that would indicate deposition under conditions of severe oxygen depletion. Alternatively, the low interstitial water Mn

F24. Pore water chemical constituents, p. 66.

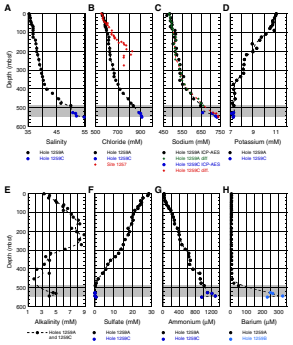

concentrations observed in Unit IV reflect the formation of Mn-rich carbonate phases (e.g., ankerite/rhodochrosite), which are common in organic matter–rich sediments. Shore-based chemical analysis of the interstitial water "squeeze cakes" will provide a definitive test of these two competing hypotheses.

Sulfate depletion is accompanied by increases in ammonium (Fig. F24G), a common respiration product of organic matter consumption. Ammonium concentrations peak in lithostratigraphic Unit IV and decrease linearly toward close to the sediment/seawater interface. In the very shallow subsurface, ammonium must be oxidized because concentrations are close to the detection limit in the two uppermost pore water samples taken. The close relation between sulfate depletion and ammonium buildup is illustrated by the linear inverse correlation shown in Figure F25.

The complete absence of sulfate in Unit IV most probably promotes two other phenomena typically seen in organic matter–rich sediments: (1) mobilization of Ba and (2) formation of dolomite. Increases in Ba concentration (Fig. F24H) are governed by barite solubility (Church and Wolgemuth, 1972) and are prone to even slight contamination by seawater sulfate. The highest dissolved Ba levels attained in Unit IV are >300 µM and exhibit a smooth profile. For this reason, we assume that seawater contamination is minimal at this site. It seems noteworthy to mention that elevated Ba levels are still present in Subunit IIIB, where authigenic barite crystals of millimeter to centimeter scale are frequently observed (see **"Lithostratigraphy,"** p. 4). Similar sedimentological and mineralogical relationships are reported elsewhere (Brumsack, 1986; Torres et al., 1996).

The downhole interstitial water concentration profile for Mg shows three different trends: an almost linear decrease from the sediment/water interface toward the P/E boundary (Hole 1259A [367 mbsf]) (see **"Lithostratigraphy,"** p. 4), constant or slightly increasing values in the clay-rich Unit III, and decreasing values from the center of Unit IV to the base of the black shales (Fig. F24K). It seems surprising that clay-rich Unit III particularly shows no sign of Mg removal with depth, even though clays may represent an important Mg sink. Because salinity increases are evident at Site 1259 (see **"Lithostratigraphic Unit IV as an Aquifer for Brines,"** p. 32), we have normalized Mg values to chloride. The downcore profile of the Mg/Cl ratio (Fig. F24Q) is quite linear, suggesting Mg removal throughout the sedimentary column. The same is essentially true for K, an element that is incorporated into clay minerals during burial diagenesis. The K profile (Fig. F24D) exhibits a stepwise decrease downcore and, again, rather constant values in Unit III. When normalized to Cl, a smooth downcore decrease is evident (Fig. F24R). The pronounced positive correlation between the Mg/Cl and K/Cl ratios (Fig. F26) suggests a common removal process, most likely incorporation into clay minerals.

In direct contrast, the downhole pore water concentration profile for Ca is nonlinear and shows a clear break at ~300 mbsf, close to the P/E boundary (Fig. F24I). Below this interval, an almost linear Ca increase toward the base of Unit IV is evident. Also, a clear relationship between Ca and alkalinity is not visible immediately. Alkalinity buildup is noticeable downcore to ~300 mbsf (Fig. F24E). Below this depth, significantly lower values are observed, most likely resulting from carbonate precipitation. Again, Cl normalization shows a much clearer picture (Fig. F24S), with increasing Ca/Cl ratios in Unit I to Subunit IIB, decreasing values in Subunit IIC, and essentially constant values down to

F25. Pore water sulfate vs. ammonium, p. 69.

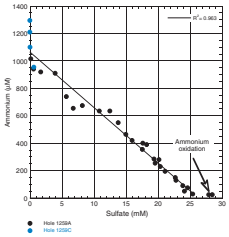


F26. Pore water Mg/Cl vs. K/Cl, p. 70.

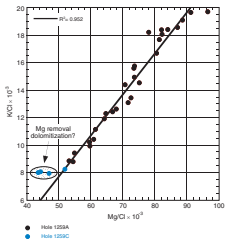

the base of Unit IV. The decrease in Ca/Cl ratio parallels the drop in alkalinity, indicating carbonate precipitation. The poor preservation of nannofossils and foraminifers in this interval supports this assumption (see "Biostratigraphy," p. 11).

The downhole pore water Sr profile at Site 1259 shows a steady increase from the sediment/water interface to increasingly high values (>1600 µM) in the deepest sample analyzed (~549 mbsf) (Fig. F24J). The shape of this pore water Sr profile contrasts with the typical ooze–chalk transition "middepth maximum" (Baker at el., 1982) and suggests that carbonate diagenesis in the Paleogene strata as inferred from the Ca and alkalinity profiles is dominated by calcite precipitation rather than dissolution or in situ "recrystallization." Even when normalized to Cl, Sr shows an almost linear increase downcore (Fig. F24T), suggesting a source (possibly aragonite-rich shallow-water carbonate sediments) underlying the section drilled.

Li concentrations (Fig. F24L) increase steadily down to 400 mbsf. Below this depth interval, a linear increase exists. Li/Cl ratios, by contrast, are almost constant below 300 mbsf (Fig. F24U), suggesting a source in the overlying sedimentary column. There is a striking linear correlation between Ca/Cl and Li/Cl ratios in the upper 270 m of the sedimentary column (Fig. F27), suggesting a common source. Whether carbonate recrystallization or ash alteration is dominating cannot be ruled out without additional isotopic investigations.

The B profile shows slight increases down to 300 mbsf (Fig. F24M), possibly resulting from B desorption processes (Brumsack and Zuleger, 1992). Below this interval, B adsorption onto clay minerals is indicated.

Increases in dissolved Si concentrations with depth to ~300 mbsf reflect biogenic Si (Fig. F24N), particularly in Subunit IIB. At greater depth, decreases in dissolved Si may also be associated with chert or silicate mineral formation. The depth profiles of B and Si concentrations are strikingly similar, suggesting clay mineralogy may influence both chemical parameters. Below the black shale unit, low Si concentrations may be attributed either to the absence of clays or to transformation of biogenic Si into opal-CT or even quartz (Dixit et al., 2001).

F27. Pore water Ca/Cl vs. Li/Cl, p. 71.

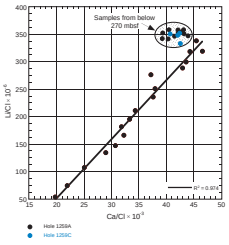


## Lithostratigraphic Unit IV as an Aquifer for Brines

Another prominent feature of interstitial water chemistry is an increase in Cl concentration with depth of >60% relative to the International Association for the Physical Sciences of the Ocean (IAPSO) value (Fig. F24A–F24C). This increase is paralleled by Na, but the Na/Cl ratio decreases toward Unit IV, from seawater values of 0.86 to below 0.80 (Fig. F24V). It is noteworthy to mention that the maximum in salt content is located at the base of Unit IV at ~549 mbsf. Unfortunately, we were unable to retrieve an interstitial water sample from below the black shales, but we assume that this unit may act as an aquifer for the brine. We cannot exclude that a fraction of the K, Ca, Sr, Mg, and Li (Fig. F24D, F24I–F24L) is also associated with this brine (Figs. F26, F27).

In summary, the interstitial water profiles from this site primarily reflect ongoing organic matter diagenesis in the black shales, carbonate diagenesis, the dissolution of biogenic Si, and, possibly, a minimal influence of ash alteration. In contrast to the findings at Site 1257, we cannot completely rule out the existence of underlying deeper-seated evaporites, as suggested for Site 144 by Waterman et al. (1972).

# PHYSICAL PROPERTIES

Physical property measurements at Site 1259 were conducted on whole cores, split cores, and discrete samples. Whole-core measurements conducted with the MST included GRA bulk density (2.5-cm spacing), magnetic susceptibility (2.5-cm spacing), NCR (5-cm spacing), and NGR (15-cm spacing). Compressional (*P*)-wave velocity was measured in the transverse direction on split cores at ~50-cm intervals and along both transverse and longitudinal directions on cube samples taken at a frequency of two per core between 310 and 480 mbsf in Hole 1259B.

Moisture and density (MAD) properties were determined on discrete samples at a frequency of one per section from all three holes at Site 1259. Sampling for MAD was reduced across critical intervals, important transitions, and throughout the Cretaceous shale sequence. A full description of the various measurement techniques is in **"Physical Properties,"** p. 33, in the "Explanatory Notes" chapter.

## Density and Porosity

MAD properties determined at Site 1259 include bulk density, porosity, grain density, water content, and void ratio (Table **T20**). Bulk density was determined on whole-core sections using the MST (GRA density) and on discrete samples. GRA-derived density tends to underestimate the true bulk density because RCB cores do not completely fill the inner diameter of the liner. The average difference between the GRA and MAD densities for Hole 1259A was 0.155 g/cm$^3$. In the absence of logging data, it is important to calibrate the MST-derived GRA density with the MAD measurements from the laboratory. Average differences in the MAD- and GRA-derived densities between lithostratigraphic units has been calculated for samples taken from all three holes of Site 1259 (Table **T21**). If the GRA data sets are to be used for quantitative purposes, it is recommended that they should first be corrected to the MAD data.

**T20.** MAD of discrete samples, p. 105.

**T21.** GRA vs. MAD bulk density, p. 109.

There is no discernible increase in the bulk density of the upper 80 mcd of sediment at Site 1259, suggesting that this interval is apparently underconsolidated (Fig. **F28**). Large variations in both porosity and grain density occur through the interval. A significant increase in the bulk density and a corresponding drop in porosity and grain density occurs between 80 and 100 mcd and coincide with a general coarsening of the sediments (see **"Lithostratigraphy,"** p. 4) as well as a hiatus in sediment accumulation rate (see **"Sedimentation Rates,"** p. 27). Below this perturbation, density increases and porosity decreases with depth from 110 to 370 mcd. Through this interval, variations in density, grain density, and porosity appear to track changes in the relative proportions of carbonate and biogenic silica (see **"Lithostratigraphy,"** p. 4). An offset in MAD data at the lithostratigraphic Subunit IIB/IIC boundary (~285 mcd) occurs through an interval of sparse recovery that marks a shift from radiolarian ooze to nannofossil chalk.

**F28.** Discrete physical property measurements, p. 72.

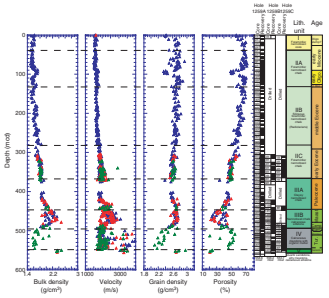


Below 400 mcd, bulk density increases significantly across the K/T boundary, which separates the clayey nannofossil chalk of Subunit IIIA from the nannofossil chalk calcareous siltstone of Subunit IIIB. Density, porosity, and velocity measurements all increase significantly in variability between 410 and 475 mcd and then gradually decrease in both magnitude and variability below 475 mcd, down to the top of Unit IV.

This variability is associated with cyclic changes in the composition and degree of lithification of the sediments. A finer-scale cyclic signal in this interval is best seen in the GRA data from the MST (Fig. F29).

Unit IV is characterized by low and variable bulk densities, decreasing grain density with depth, and a peak in porosity in the middle of the unit. Two anomalously low porosity values can be matched with peaks in the bulk density and are from limestone layers commonly found interbedded through the Unit IV shale sequences. A distinct increase in porosity through the middle part of Unit IV is unexplained. The frequency of MAD sampling is not sufficient to fully characterize the variability of Unit IV, and a better representation is given by the MST data described below. Limited sampling in Unit V reveals an abrupt increase in bulk density and grain density and a drop in porosity.

## Acoustic Velocity

*P*-wave velocity was measured on split cores using the modified Hamilton Frame apparatus. In addition, measurements of transverse (x- and y-direction) and longitudinal (z-direction) velocity were conducted on cube samples from Hole 1259B (Table T22).

The general depth trend of acoustic velocity correlates directly with bulk density and inversely with porosity (Fig. F28). However, variability in the velocity is more pronounced through Subunit IIC and into the top of Subunit IIIA. This variability coincides with alternations between bands of light greenish gray sediment with high clay content (low velocity) and intervals rich in zeolite and calcite (high velocity) (see "Lithostratigraphy," p. 4).

Beginning in the middle of Subunit IIIA and throughout Subunit IIIB, velocities increase to values between 1800 and 3000 m/s. This large range in velocities reflects the cyclic alternations between dark clay-rich intervals and light-colored calcite intervals. Just below the K/T boundary, velocity values reach ~3200 m/s before gradually decreasing to ~1900 m/s at the transition into Unit IV. In Unit IV (calcareous claystone with organic matter), velocity of the laminated organic-rich claystones averages 1800 m/s, whereas sandstone/limestone velocities vary between 2000 and >4000 m/s (Figs. F28, F29).

Anisotropy of velocity measurements were performed on cubes taken from Hole 1259B between 310 and 480 mbsf (Fig. F29). This interval coincides with the greatest variability in the velocity, density, and porosity measurements. Anisotropy increases downhole. At 300 mcd, velocities are ~1% faster along the longitudinal z-axis, but by 350 mcd, velocities are 2%–3% higher in the transverse direction. Transverse velocity is generally 1%–6% higher in Unit III, reflecting changes in sediment composition, varying rebound effects through clayey intervals, or a combination of both (Fig. F29).

## Whole-Core Multisensor Track

Poor core recovery hampers the interpretation of MST data trends in Unit I and Subunit IIA. Unit II tends to have a somewhat higher magnetic susceptibility and gamma ray signal than Unit I, with a drop in the density, magnetic susceptibility, and NGR signals at 100 mcd (Fig. F30).

The transition into the siliceous foraminifer nannofossil chalk of Subunit IIB is marked by a decrease in both the magnetic susceptibility

F29. Acoustic velocity and velocity anisotropy, p. 73.

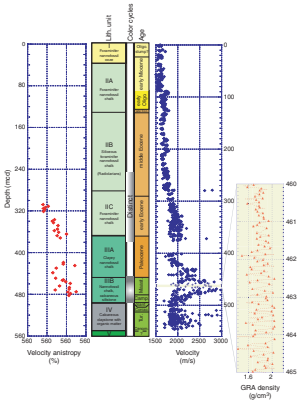

T22. *P*-wave velocity, p. 110.

F30. MST data, p. 74.

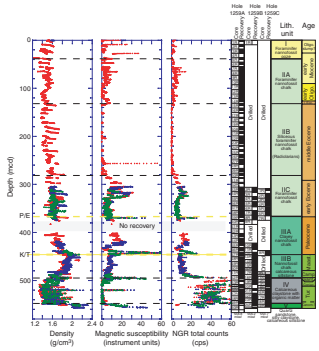

and NGR data to background noise levels. Near the bottom of Subunit IIB, beginning at ~250 mcd, a gradual increase in magnetic susceptibility and NGR can be discerned. This increase continues across the boundary into Subunit IIC and culminates at 310 mcd, where recovery in Holes 1259B and 1259C supplement the record and a distinct series of peaks in both magnetic susceptibility and NGR sensors is seen. NGR counts through the middle part of Subunit IIC, an interval of alternating clay and zeolite/calcite–rich layers reach 20 counts per second (cps), whereas magnetic susceptibility rises to >15 (magnetic susceptibility values are reported herein as raw instrument units; see **"Physical Properties,"** p. 33, in the "Explanatory Notes" chapter for conversion of these data to SI units).

NGR and magnetic susceptibility signals are cyclical through the lower 40 m of Subunit IIC, where the P/E boundary is recovered, and are represented by a short pronounced excursion in magnetic susceptibility values to 25 and NGR emissions of 30 cps. Just below the P/E boundary, there is a 30-m gap in recovery in the upper part of lithostratigraphic Subunit IIIA.

Following this gap in recovery, a continuous spliced sequence is made (see **"Composite Depths,"** p. 25) that extends from the middle of Subunit IIIA, across the K/T boundary, through the nannofossil chalk and calcareous silstone of Subunit IIIB, and down to the transition into Unit IV. Alternating dark clay-rich intervals and light-colored carbonate intervals bracket the K/T boundary, which is seen in all three holes as a peak in magnetic susceptibility (>30) and a sharp rise to just less than 30 cps in NGR emissions.

GRA density gradually decreases below the K/T boundary. NGR emissions through this same interval remain relatively constant until ~485 mcd, where a gradual rise correlates with the appearance of the glauconitic sands transitioning into the organic-rich interval of Unit IV.

Unit IV is characterized by highly variable GRA and NGR signals that correspond to the alternation of laminated organic-rich intervals and cemented limestone and sandstone intervals (Fig. **F31**). In general, the NGR readings are highest near the top of the unit, with emissions reaching 120 cps. NGR counts decrease until ~520 mcd, where a spike in the magnetic susceptibility and GRA records represents a distinct coarse-grained glauconite-rich calcareous claystone (see **"Lithostratigraphy,"** p. 4). Below this spike, NGR emissions vary around an average of ~35 cps.

Excellent covariance is shown between the NGR and GRA signals in Unit IV, with organic-rich layers having lower density and higher radioactivity and limestone intervals with higher density but lower radioactivity. A density minima occurs through the interval from 490 to 550 mcd (Fig **F31**) that may reflect higher organic carbon content (higher porosity). The magnetic susceptibility signal through Unit IV shows a small but gradual increase beginning below the glauconitic calcareous claystone at ~520 mcd. This change may indicate a concomitant change in sediment composition that explains the observed trend in GRA density.

The boundary between Units IV and V is sharp and best defined by a large increase in GRA density. An increase in susceptibility across this boundary, however, is more gradual. NGR emissions drop upon entering Unit V but remain above 25 cps.

**F31.** MST data across the K/T boundary, p. 75.

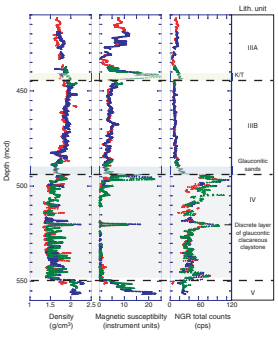

## Synthetic Seismograms

A synthetic seismogram is generated from formation velocity and density. In the absence of logging data at Site 1259 and reliable MST data from RCB cores, density and velocity measurements were obtained from MAD properties and Hamilton Frame measurements, respectively. MAD samples taken within 2.5 cm of Hamilton Frame velocity measurements were used in the calculation of downhole impedance:

velocity (m/s) × density (Mg/m³).

Downhole impedance contrasts across successive layers yield the reflection coefficient series (Fig. F32). An Ormsby wavelet was convolved with the reflection coefficient series to generate a synthetic seismogram (Fig F33).

Hole 1259A was offset 300 m from the seismic line, and changes in the depth structure of the shallowest sediments are difficult to account for over this offset; however, by aligning Reflector C on the seismic section with the prominent reflection at the base of the synthetic seismogram there is excellent agreement between marked impedance contrasts and major reflectors. Once shifted, the synthetic seismogram matches accurately to the seismic data, which allowed regional Reflectors B, B′, and C to be correctly identified in the time domain (Fig. F33). Reflector C represents the base of the black shales. Reflector B′ matches the impedance spike found at ~520 ms (two-way traveltime) (Fig. F32), the height of distinct cyclical alternations between dark clay-rich intervals and light-colored limestone intervals (~475 mbsf) (Fig. F32), whereas Reflector B is the density and velocity step across the K/T boundary denoting the transition from Subunits IIIA to IIIB (see "Lithostratigraphy," p. 4).

F32. Impedance and reflection coefficient profiles, p. 76.

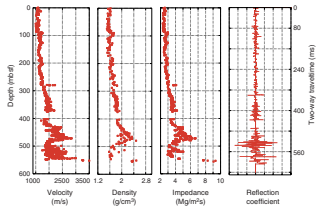


F33. Impedance contrasts, p. 77.

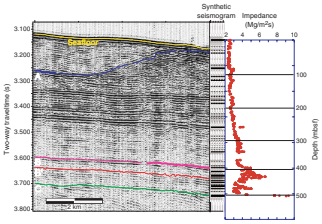

# REFERENCES

Baker, P.A., Gieskes, J.M., and Elderfield, H., 1982. Diagenesis of carbonates in deep-sea sediments—evidence from $Sr^{2+}/Ca^{2+}$ ratios and interstitial dissolved $Sr^{2+}$ data. *J. Sediment. Petrol.,* 52:71–82.

Boetius, A., Ravenschlag, K., Schubert, C.J., Rickert, D., Widdel, F., Gieseke, A., Amann, R., Jørgensen, B.B., Witte, U., and Pfannkuche, O., 2000. Microscopic identification of a microbial consortium apparently mediating anaerobic methane oxidation above marine gas hydrate. *Nature,* 407:623–626.

Borowski, W.S., Paull, C.K., and Ussler, W., III, 1999. Global and local variations of interstitial sulfate gradients in deep-water, continental margin sediments: sensitivity to underlying methane and gas hydrates. *Mar. Geol.,* 159:131–154.

Brumsack, H.-J., 1986. The inorganic geochemistry of Cretaceous black shales (DSDP Leg 41) in comparison to modern upwelling sediments from the Gulf of California. *In* Summerhayes, C.P., and Shackleton, N.J. (Eds.), *North Atlantic Palaeoceanography.* Geol. Soc. Spec. Publ., 21:447–462.

Brumsack, H.-J., and Zuleger, E., 1992. Boron and boron isotopes in pore waters from ODP Leg 127, Sea of Japan. *Earth Planet. Sci. Lett.,* 113:427–433.

Claypool, G.E., and Kvenvolden, K.A., 1983. Methane and other hydrocarbon gases in marine sediment. *Annu. Rev. Earth Planet. Sci.,* 11:299–327.

Church, T.M., and Wolgemuth, K., 1972. Marine barite saturation. *Earth Planet. Sci. Lett.,* 15:35–44.

Dixit, S., van Cappellen, P., and van Bennekom, A.J., 2001. Processes controlling solubility of biogenic silica and pore water buildup of silicic acid in marine sediments. *Mar. Chem.,* 73:333–352.

Espitalié, J., Laporte, J.L., Madec, M., Marquis, F., Leplat, P., Paulet, J., and Boutefeu, A., 1977. Méthode rapide de caractérisation des roches mères, de leur potentiel pétrolier et de leur degré d'évolution. *Rev. Inst. Fr. Pet.,* 32:23–42.

Hayes, D.E., Pimm, A.C., et al., 1972. *Init. Repts. DSDP,* 14: Washington (U.S. Govt. Printing Office).

Jenkins, D.G., 1966. Planktonic foraminiferal datum planes in the Pacific and Trinidad Tertiary. *N. Z. J. Geol. Geophys.,* 9:424–427.

Kelly, D.C., Bralower, T.J., and Zachos, J.C., 1998. Evolutionary consequences of the Latest Paleocene Thermal Maximum for tropical planktonic foraminifera. *Palaeogeogr., Palaeoclimatol., Palaeoecol.,* 141:139–161.

Meyers, P.A., 1997. Organic geochemical proxies of paleoceanographic, paleolimnologic, and paleoclimatic processes. *Org. Geochem.,* 27:213–250.

Müller, P.J., 1977. C/N ratios in Pacific deep sea sediments: effect of inorganic ammonium and organic nitrogen compounds sorbed by clays. *Geochim. Cosmochim. Acta,* 41:765–776.

Ogg, J.G., and Bardot, L., 2001. Aptian through Eocene magnetostratigraphic correlation of the Blake Nose Transect (Leg 171B), Florida continental margin. *In* Kroon, D., Norris, R.D., and Klaus, A. (Eds.), *Proc. ODP, Sci. Results,* 171B, 1–58 [CD-ROM]. Available from: Ocean Drilling Program, Texas A&M University, College Station TX 77845-9547, USA.

Peters, K.E., 1986. Guidelines for evaluating petroleum source rock using programmed pyrolysis. *AAPG Bull.,* 70:318–329.

Torres, M.E., Brumsack, H.-J., Bohrmann, G., and Emeis, K.C., 1996. Barite fronts in continental margin sediments: a new look at barium remobilization in the zone of sulfate reduction and formation of heavy barites in diagenetic fronts. *Chem. Geol.,* 127:125–139.

Twichell, S.C., Meyers, P.A., and Diester-Haass, L., 2002. Significance of high C/N ratios in organic-carbon-rich Neogene sediments under the Benguela Current upwelling system. *Org. Geochem.,* 33:715–722.

Waterman, L.S., Sayles, F.L., and Manheim, F.T., 1972. Interstitial water studies on small core samples, Leg 14. *In* Hays, D.E., Pimm, A.C., et al., *Init. Repts. DSDP,* 14: Washington (U.S. Govt. Printing Office), 753–762.

**Figure F1.** Seismic line GeoB219 at Site 1259 and GeoB220 at Site 1257. Seismic Unit 1 is above Horizon A, Unit 2 is between Horizons A and B, Subunit 3a is between Reflectors B and B′, and Unit 4 is below Horizon C. See Figure **F1**, p. 5, in Shipboard Scientific Party, this volume [“Seismic Stratigraphy and Underway Geophysics”] for a location map for this line.

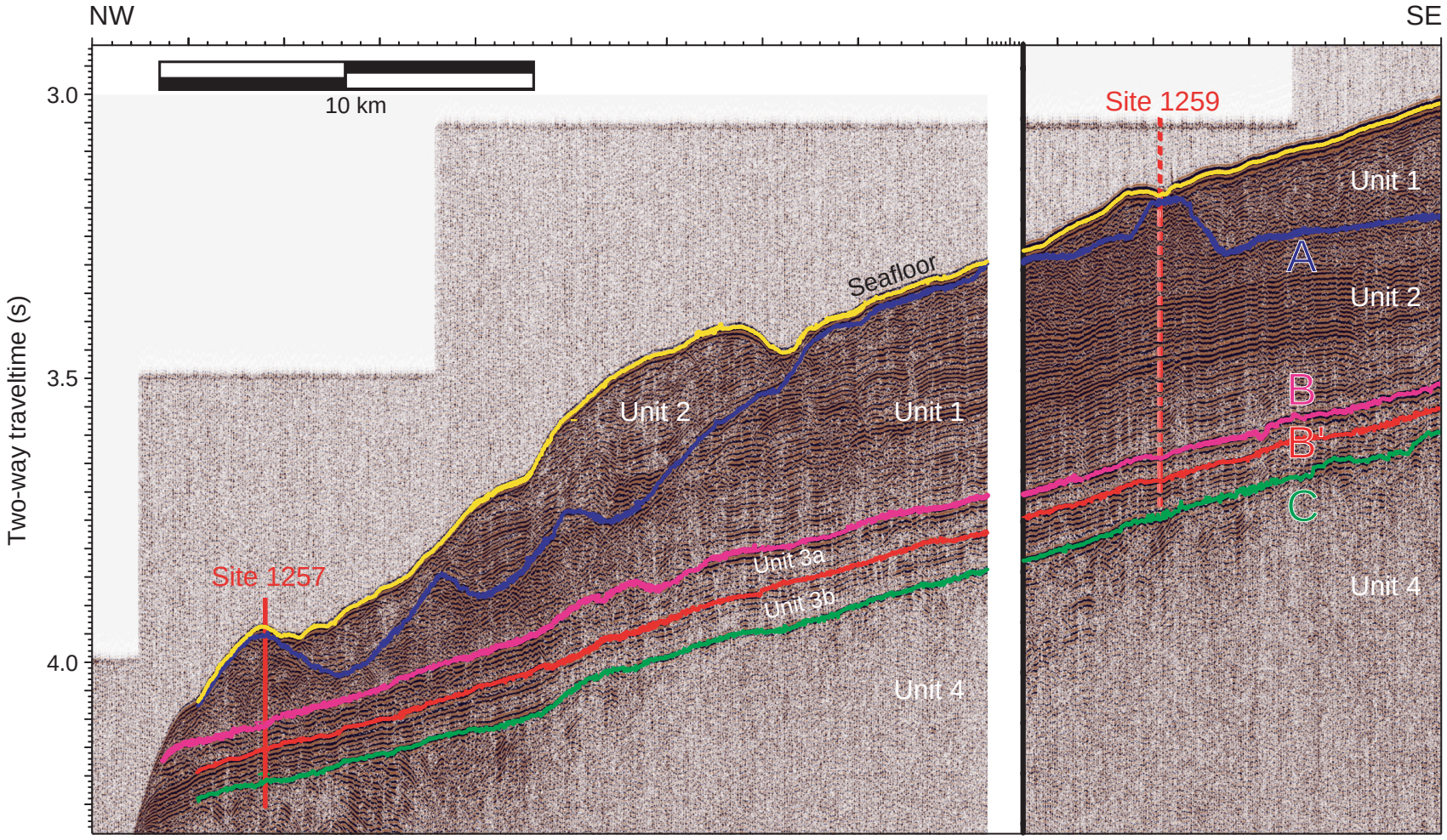

**Figure F2.** Industry multichannel seismic reflection line C2206a passing orthogonal to line GeoB219 across Site 1259. See Figure F1, p. 5, in Shipboard Scientific Party, this volume ("Seismic Stratigraphy and Underway Geophysics") for a location map for this line. It shows the seismic tie from this site to Site 1260. The position of Reflector A is uncertain on this low-resolution profile.

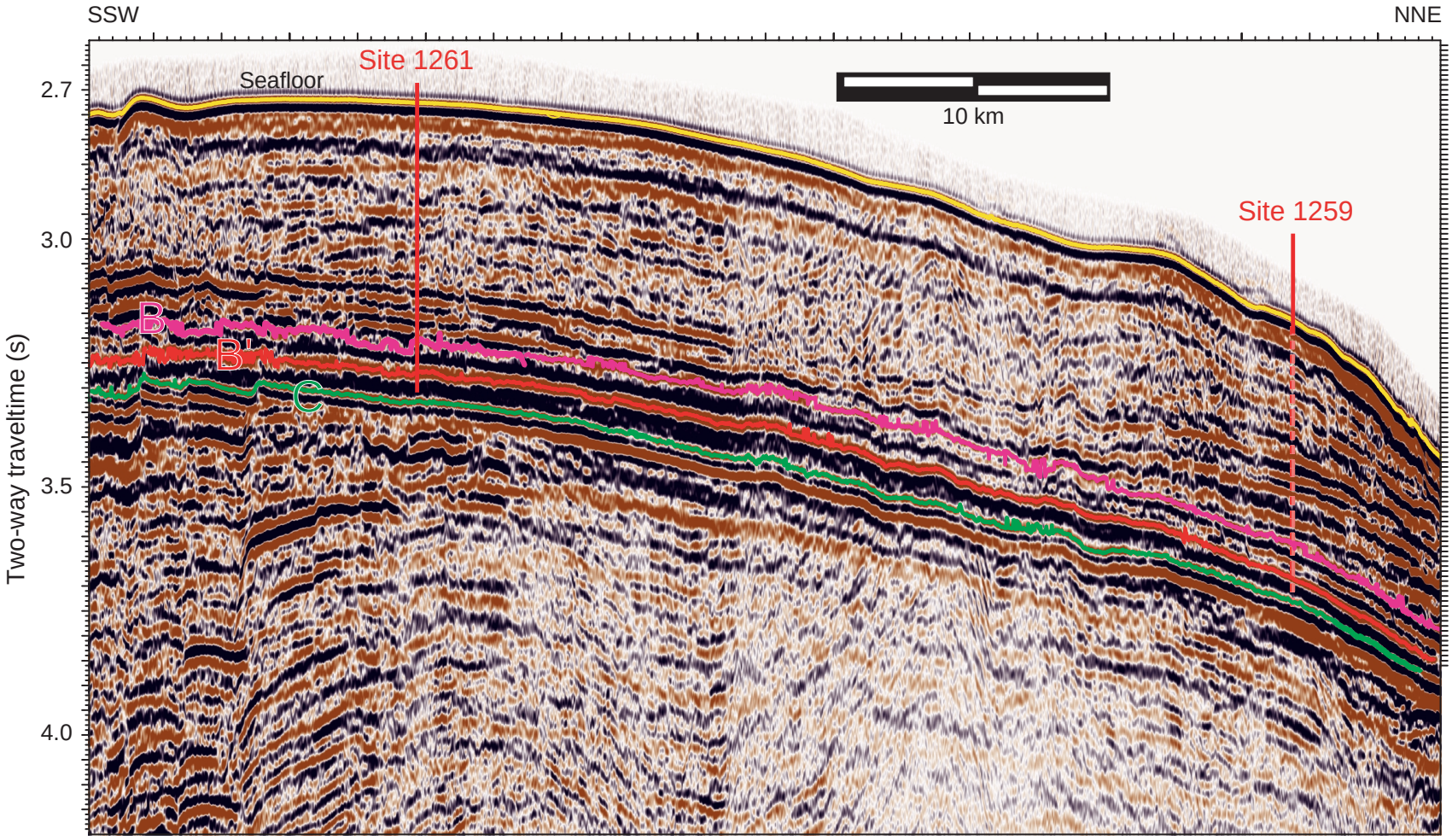

**Figure F3.** Comparison of core recovery, lithostratigraphic units, ages, carbonate, and total organic carbon (TOC) content at Site 1259. Carbonate and TOC content values are primarily from Hole 1259A (red dots), with few additional carbonate data from Holes 1259B (blue squares) and 1259C (green diamonds).

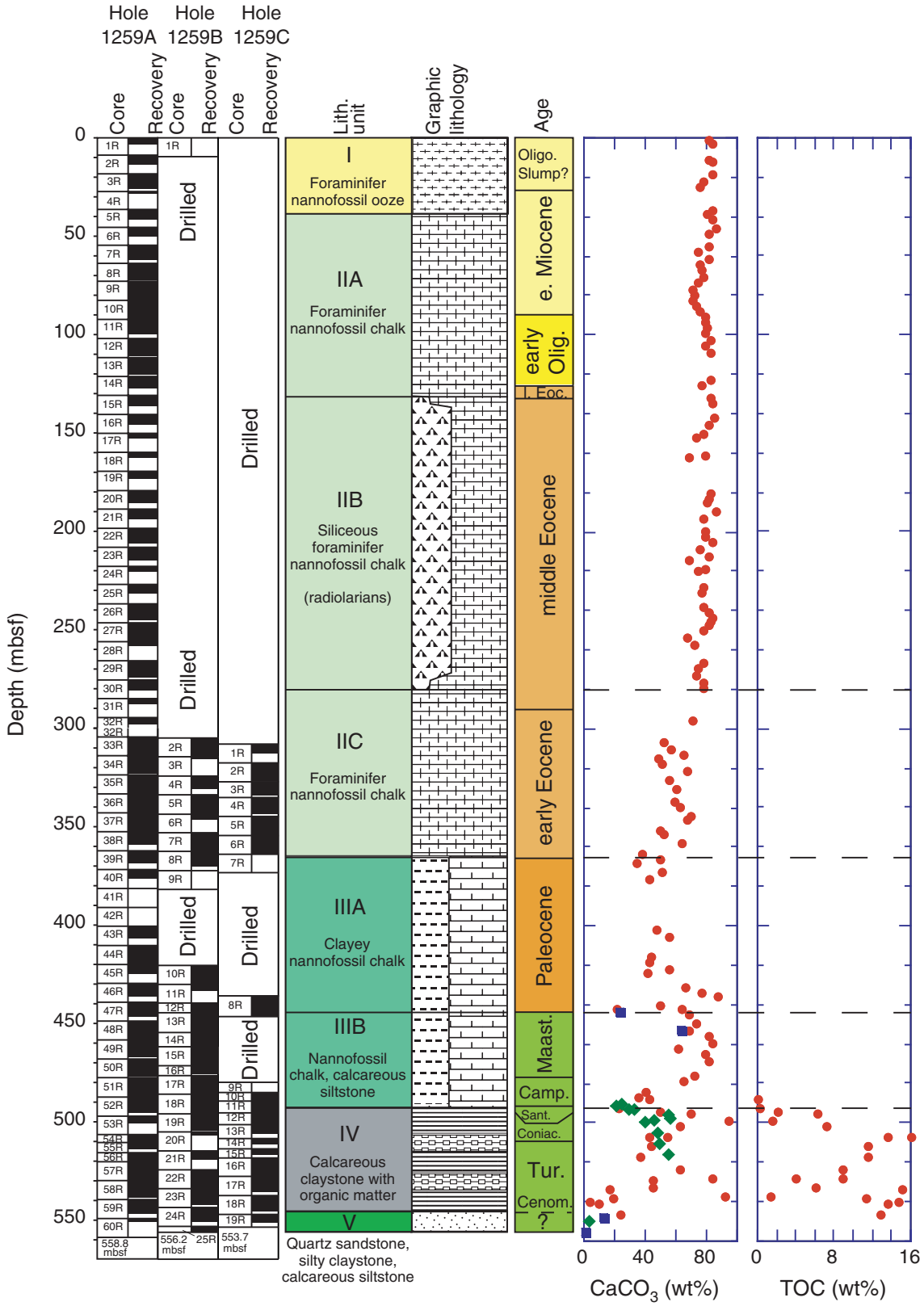

**Figure F4.** Close-up photographs of representative lithologies from Unit II at Site 1259. **A.** Light greenish gray siliceous foraminifer nannofossil chalk, with pervasive burrows from Subunit IIB (interval 207-1259A-27R-6, 70–90 cm). The darker (higher clay content) interval at 83–86 cm is characteristic of the rhythmic color cycles observed at the base of the subunit. **B.** Typical finely mottled sediments of Subunit IIC right above the biostratigraphic P/E boundary (interval 207-1259B-8R-4, 35–50 cm).

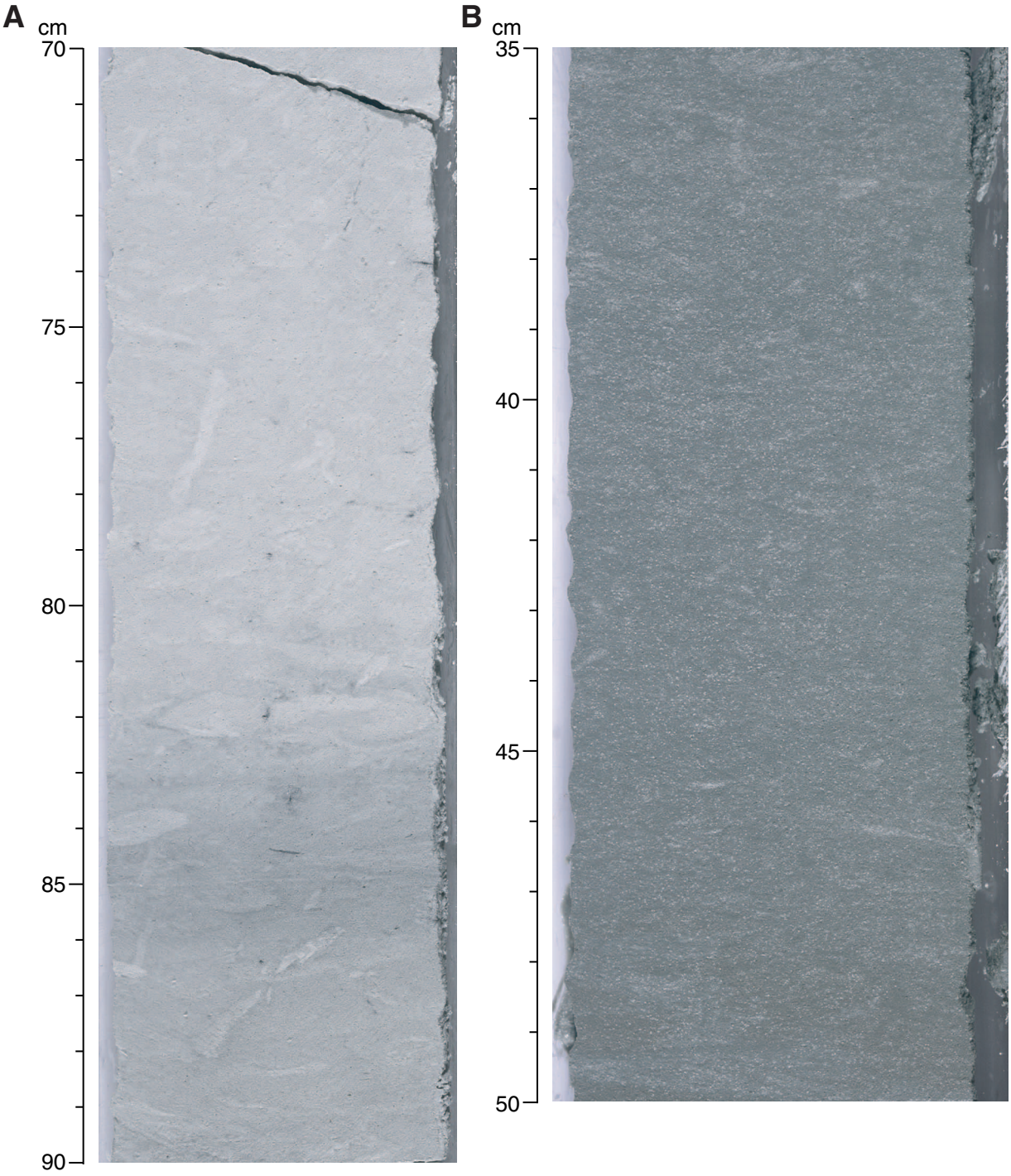

**Figure F5.** Close-up photographs of representative lithologies from the lithostratigraphic unit boundary between Units II and III which corresponds to the P/E boundary at Site 1259. **A.** Sharp contact with a distinct lithologic change from the finely mottled nannofossil chalk of Subunit IIC to the more clayey nannofossil chalk of Subunit IIIA (interval 207-1259A-39R-5, 130–145 cm). Note there are few darker burrows in underlying lithology. The unit boundary was placed at interval 207-1259A-39R-5, 139 cm. **B.** The apparently complete P/E boundary interval in Hole 1259B (interval 207-1259B-8R-5, 95–115 cm). An interval with darker burrows can be observed (interval 207-1259B-8R-5, 106–107 cm) at the top of Subunit IIIA. The unit boundary is placed at interval 207-1259B-8R-5, 106 cm.

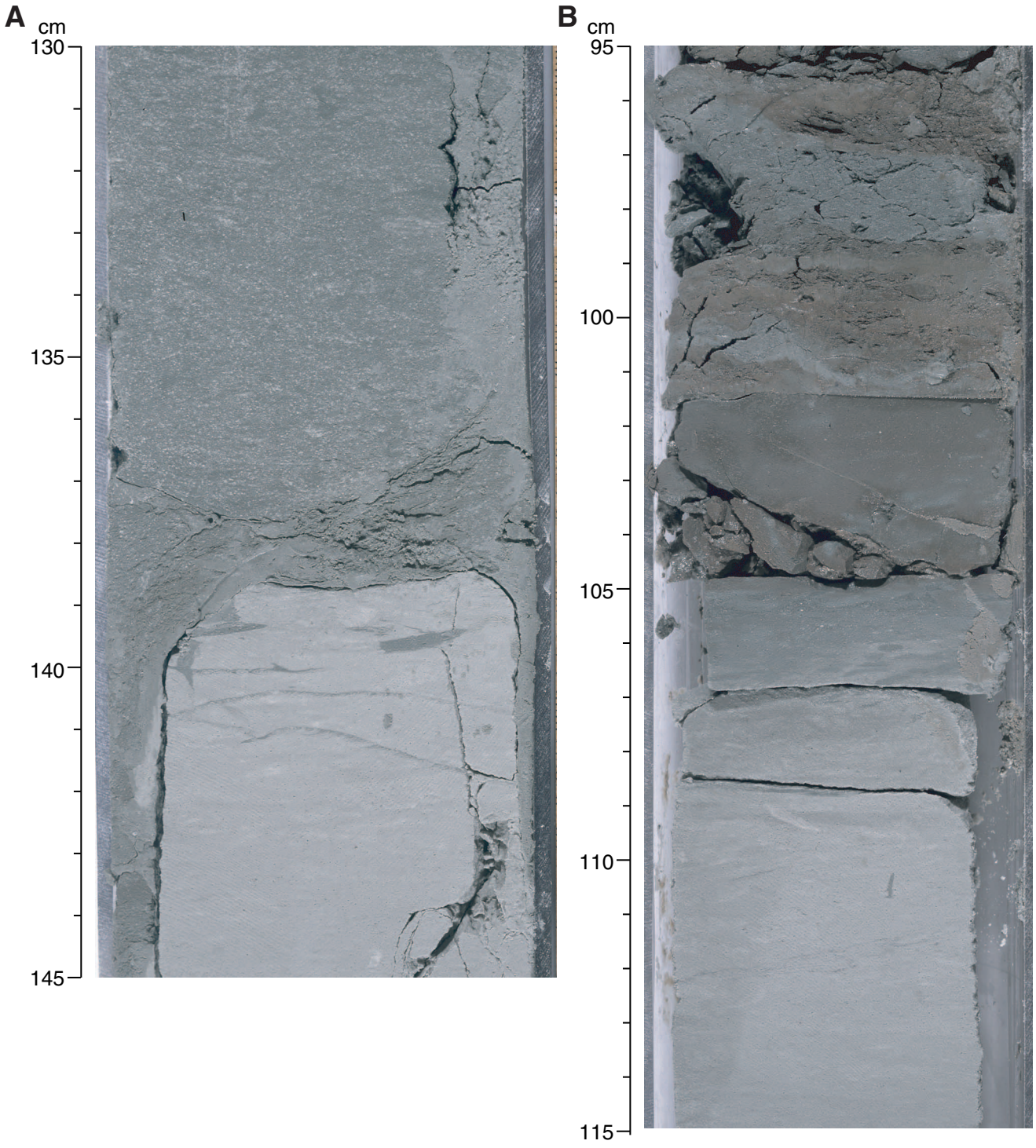

**Figure F6.** Close-up photographs of representative lithologies from Subunits IIIA and IIIB and the K/T boundary. **A.** Typical fine-scaled mottled structure and colors (light greenish gray and reddish brown) of Subunit IIIA (interval 207-1259A-47R-1, 90–110 cm). Note the light greenish gray halos around discrete burrows in the reddish brown sediments. **B.** Apparently complete K/T boundary interval including a graded 1.9-cm-thick ejecta layer (interval 207-1259B-13R-1, 33–53 cm). (Continued on next page.)

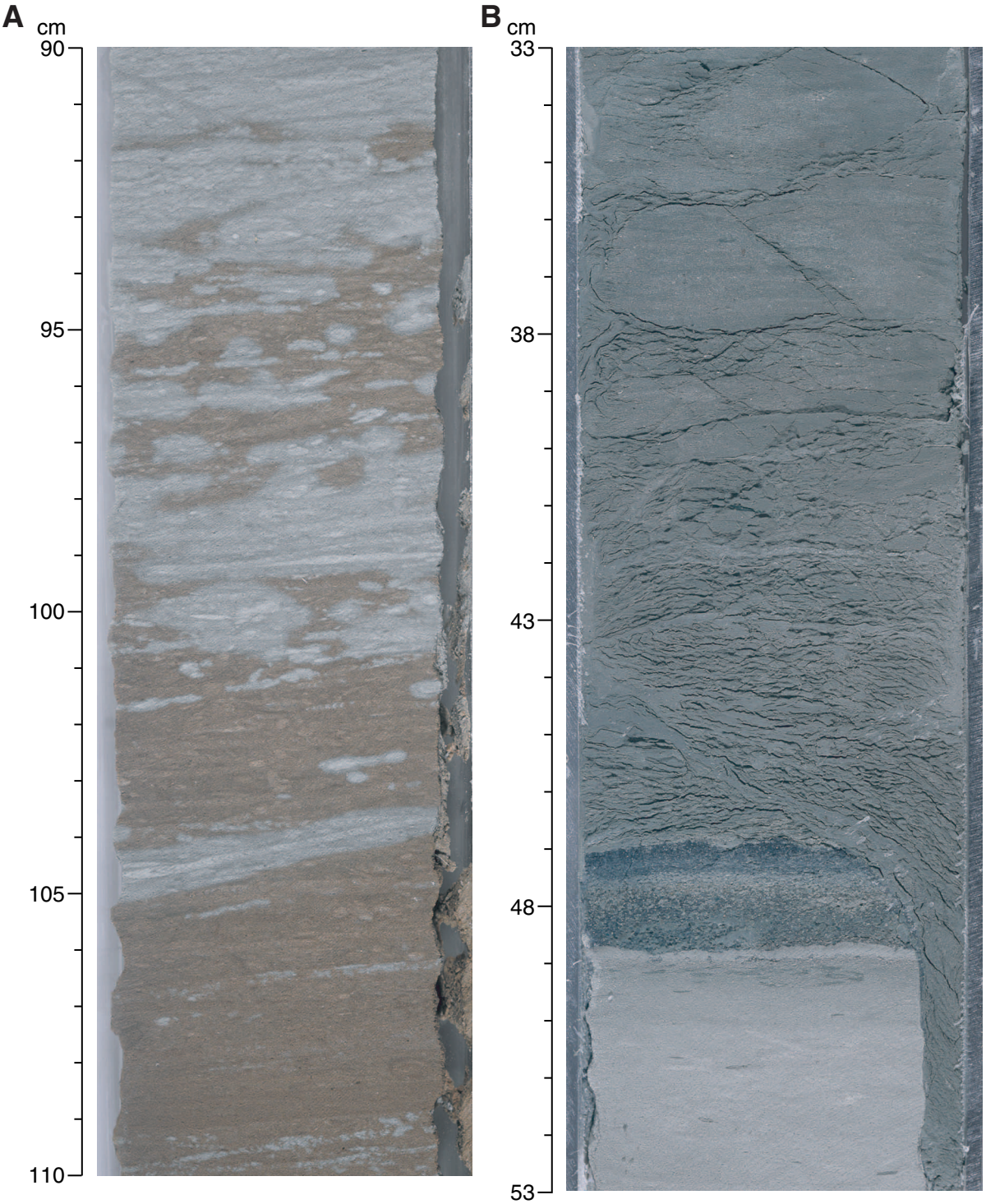

**Figure F6 (continued).** C. Mottled nannofossil chalk of late Maastrichtian age (interval 207-1259A-47R-4, 90–110 cm).

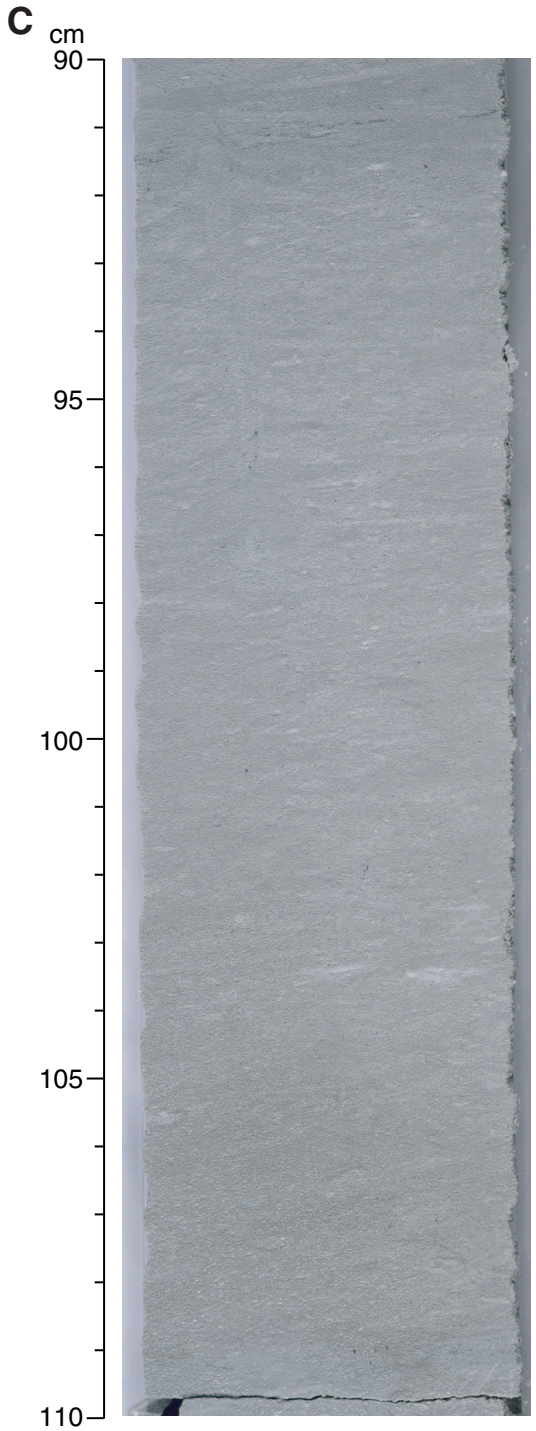

**Figure F7.** Close-up photographs of details of the boundary between Unit III and Unit IV at Site 1259. **A.** Glauconite-rich greenish gray claystone mixed by pervasive bioturbation with darker brown glauconitic claystone over an interval of ~12 cm (interval 207-1259B-18R-7, 36–56). **B.** Sharp contact without obvious bioturbation between glauconite-rich greenish gray claystone and darker brown claystone (interval 207-1259C-11R-3, 45–55 cm).

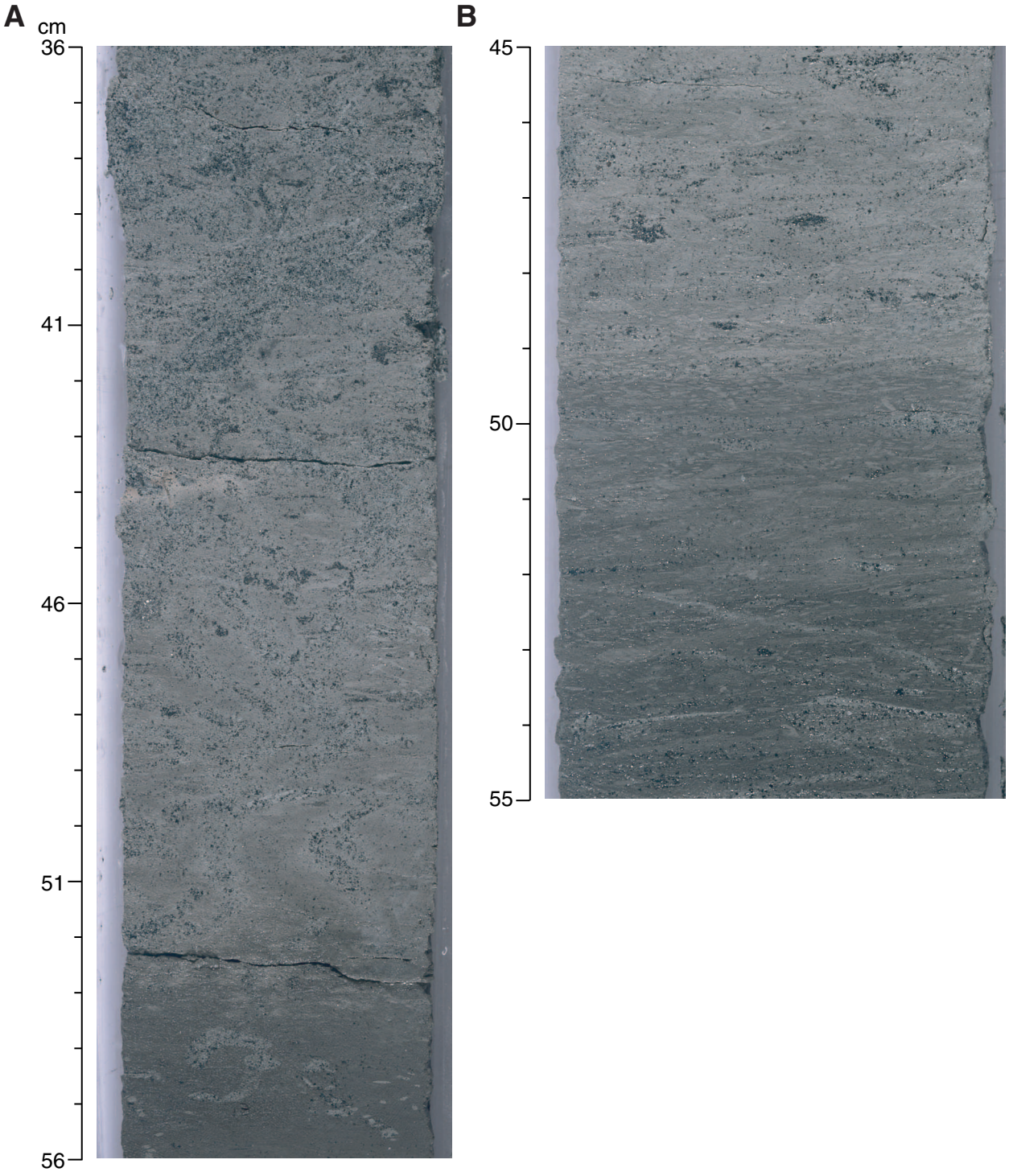

**Figure F8.** Close-up photographs of lithologies and sedimentary structures of lower Subunit IIIB at Site 1259. **A.** Campanian nannofossil chalk with pyrite crystals and common discrete black *Zoophycos* and *Chondrites* burrows (interval 207-1259A-52R-2, 60–80 cm). **B.** Top of the gradational change from calcareous chalk to glauconitic claystone at the base of Unit III (interval 207-1259B-18R-6, 25–45 cm). Darkening of the sediment downcore corresponds to an increase in clay content. (Continued on next page.)

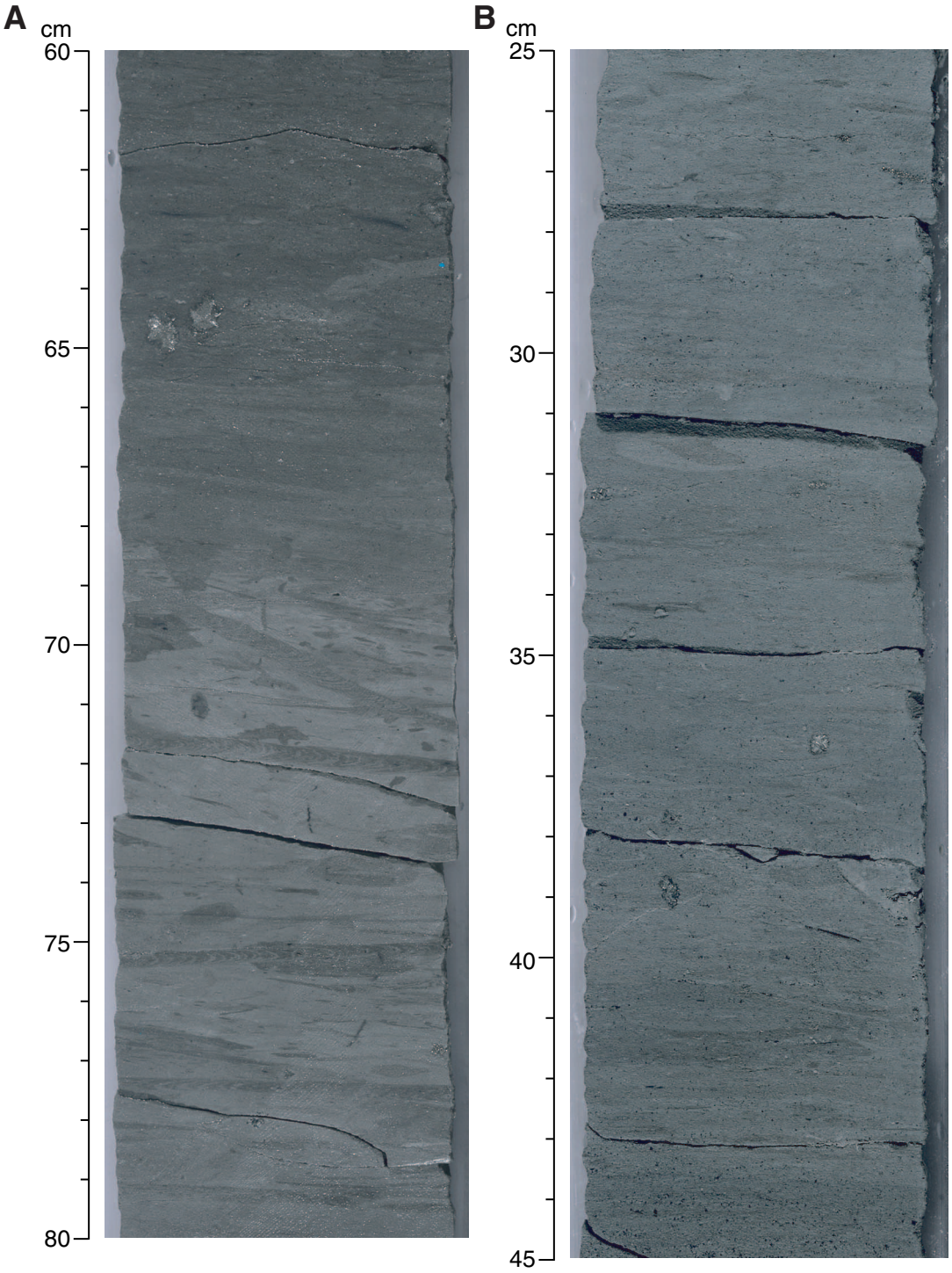

**Figure F8 (continued).** C. Gradational change from brownish to greenish gray glauconitic claystone (interval 207-1258B-18R-6, 44–68 cm). Glauconitic grains appear to be coarser and more concentrated in planar layers in the lowest portions of Subunit IIIB.

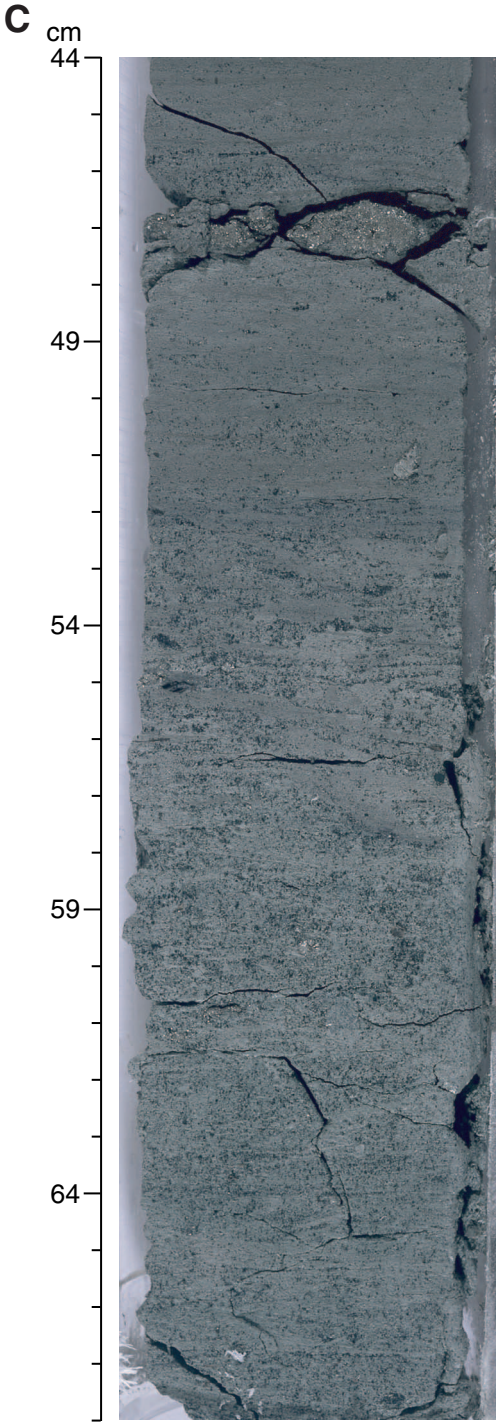

**Figure F9.** Close-up photographs of typical lithologies encountered in Unit IV at Site 1259. **A.** Black submillimeter-scale laminated claystone with organic matter (interval 207-1259A-57R-1, 123–137 cm). Note concentrations of phosphatic streaks and nodules at 133.5 cm. **B.** Black submillimeter-scale laminated claystone with organic matter intercalated with olive-gray laminated limestone that is strongly cemented by calcite (interval 207-1259A-57R-2, 10–28 cm). (Continued on next page.)

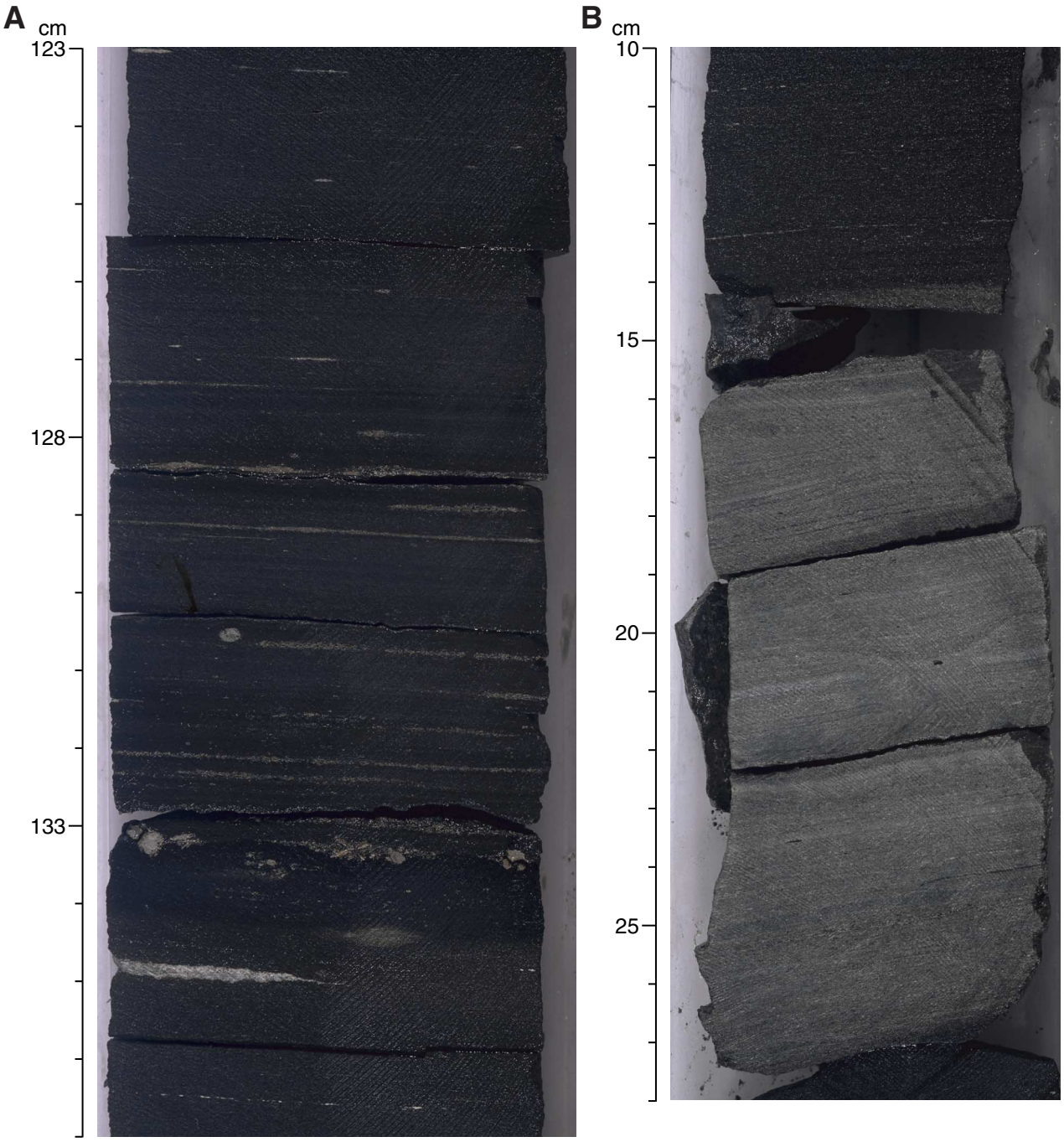

**Figure F9 (continued).** C. Close up of black submillimeter-scale laminated claystone with organic matter that contains layers of white calcite (infilled foraminifers) (interval 207-1259A-59R-4, 64–74 cm).

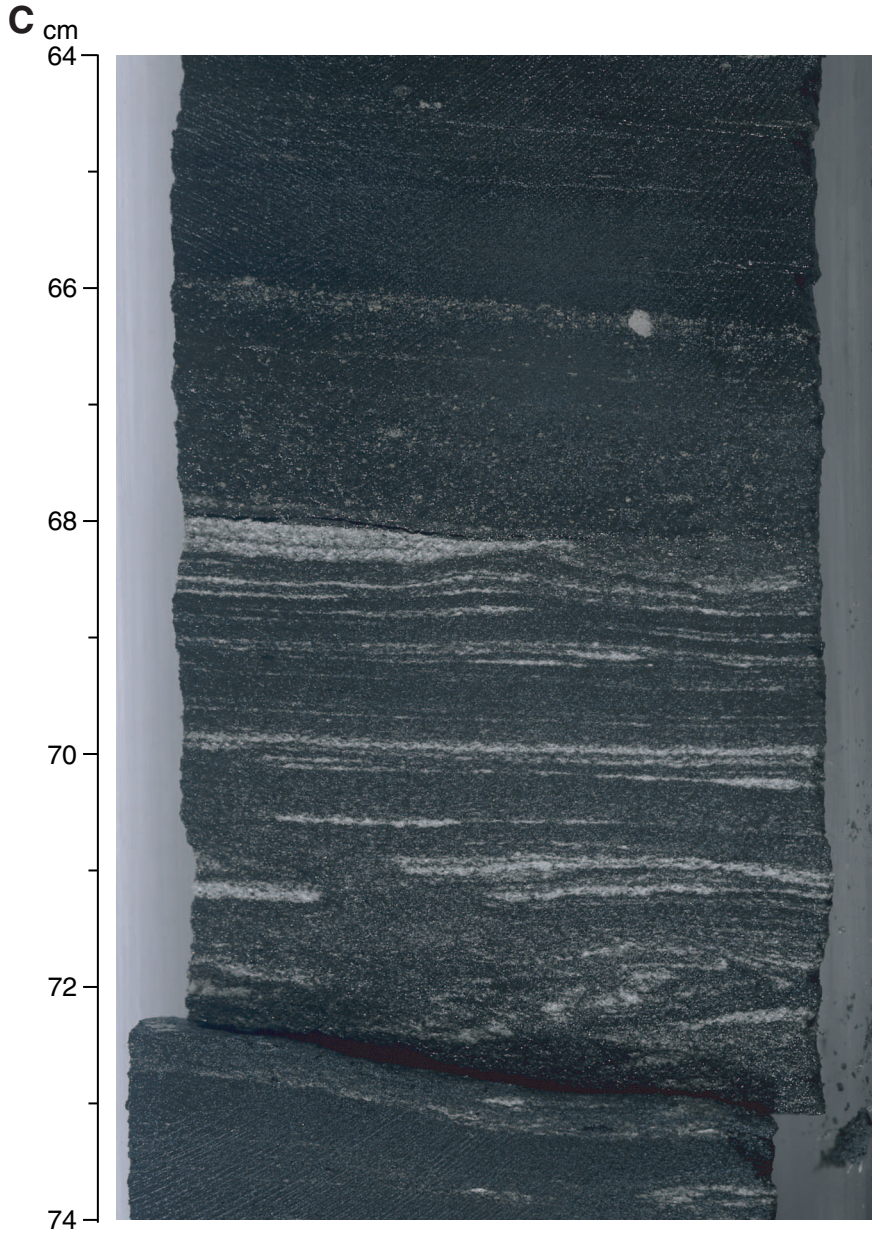

**Figure F10.** Close-up photograph of typical lithology and sedimentary structures of Unit V at Site 1259. Intercalated dark gray and brownish calcareous siltstone and silty claystone showing strongly bioturbated intervals and tepee structures. The latter are indicative of shallow marine, possibly tidal-flat, deposits (interval 207-1259B-25R-2, 45–65 cm).

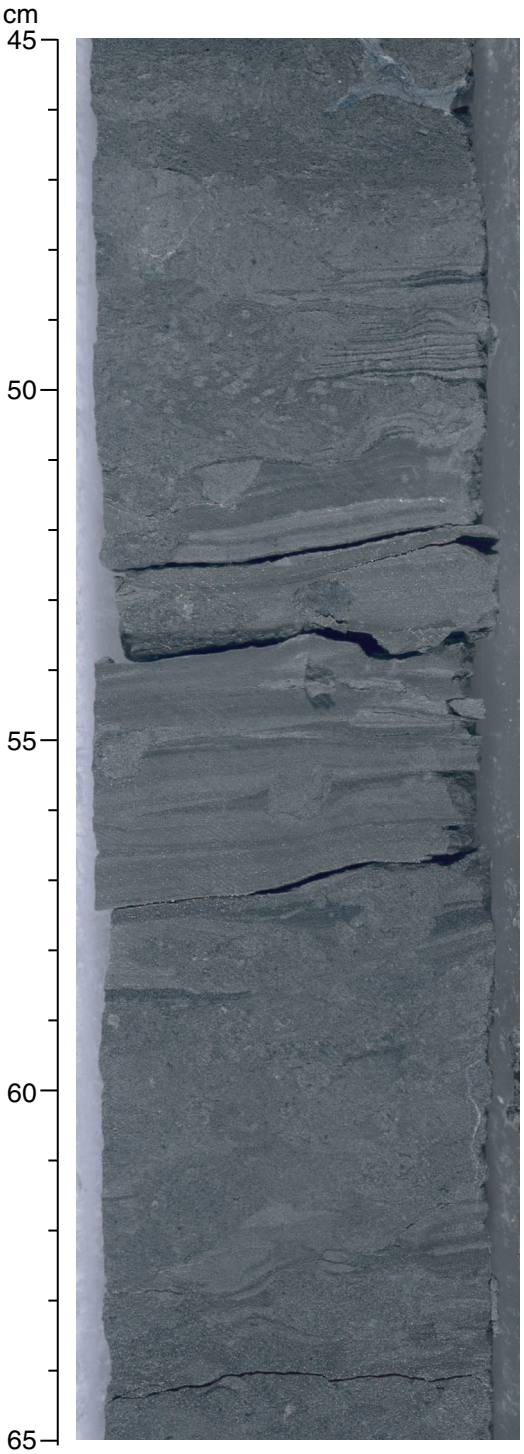

**Figure F11.** Planktonic foraminifer, calcareous nannofossil, and radiolarian biozonation at Site 1259. LO = last occurrence.

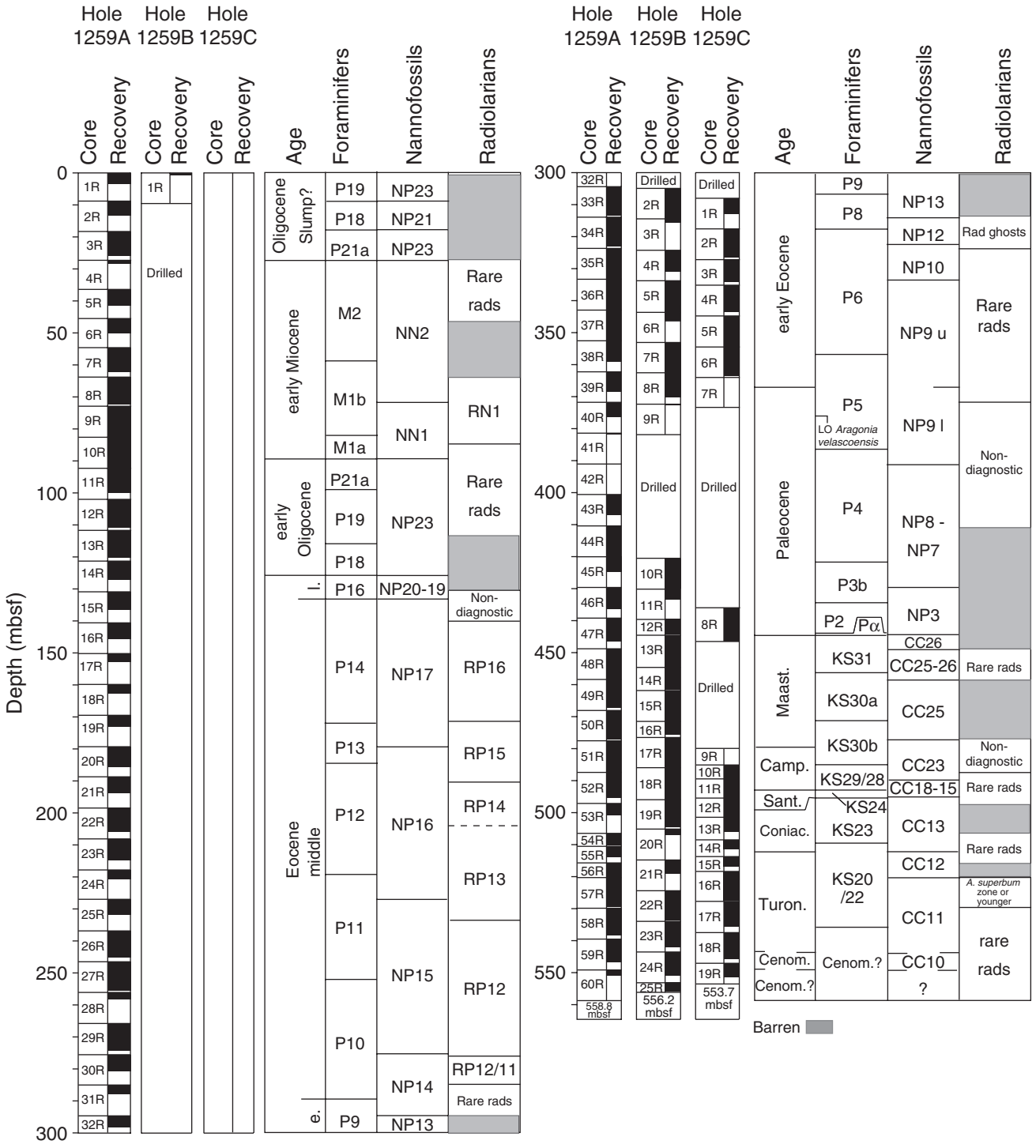

**Figure F12.** Shipboard paleomagnetic data and initial interpretations of inclination clusters of the Cretaceous–Miocene from Holes 1259A, 1259B, and 1259C. Visual color variations in the sediment succession generally correspond to changes in magnetic properties and are displayed as an exaggerated schematic column to the right of the shipboard lithologic units. The paleomagnetic data from the holes have been compared using the composite depth offsets, which rarely exceeded a relative displacement of 4 m at this site, and those of the main record from Hole 1259A are within 1 m of the composite depth scale (mcd). Magnetic inclinations are from intact blocks (excluding measurements within 5 cm of the end of each blocks) after 15-mT demagnetization. The inclination data exclude measurements near the background noise limit of the cryogenic magnetometer ($<3 \times 10^{-5}$ A/m), therefore measurements with intensities $<5 \times 10^{-5}$ A/m are not considered reliable. In addition, the upper 20 cm of each core that commonly displays spurious high-intensity magnetization or downhole contamination, and the upper 5 cm of each section that is influenced by magnetization carried by the blue-colored end-cap are excluded. Magnetic inclinations are either 3-point running means (solid circles), 2-point means (open circles, for blocks <20 cm long) or single-level data (open triangles, for blocks <15 cm long, or from isolated levels within a larger block in which the adjacent measurements were $<5 \times 10^{-5}$ A/m) of magnetic directions from intact blocks (excluding measurements within 5 cm of the end of each blocks) after 15-mT demagnetization. The magnetic intensity column is from Hole 1259A and includes NRM (small orange dots are a 21-point running mean) and after 15-mT demagnetization (small black dots, with the large blue dots being a 101-point logging-mean average). Magnetic susceptibility of Hole 1259A, obtained using a magnetic susceptibility core logger (MSCL), is shown by green dots in the right most column. Shipboard assignment of polarity zones were based on clusters of magnetic inclinations from intact blocks (to right of polarity zone column), as delimited by the thin lines. Zones of positive inclinations (originally considered to be normal polarity zones) = black or medium gray, if reliability is less certain; negative or mixed inclinations (originally considered to be reversed polarity zones) = white or light gray, if reliability is less certain. Uncertain inclination characteristics or gaps in data coverage = cross hatched. The shipboard interpretations of polarity zones were not always supported by analyses of magnetic characteristics during progressive thermal demagnetization of minicores (Fig. **F13,** p. 54). F = foraminifer, R = radiolarian. (This figure is available in an **oversized format.**)

**Figure F13.** Magnetostratigraphy and characteristic directions of Cretaceous–Eocene of Holes 1259A and 1259B based on shore-based analysis of minicores. The minicore data from the two holes have been merged using composite depth scales from each hole. Polarity ratings are graded according to reliability and number of vectors utilized in the characteristic direction. R = reliable reversed polarity, INT = indeterminate, N = reliable normal polarity) (relative placement of other points indicates degree of precision or uncertainty). Methods of polarity interpretation, polarity ratings, and derivation of characteristic inclinations and intensities are in "**Paleomagnetism**," p. 16, in the "Explanatory Notes" chapter). Polarity zones are assigned according to clusters of individual polarity interpretations. Normal polarity zones = dark gray; reversed polarity zones = white; uncertain polarity or gaps in data coverage = cross hatched. Assignments of polarity chrons are based on the polarity zone pattern and the constraints from microfossil biostratigraphy. F = foraminifer, R = radiolarian. (**Figure shown on next page.**)

**Figure F13 (continued).** (Caption shown on previous page.)

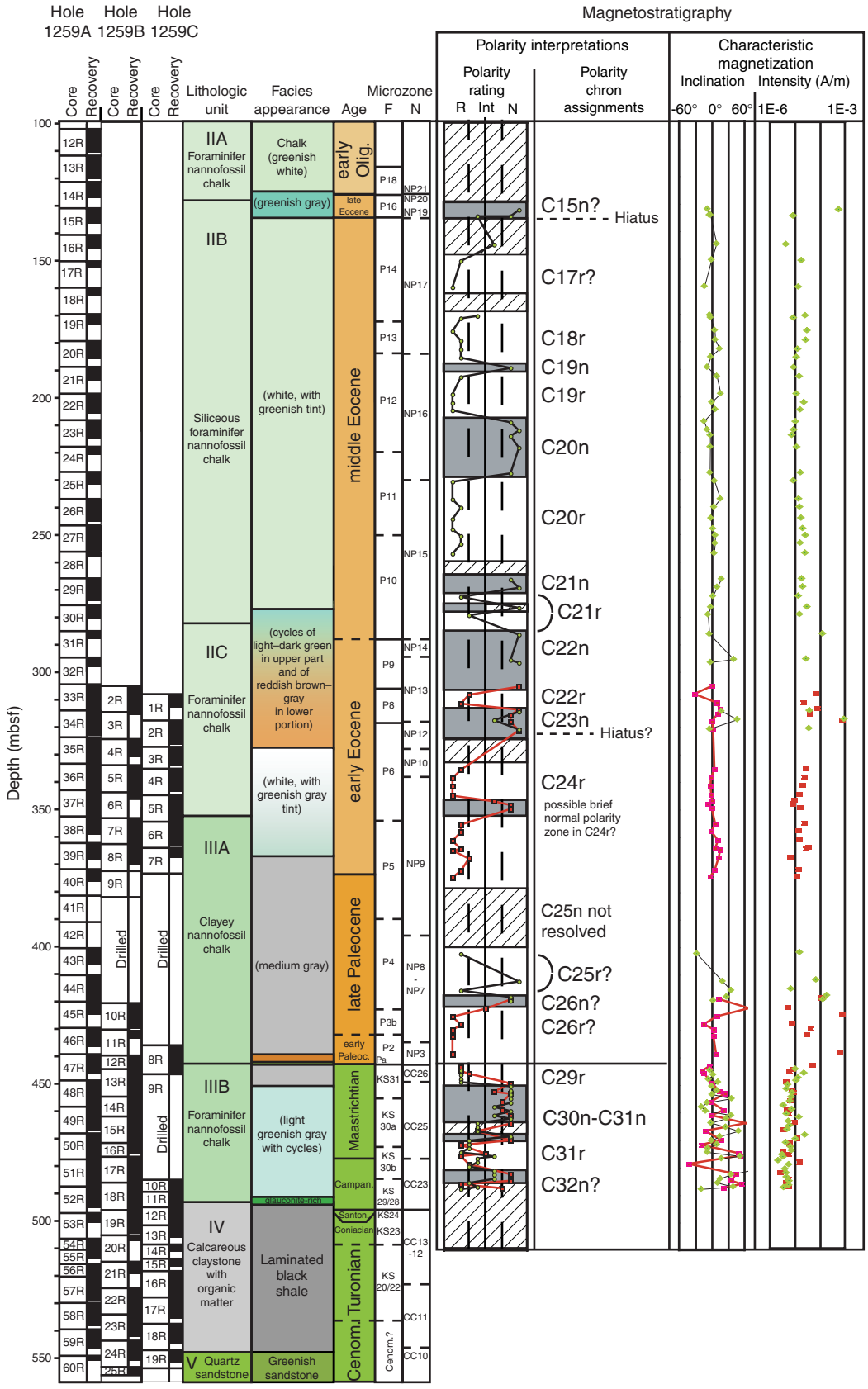

**Figure F14.** Composite and spliced magnetic susceptibility data for the lower Eocene section from Holes 1259A (black), 1259B (blue), and 1259C (green). The composite data from Holes 1259B and 1259C are offset by a constant (5 and 10 units, respectively) for illustration purposes. All data sets are smoothed with a 9-point Gaussian filter.

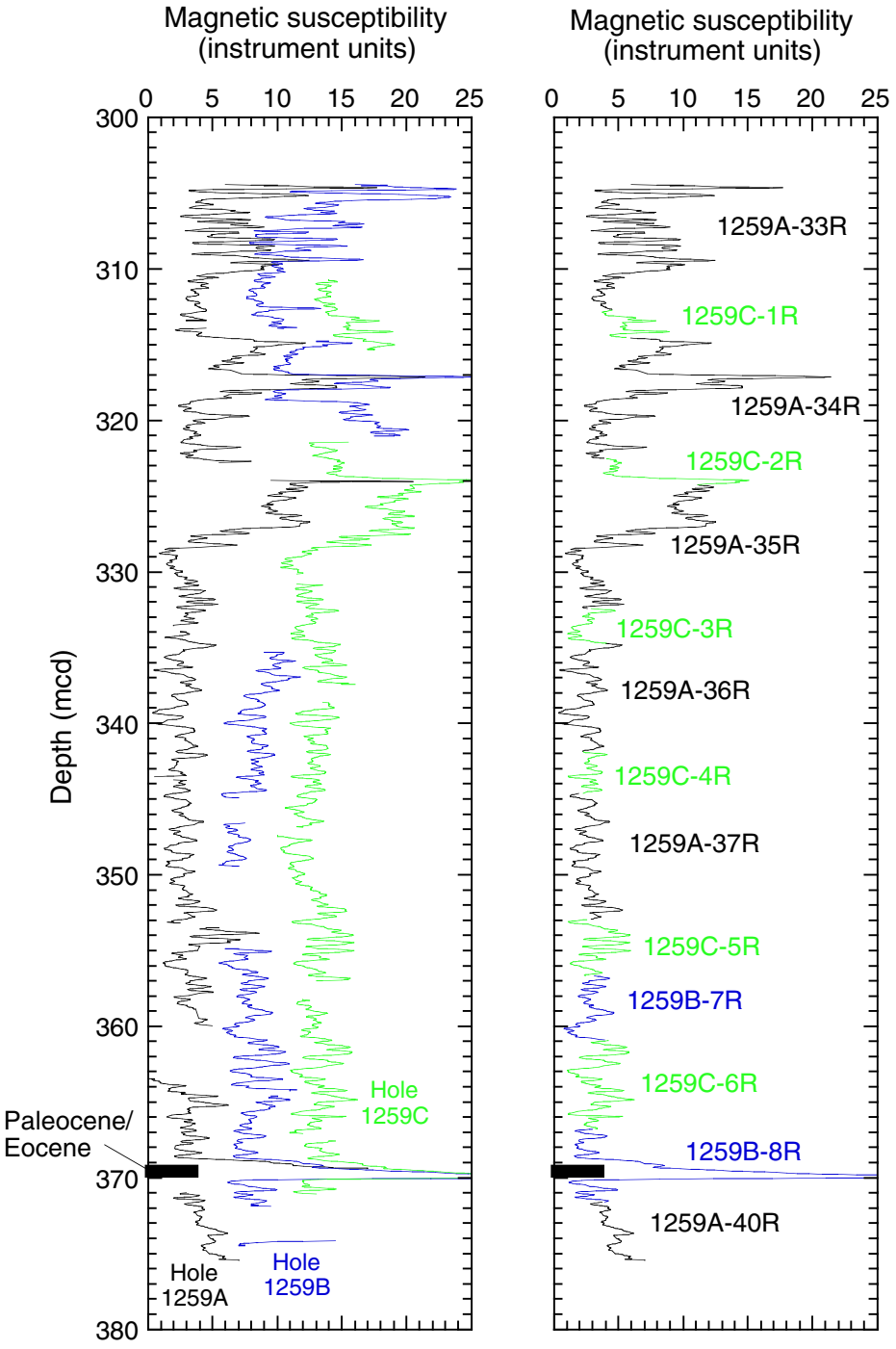

**Figure F15.** Composite and spliced magnetic susceptibility data for the Campanian–Maastrichtian section from Holes 1259A (black), 1259B (blue), and 1259C (green). The composite data from Holes 1259B and 1259C are offset by a constant (5 and 10 units, respectively) for illustration purposes. All data sets are smoothed with a 9-point Gaussian filter.

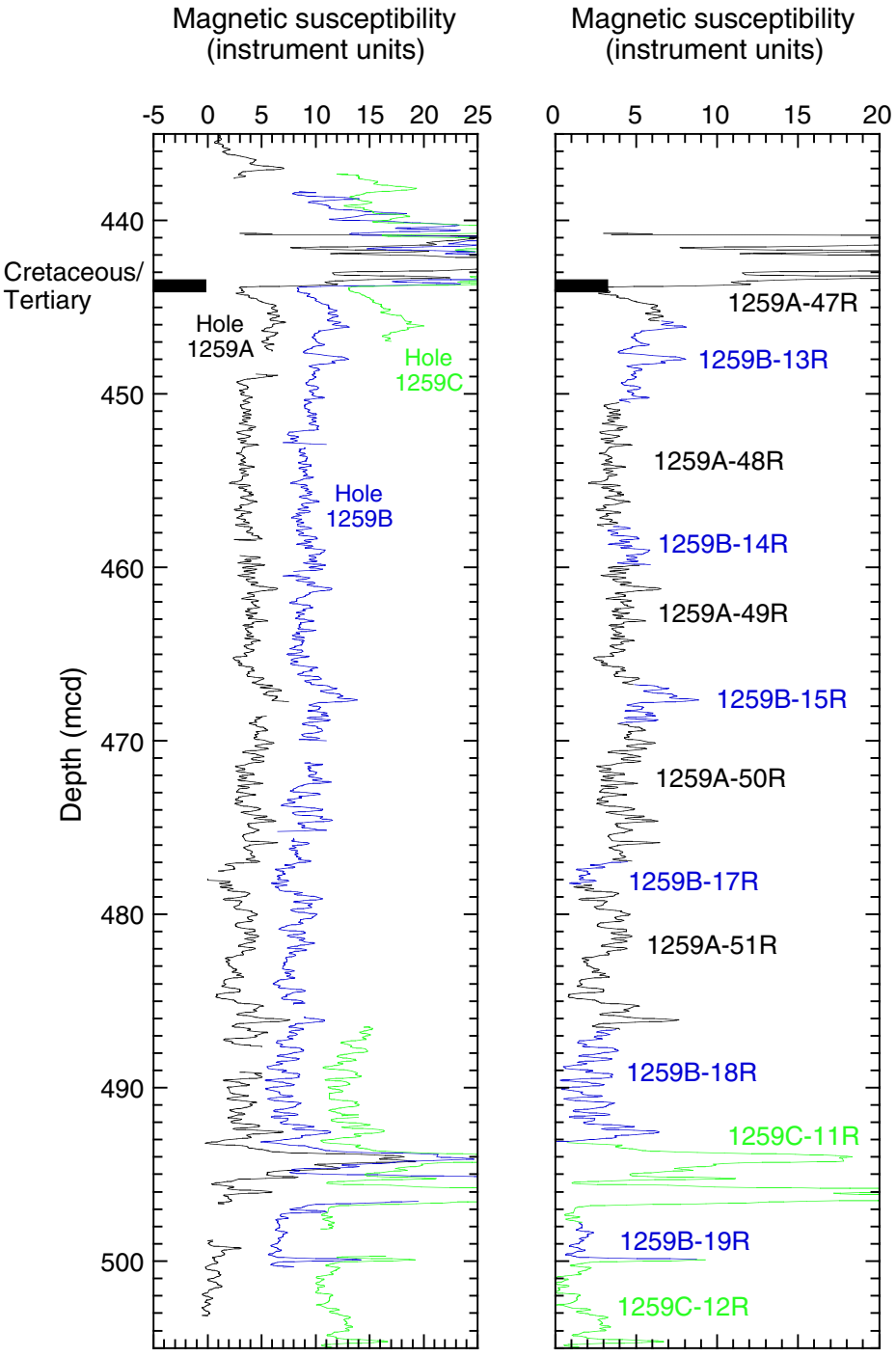

**Figure F16.** Composite and spliced gamma ray attenuation (GRA) bulk density data for the black shale sequence from Holes 1259A (black), 1259B (blue), and 1259C (green). The composite data from Holes 1259B and 1259C are offset by a constant (0.5 and 1.0 units, respectively) for illustration purposes. All data sets are smoothed with a 9-point Gaussian filter.

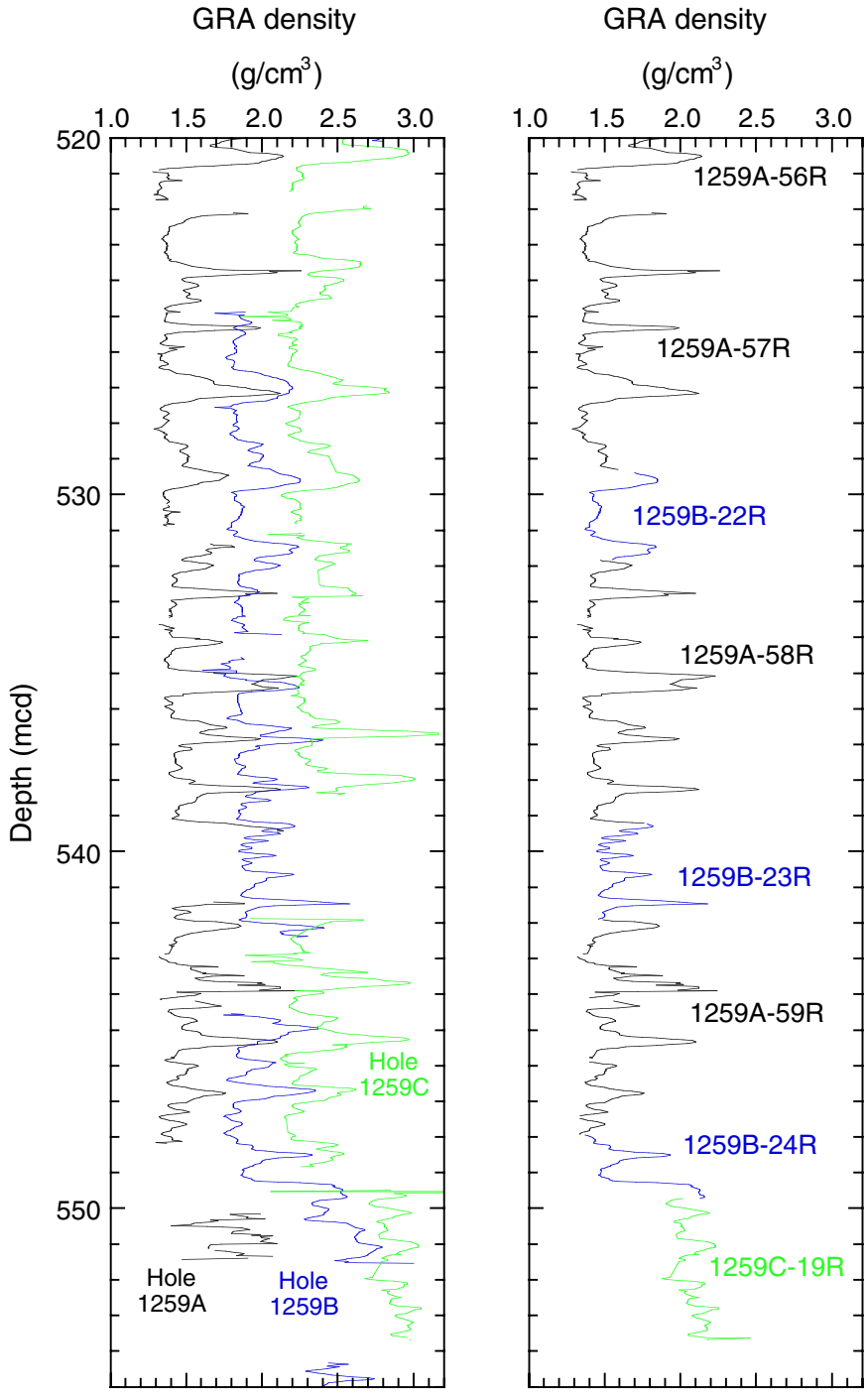

**Figure F17.** Magnetic susceptibility data plotted along with a qualitative estimate of the confidence of the core-to-core correlations among holes at Site 1259. **A.** Magnetic susceptibility data for Holes 1259A (black), 1259B (blue), and 1259C (green). The composite data from Holes 1259A and 1259B are offset by a constant (5 and 10 units, respectively) for illustration purposes. All data sets are smoothed with a 9-point Gaussian filter. **B.** Green indicates intervals with definitive hole-to-hole correlations and a high-quality splice (i.e., core gaps spanned). Yellow indicates intervals where good core-to-core correlations could be made (i.e., a one-to-one match of signals between holes) but definitive depth positions could not be established because core gaps could not be spanned. The diagonal line pattern indicates intervals where hole-to-hole correlations could not be made (primarily a result of only one hole in that interval). P/E = Paleocene/Eocene boundary, K/T = Cretaceous/Tertiary boundary.

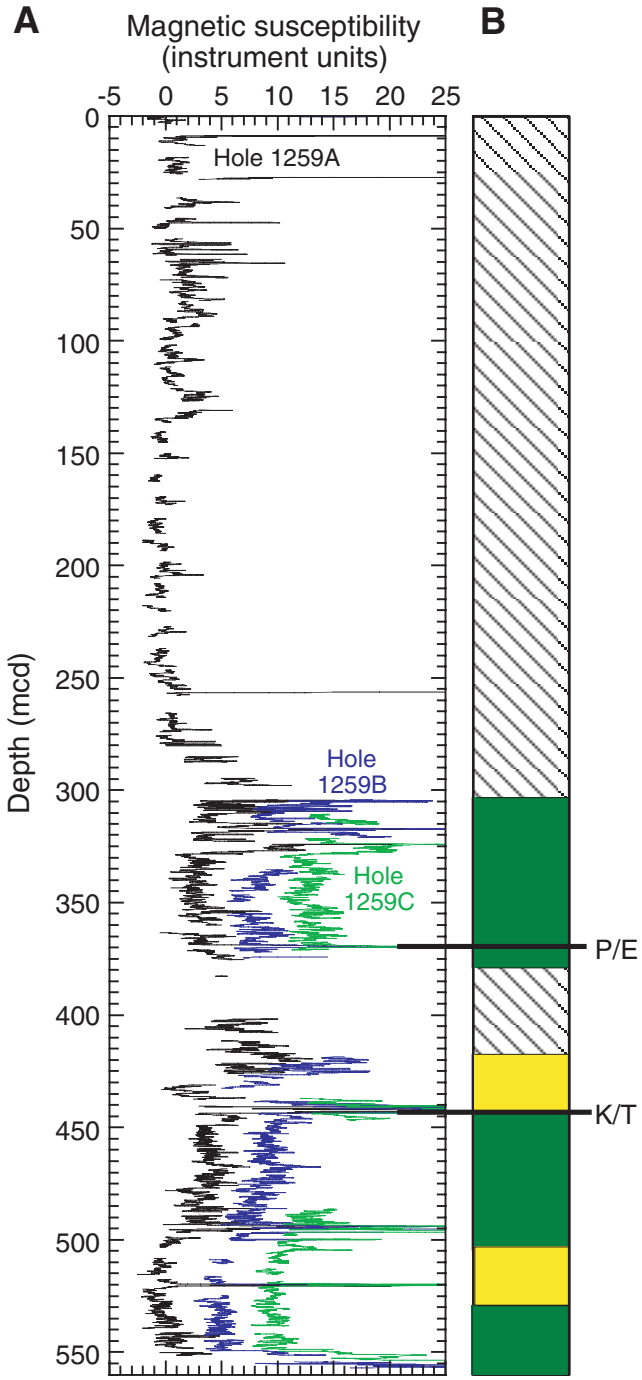

**Figure F18.** Age-depth plot combining all available biostratigraphic and magnetostratigraphic datums from Hole 1259A. Letters A–F indicate six distinct hiatuses in between those intervals. See **"Sedimentation Rates and Hiatuses,"** p. 27, for more details.

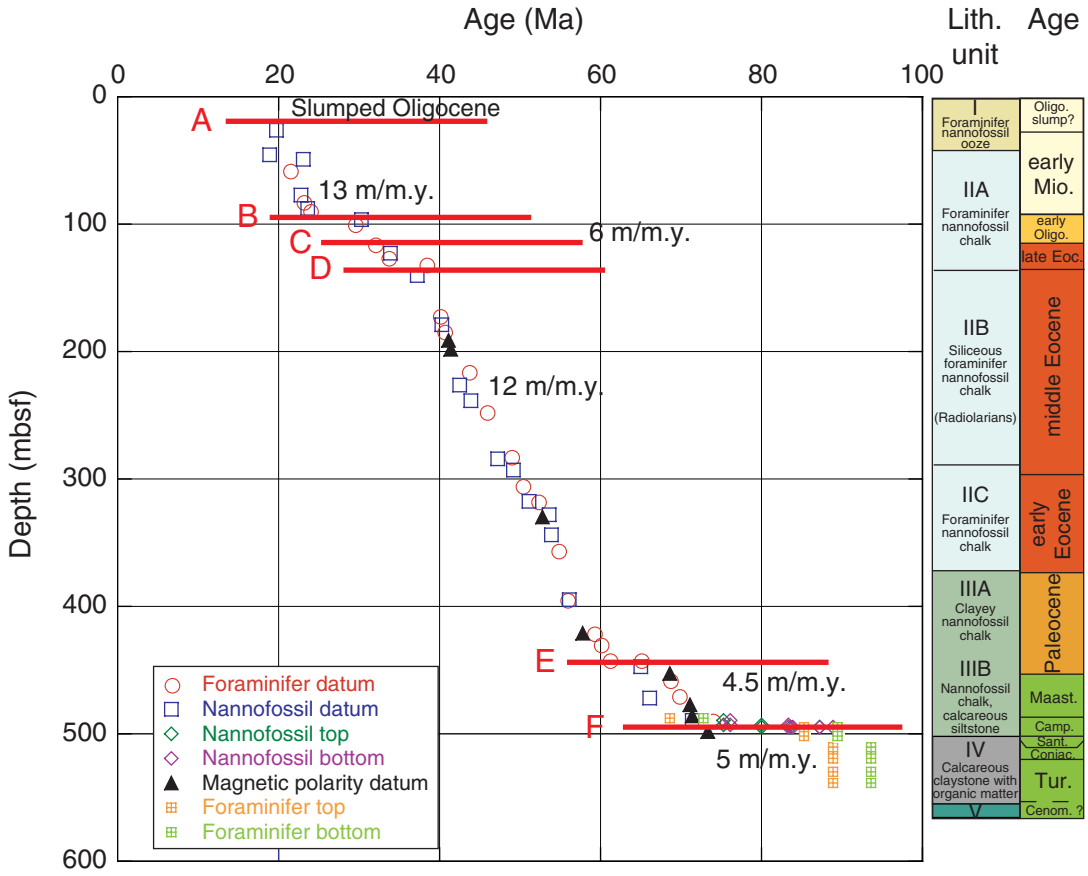

**Figure F19.** Age-depth plot with an expanded view of Hole 1259A (380–540 mbsf). See **"Sedimentation Rates and Hiatuses,"** p. 27, for more details.

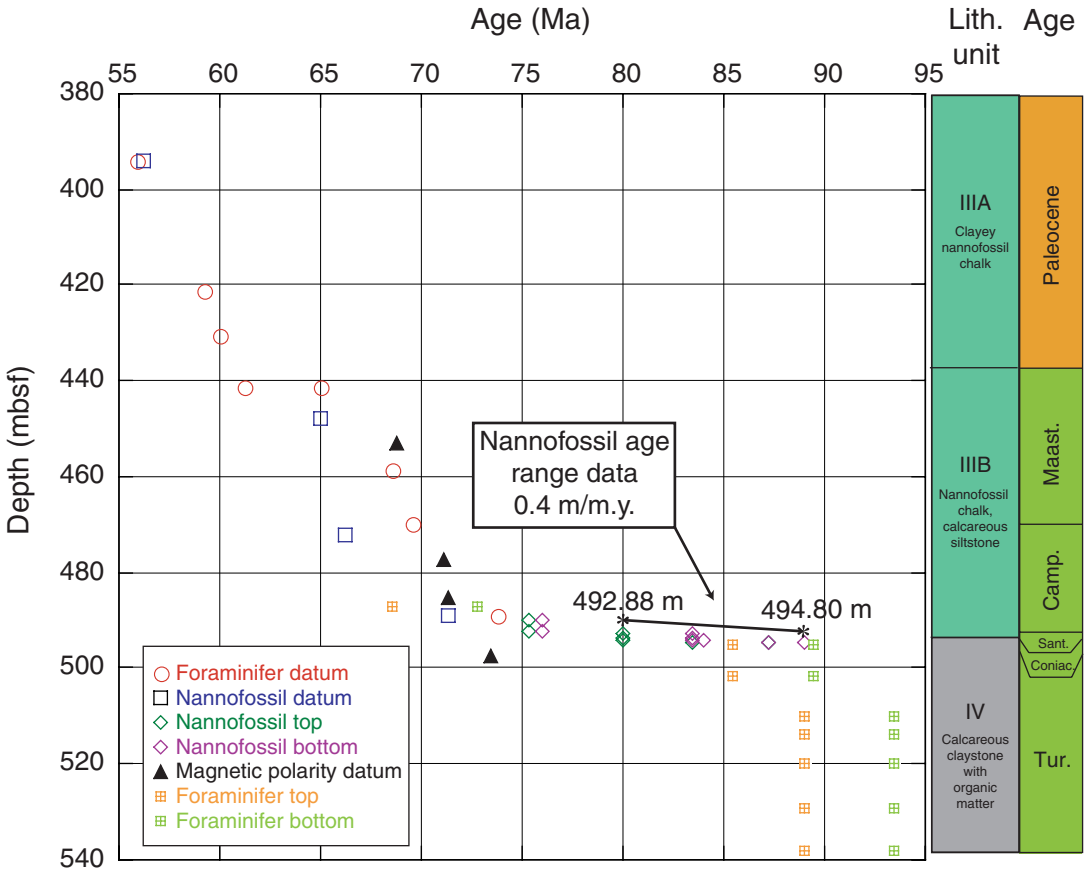

**Figure F20.** Mass accumulation rate (MAR) and carbonate MAR depth plot of the middle Eocene–Paleocene interval. See "Mass Accumulation Rates," p. 27, for more details.

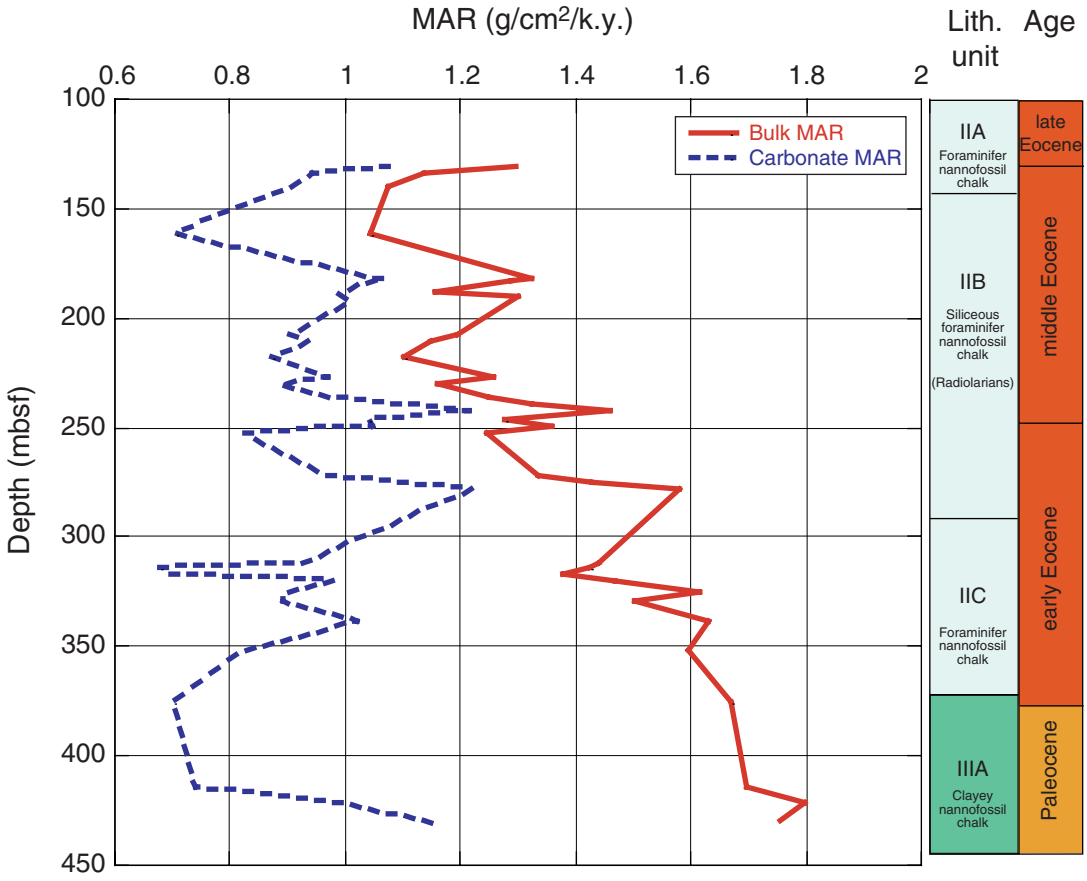

**Figure F21.** Rock-Eval van Krevelen-type diagram of sediment samples from Hole 1259A. Organic matter appears to be predominantly Type II algal material that has been variably oxidized. Incorporation of organic detrital material possibly gives rise to those samples that fall between Types II and III. TOC = total organic carbon.

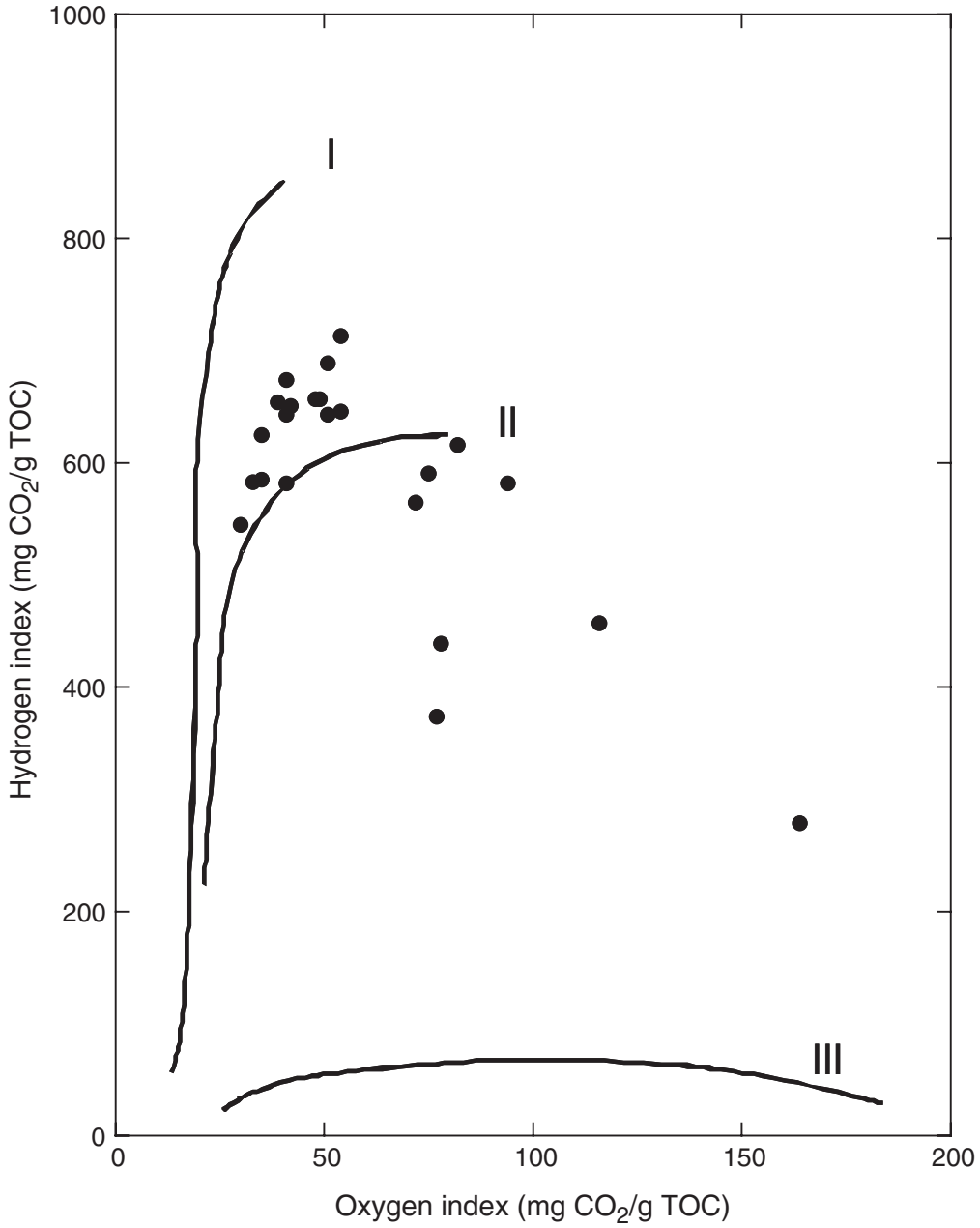

**Figure F22.** Comparison of concentrations of routine headspace gas (HS) and microbial methane in sediments from Hole 1259A.

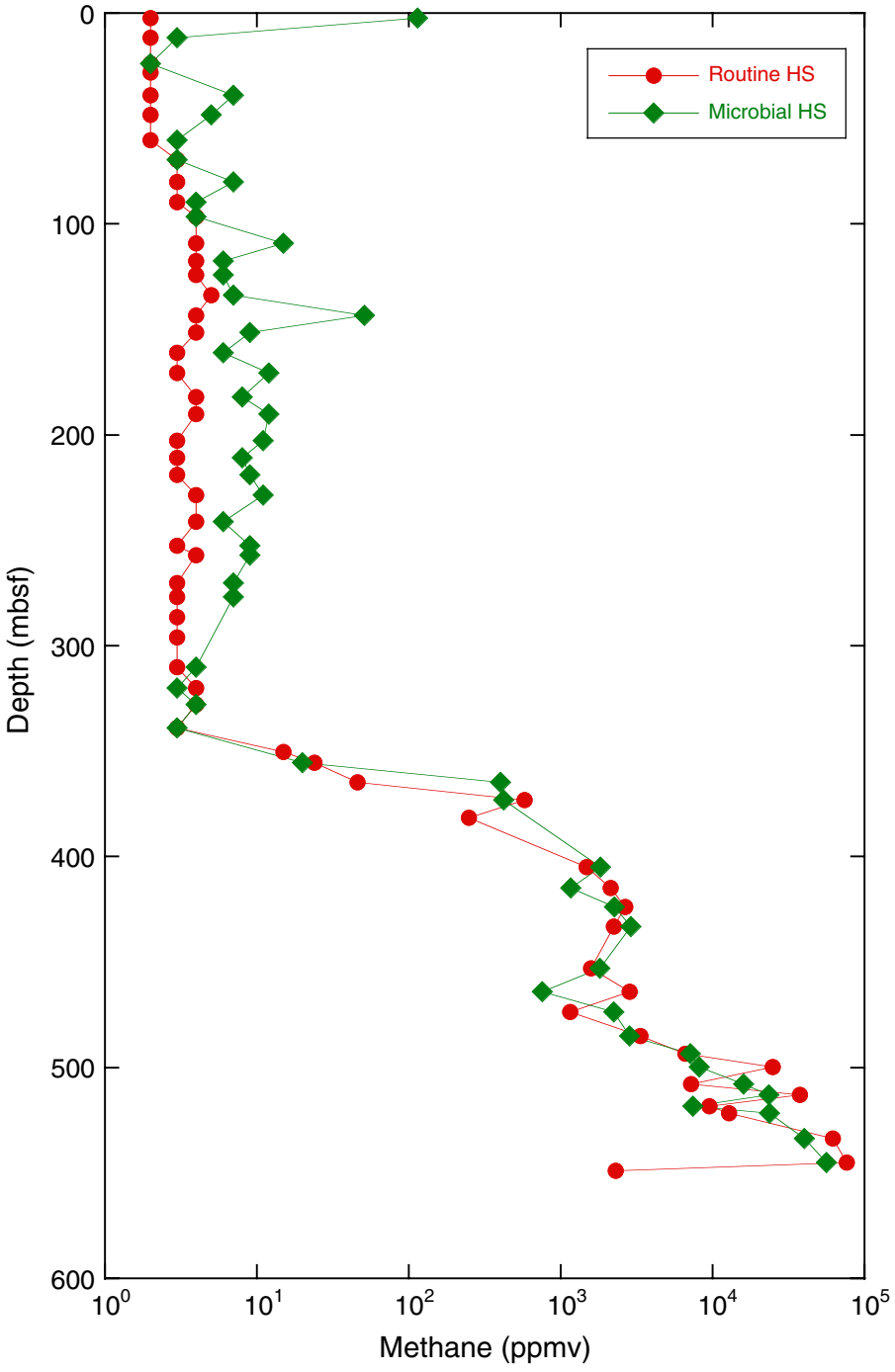

**Figure F23.** Correlation of total organic carbon (TOC) with interstitial methane concentrations in Hole 1259A.

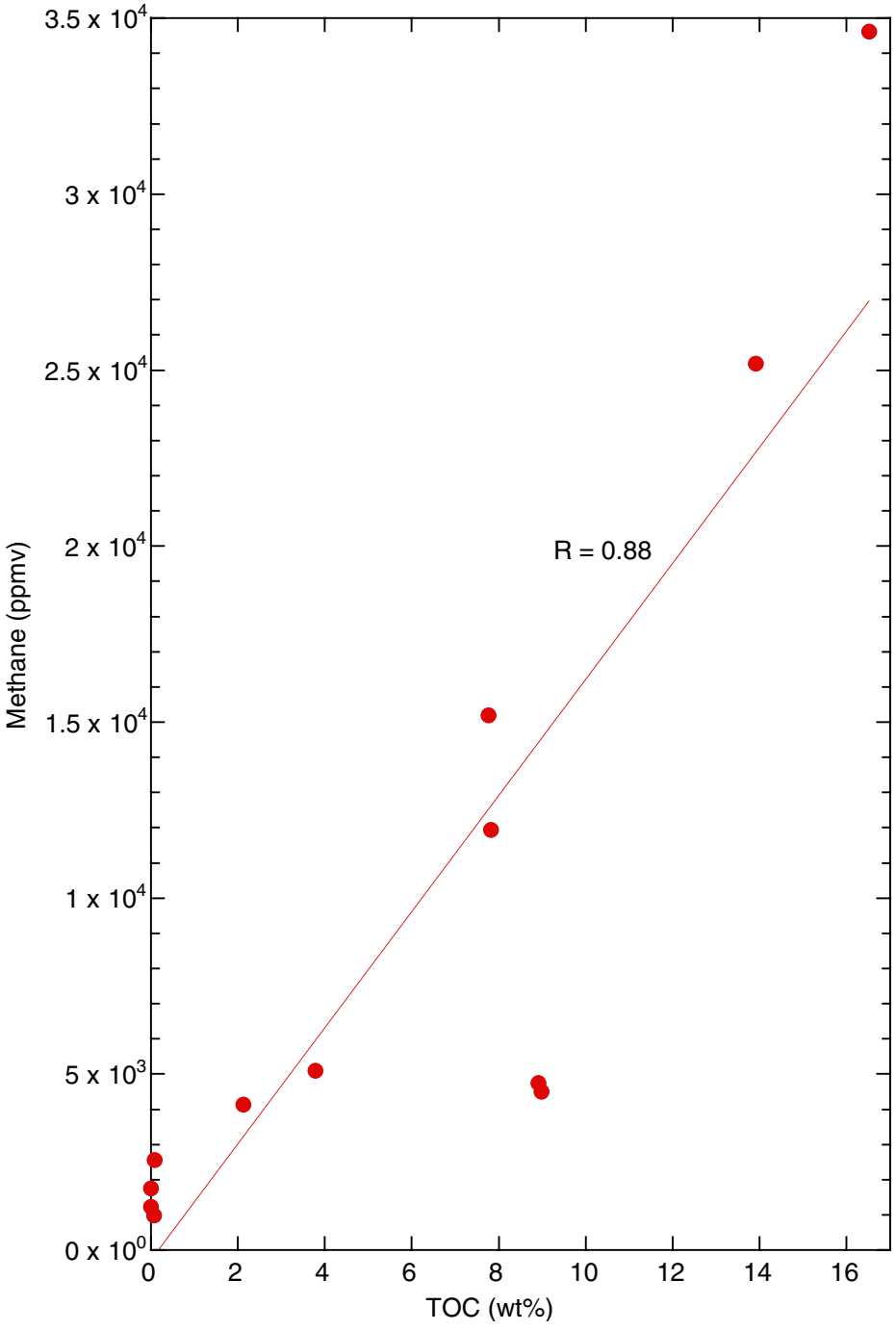

**Figure F24.** Profiles of chemical constituents in interstitial water at Site 1259. **A.** Salinity. **B.** Chloride. **C.** Sodium. **D.** Potassium. **E.** Alkalinity. **F.** Sulfate. **G.** Ammonium. **H.** Barium. (Continued on next two pages.)

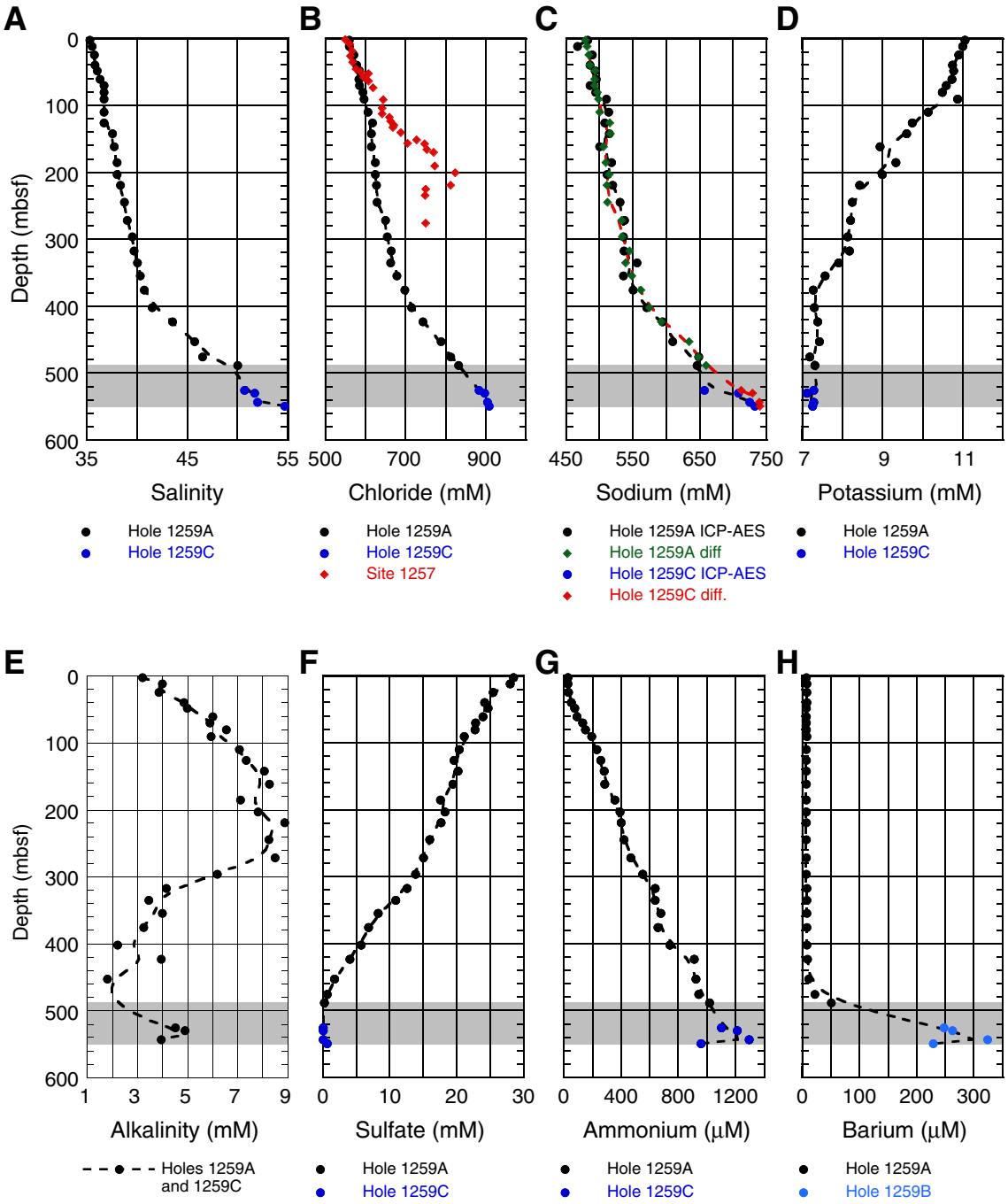

**Figure F24 (continued).** **I.** Calcium. **J.** Strontium. **K.** Magnesium. **L.** Lithium. **M.** Boron. **N.** Silica. **O.** Iron. **P.** Managanese.

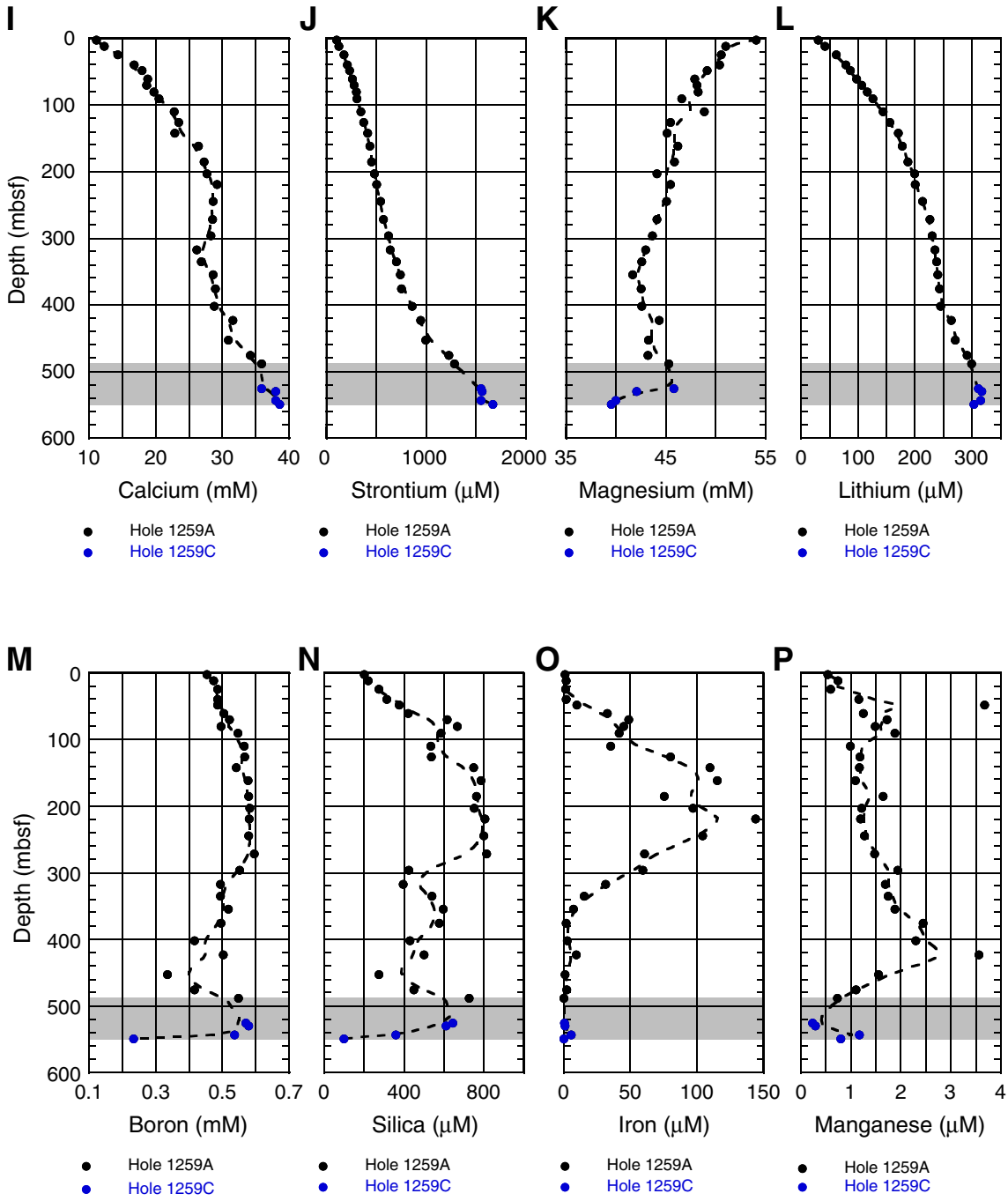

**Figure F24 (continued).** **Q.** Mg/Cl × $10^{-3}$. **R.** K/Cl × $10^{-3}$. **S.** Ca/Cl × $10^{-3}$. **T.** Sr/Cl × $10^{-3}$. **U.** Li/Cl × $10^{-6}$. **V.** Na/Cl. diff. = calculated by difference, IAP-AES = inductively coupled plasma–atomic emission spectroscopy. Gray bars = black shale interval.

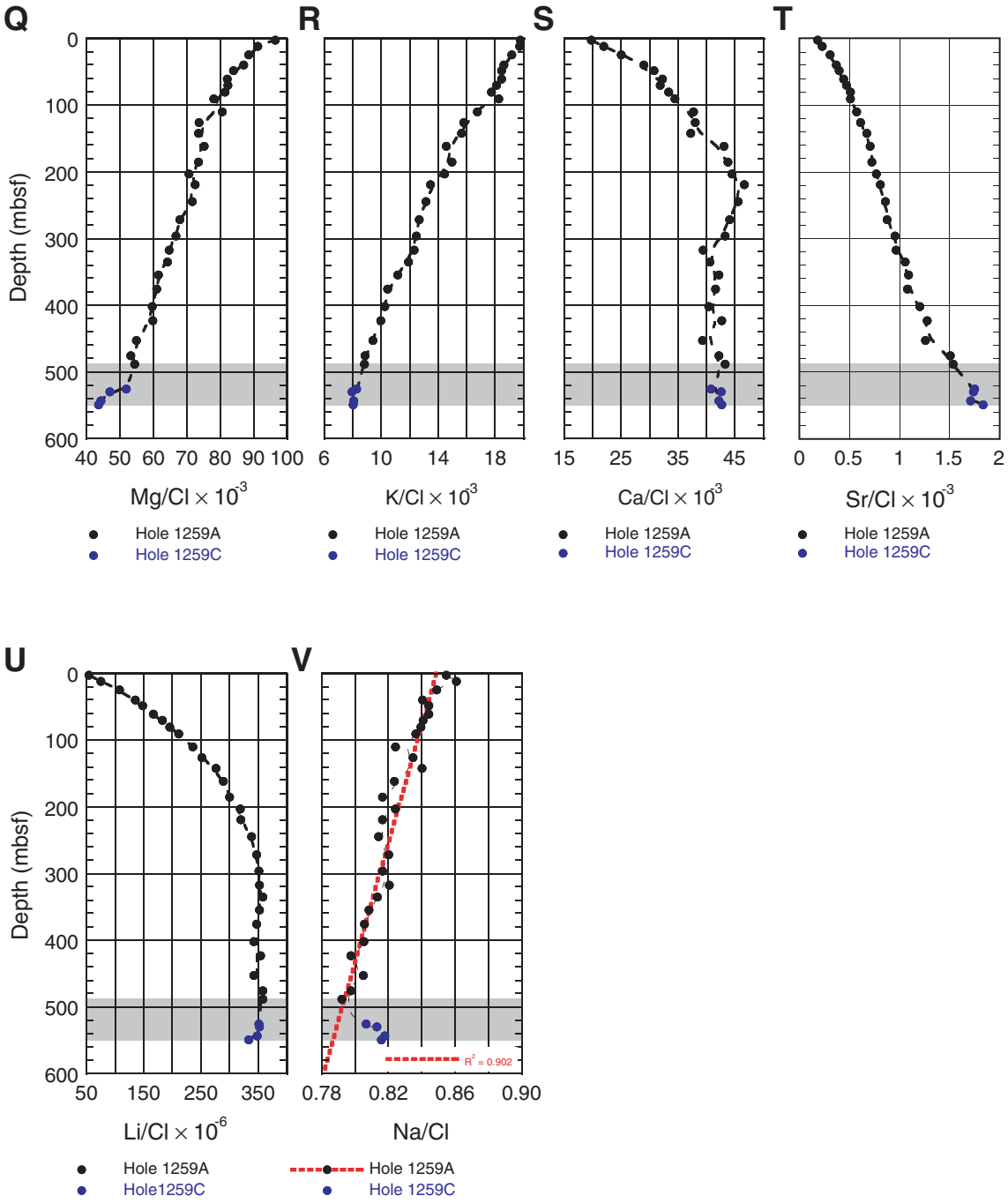

**Figure F25.** Correlation of sulfate vs. ammonium in interstitial water.

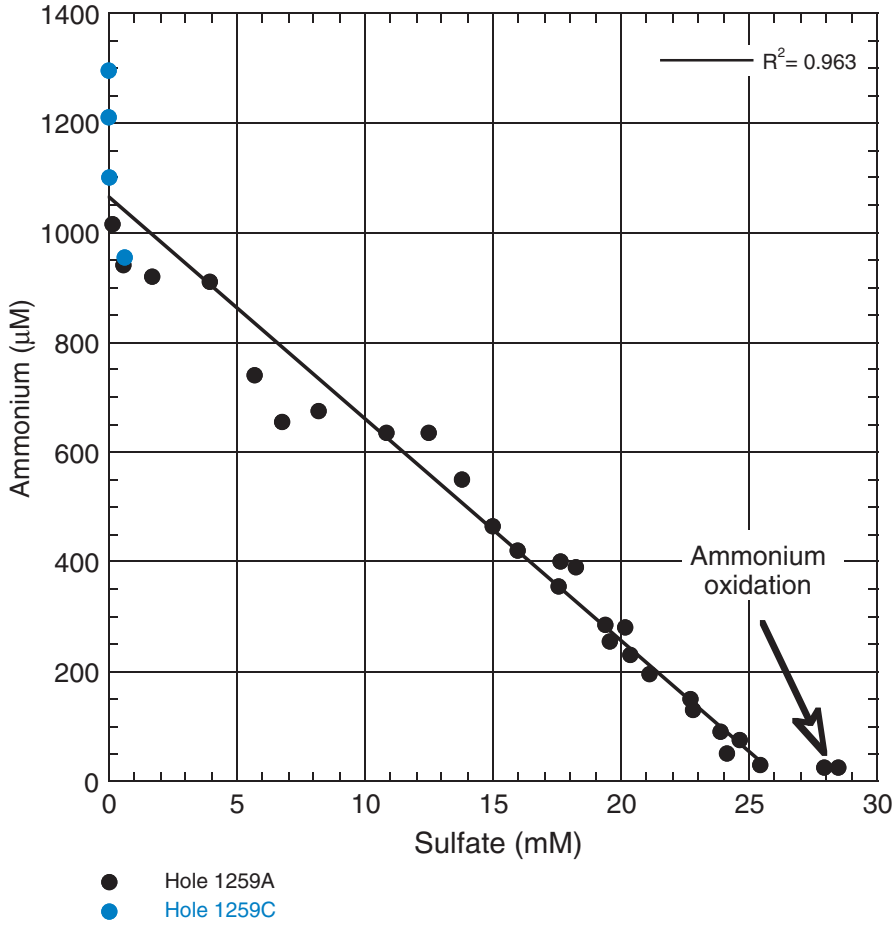

**Figure F26.** Correlation of Mg/Cl vs. K/Cl in interstitial water from Site 1259.

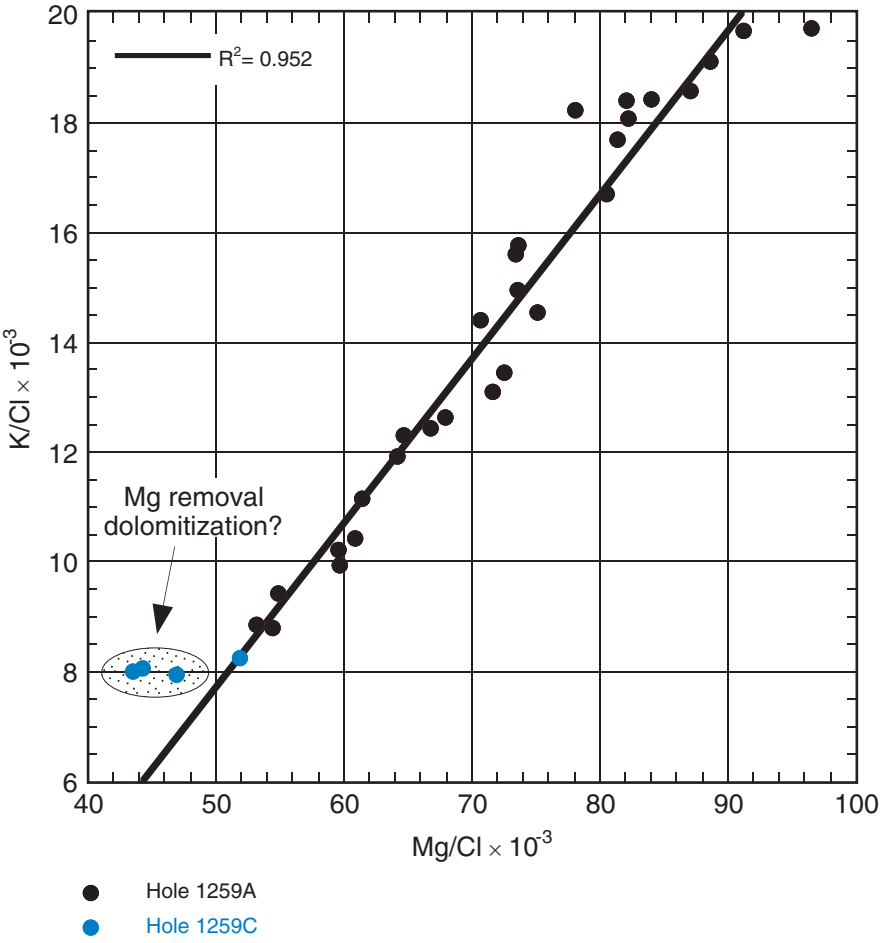

**Figure F27.** Correlation of Ca/Cl vs. Li/Cl in interstitial water from Site 1259.

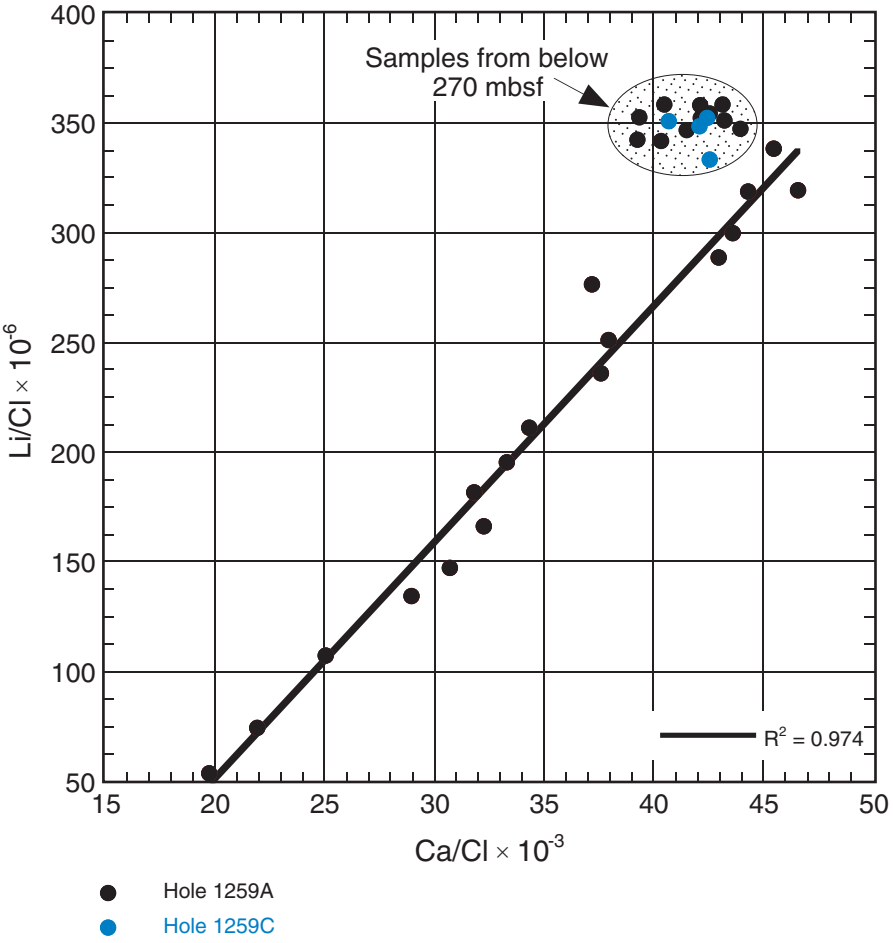

**Figure F28.** Bulk density, grain density, porosity of discrete samples, and acoustic velocity measurements made with the Hamilton Frame on split-core sections from Site 1259. Red = Hole 1257A, blue = Hole 1257B, green = Hole 1257C.

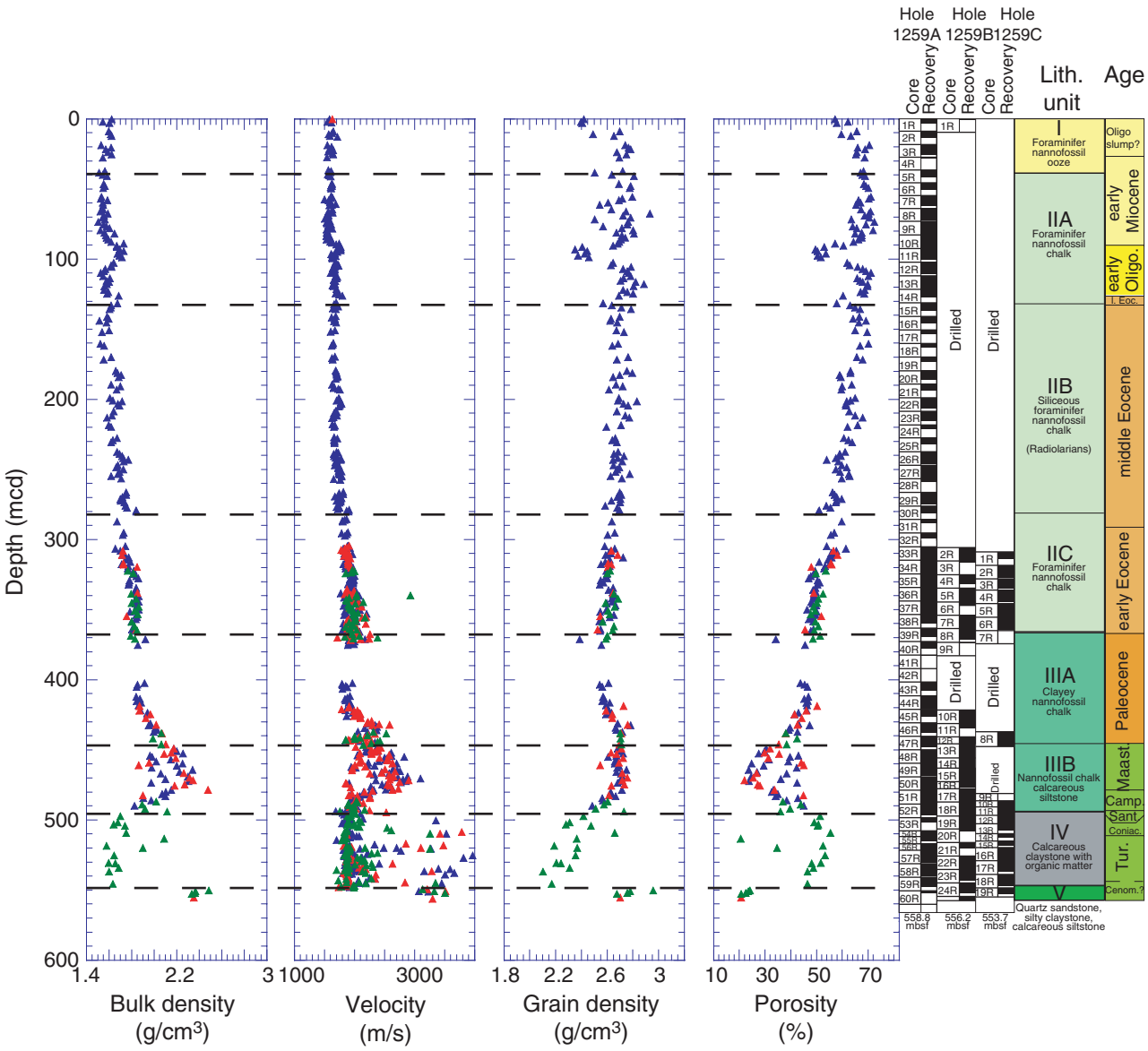

**Figure F29.** Acoustic velocity and velocity anisotropy measured on samples from Hole 1259B. Variation in GRA density over a 5-m interval (every third datum plotted with no smoothing or interpolation) is shown to account for the observed variability in both the velocity and velocity anisotropy between 400 and 500 mcd. For anisotropy calculations, see **"Physical Properties,"** p. 33, in the "Explanatory Notes" chapter.

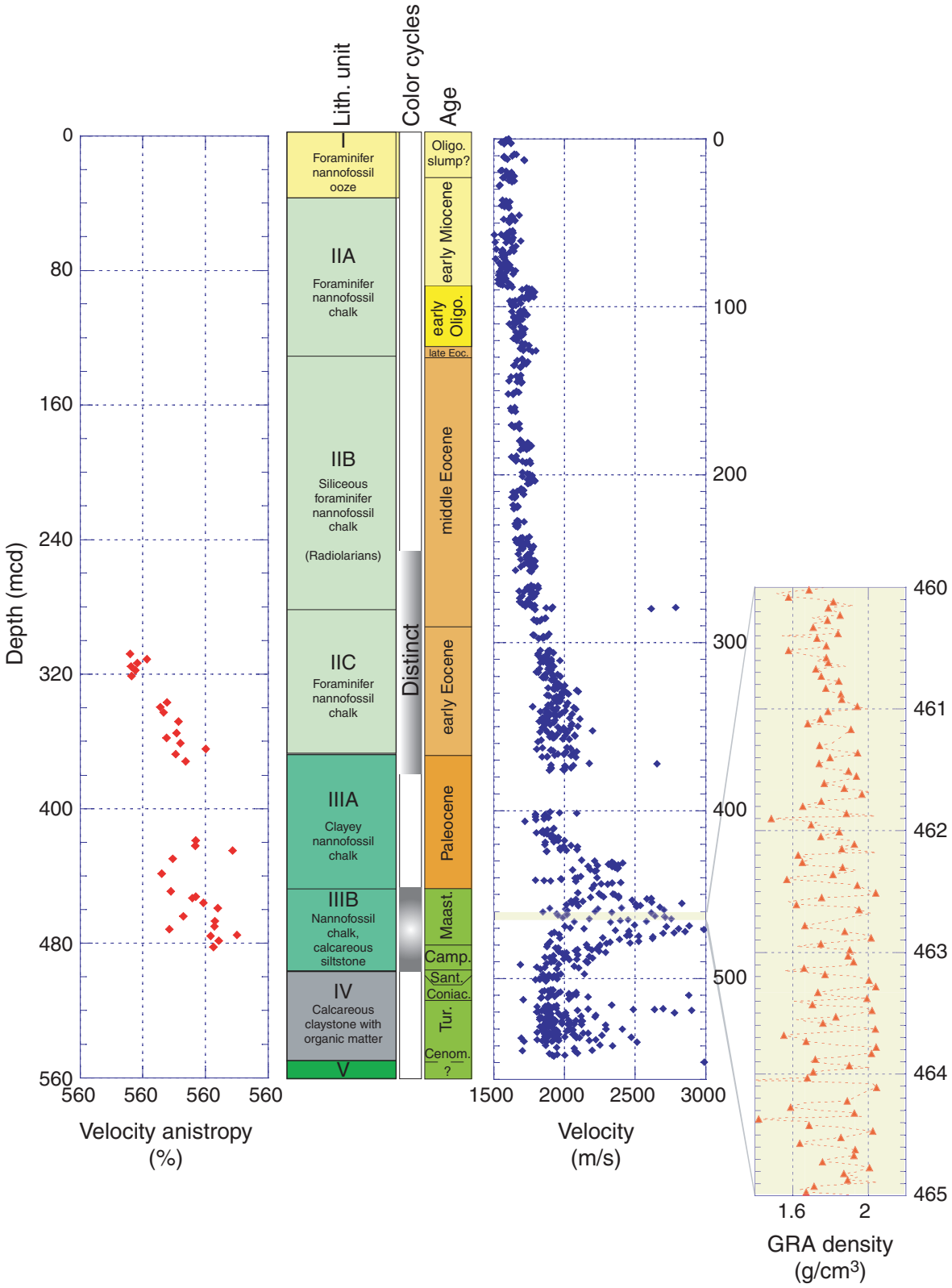

**Figure F30.** MST data vs. lithostratigraphic units from Holes 1259A (red), 1259B (blue), and 1259C (green). Data have been smoothed using a 75-cm moving window. NGR = natural gamma radiation. P/E = Paleocene/Eocene boundary, K/T = Cretaceous/Tertiary boundary.

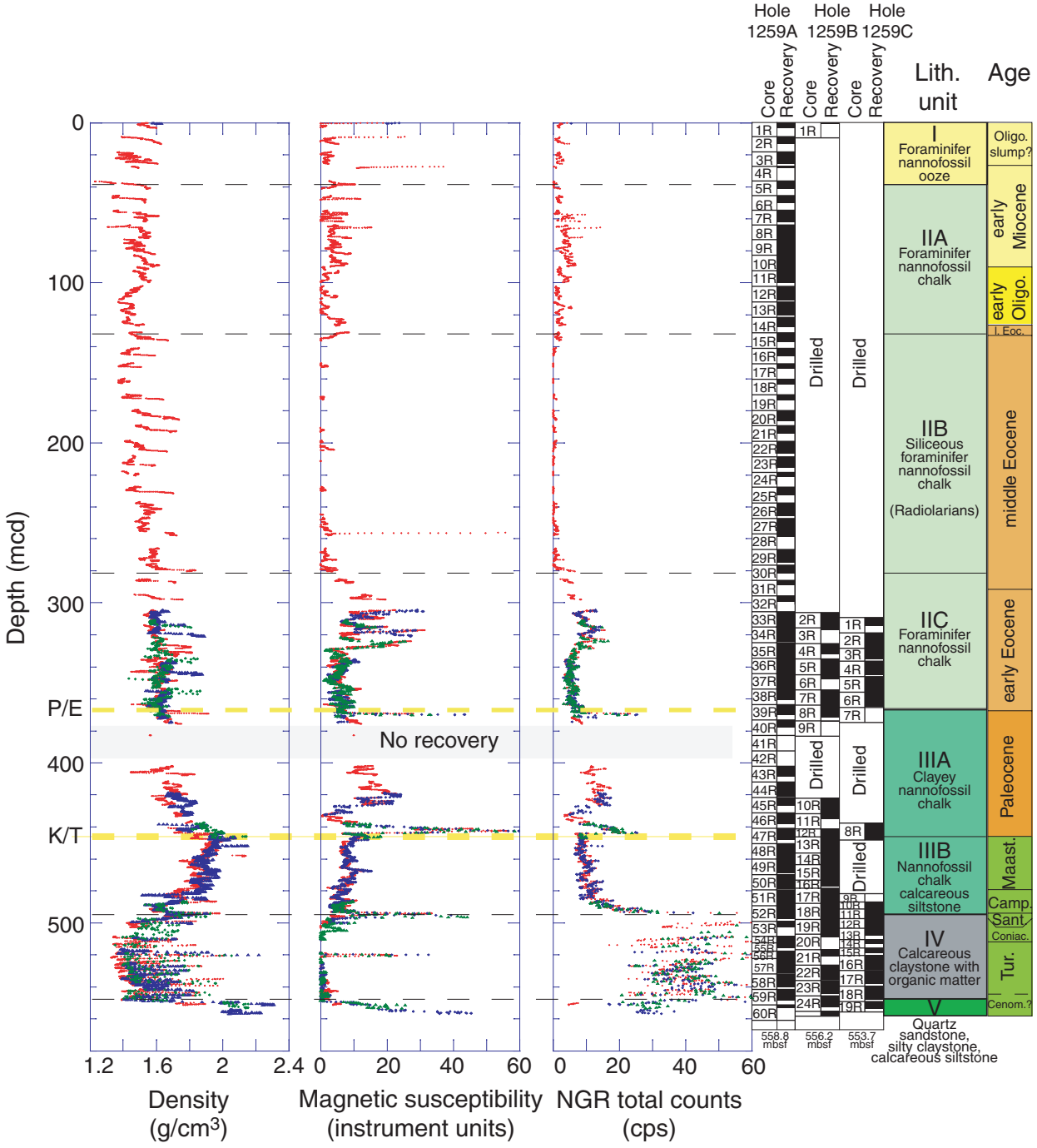

**Figure F31.** MST data across the Cretaceous/Tertiary (K/T) boundary and through the shale sequence at Site 1259. Red = Hole 1259A; blue = Hole 1259B; green = 1259C. NGR = natural gamma radiation.

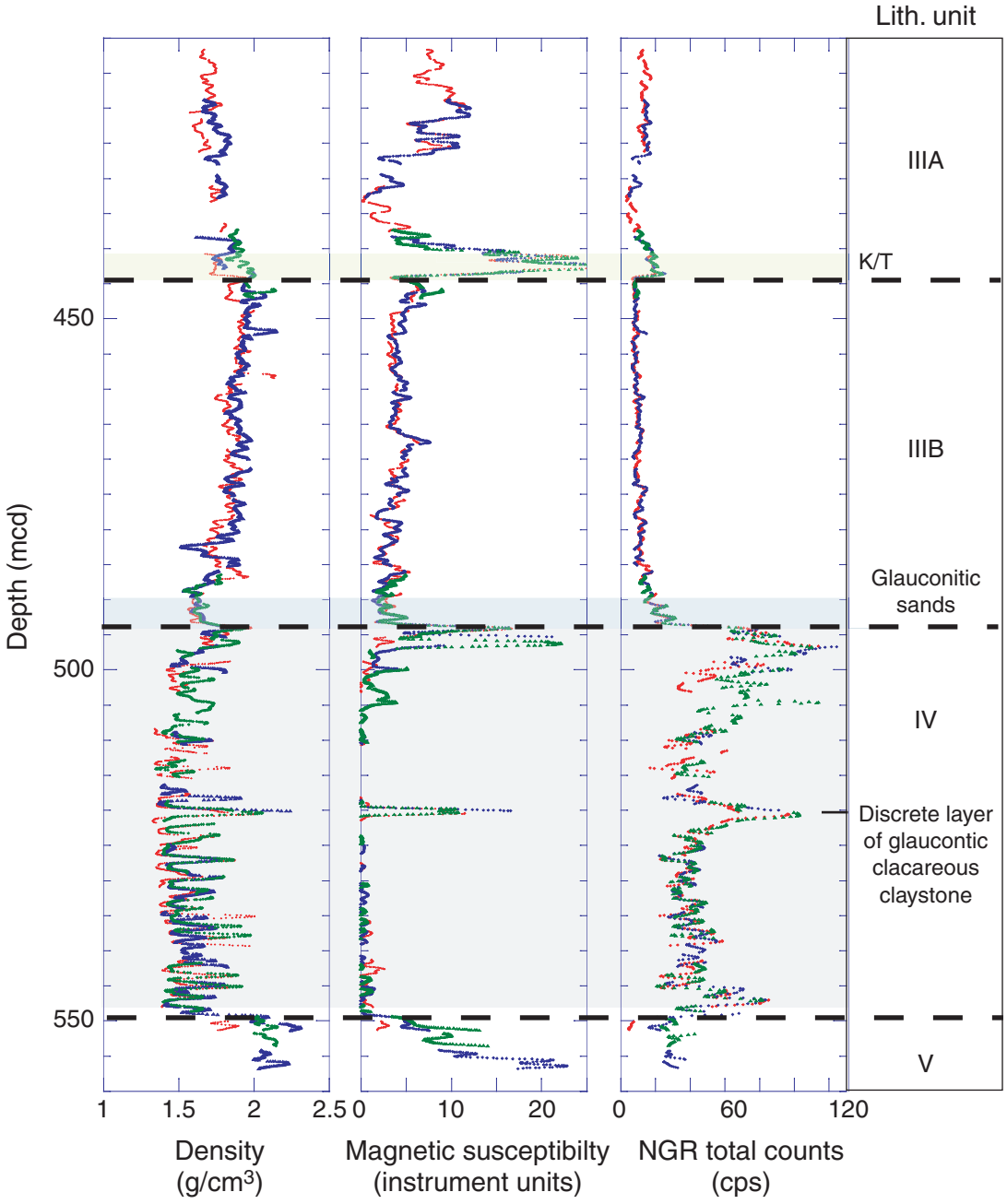

**Figure F32.** Impedance and reflection coefficient profiles used to generate the synthetic seismogram at Site 1259.

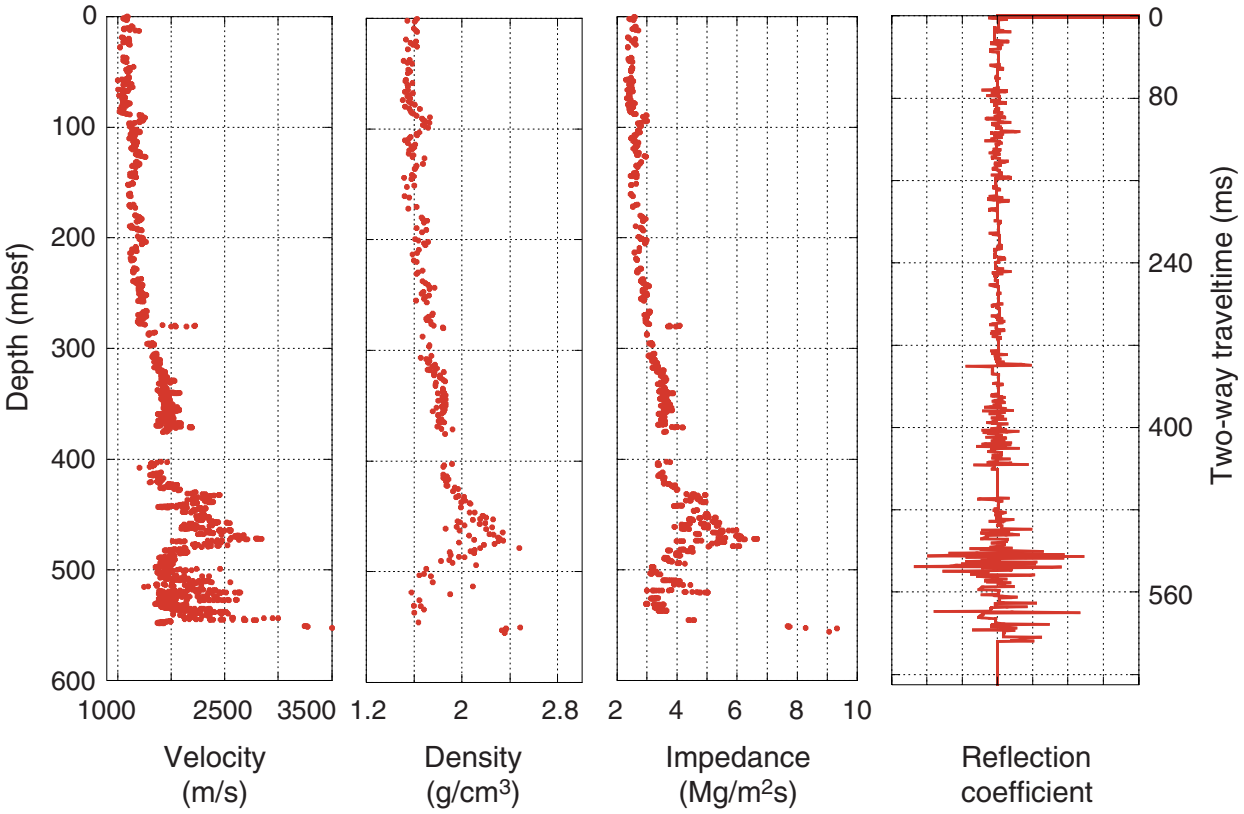

**Figure F33.** Impedance contrasts showing close agreement with major reflectors at Site 1259. The seafloor is shifted because the actual drill site was 300 m upslope from the seismic line's nearest crossing. The synthetic seismic match was made by aligning Reflector C at the base of the section.

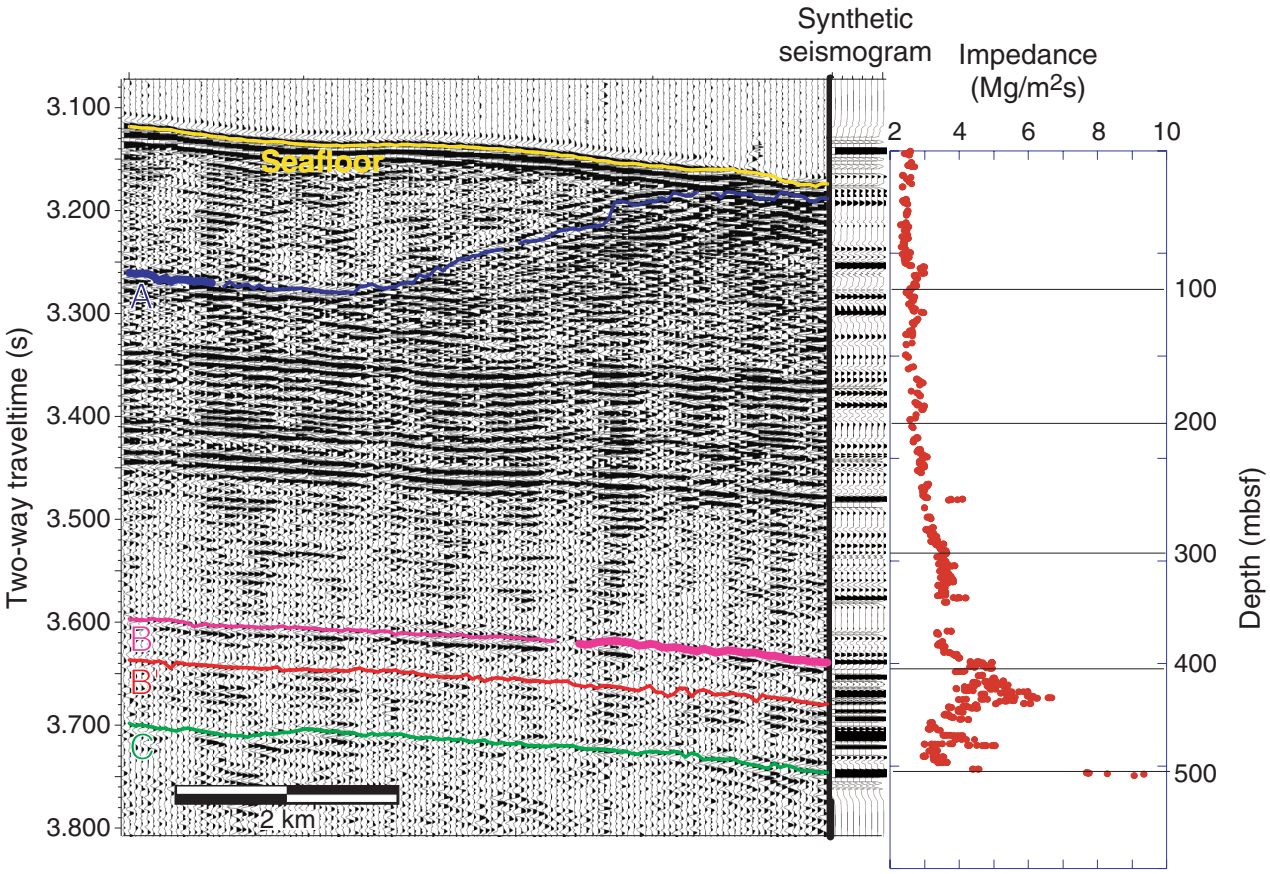

**Table T1.** Coring summary, Site 1259. (See table note. Continued on next two pages.)

**Hole 1259A**
Latitude: 9°17.9989′N
Longitude: 54°11.9984′W
Time on site: 145.12 (1208 hr, 1 Feb–2135 hr, 14 Feb 2003)
Time on hole: 62.87 (1208 hr, 1 Feb–0300 hr, 4 Feb 2003)
Seafloor (drill pipe measurement from rig floor, mbrf): 2365.0
Distance between rig floor and sea level (m): 11.2
Water depth (drill pipe measurement from sea level, m): 2353.8
Total depth (drill pipe measurement from rig floor, mbrf): 2923.8
Total penetration (meters below seafloor, mbsf): 558.8
Total length of cored section (m): 558.8
Total core recovered (m): 372.13
Core recovery (%): 66.6
Total number of cores: 60
Total number of drilled intervals: 0

**Hole 1259B**
Latitude: 9°18.0485′N
Longitude: 54°11.9448′W
Time on hole: 42.58 (0300 hr, 13 Feb–2135 hr, 14 Feb 2003)
Seafloor (drill pipe measurement from rig floor, mbrf): 2365.0
Distance between rig floor and sea level (m): 11.2
Water depth (drill pipe measurement from sea level, m): 2353.8
Total depth (drill pipe measurement from rig floor, mbrf): 2921.2
Total penetration (meters below seafloor, mbsf): 556.2
Total length of cored section (m): 222.2
Total length of drilled intervals (m): 334.0
Total core recovered (m): 153.78
Core recovery (%): 69.2
Total number of cores: 25
Total number of drilled intervals: 2

**Hole 1259C**
Latitude: 9°18.0240′N
Longitude: 54°11.9694′W
Time on hole: 39.67 (2135 hr, 14 Feb–1315 hr, 16 Feb 2003)
Seafloor (drill pipe measurement from rig floor, mbrf): 2367.0
Distance between rig floor and sea level (m): 11.2
Water depth (drill pipe measurement from sea level, m): 2355.8
Total depth (drill pipe measurement from rig floor, mbrf): 2920.7
Total penetration (meters below seafloor, mbsf): 553.7
Total length of cored section (m): 148.6
Total length of drilled intervals (m): 405.1
Total core recovered (m): 118.94
Core recovery (%): 80.0
Total number of cores: 19
Total number of drilled intervals: 3

| Core | Date (Feb 2003) | Local time (hr) | Depth (mbsf) Top | Depth (mbsf) Bottom | Length (m) Cored | Length (m) Recovered | Recovery (%) | Remarks |
|---|---|---|---|---|---|---|---|---|
| 207-1259A- | | | | | | | | |
| 1R | 1 | 1850 | 0.0 | 8.8 | 8.8 | 3.40 | 38.6 | |
| 2R | 1 | 1935 | 8.8 | 18.3 | 9.5 | 4.62 | 48.6 | |
| 3R | 1 | 2005 | 18.3 | 27.3 | 9.0 | 7.59 | 84.3 | |
| 4R | 1 | 2035 | 27.3 | 36.4 | 9.1 | 1.07 | 11.8 | |
| 5R | 1 | 2105 | 36.4 | 45.5 | 9.1 | 4.97 | 54.6 | |
| 6R | 1 | 2135 | 45.5 | 54.6 | 9.1 | 4.64 | 51.0 | |
| 7R | 1 | 2205 | 54.6 | 63.8 | 9.2 | 7.45 | 81.0 | |
| 8R | 1 | 2235 | 63.8 | 72.9 | 9.1 | 8.46 | 93.0 | |
| 9R | 1 | 2305 | 72.9 | 82.6 | 9.7 | 9.48 | 97.7 | |
| 10R | 1 | 2335 | 82.6 | 92.3 | 9.7 | 9.41 | 97.0 | |
| 11R | 2 | 0005 | 92.3 | 102.0 | 9.7 | 7.70 | 79.4 | |
| 12R | 2 | 0035 | 102.0 | 111.7 | 9.7 | 8.66 | 89.3 | |
| 13R | 2 | 0105 | 111.7 | 121.3 | 9.6 | 8.59 | 89.5 | |
| 14R | 2 | 0135 | 121.3 | 130.9 | 9.6 | 5.75 | 59.9 | |
| 15R | 2 | 0205 | 130.9 | 140.6 | 9.7 | 5.50 | 56.7 | |
| 16R | 2 | 0235 | 140.6 | 150.2 | 9.6 | 5.06 | 52.7 | |
| 17R | 2 | 0310 | 150.2 | 159.8 | 9.6 | 2.70 | 28.1 | |
| 18R | 2 | 0340 | 159.8 | 169.5 | 9.7 | 3.01 | 31.0 | |
| 19R | 2 | 0410 | 169.5 | 179.2 | 9.7 | 3.58 | 36.9 | |

Table T1 (continued).

| Core | Date (Feb 2003) | Local time (hr) | Depth (mbsf) Top | Depth (mbsf) Bottom | Length (m) Cored | Length (m) Recovered | Recovery (%) | Remarks |
|---|---|---|---|---|---|---|---|---|
| 20R | 2 | 0440 | 179.2 | 188.8 | 9.6 | 6.62 | 69.0 | |
| 21R | 2 | 0510 | 188.8 | 198.5 | 9.7 | 4.85 | 50.0 | |
| 22R | 2 | 0545 | 198.5 | 208.1 | 9.6 | 7.31 | 76.2 | |
| 23R | 2 | 0615 | 208.1 | 217.8 | 9.7 | 6.38 | 65.8 | |
| 24R | 2 | 0710 | 217.8 | 227.2 | 9.4 | 2.90 | 30.9 | |
| 25R | 2 | 0745 | 227.2 | 236.9 | 9.7 | 4.64 | 47.8 | |
| 26R | 2 | 0815 | 236.9 | 246.5 | 9.6 | 8.43 | 87.8 | |
| 27R | 2 | 0845 | 246.5 | 256.2 | 9.7 | 9.11 | 93.9 | |
| 28R | 2 | 1000 | 256.2 | 265.8 | 9.6 | 1.94 | 20.2 | |
| 29R | 2 | 1035 | 265.8 | 275.5 | 9.7 | 8.42 | 86.8 | |
| 30R | 2 | 1110 | 275.5 | 285.1 | 9.6 | 5.08 | 52.9 | |
| 31R | 2 | 1150 | 285.1 | 294.7 | 9.6 | 2.75 | 28.7 | |
| 32R | 2 | 1220 | 294.7 | 304.4 | 9.7 | 3.62 | 37.3 | |
| 33R | 2 | 1250 | 304.4 | 314.0 | 9.6 | 9.17 | 95.5 | |
| 34R | 2 | 1320 | 314.0 | 323.7 | 9.7 | 9.05 | 93.3 | |
| 35R | 2 | 1355 | 323.7 | 333.3 | 9.6 | 9.98 | 104.0 | |
| 36R | 2 | 1440 | 333.3 | 343.0 | 9.7 | 9.74 | 100.4 | |
| 37R | 2 | 1515 | 343.0 | 352.6 | 9.6 | 9.74 | 101.5 | |
| 38R | 2 | 1555 | 352.6 | 362.2 | 9.6 | 6.64 | 69.2 | |
| 39R | 2 | 1645 | 362.2 | 371.8 | 9.6 | 6.41 | 66.8 | |
| 40R | 2 | 1745 | 371.8 | 381.4 | 9.6 | 4.70 | 49.0 | |
| 41R | 2 | 1855 | 381.4 | 391.1 | 9.7 | 0.41 | 4.2 | |
| 42R | 2 | 2020 | 391.1 | 400.7 | 9.6 | 0.00 | 0.0 | Dropped deplugger; no recovery |
| 43R | 2 | 2240 | 400.7 | 410.4 | 9.7 | 6.15 | 63.4 | |
| 44R | 2 | 2350 | 410.4 | 420.0 | 9.6 | 9.30 | 96.9 | |
| 45R | 3 | 0050 | 420.0 | 429.6 | 9.6 | 4.88 | 50.8 | |
| 46R | 3 | 0150 | 429.6 | 439.2 | 9.6 | 6.88 | 71.7 | |
| 47R | 3 | 0300 | 439.2 | 448.8 | 9.6 | 7.33 | 76.4 | K/T boundary recovered |
| 48R | 3 | 0350 | 448.8 | 458.4 | 9.6 | 9.92 | 103.3 | |
| 49R | 3 | 0445 | 458.4 | 468.0 | 9.6 | 8.71 | 90.7 | |
| 50R | 3 | 0540 | 468.0 | 477.6 | 9.6 | 9.17 | 95.5 | |
| 51R | 3 | 0705 | 477.6 | 487.3 | 9.7 | 10.06 | 103.7 | |
| 52R | 3 | 0830 | 487.3 | 497.0 | 9.7 | 7.97 | 82.2 | |
| 53R | 3 | 0945 | 497.0 | 506.6 | 9.6 | 4.72 | 49.2 | |
| 54R | 3 | 1235 | 506.6 | 510.6 | 4.0 | 3.76 | 94.0 | |
| 55R | 3 | 1345 | 510.6 | 515.8 | 5.2 | 3.38 | 65.0 | |
| 56R | 3 | 1455 | 515.8 | 520.3 | 4.5 | 4.47 | 99.3 | |
| 57R | 3 | 1620 | 520.3 | 529.9 | 9.6 | 9.04 | 94.2 | |
| 58R | 3 | 1755 | 529.9 | 539.5 | 9.6 | 8.32 | 86.7 | |
| 59R | 3 | 1930 | 539.5 | 549.1 | 9.6 | 7.14 | 74.4 | |
| 60R | 3 | 2050 | 549.1 | 558.8 | 9.7 | 1.40 | 14.4 | |
| | | | Cored totals: | | 558.8 | 372.13 | 66.6 | |
| 207-1259B- | | | | | | | | |
| 1R | 13 | 0855 | 0.0 | 9.6 | 9.6 | 0.67 | 7.0 | |
| | | | *****Drilled from 9.6 to 305.0 mbsf***** | | | | | |
| 2R | 13 | 1620 | 305.0 | 314.6 | 9.6 | 9.83 | 102.4 | |
| 3R | 13 | 1655 | 314.6 | 324.2 | 9.6 | 0.00 | 0.0 | No recovery |
| 4R | 13 | 1745 | 324.2 | 333.8 | 9.6 | 6.59 | 68.7 | |
| 5R | 13 | 1835 | 333.8 | 343.4 | 9.6 | 9.91 | 103.2 | |
| 6R | 13 | 1915 | 343.4 | 353.1 | 9.7 | 3.11 | 32.1 | |
| 7R | 13 | 2000 | 353.1 | 362.7 | 9.6 | 9.68 | 100.8 | |
| 8R | 13 | 2050 | 362.7 | 372.3 | 9.6 | 7.51 | 78.2 | |
| 9R | 13 | 2145 | 372.3 | 381.9 | 9.6 | 0.42 | 4.4 | |
| | | | *****Drilled from 381.9 to 420.5 mbsf***** | | | | | |
| 10R | 14 | 0145 | 420.5 | 430.1 | 9.6 | 9.38 | 97.7 | |
| 11R | 14 | 0225 | 430.1 | 439.7 | 9.6 | 3.30 | 34.4 | |
| 12R | 14 | 0300 | 439.7 | 444.7 | 5.0 | 4.86 | 97.2 | |
| 13R | 14 | 0345 | 444.7 | 454.3 | 9.6 | 9.85 | 102.6 | K/T boundary recovered |
| 14R | 14 | 0435 | 454.3 | 461.9 | 7.6 | 7.26 | 95.5 | |
| 15R | 14 | 0525 | 461.9 | 471.5 | 9.6 | 9.90 | 103.1 | |
| 16R | 14 | 0615 | 471.5 | 476.5 | 5.0 | 4.03 | 80.6 | |
| 17R | 14 | 0710 | 476.5 | 485.9 | 9.4 | 9.94 | 105.7 | |
| 18R | 14 | 0845 | 485.9 | 495.5 | 9.6 | 9.73 | 101.4 | |
| 19R | 14 | 0950 | 495.5 | 505.1 | 9.6 | 4.16 | 43.3 | |
| 20R | 14 | 1110 | 505.1 | 514.8 | 9.7 | 2.02 | 20.8 | |
| 21R | 14 | 1230 | 514.8 | 524.4 | 9.6 | 4.27 | 44.5 | |
| 22R | 14 | 1340 | 524.4 | 534.0 | 9.6 | 9.35 | 97.4 | |
| 23R | 14 | 1510 | 534.0 | 543.6 | 9.6 | 8.03 | 83.7 | |

**Table T1 (continued).**

| Core | Date (Feb 2003) | Local time (hr) | Depth (mbsf) Top | Depth (mbsf) Bottom | Length (m) Cored | Length (m) Recovered | Recovery (%) | Remarks |
|---|---|---|---|---|---|---|---|---|
| 24R | 14 | 1705 | 543.6 | 553.2 | 9.6 | 7.17 | 74.7 | |
| 25R | 14 | 1940 | 553.2 | 556.2 | 3.0 | 2.81 | 93.7 | |
| | | | | Cored totals: | 222.2 | 153.78 | 69.2 | |
| | | | | Drilled total: | 334.0 | | | |
| | | | | Total: | 556.2 | | | |
| 207-1259C- | | | | | | | | |
| | | | *****Drilled from 0.0 to 308.0 mbsf***** | | | | | |
| 1R | 15 | 0515 | 308.0 | 317.6 | 9.6 | 4.91 | 51.2 | |
| 2R | 15 | 0555 | 317.6 | 327.2 | 9.6 | 8.93 | 93.0 | |
| 3R | 15 | 0635 | 327.2 | 335.2 | 8.0 | 6.93 | 86.6 | |
| 4R | 15 | 0720 | 335.2 | 344.8 | 9.6 | 8.38 | 87.3 | |
| 5R | 15 | 0810 | 344.8 | 354.4 | 9.6 | 9.96 | 103.8 | |
| 6R | 15 | 0855 | 354.4 | 364.0 | 9.6 | 9.12 | 95.0 | |
| 7R | 15 | 0950 | 364.0 | 373.3 | 9.3 | 3.74 | 40.2 | |
| | | | *****Drilled from 373.3 to 436.0 mbsf***** | | | | | |
| 8R | 15 | 1420 | 436.0 | 445.6 | 9.6 | 10.00 | 104.2 | K/T boundary recovered |
| | | | *****Drilled from 445.6 to 480.0 mbsf***** | | | | | |
| 9R | 15 | 1825 | 480.0 | 485.0 | 5.0 | 0.00 | 0.0 | No recovery |
| 10R | 15 | 1930 | 485.0 | 489.4 | 4.4 | 5.31 | 120.7 | |
| 11R | 15 | 2020 | 489.4 | 495.4 | 6.0 | 6.64 | 110.7 | |
| 12R | 15 | 2115 | 495.4 | 501.6 | 6.2 | 6.56 | 105.8 | |
| 13R | 15 | 2205 | 501.6 | 508.6 | 7.0 | 4.39 | 62.7 | |
| 14R | 15 | 2305 | 508.6 | 513.8 | 5.2 | 2.67 | 51.4 | |
| 15R | 15 | 2350 | 513.8 | 518.3 | 4.5 | 2.96 | 65.8 | |
| 16R | 16 | 0100 | 518.3 | 527.9 | 9.6 | 9.13 | 95.1 | |
| 17R | 16 | 0215 | 527.9 | 537.5 | 9.6 | 7.77 | 80.9 | |
| 18R | 16 | 0330 | 537.5 | 547.1 | 9.6 | 7.24 | 75.4 | |
| 19R | 16 | 0610 | 547.1 | 553.7 | 6.6 | 4.30 | 65.2 | |
| | | | | Cored totals: | 148.6 | 118.94 | 80.0 | |
| | | | | Drilled total: | 405.1 | | | |
| | | | | Total: | 553.7 | | | |

Note: K/T = Cretaceous/Tertiary.

**Table T2.** Lithostratigraphic units and subunits, Site 1259.

| Unit/Subunit | Hole, core, section, interval (cm) | Depth (mbsf) | Thickness (m) | Age | Lithology |
|---|---|---|---|---|---|
| | 207- | | | | |
| I | 1259A-1R-1, 0, through 1259A-5R-2, 0 | 0.00–37.90 | 37.90 | early Miocene and slumped Oligocene | Foraminifer nannofossil ooze |
| IIA | 1259A-5R-2, 0, through 1259A-15R-1, 0 | 37.90–130.90 | 93.00 | late Eocene, early Oligocene, and early Miocene | Foraminifer nannofossil chalk |
| IIB | 1259A-15R-1, 0, through 1259A-31R-1, 0 | 130.90–285.10 | 154.20 | middle–late Eocene | Siliceous (radiolarian) foraminifer nannofossil chalk |
| IIC | 1259A-31R-1, 0, through 1259A-39R-5, 139 | 285.10–368.24 | 83.14 | early–middle Eocene | Foraminifer nannofossil chalk |
| (P/E at base) | 1259B-2R-1, 0, through 1259B-8R-4, 106 | 305.00–368.26 | 63.26 | | |
| | 1259C-1R-1, 0, through 1259C-7R-2, 120 | 308.00–366.55 | 58.55 | | |
| IIIA | 1259A-39R-5, 139, through 1259A-47R-3, 75 | 368.24–442.33 | 74.09 | late Paleocene | Clayey nannofossil chalk |
| (K/T at base) | 1259B-8R-4, 106, through 1259B-13R-1, 48 | 368.26–445.18 | 76.92 | | |
| | 1259C-7R-2, 120, through 1259C-8R-5, 98 | 366.55–442.47 | 75.92 | | |
| IIIB | 1259A-47R-3, 75, through 1259A-52R-5, 13 | 442.33–492.96 | 50.63 | Campanian–Maastrichtian | Nannofossil chalk, calcareous siltstone, and glauconitic claystone |
| | 1259B-13R-1, 48, through 1259B-18R-7, 53 | 445.18–494.52 | 49.34 | | |
| | 1259C-8R-5, 98, through 1259C-11R-3, 50 | 442.47–492.43 | 49.96 | | |
| IV | 1259A-52R-5, 13, through 1259A-60R-1, 0 | 492.96–549.10 | 56.14 | Santonian, Coniacian, and Turonian | Calcareous claystone with organic matter |
| | 1259B-18R-7, 53, through 1259B-24R-4, 42 | 494.52–548.52 | 54.08 | | |
| | 1259C-11R-3, 50, through 1259C-19R-1, 0 | 492.43–547.10 | 53.29 | | |
| V | 1259A-60R-1, 0, through 1259A-60R-1, 140 | 549.10–550.50 | 1.40 | Age unknown | Quartz sandstone, silty claystone, and calcareous siltstone |
| | 1259B-24R-4, 42, through 1259B-25R-CC, 9 | 548.52–556.01 | 7.49 | | |
| | 1259C-19R-1, 0, through 1259C-19R-4, 86 | 547.10–551.40 | 4.30 | | |

Note: P/E = Paleocene/Eocene boundary, K/T = Cretaceous/Tertiary boundary.

**Table T3.** Datum levels for calcareous nannofossils, Hole 1259A.

| Core, section, interval (cm) | Depth (mbsf) | | Depth (mcd) | | Datum | Species | Zone | Age | Age (Ma) |
|---|---|---|---|---|---|---|---|---|---|
| | Top | Bottom | Top | Bottom | | | | | |
| 207-1259A- | | | | | | | | | |
| 1R-CC, 12–17 | 0.00 | 3.35 | 0.00 | 3.35 | Slump; no datums given | | NP23 (= CP17) | early Oligocene | 30.4–31.7 |
| 2R-CC, 12–17 | 3.35 | 13.37 | 3.35 | 13.37 | Slump; no datums given | | NP21 | early Oligocene | 32.9–33.8 |
| 3R-CC, 15–18 | 13.37 | 25.86 | 13.37 | 25.86 | Slump; no datums given | | NP23 (= CP17) | early Oligocene | 30.4–31.7 |
| 4R-CC, 0–8 | 25.86 | 28.29 | 25.86 | 28.29 | T | *Triquetrorhabdulus carinatus* | NN2 | early Miocene | 19.6 |
| 5R-CC, 5–13 | 41.29 | 50.06 | 41.29 | 50.06 | B | *Sphenolithus belemnos* | NN2 | early Miocene | 18.9 |
| 6R-CC, 8–16 | 50.06 | 50.06 | 50.06 | 50.06 | B | *Discoaster druggii* | NN2 | early Miocene | 23.2 |
| 8R-CC, 11–17 | 62.00 | 72.20 | 62.00 | 72.20 | T acme | *Triquetrorhabdulus carinatus* | NN2 | early Miocene | 22.9 |
| 9R-CC, 18–23 | 82.33 | 91.95 | 82.33 | 91.95 | B | *Sphenolithus disbelemnos* | NN1 | early Miocene | 23.5 |
| 10R-CC, 6–12 | 91.95 | 99.95 | 91.95 | 99.95 | B | *Sphenolithus distentus* | NP23 (= CP18) | late Oligocene | 30.4 |
| 14R-4, 27.5–27.5 | 126.07 | 126.07 | 126.07 | 126.07 | Disconformity | Oligocene/Eocene boundary | | | 33.7 |
| 14R-CC, 17–22 | 120.24 | 127.00 | 120.24 | 127.00 | T | *Cribrocentrum reticulatum* | NP20/19 | late Eocene | 33.9 |
| 16R-CC, 10–15 | 136.35 | 145.61 | 136.35 | 145.61 | T | *Chiasmolithus grandis* | NP17 | middle Eocene | 37.1 |
| 20R-CC, 8–13 | 173.03 | 185.77 | 173.03 | 185.77 | T | *Chiasmolithus solitus* | NP16 | middle Eocene | 40.4 |
| 24R-CC, 21–24 | 220.67 | 231.79 | 220.67 | 231.79 | B | *Reticulofenestra umbilica* | NP16 (= CP13c) | middle Eocene | 42.5 |
| 26R-CC, 14–19 | 231.79 | 245.28 | 231.79 | 245.28 | T | *Chiasmolithus gigas* | mid NP15 (= CP13b) | middle Eocene | 44.0 |
| 29R-CC, 12–17 | 274.17 | 280.39 | 274.17 | 280.39 | B | *Chiasmolithus gigas* | mid NP15 (= CP13b) | middle Eocene | 46.1 |
| 31R-CC, 15–19 | 280.39 | 287.81 | 280.39 | 287.81 | T | *Discoaster sublodoensis* | NP14 | middle Eocene | 47.2 |
| 31R-CC, 15–19 | 287.81 | 298.12 | 287.81 | 298.12 | B | *Discoaster sublodoensis* | NP14 | middle Eocene | 49.3 |
| 34R-CC, 0–5 | 313.52 | 323.00 | 313.37 | 322.85 | T | *Tribrachiatus orthostylus* | NP12 | early Eocene | 51.0 |
| 35R-CC, 21–26 | 323.00 | 334.70 | 323.21 | 334.91 | X | *T. bramlettei/T. contortus* | NP10 | early Eocene | 53.7 |
| 39R-5, 139–139 | 368.24 | 368.24 | 369.42 | 369.42 | X at PETM | *Z. bijugatus*/fasciculiths | NP9 | Eocene/Paleocene | 55.5 |
| 41R-CC, 9–13 | 381.77 | 406.80 | 382.94 | 407.97 | B | *Discoaster multiradiatus* | NP9 | late Paleocene | 56.2 |
| 47R-3, 72–72 | 442.30 | 442.30 | 443.78 | 443.78 | T at K/T | *Micula prinsii* | CC26 | late Maastrichtian | 65.0 |
| 49R-CC, 11–17 | 467.05 | 477.12 | 467.91 | 477.98 | B | *Micula murus* | CC25 | late Maastrichtian | 66.2 |
| 51R-CC, 14–16 | 477.12 | 487.51 | 477.45 | 487.84 | T | *Uniplanarius trifidum* | CC23 | Campanian/Maastrichtian boundary | 71.3 |
| 52R-6, 104–104 | 494.64 | 494.70 | 496.39 | 496.45 | B | *Micula decussata* | CC13 | early Coniacian | 87.2 |
| 54R-CC, 10–15 | 510.31 | 513.82 | 512.06 | 515.57 | B | *Marthasterites furcatus* | CC13 | Cenomanian/Turonian boundary | 89.3 |
| 56R-CC, 14–19 | 520.22 | 529.29 | 521.97 | 531.04 | B | *Eiffellithus eximius* | CC12 | Turonian | 91.0 |
| 59R-1, 138–138 | 540.88 | 541.00 | 542.72 | 542.84 | B | *Liliasterites angularis* | | Turonian | 93.2 |

Notes: T = top, B = bottom, X = crossover in abundance. K/T = Cretaceous/Tertiary boundary. PETM = Paleocene/Eocene Thermal Maximum.

**Table T4.** Distribution of planktonic foraminifers, Hole 1259A. (This table is available in an **oversized format.**)

**Table T5.** Datum levels for planktonic foraminifers, Site 1259.

| Core, section, interval (cm) | Depth (mbsf) Top | Bottom | Datum | Species | Zone | Age | Age (Ma) |
|---|---|---|---|---|---|---|---|
| 207-1259A- | | | | | | | |
| 7R-3, 50–54 | 56.60 | 58.10 | T | *Paragloborotalia kugleri* | M1b | early Miocene | 21.5 |
| 9R-7, 50–54 | 82.00 | 82.33 | B | *Globoquadrina dehiscens* | M1b | early Miocene | 23.2 |
| 10R-5, 50–54 | 89.10 | 90.60 | B | *Paragloborotalia kugleri* | M1a | early Miocene | 23.8 |
| 11R-5, 50–54 | 98.80 | 99.95 | B | *Globigerina angulosuturalis** | P21a | early Oligocene | 29.4 |
| 13R-4, 50–54 | 115.20 | 116.70 | T | *Pseudohastigerina* spp. | P18 | early Oligocene | 32.0 |
| 14R-4, 50–54 | 124.80 | 126.30 | T | *Hantkenina* spp. | P16 | late Eocene | 33.7 |
| 15R-2, 50–54 | 131.40 | 132.90 | T | *Morozovella* and *Acarinina* spp. | P14 | middle Eocene | |
| 19R-3, 50–53 | 171.50 | 172.70 | T | *Orbulinoides beckmanni* | P13 | middle Eocene | 40.1 |
| 20R-4, 50–53 | 184.20 | 185.60 | B | *Orbulinoides beckmanni* | P13 | middle Eocene | 40.5 |
| 24R-1, 50–54 | 214.45 | 218.30 | T | *Morozovella aragonensis* | P11 | middle Eocene | 43.6 |
| 27R-1, 50–54 | 247.00 | 248.50 | B | *Globigerinatheka mexicana* | P11 | middle Eocene | 45.8 |
| 30R-CC, 9–12 | 280.39 | 285.60 | B | *Guembelitroides nuttali* | P10 | middle Eocene | 49.0 |
| 33R-1, 50–54 | 304.90 | 306.40 | B | *Planorotalites palmerae* | P9 | early Eocene | 50.4 |
| 33R-CC, 0–5 | 313.52 | 323.00 | B | *Morozovella aragonensis** | P8 | early Eocene | 52.3 |
| 38R-4, 49–52 | 356.12 | 357.59 | T | *Morozovella velascoensis* group | P5 | early Eocene | 54.7 |
| 43R-CC, 13–18 | 381.77 | 406.80 | T | *Globanomalina pseudomenardii* | P4 | late Paleocene | 55.9 |
| 45R-1, 50–54 | 420.50 | 422.00 | B | *Globanomalina pseudomenardii* | P4 | late Paleocene | 59.2 |
| 45R-CC, 5–11 | 424.82 | 436.43 | B | *Igorina albeari* | P3b | late Paleocene | 60.0 |
| 46R-CC, 29–34 | 436.43 | 446.48 | B | *Praemurica uncinata* | P2 | early Paleocene | 61.2 |
| 47R-CC, 38–43 | 436.43 | 446.48 | T | *Abathomphalus mayaroensis* | KS31 | Maastrichtian | 65.0 |
| 48R-7, 50–54 | 458.30 | 458.67 | B | *Abathomphalus mayaroensis* | KS31 | Maastrichtian | 68.6 |
| 49R-CC, 11–17 | 467.05 | 472.75 | B | *Contusotruncana contusa* | KS30a | Maastrichtian | 69.6 |
| 51R-CC, 14–16 | 487.51 | 490.37 | B | *Globotruncana aegyptiaca* | KS29 | late Campanian | 73.8 |
| 207-1259B- | | | | | | | |
| 4R-CC, 15–20 | 314.78 | 330.74 | T | *Morozovella formosa** | P7 | early Eocene | 50.8 |
| 4R-CC, 15–20 | 330.74 | 343.68 | B | *Morozovella aragonensis** | | | 52.3 |
| 6R-CC, 10–16 | 343.68 | 346.45 | T | *Morozovella velascoensis* group | P5 | early Eocene | 54.7 |
| 11R-3, 56–60 | 433.36 | 442.14 | B | *Igorina albeari** | P3b | late Paleocene | 60.0 |
| 12R-4, 53–54 | 443.37 | 444.23 | T | *Parvularugoglobigerina eugubina* | Pa | early Paleocene | 63.7–64.9 |
| 13R-1, 24–25 | 444.94 | 454.51 | B | *Parvularugoglobigerina eugubina* | Pa | early Paleocene | 64.97 |
| 13R-CC, 13–17 | 444.94 | 454.51 | T | *Abathomphalus mayaroensis* | KS31 | Maastrichtian | 65.0 |
| 14R-CC, 0–5 | 461.51 | 471.75 | B | *Contusotruncana contusa* | KS30a | Maastrichtian | 69.6 |
| 15R-CC, 17–22 | 471.75 | 475.48 | B | *Gansserina gansseri* | KS30b | Maastrichtian–late Campanian | 72.8 |
| 17R-CC, 21–25 | 486.40 | 495.59 | B | *Globotruncana aegyptiaca* | KS29 | late Campanian | 73.8 |
| 207-1259C- | | | | | | | |
| 1R-CC, 13–18 | 312.86 | 326.48 | B | *Morozovella aragonensis* | P7 | early Eocene | 52.3 |
| 6R-CC, 10–13 | 354.74 | 363.49 | T | *Morozovella velascoensis* group | P5 | early Eocene | 54.7 |
| 8R-7, 66–68 | 439.20 | 445.15 | T | *Abathomphalus mayaroensis* | KS31 | Maastrichtian | 65.0 |

Notes: Top and bottom depth values refer to the range of possible depth in the core within which the datum is believed to fall. T = top, B = bottom. * = datums that probably reflect incomplete ranges of the foraminiferal marker species.

**Table T6.** Datum levels for radiolarians, Hole 1259A.

| Core, section, interval (cm) | Depth (mbsf) | Depth (mcd) | Datum | Species | Zone | Age | Age (Ma) |
|---|---|---|---|---|---|---|---|
| 207-1259A- | | | | | | | |
| 8R-CC, 11–17 | 72.20 | 72.20 | LO | *Calocycletta serrata* | RN1 | early Miocene | ~20.5 |
| 9R-CC, 18–23 | 82.33 | 82.33 | B | *Cyrtocapsella tetrapera* | RN1 | early Miocene | 23.6 |
| 16R-CC, 10–15 | 145.61 | 145.61 | LO | *Spongatractus pachystylus* | RP16 | middle Eocene | ~37.7 |
| 18R-CC, 15–20 | 162.76 | 162.76 | B | *Podocyrtis goetheana* | RP16 | middle Eocene | ~38.8 |
| 20R-CC, 8–13 | 185.77 | 185.77 | EVOL | *Podocyrtis chalara* | RP15 | middle Eocene | ~39.5 |
| 21R-CC, 14–20 | 193.59 | 193.59 | FO | *Sethochytris triconiscus* | Upper RP14 | middle Eocene | 40.0–42.0 |
| 22R-CC, 2–8 | 205.70 | 205.70 | LO | *Podocyrtis fasciolata* | Lower RP14 | middle Eocene | 40.0–42.0 |
| 22R-CC, 2–8 | 205.70 | 205.70 | FO | *Podocyrtis trachodes* | Top RP13 | middle Eocene | ~43.0 |
| 24R-CC, 21–24 | 220.67 | 220.67 | EVOL | *Eusyringium fistuligerum* | Upper RP13 | middle Eocene | 43.0–44.0 |
| 25R-CC, 16–21 | 231.79 | 231.79 | FO | *Eusyringium fistuligerum* | Top RP13 | middle Eocene | ~44.5 |
| 29R-CC, 12–17 | 274.17 | 274.17 | EVOL | *Thyrsocyrtis triacantha* | RP12 | middle Eocene | ~47.5 |
| 30R-CC, 9–12 | 280.39 | 280.39 | FO | *Dictyoprora mongolfieri* | RP11 | middle Eocene | ~48.5 |

Note: LO = last occurrence, B = bottom, FO = first occurrence, EVOL = evolutionary transition between species.

**Table T7.** Datum levels, ages, and preservation of samples for calcareous nannofossils, Site 1259.

| Core, section, interval (cm) | Depth (mbsf) | Zone | Age | Preservation | Group abundance |
|---|---|---|---|---|---|
| 207-1259A- | | | | | |
| 1R-CC, 12–17 | 3.35 | NP23 | early Oligocene | G | C |
| 2R-CC, 12–17 | 13.37 | NP21 | early Oligocene | G | C |
| 3R-CC, 15–18 | 25.86 | NP23 | early Oligocene | G | C |
| 4R-CC, 0–8 | 28.29 | NN2 | early Miocene | G | C |
| 5R-CC, 5–13 | 41.29 | NN2 | early Miocene | G | C |
| 6R-CC, 8–16 | 50.06 | NN2 | early Miocene | G | C |
| 7R-CC, 13–18 | 62.00 | NN2 | early Miocene | G | C |
| 8R-CC, 11–17 | 72.20 | NN2 | early Miocene | G | C |
| 9R-CC, 18–23 | 82.33 | NN1 | early Miocene | | |
| 10R-CC, 6–12 | 91.95 | NP23 | early Oligocene | | |
| 11R-CC, 21–26 | 99.95 | NP23 | early Oligocene | G | C |
| 12R-CC, 7–14 | 110.59 | NP23 | early Oligocene | G | C |
| 13R-CC, 9–14 | 120.24 | NP23 | early Oligocene | G | C |
| 14R-CC, 17–22 | 127.00 | NP20/19 | late Eocene | G | C |
| 15R-CC, 13–18 | 136.35 | NP17 | middle Eocene | G | C |
| 16R-CC, 10–15 | 145.61 | NP17 | middle Eocene | G | C |
| 17R-CC, 16–21 | 152.85 | NP17 | middle Eocene | G | C |
| 18R-CC, 15–20 | 162.76 | NP17 | middle Eocene | G | C |
| 19R-CC, 11–16 | 173.03 | NP17 | middle Eocene | G | C |
| 20R-CC, 8–13 | 185.77 | NP16 | middle Eocene | G | C |
| 21R-CC, 14–20 | 193.59 | NP16 | middle Eocene | P | F |
| 22R-CC, 2–8 | 205.70 | NP16 | middle Eocene | G | C |
| 23R-CC, 10–13 | 214.45 | NP16 | middle Eocene | G | C |
| 24R-CC, 21–24 | 220.67 | NP16 | middle Eocene | G | C |
| 25R-CC, 16–21 | 231.79 | NP15 | middle Eocene | G | C |
| 26R-CC, 14–19 | 245.28 | NP15 | middle Eocene | G | C |
| 27R-CC, 7–10 | 255.58 | NP15 | middle Eocene | G | C |
| 28R-CC, 18–23 | 258.09 | NP15 | middle Eocene | G | C |
| 29R-CC, 12–17 | 274.17 | NP15 | middle Eocene | G | C |
| 30R-CC, 9–12 | 280.39 | NP14 | middle Eocene | G | C |
| 31R-CC, 15–19 | 287.81 | NP14 | middle Eocene | G | C |
| 32R-CC, 0–5 | 298.12 | NP13 | early Eocene | M | F |
| 33R-CC, 0–5 | 313.52 | NP13 | early Eocene | M | F |
| 34R-CC, 0–5 | 323.00 | NP12 | early Eocene | G | C |
| 35R-CC, 21–26 | 333.63 | NP10 | early Eocene | G | C |
| 36R-1, 140–150 | 334.70 | | | | |
| 36R-CC, 0–5 | 342.99 | NP9 | early Eocene | | |
| 37R-CC, 12–18 | 352.68 | NP9 | early Eocene | | |
| 38R-CC, 0–5 | 359.19 | NP9 | early Eocene | | |
| 39R-5, 148–150 | 368.33 | NP9 | late Paleocene | | |
| 39R-CC, 21–26 | 368.56 | NP9 | late Paleocene | | |
| 40R-CC, 10–15 | 376.45 | NP9 | late Paleocene | M | C |
| 41R-CC, 9–13 | 381.77 | NP9 | late Paleocene | G | C |
| 43R-CC, 13–18 | 406.80 | NP7 | late Paleocene | G | C |
| 44R-CC, 13–18 | 419.65 | NP7 | late Paleocene | G | C |
| 45R-CC, 5–11 | 424.82 | | | | |
| 46R-CC, 29–34 | 436.43 | NP3 | early Paleocene | P | R |
| 47R-CC, 38–43 | 446.48 | CC26 | Maastrichtian | M | F |
| 48R-CC, 18–23 | 458.67 | CC26 | Maastrichtian | M | F |
| 49R-CC, 11–17 | 467.05 | CC25 | Maastrichtian | M | F |
| 50R-CC, 7–12 | 477.12 | CC25 | Maastrichtian | M | F |
| 51R-CC, 14–16 | 487.51 | CC23 | Campanian | P | R |
| 52R-CC, 23–26 | 495.24 | CC13 | Coniacian | P | R |
| 53R-CC, 20–22 | 501.70 | CC13 | Coniacian | P | R |
| 54R-CC, 10–15 | 510.31 | CC13 | Coniacian | G | C |
| 55R-CC, 0–3 | 513.82 | CC12 | Turonian | | |
| 56R-CC, 14–19 | 520.22 | CC12 | Turonian | G | F |
| 57R-CC, 10–15 | 529.29 | CC11 | Turonian | P | R |
| 58R-CC, 11–16 | 538.17 | CC11 | Turonian | | |
| 59R-4, 130–131 | 545.13 | | | | |
| 59R-CC, 12–17 | 546.54 | | | | |
| 60R-1, 9–13 | 549.19 | | | | |
| 207-1259B- | | | | | |
| 1R-CC, 19–23 | 0.63 | NP24 | late Oligocene | G | C |
| 2R-CC, 16–21 | 314.78 | NP13 | early Eocene | G | R |
| 4R-CC, 15–20 | 330.74 | NP10 | early Eocene | G | C |
| 5R-CC, 15–18 | 343.68 | NP9 | early Eocene | G | C |
| 6R-CC, 10–16 | 346.45 | NP9 | early Eocene | G | C |
| 7R-CC, 0–4 | 362.57 | NP9 | early Eocene | G | C |
| 8R-CC, 8–13 | 370.16 | NP9 | late Paleocene | G | C |
| 9R-1, 40–42 | 372.70 | NP9 | late Paleocene | G | C |
| 10R-CC, 6–12 | 429.82 | NP5 | late Paleocene | M | C |
| 11R-3, 56–60 | 433.36 | NP3 | early Paleocene | P | F |
| 12R-CC, 17–21 | 444.52 | NP1 | early Paleocene | P | F |
| 13R-CC, 13–17 | 454.51 | CC26 | Maastrichtian | G | C |
| 14R-CC, 0–5 | 461.51 | CC25 | Maastrichtian | M | F |
| 15R-CC, 17–22 | 471.75 | | | | |
| 16R-3, 98–103 | 475.48 | CC24 | Maastrichtian | P | R |
| 17R-CC, 21–25 | 486.40 | CC23 | Campanian | P | R |
| 18R-CC, 10–14 | 495.59 | CC18 | Campanian | G | R |
| 19R-3, 91–92 | 499.41 | | | | |
| 19R-CC, 19–24 | 499.61 | CC15 | Santonian | P | R |
| 20R-CC, 14–16 | 507.10 | CC12 | Turonian | M | F |
| 21R-CC, 34–40 | 519.01 | CC11 | Turonian | | B |
| 22R-CC, 16–21 | 533.70 | CC11 | Turonian | | B |
| 23R-CC, 0–5 | 541.98 | CC11 | Turonian | | B |
| 24R-CC, 0–5 | 550.72 | | | | B |
| 25R-CC, 4–7 | 555.96 | | | | B |
| 207-1259C- | | | | | |
| 1R-CC, 13–18 | 312.86 | NP12 | early Eocene | G | C |
| 2R-CC, 9–14 | 326.48 | NP11 | early Eocene | G | C |
| 3R-CC, 15–20 | 334.08 | NP10 | early Eocene | G | C |
| 4R-CC, 0–5 | 343.53 | NP9 | early Eocene | G | C |
| 5R-CC, 21–23 | 354.74 | NP9 | early Eocene | G | C |
| 6R-CC, 10–13 | 363.49 | NP9 | early Eocene | G | C |
| 7R-CC, 8–10 | 367.72 | NP9 | late Paleocene | G | C |
| 8R-CC, 16–21 | 445.95 | CC25 | Maastrichtian | G | C |
| 10R-CC, 0–5 | 490.26 | | | | |
| 11R-5, 106–111 | 495.99 | CC13 | Coniacian | | |
| 12R-CC, 21–26 | 501.91 | CC13 | Coniacian | | |
| 13R-CC, 0–5 | 505.75 | CC12 | Turonian | | |
| 14R-CC, 18–23 | 511.22 | CC12 | Turonian | | |
| 15R-2, 141–146 | 516.71 | | | | |
| 16R-CC, 5–10 | 527.38 | CC11 | Turonian | M | F |
| 17R-CC, 26–31 | 535.62 | CC11 | Turonian | M | F |
| 18R-CC, 0–5 | 544.54 | CC11 | Turonian | G | F |

Notes: Preservation: G = good, M = moderate, P = poor. Abundance: C = common, F = few, R = rare, B = barren.

**Table T8.** Distribution of planktonic foraminifers, Hole 1259B. (Continued on next page.)

| Core, section, interval (cm) | Depth (mbsf) | Zone | Age | Preservation | Group abundance | *Clavihedbergella simplex* | *Heterohelix moremani* | *Whiteinella archaeocretacea* | *Whiteinella baltica* | *Whiteinella inornata* | *Hastigerinoides watersi* | *Heterohelix globulosa* | *Archaeoglobigerina cretacea* | *Dicarinella hagni* | *Marginotruncana pseudolinneiana* | *Dicarinella* sp. 1 | *Contusotruncana fornicata* | *Marginotruncana sinuosa* | *Globigerinelloides prairiehillensis* | *Heterohelix sphenoides* | *Heterohelix striata* | *Pseudoguembelina costellifera* | *Globotruncana aegyptiaca* | *Globotruncana linneiana* | *Pseudotextularia elegans* | *Rugoglobigerina rugosa* | *Rugotruncana subcircumnodifer* | *Contusotruncana patelliformis* | *Globotruncanita stuartiformis* | *Globotruncanita subspinosa* | *Gansserina gansseri* | *Globotruncana arca* | *Globotruncana esnehensis* | *Globotruncanita stuarti* | *Contusotruncana contusa* | *Rugoglobigerina hexacamerata* | *Rugoglobigerina rotundata* | *Abathomphalus mayaroensis* | *Globoconusa daubjergensis* | *Parvularugoglobigerina eugubina* | *Woodringina hornerstownensis* | *Guembelitria cretacea* | *Parvularugoglobigerina alabamensis* | *Eoglobigerina eobulloides* | *Parasubbotina pseudobulloides* |
|---|---|---|---|---|---|---|---|---|---|---|---|---|---|---|---|---|---|---|---|---|---|---|---|---|---|---|---|---|---|---|---|---|---|---|---|---|---|---|---|---|---|---|---|---|
| 207-1259B- | | | | | | | | | | | | | | | | | | | | | | | | | | | | | | | | | | | | | | | | | | | | |
| 1R-CC, 19–23 | 0.63 | P21b | early Oligocene | G | A | | | | | | | | | | | | | | | | | | | | | | | | | | | | | | | | | | | | | | | |
| 2R-CC, 16–21 | 314.78 | P8 | early Eocene | P | C | | | | | | | | | | | | | | | | | | | | | | | | | | | | | | | | | | | | | | | |
| 4R-CC, 15–20 | 330.74 | P7 | early Eocene | P | C | | | | | | | | | | | | | | | | | | | | | | | | | | | | | | | | | | | | | | | |
| 5R-CC, 15–18 | 343.68 | P6 | early Eocene | P | C | | | | | | | | | | | | | | | | | | | | | | | | | | | | | | | | | | | | | | | |
| 6R-CC, 10–16 | 346.45 | P5 | early Eocene | P | C | | | | | | | | | | | | | | | | | | | | | | | | | | | | | | | | | | | | | | | |
| 7R-CC, 0–4 | 362.57 | P5 | early Eocene | P | C | | | | | | | | | | | | | | | | | | | | | | | | | | | | | | | | | | | | | | | |
| 8R-CC, 8–13 | 370.16 | P5 | late Paleocene | M | C | | | | | | | | | | | | | | | | | | | | | | | | | | | | | | | | | | | | | | | |
| 9R-1, 40–42 | 372.70 | P5 | late Paleocene | M | C | | | | | | | | | | | | | | | | | | | | | | | | | | | | | | | | | | | | | | | |
| 10R-CC, 6–12 | 429.82 | P3 | late Paleocene | P | A | | | | | | | | | | | | | | | | | | | | | | | | | | | | | | | | | | | | | | | |
| 11R-3, 56–60 | 433.36 | P3 | late Paleocene | P | C | | | | | | | | | | | | | | | | | | | | | | | | | | | | | | | | | | | | | | | |
| 12R-2, 94–95 | 442.14 | P1 | early Paleocene | P | C | | | | | | | | | | | | | | | | | | | | | | | | | | | | | | | | | | | | | | | X |
| 12R-3, 67–68 | 443.37 | P1 | early Paleocene | P | C | | | | | | | | | | | | | | | | | | | | | | | | | | | | | | | | | | | | | | | X X |
| 12R-4, 53–54 | 444.23 | Pα | early Paleocene | P | C | | | | | | | | | | | | | | | | | | | | | | | | | | | | | | | | | | | | | | X | X X | | X | |
| 12R-CC, 17–21 | 444.52 | Pα | early Paleocene | M | A | | | | | | | | | | | | | | | | | | | | | | | | | | | | | | | | | | | | | | | X X | | | |
| 13R-1, 24–25 | 444.94 | Pα | early Paleocene | M | A | | | | | | | | | | | | | | | | | | | | | | | | | | | | | | | | | | | | | | X | | | | |
| 13R-CC, 13–17 | 454.51 | KS31 | Maastrichtian | P | A | | | | | | | | | | | | | | | | | | | | | | X | | | | X | | | | X | | X X | | | | X | | | | |
| 14R-CC, 0–5 | 461.51 | KS30a | Maastrichtian | M | C | | | | | | | X | | | | | | | | | | | X | | | | | | | | | | X | | X | X X | | | | | | | | |
| 15R-CC, 17–22 | 471.75 | KS30b | Maastrichtian–late Campanian | P | A | | | | | | | | | | | | | | | | | | | | | | | | X | | | X | X X X X | | | | | | | | | | | |
| 16R-3, 98–103 | 475.48 | KS29–30b | Maastrichtian–late Campanian | P | C | | | | | | | | | | | | | | | | | | | | | | X | | X X X | | | | | | | | | | | | | | | |
| 17R-CC, 21–25 | 486.40 | KS29 | late Campanian | M | F | | | | | | | | | | | | | | | | | | X X X | | X X | | | | | | | | | | | | | | | | | | |
| 18R-CC, 10–14 | 495.59 | Not defined | Santonian | M | F | | X | | | | X | | X | | X | | | | X X | | X X | | | | | | | | | | | | | | | | | | | | | | |
| 19R-3, 91–92 | 499.41 | Not defined | Santonian | G | C | | | | | | | X | | | X | | X X | | | | | | | | | | | | | | | | | | | | | | | | | | | |
| 20R-CC, 14–16 | 507.10 | Not defined | Turonian | G | F | | | X | | X | | X | X X | X | X | X | | | | | | | | | | | | | | | | | | | | | | | | | | | |
| 21R-CC, 34–40 | 519.01 | Not defined | Turonian | G | C | | | X | X X | | | X | | | | | | | | | | | | | | | | | | | | | | | | | | | | | | | |
| 22R-CC, 16–21 | 533.70 | Not defined | Turonian | M | C | X | | | X | | X | X | | | | | | | | | | | | | | | | | | | | | | | | | | | | | | | |
| 23R-CC, 0–5 | 541.98 | Not defined | Turonian | P | C | X | X | X | X | X | | | | | | | | | | | | | | | | | | | | | | | | | | | | | | | | | |
| 24R-CC, 0–5 | 550.72 | Barren | No age assignment | | B | | | | | | | | | | | | | | | | | | | | | | | | | | | | | | | | | | | | | | | |
| 25R-CC, 4–7 | 555.96 | Barren | No age assignment | | B | | | | | | | | | | | | | | | | | | | | | | | | | | | | | | | | | | | | | | | |

Notes: Preservation: G = good, M = moderate, P = poor. Abundance: A = abundant, C = common, F = few, R = rare, B = barren. Time constraints in shipboard observation of samples prevented us from recording all species observed in some samples between biostratigraphic datums. Hence, gaps in the ranges of some species should not be assumed to represent genuine absence of the species.

**Table T8 (continued).**

| Core, section, interval (cm) | Depth (mbsf) | Zone | Age | Preservation | Group abundance | *Praemurica taurica* | *Praemurica pseudoinconstans* | *Subbotina triloculinoides* | *Globanomalina ehrenbergi* | *Igorina albeari* | *Morozovella angulata* | *Parasubbotina varianta* | *Morozovella velascoensis* | *Subbotina velascoensis* | *Acarinina coalingensis* | *Acarinina soldadoensis* | *Morozovella acuta* | *Morozovella aequa* | *Morozovella occlusa* | *Chiloguembelina wilcoxensis* | *Morozovella apanthesma* | *Morozovella subbotinae* | *Subbotina triangularis* | *Pseudohastigerina micra* | *Morozovella gracilis* | *Morozovella marginodentata* | *Acarinina quetra* | *Acarinina wilcoxensis* | *Igorina broedermanni* | *Morozovella aragonensis* | *Morozovella formosa* | *Turborotalia praecentralis* | *Cassigerinella chipolensis* | *Chiloguembelina cubensis* | *Globigerina angulosuturalis* | *Globigerina ciperoensis* | *Globigerina praebulloides* | *Globoquadrina altispira globosa* | *Paragloborotalia opima nana* | *Tenuitella angustiumbilicata* | *Tenuitella munda* | *Turborotalia ampliapertura* |
|---|---|---|---|---|---|---|---|---|---|---|---|---|---|---|---|---|---|---|---|---|---|---|---|---|---|---|---|---|---|---|---|---|---|---|---|---|---|---|---|---|
| 207-1259B- | | | | | | | | | | | | | | | | | | | | | | | | | | | | | | | | | | | | | | | | |
| 1R-CC, 19–23 | 0.63 | P21b | early Oligocene | G | A | | | | | | | | | | | | | | | | | | | | | | | | | | | | X | | | X | X | X | X | X | X |
| 2R-CC, 16–21 | 314.78 | P8 | early Eocene | P | C | | | | | | | | | | | X | | | | | | | | | | X | X | X | X | | X | | | | | | | | | |
| 4R-CC, 15–20 | 330.74 | P7 | early Eocene | P | C | | | | | | | | | | | X | | | | | | | | X | X | X | X | X | X | | X | | | | | | | | | |
| 5R-CC, 15–18 | 343.68 | P6 | early Eocene | P | C | | | | | | | | | | | X | | | | | | X | X | | X | X | | | | | | | | | | | | | | |
| 6R-CC, 10–16 | 346.45 | P5 | early Eocene | P | C | | | | | | | | | | | X | X | | | X | | X | X | X | | | | | | | | | | | | | | | | |
| 7R-CC, 0–4 | 362.57 | P5 | early Eocene | P | C | | | | | | | | | | | X | X | | X | X | X | X | X | | | | | | | | | | | | | | | | | |
| 8R-CC, 8–13 | 370.16 | P5 | late Paleocene | M | C | | | | | | | | X | | X | X | X | X | X | | | | | | | | | | | | | | | | | | | | | |
| 9R-1, 40–42 | 372.7 | P5 | late Paleocene | M | C | | | | | | | | X | | X | X | X | X | X | | | | | | | | | | | | | | | | | | | | | |
| 10R-CC, 6–12 | 429.82 | P3 | late Paleocene | P | A | | | | | X | X | | X | X | | | | | | | | | | | | | | | | | | | | | | | | | | |
| 11R-3, 56–60 | 433.36 | P3 | late Paleocene | P | C | | | X | X | X | X | X | | | | | | | | | | | | | | | | | | | | | | | | | | | | |
| 12R-2, 94–95 | 442.14 | P1 | early Paleocene | P | C | | X | X | | | | | | | | | | | | | | | | | | | | | | | | | | | | | | | | |
| 12R-3, 67–68 | 443.37 | P1 | early Paleocene | P | C | X | | | | | | | | | | | | | | | | | | | | | | | | | | | | | | | | | | |
| 12R-4, 53–54 | 444.23 | Pα | early Paleocene | P | C | | | | | | | | | | | | | | | | | | | | | | | | | | | | | | | | | | | |
| 12R-CC, 17–21 | 444.52 | Pα | early Paleocene | M | A | | | | | | | | | | | | | | | | | | | | | | | | | | | | | | | | | | | |
| 13R-1, 24–25 | 444.94 | Pα | early Paleocene | M | A | | | | | | | | | | | | | | | | | | | | | | | | | | | | | | | | | | | |
| 13R-CC, 13–17 | 454.51 | KS31 | Maastrichtian | P | A | | | | | | | | | | | | | | | | | | | | | | | | | | | | | | | | | | | |
| 14R-CC, 0–5 | 461.51 | KS30a | Maastrichtian | M | C | | | | | | | | | | | | | | | | | | | | | | | | | | | | | | | | | | | |
| 15R-CC, 17–22 | 471.75 | KS30b | Maastrichtian–late Campanian | P | A | | | | | | | | | | | | | | | | | | | | | | | | | | | | | | | | | | | |
| 16R-3, 98–103 | 475.48 | KS29-30b | Maastrichtian–late Campanian | P | C | | | | | | | | | | | | | | | | | | | | | | | | | | | | | | | | | | | |
| 17R-CC, 21–25 | 486.4 | KS29 | late Campanian | M | F | | | | | | | | | | | | | | | | | | | | | | | | | | | | | | | | | | | |
| 18R-CC, 10–14 | 495.59 | Not defined | Santonian | M | F | | | | | | | | | | | | | | | | | | | | | | | | | | | | | | | | | | | |
| 19R-3, 91–92 | 499.41 | Not defined | Santonian | G | C | | | | | | | | | | | | | | | | | | | | | | | | | | | | | | | | | | | |
| 20R-CC, 14–16 | 507.1 | Not defined | Turonian | G | F | | | | | | | | | | | | | | | | | | | | | | | | | | | | | | | | | | | |
| 21R-CC, 34–40 | 519.01 | Not defined | Turonian | G | C | | | | | | | | | | | | | | | | | | | | | | | | | | | | | | | | | | | |
| 22R-CC, 16–21 | 533.7 | Not defined | Turonian | M | C | | | | | | | | | | | | | | | | | | | | | | | | | | | | | | | | | | | |
| 23R-CC, 0–5 | 541.98 | Not defined | Turonian | P | C | | | | | | | | | | | | | | | | | | | | | | | | | | | | | | | | | | | |
| 24R-CC, 0–5 | 550.72 | Barren | No age assignment | | B | | | | | | | | | | | | | | | | | | | | | | | | | | | | | | | | | | | |
| 25R-CC, 4–7 | 555.96 | Barren | No age assignment | | B | | | | | | | | | | | | | | | | | | | | | | | | | | | | | | | | | | | |

**Table T9.** Distribution of planktonic foraminifers, Hole 1259C. (Continued on next page.)

| Core, section, interval (cm) | Depth (mbsf) | Zone | Age | Preservation | Group abundance | *Heterohelix globulosa* | *Whiteinella bosquensis* | *Hedbergella delrioensis* | *Whiteinella baltica* | *Whiteinella archaeocretacea* | *Whiteinella inornata* | *Dicarinella* sp. 1 | *Archaeoglobigerina cretacea* | *Contusotruncana fornicata* | *Abathomphalus mayaroensis* | *Contusotruncana contusa* | *Gansserina gansseri* | *Globotruncanita stuarti* | *Pseudotextularia elegans* | *Rugoglobigerina rugosa* | *Globigerinelloides prairiehillensis* | *Globotruncana aegyptiaca* | *Pseudoguembelina excolata* | *Rugoglobigerina rotundata* | *Rugoglobigerina scotti* | *Parasubbotina pseudobulloides* | *Praemurica inconstans* | *Praemurica taurica* | *Globanomalina compressa* | *Praemurica pseudoinconstans* | *Subbotina triloculinoides* | *Acarininasibaiyaensis* | *Acarinina africana* | *Acarinina soldadoensis* | *Morozovella allisonensis* | *Parasubbotina varianta* | *Subbotina patagonica* | *Acarinina coalingensis* | *Chiloguembelina wilcoxensis* | *Morozovella aequa* |
|---|---|---|---|---|---|---|---|---|---|---|---|---|---|---|---|---|---|---|---|---|---|---|---|---|---|---|---|---|---|---|---|---|---|---|---|---|---|---|---|
| 207-1259C- | | | | | | | | | | | | | | | | | | | | | | | | | | | | | | | | | | | | | | | |
| 1R-CC, 13–18 | 312.86 | P7 | early Eocene | P | C | | | | | | | | | | | | | | | | | | | | | | | | | | | | | X | | | | | |
| 2R-CC, 9–14 | 326.48 | P6 | early Eocene | P | A | | | | | | | | | | | | | | | | | | | | | | | | | | | | | X | | | X | | |
| 3R-CC, 15–20 | 334.08 | P6 | early Eocene | P | A | | | | | | | | | | | | | | | | | | | | | | | | | | | | | X | | | X | | X |
| 4R-CC, 0–5 | 343.53 | P6 | early Eocene | P | C | | | | | | | | | | | | | | | | | | | | | | | | | | | | | X | | | X | | X |
| 5R-CC, 21–23 | 354.74 | P6 | early Eocene | M | C | | | | | | | | | | | | | | | | | | | | | | | | | | | | | X | | | | | X |
| 6R-CC, 10–13 | 363.49 | P5 | early Eocene | M | A | | | | | | | | | | | | | | | | | | | | | | | | | | | | | X | X | | X | X | X |
| 7R-2, 0–2 | 365.35 | P5 | early Eocene | P | F | | | | | | | | | | | | | | | | | | | | | | | | | | | | | X | | | X | X | X |
| 7R-2, 70–72 | 366.05 | P5 | early Eocene | M | A | | | | | | | | | | | | | | | | | | | | | | | | | | | X | X | X | X | X | X | | |
| 7R-2, 100–102 | 366.35 | | | B | B | | | | | | | | | | | | | | | | | | | | | | | | | | | | | | | | | | |
| 7R-2, 108–110 | 366.43 | | | B | B | | | | | | | | | | | | | | | | | | | | | | | | | | | | | | | | | | |
| 7R-2, 115–117 | 366.50 | | | B | B | | | | | | | | | | | | | | | | | | | | | | | | | | | | | | | | | | |
| 7R-CC, 8–10 | 367.72 | | | B | B | | | | | | | | | | | | | | | | | | | | | | | | | | | | | | | | | | |
| 8R-1, 89–91 | 436.89 | P1c | late Paleocene | P | A | | | | | | | | | | | | | | | | | | | | | | | X | | X | X | X | | | | | | | |
| 8R-3, 20–22 | 439.20 | P1c | late Paleocene | P | A | | | | | | | | | | | | | | | | | | | | | X | X | X | | | | | | | | | | | |
| 8R-7, 66–68 | 445.15 | KS31 | Maastrichtian | P | A | | | | | | | | | | X | | | X | X | X | X | X | X | X | X | | | | | | | | | | | | | | |
| 8R-CC, 16–21 | 445.95 | KS31 | Maastrichtian | P | A | | | | | | | | | | X | X | X | X | X | X | | | | | | | | | | | | | | | | | | | |
| 10R-CC, 0–5 | 490.26 | | | B | B | | | | | | | | | | | | | | | | | | | | | | | | | | | | | | | | | | |
| 11R-5, 106–111 | 495.99 | Not defined | Santonian | M | C | X | | | | | | X | X | X | | | | | | | | | | | | | | | | | | | | | | | | | |
| 12R-CC, 21–26 | 501.91 | Not defined | No age assignment | P | C | X | | | | | | | | | | | | | | | | | | | | | | | | | | | | | | | | | |
| 13R-CC, 0–5 | 505.75 | Not defined | No age assignment | P | R | X | | | X | | | | | | | | | | | | | | | | | | | | | | | | | | | | | | |
| 14R-CC, 18–23 | 511.22 | | | B | B | | | | | | | | | | | | | | | | | | | | | | | | | | | | | | | | | | |
| 15R-2, 141–146 | 516.71 | Not defined | Turonian | G | C | X | | X | | X | X | | | | | | | | | | | | | | | | | | | | | | | | | | | | |
| 16R-CC, 5–10 | 527.38 | Not defined | Turonian | G | C | X | X | X | | | | | | | | | | | | | | | | | | | | | | | | | | | | | | | |
| 17R-CC, 26–31 | 535.62 | Not defined | No age assignment | P | R | X | | | | | | | | | | | | | | | | | | | | | | | | | | | | | | | | | |
| 18R-CC, 0–5 | 544.54 | | | B | B | | | | | | | | | | | | | | | | | | | | | | | | | | | | | | | | | | |

Notes: Preservation: G = good, M = moderate, P = poor, B = barren. Abundance: A = abundant, C = common, F = few, R = rare, B = barren. Time constraints in shipboard observation of samples prevented the scientific party from recording all species observed in some samples between biostratigraphic datums. Hence, gaps in the ranges of some species should not be assumed to represent genuine absence of the species.

**Table T9 (continued).**

| Core, section, interval (cm) | Depth (mbsf) | Zone | Age | Preservation | Group abundance | *Morozovella subbotinae* | *Acarinina wilcoxensis* | *Igorina broedermanni* | *Morozovella velascoensis* | *Acarinina quetra* | *Morozovella gracilis* | *Morozovella marginodentata* | *Morozovella lensiformis* | *Subbotina triangularis* | *Morozovella aragonensis* | *Morozovella formosa* |
|---|---|---|---|---|---|---|---|---|---|---|---|---|---|---|---|---|
| 207-1259C- | | | | | | | | | | | | | | | | |
| 1R-CC, 13–18 | 312.86 | P7 | early Eocene | P | C | | | X | | X | | | | | X | X |
| 2R-CC, 9–14 | 326.48 | P6 | early Eocene | P | A | X | | | | X | X | | X | X | | |
| 3R-CC, 15–20 | 334.08 | P6 | early Eocene | P | A | X | | | | X | X | X | | | | |
| 4R-CC, 0–5 | 343.53 | P6 | early Eocene | P | C | X | | | | X | | | | | | |
| 5R-CC, 21–23 | 354.74 | P6 | early Eocene | M | C | X | X | | | X | | | | | | |
| 6R-CC, 10–13 | 363.49 | P5 | early Eocene | M | A | X | X | X | X | | | | | | | |
| 7R-2, 0–2 | 365.35 | P5 | early Eocene | P | F | X | | | | | | | | | | |
| 7R-2, 70–72 | 366.05 | P5 | early Eocene | M | A | | | | | | | | | | | |
| 7R-2, 100–102 | 366.35 | | | B | B | | | | | | | | | | | |
| 7R-2, 108–110 | 366.43 | | | B | B | | | | | | | | | | | |
| 7R-2, 115–117 | 366.50 | | | B | B | | | | | | | | | | | |
| 7R-CC, 8–10 | 367.72 | | | B | B | | | | | | | | | | | |
| 8R-1, 89–91 | 436.89 | P1c | late Paleocene | P | A | | | | | | | | | | | |
| 8R-3, 20–22 | 439.20 | P1c | late Paleocene | P | A | | | | | | | | | | | |
| 8R-7, 66–68 | 445.15 | KS31 | Maastrichtian | P | A | | | | | | | | | | | |
| 8R-CC, 16–21 | 445.95 | KS31 | Maastrichtian | P | A | | | | | | | | | | | |
| 10R-CC, 0–5 | 490.26 | | | B | B | | | | | | | | | | | |
| 11R-5, 106–111 | 495.99 | Not defined | Santonian | M | C | | | | | | | | | | | |
| 12R-CC, 21–26 | 501.91 | Not defined | No age assignment | P | C | | | | | | | | | | | |
| 13R-CC, 0–5 | 505.75 | Not defined | No age assignment | P | R | | | | | | | | | | | |
| 14R-CC, 18–23 | 511.22 | | | B | B | | | | | | | | | | | |
| 15R-2, 141–146 | 516.71 | Not defined | Turonian | G | C | | | | | | | | | | | |
| 16R-CC, 5–10 | 527.38 | Not defined | Turonian | G | C | | | | | | | | | | | |
| 17R-CC, 26–31 | 535.62 | Not defined | No age assignment | P | R | | | | | | | | | | | |
| 18R-CC, 0–5 | 544.54 | | | B | B | | | | | | | | | | | |

**Table T10.** Characteristic directions of minicores, Holes 1259A and 1259B. (**See table notes.** Continued on next two pages.)

| Core, section, interval (cm) | PMAG code | Depth (mcd) | Polarity Label | Polarity Code | Chron/ subchron | Declination (°) | Inclination (°) | Intensity (mA/m) | MAD (°) | N | Temperature steps used in least-square analysis (°C) 1 | 2 | 3 | 4 | 5 | 6 | 7 | 8 | 9 | 10 | 11 | 12 |
|---|---|---|---|---|---|---|---|---|---|---|---|---|---|---|---|---|---|---|---|---|---|---|
| 207-1259A- | | | | | | | | | | | | | | | | | | | | | | |
| 15R-1, 86 | 151.086 | 131.76 | N | 4 | C15n? | 11.2 | –8.6 | 5.67E–01 | 1.9 | 6 | 150 | 200 | 250 | 300 | 350 | 400 | Org | Tied | | | | |
| 15R-3, 13 | 153.013 | 134.03 | NP | 3 | | 57.1 | –5.0 | 8.42E–03 | 8.3 | 8 | 150 | 200 | 250 | 300 | 350 | 350 | 400 | 400 | Org | Tied | | |
| 16R-1, 6 | 161.006 | 140.66 | R? | –1 | | 66.2 | –2.8 | 8.66E–03 | 7.8 | 4 | 250 | 350 | 400 | 400 | Org | Tied | | | | | | |
| | | | | | Hiatus | | | | | | | | | | | | | | | | | |
| 16R-3, 83 | 163.083 | 144.43 | N? | 1 | C17r? | 356.3 | 8.4 | 4.37E–03 | 3.8 | 2 | 50 | 50 | Org | Tied | | | | | | | | |
| 17R-1, 11 | 171.011 | 150.31 | RP | –3 | | 93.7 | –0.8 | 1.81E–02 | 3.8 | 4 | 250 | 300 | 350 | 400 | Org | Tied | | | | | | |
| 18R-1, 10 | 181.010 | 159.90 | R | –4 | | 106.0 | –13.7 | 1.35E–02 | 3.6 | 5 | 200 | 250 | 300 | 350 | 400 | Org | Tied | | | | | |
| | | | | | Gap in coverage | | | | | | | | | | | | | | | | | |
| 19R-1, 84 | 191.084 | 170.34 | R? | –1 | | 194.9 | –4.5 | 2.54E–02 | 0.6 | 5 | 200 | 250 | 300 | 350 | 400 | Org | Tied | | | | | |
| 19R-2, 15 | 192.015 | 171.15 | RP | –3 | C18r | 277.2 | –3.2 | 8.54E–03 | 4.9 | 7 | 200 | 250 | 300 | 350 | 350 | 400 | 400 | Org | Tied | | | |
| 19R-5, 31 | 195.031 | 175.81 | R | –4 | | 297.5 | 4.9 | 3.02E–02 | 2.5 | 6 | 150 | 200 | 250 | 300 | 350 | 400 | Org | Tied | | | | |
| 20R-1, 8 | 201.008 | 179.28 | RP | –3 | | 56.1 | 5.9 | 2.71E–02 | 2.6 | 5 | 200 | 250 | 300 | 350 | 400 | Org | Tied | | | | | |
| 20R-3, 34 | 203.034 | 182.54 | RP | –3 | | 269.5 | 13.8 | 1.29E–02 | 2.5 | 5 | 200 | 250 | 300 | 350 | 400 | Org | Tied | | | | | |
| 20R-5, 42 | 205.042 | 185.52 | RP | –3 | | 109.7 | –2.5 | 1.15E–02 | 4.3 | 5 | 200 | 250 | 300 | 350 | 400 | Org | Tied | | | | | |
| 21R-1, 43 | 211.043 | 189.23 | NP | 3 | C19n | 109.2 | –8.9 | 8.88E–03 | 2.6 | 2 | 350 | 400 | Org | Tied | | | | | | | | |
| 21R-3, 71 | 213.071 | 192.51 | RP | –3 | C19r | 163.8 | 9.0 | 1.50E–02 | 2.9 | 3 | 300 | 350 | 400 | Org | Tied | | | | | | | |
| 22R-1, 31 | 221.031 | 198.81 | R | –4 | | 327.7 | 15.7 | 1.15E–02 | 3.3 | 4 | 250 | 300 | 350 | 400 | Org | Tied | | | | | | |
| 22R-3, 44 | 223.044 | 201.94 | R | –4 | | 126.6 | –0.6 | 2.26E–02 | 2.2 | 4 | 250 | 300 | 350 | 400 | Org | Tied | | | | | | |
| 22R-5, 12 | 225.012 | 204.62 | R | –4 | | 308.0 | 5.9 | 1.60E–02 | 3.5 | 5 | 200 | 250 | 300 | 350 | 400 | Org | Tied | | | | | |
| 23R-1, 83 | 231.083 | 208.93 | NP | 3 | C20n | 81.5 | –14.7 | 1.04E–02 | 7.0 | 5 | 200 | 250 | 300 | 350 | 400 | Org | Tied | | | | | |
| 23R-3, 85 | 233.085 | 211.93 | N | 4 | | 343.3 | –9.1 | 8.72E–03 | 2.6 | 5 | 200 | 250 | 300 | 350 | 400 | Org | Tied | | | | | |
| 23R-5, 33 | 235.033 | 213.93 | NP | 3 | | 206.6 | –3.3 | 7.51E–03 | 3.4 | 7 | 200 | 200 | 250 | 300 | 350 | 400 | 400 | Org | Tied | | | |
| 24R-1, 40 | 241.040 | 218.20 | N | 4 | | 270.3 | –3.6 | 1.19E–02 | 2.3 | 4 | 200 | 250 | 300 | 350 | Org | Tied | | | | | | |
| 25R-1, 31 | 251.031 | 227.51 | NP | 3 | | 82.5 | –4.0 | 1.67E–02 | 3.2 | 4 | 200 | 250 | 300 | 350 | Org | Tied | | | | | | |
| 25R-3, 33 | 253.033 | 230.53 | R | –4 | C20r | 30.6 | 4.4 | 8.70E–03 | 4.1 | 6 | 200 | 250 | 300 | 350 | 400 | 400 | Org | Tied | | | | |
| 26R-1, 13 | 261.013 | 237.04 | R | –4 | | 138.8 | 15.1 | 1.40E–02 | 3.0 | 5 | 200 | 250 | 300 | 350 | 400 | Org | Tied | | | | | |
| 26R-3, 11 | 263.011 | 240.01 | RP | –3 | | 105.7 | 3.3 | 1.52E–02 | 3.5 | 5 | 200 | 250 | 300 | 350 | 400 | Org | Tied | | | | | |
| 26R-5, 119 | 265.119 | 244.09 | R | –4 | | 21.5 | –1.8 | 1.77E–02 | 2.9 | 5 | 200 | 250 | 300 | 350 | 400 | Org | Tied | | | | | |
| 27R-1, 138 | 271.138 | 247.88 | R | –4 | | 245.1 | 1.4 | 2.03E–02 | 2.7 | 4 | 250 | 300 | 350 | 400 | Org | Tied | | | | | | |
| 27R-3, 84 | 273.084 | 250.34 | RP | –3 | | 117.6 | 6.0 | 2.66E–02 | 3.8 | 4 | 200 | 250 | 300 | 350 | Org | Tied | | | | | | |
| 27R-5, 65 | 275.065 | 253.15 | RP | –3 | | 195.0 | 5.7 | 1.63E–02 | 4.6 | 2 | 300 | 350 | Org | Tied | | | | | | | | |
| 28R-1, 58 | 281.058 | 256.78 | R | –4 | | 121.0 | 4.1 | 2.57E–02 | 2.9 | 6 | 200 | 250 | 300 | 350 | 350 | 400 | Org | Tied | | | | |
| | | | | | Gap in coverage | | | | | | | | | | | | | | | | | |
| 29R-1, 32 | 291.032 | 266.12 | NP | 3 | C21n | 295.3 | 17.0 | 1.87E–02 | 3.6 | 6 | 150 | 200 | 250 | 300 | 350 | 400 | Org | Tied | | | | |
| 29R-3, 28 | 293.028 | 269.08 | N | 4 | | 3.7 | 9.5 | 2.02E–02 | 2.5 | 6 | 150 | 200 | 250 | 300 | 350 | 400 | Org | Tied | | | | |
| 29R-5, 63 | 295.063 | 272.43 | RP | –3 | C21r | 99.4 | 1.3 | 1.35E–02 | 2.0 | 3 | 250 | 300 | 350 | Org | Tied | | | | | | | |
| 30R-1, 90 | 301.090 | 276.40 | N | 4 | ? | 250.0 | –2.6 | 3.01E–02 | 1.4 | 5 | 200 | 250 | 300 | 350 | 400 | Org | Tied | | | | | |
| 30R-3, 58 | 303.058 | 279.08 | RPP | –2 | | 99.9 | –7.4 | 1.52E–02 | 1.3 | 2 | 350 | 400 | Org | Tied | | | | | | | | |
| 31R-1, 108 | 311.108 | 286.18 | N | 4 | C22n | 304.4 | –5.1 | 1.27E–01 | 2.7 | 6 | 150 | 200 | 250 | 300 | 350 | 400 | Org | Tied | | | | |
| 32R-1, 67 | 321.067 | 295.38 | NP | 3 | | 11.0 | 39.7 | 2.76E–02 | 6.5 | 5 | 200 | 250 | 300 | 350 | 400 | Org | Tied | | | | | |
| 32R-2, 29 | 322.029 | 296.42 | N | 4 | | 331.2 | –3.1 | 1.39E+00 | 1.4 | 6 | 150 | 200 | 250 | 300 | 350 | 400 | Org | Tied | | | | |
| | | | | | Hiatus? and gap in coverage | | | | | | | | | | | | | | | | | |
| 34R-1, 31 | 341.031 | 314.17 | N | 4 | | 27.0 | 17.2 | 3.86E–02 | 2.6 | 5 | 200 | 250 | 300 | 350 | 400 | Org | Tied | | | | | |
| 34R-3, 35 | 343.035 | 317.22 | N? | 1 | | 347.8 | 46.3 | 9.08E–01 | 2.1 | 5 | 200 | 250 | 300 | 350 | 400 | Org | Tied | | | | | |
| 34R-5, 78 | 345.078 | 320.65 | N | 4 | | 275.4 | –4.5 | 3.58E–02 | 5.0 | 4 | 250 | 300 | 350 | 400 | Org | Tied | | | | | | |
| 43R-1, 33 | 431.033 | 402.20 | RP | –3 | C25r? | 236.0 | –28.1 | 1.52E–02 | 9.3 | 4 | 200 | 250 | 300 | 400 | Org | Tied | | | | | | |
| 44R-1, 65 | 441.065 | 412.23 | N | 4 | ? | 341.4 | 19.1 | 7.03E–02 | 2.1 | 3 | 250 | 300 | 350 | Org | Tied | | | | | | | |

## Table T10 (continued).

| Core, section, interval (cm) | PMAG code | Depth (mcd) | Polarity Label | Polarity Code | Chron/ subchron | Declination (°) | Inclination (°) | Intensity (mA/m) | MAD (°) | N | Temperature steps used in least-square analysis (°C) 1 | 2 | 3 | 4 | 5 | 6 | 7 | 8 | 9 | 10 | 11 | 12 |
|---|---|---|---|---|---|---|---|---|---|---|---|---|---|---|---|---|---|---|---|---|---|---|
| 44R-3, 94 | 443.094 | 415.51 | RP | –3 | | 346.0 | 34.8 | 6.83E–03 | 4.0 | 4 | 200 | 250 | 300 | 300 | Org | Tied | | | | | | |
| 44R-5, 31 | 445.031 | 417.88 | NP | 3 | C26n? | 95.8 | 26.4 | 1.82E–01 | 3.2 | 3 | 250 | 300 | 350 | Org | Tied | | | | | | | |
| 44R-6, 17 | 446.017 | 419.24 | NP | 3 | | 102.4 | 2.0 | 1.30E–01 | 3.6 | 6 | 150 | 200 | 250 | 300 | 350 | 400 | Org | Tied | | | | |
| 47R-4, 3 | 474.003 | 444.59 | RP | –3 | C29r | 155.8 | –4.2 | 1.02E–02 | 8.7 | 8 | 200 | 200 | 225 | 225 | 250 | 300 | 300 | 350 | Org | Tied | | |
| 47R-5, 11 | 475.011 | 446.17 | RP | –3 | | 125.9 | 1.8 | 2.29E–02 | 6.8 | 4 | 300 | 300 | 330 | 360 | Org | Tied | | | | | | |
| 47R-CC, 24 | 479.024 | 447.82 | RP | –3 | | 90.5 | –6.2 | 1.33E–02 | 8.3 | 6 | 200 | 200 | 225 | 250 | 300 | 350 | Org | Tied | | | | |
| 48R-1, 5 | 481.005 | 448.86 | RP | –3 | | 143.2 | 10.8 | 1.12E–02 | 12.5 | 4 | 250 | 300 | 350 | 350 | Org | Tied | | | | | | |
| 48R-2, 3 | 482.003 | 450.34 | NP | 3 | C30n | 60.2 | –0.3 | 5.12E–03 | 8.4 | 5 | 150 | 150 | 200 | 200 | 240 | Org | Tied | | | | | |
| 48R-3, 7 | 483.007 | 451.88 | NP | 3 | to | 354.3 | 9.1 | 4.53E–03 | 3.1 | 4 | 225 | 225 | 225 | 225 | Org | Tied | | | | | | |
| 48R-4, 3 | 484.003 | 453.34 | NP | 3 | C31n | 25.1 | –0.1 | 7.67E–03 | 10.3 | 7 | 150 | 200 | 200 | 225 | 225 | 250 | 250 | Org | Tied | | | |
| 48R-5, 4 | 485.004 | 454.84 | NP | 3 | | 33.1 | 36.0 | 7.06E–03 | 8.0 | 4 | 150 | 150 | 200 | 200 | Org | Tied | | | | | | |
| 48R-6, 6 | 486.006 | 456.37 | NP | 3 | | 46.1 | –8.7 | 6.26E–03 | 9.8 | 8 | 150 | 150 | 200 | 200 | 225 | 225 | 250 | 250 | Org | Tied | | |
| 48R-7, 3 | 487.003 | 457.84 | N? | 1 | | 64.4 | –19.6 | 3.46E–03 | 3.4 | 3 | 150 | 150 | 150 | Org | Tied | | | | | | | |
| 49R-1, 4 | 491.004 | 459.30 | NP | 3 | | 11.1 | –11.8 | 7.36E–03 | 4.8 | 6 | 150 | 200 | 200 | 240 | 240 | 270 | Org | Tied | | | | |
| 49R-2, 18 | 492.018 | 460.94 | N? | 1 | | 13.2 | 34.9 | 4.51E–03 | 0.7 | 2 | 150 | 150 | Org | Tied | | | | | | | | |
| 49R-3, 3 | 493.003 | 462.12 | NP | 3 | | 2.7 | 25.9 | 1.42E–02 | 7.0 | 4 | 50 | 150 | 200 | 200 | | | | | | | | |
| 49R-4, 11 | 494.011 | 463.70 | R? | –1 | | 95.5 | –2.2 | 5.49E–03 | 7.8 | 6 | 150 | 150 | 200 | 200 | 225 | 225 | Org | Tied | | | | |
| 49R-5, 16 | 495.016 | 465.19 | R? | –1 | | 119.2 | 25.0 | 6.09E–03 | 4.5 | 4 | 150 | 150 | 200 | 200 | Org | Tied | | | | | | |
| 49R-6, 14 | 496.014 | 466.65 | R? | –1 | | 260.0 | 48.8 | 4.82E–03 | 0.0 | 0 | 200 | Org | Tied | | | | | | | | | |
| 50R-1, 7 | 501.007 | 468.60 | NP | 3 | | 43.7 | 14.5 | 2.48E–02 | 1.6 | 4 | 50 | 150 | 200 | 250 | | | | | | | | |
| 50R-2, 7 | 502.007 | 470.10 | RPP | –2 | C31r | 261.4 | –1.2 | 1.05E–02 | 6.7 | 4 | 250 | 300 | 350 | 400 | Org | Tied | | | | | | |
| 50R-3, 7 | 503.007 | 471.42 | RPP | –2 | | 147.2 | 9.1 | 4.26E–03 | 3.5 | 2 | 250 | 250 | Org | Tied | | | | | | | | |
| 50R-4, 7 | 504.007 | 472.92 | RPP | –2 | | 247.4 | –7.9 | 6.61E–03 | 1.8 | 2 | 240 | 240 | Org | Tied | | | | | | | | |
| 50R-5, 7 | 505.007 | 474.29 | RP | –3 | | 309.3 | –8.3 | 7.29E–03 | 4.7 | 4 | 200 | 250 | 300 | 300 | Org | Tied | | | | | | |
| 50R-6, 7 | 506.007 | 475.78 | N? | 1 | | 338.1 | 51.6 | 3.10E–03 | 3.7 | 2 | 150 | 150 | Org | Tied | | | | | | | | |
| 50R-7, 7 | 507.007 | 476.63 | R? | –1 | | 121.8 | 17.2 | 3.38E–03 | 20.9 | 2 | 150 | 200 | Org | Tied | | | | | | | | |
| 51R-1, 5 | 511.005 | 477.98 | R? | –1 | | 216.8 | –74.1 | 2.09E–03 | 11.8 | 2 | 200 | 200 | Org | Tied | | | | | | | | |
| 51R-2, 3 | 512.003 | 479.46 | RPP | –2 | | 316.1 | –73.5 | 5.59E–03 | 3.2 | 4 | 250 | 250 | 300 | 300 | Org | Tied | | | | | | |
| 51R-3, 10 | 513.010 | 481.03 | N? | 1 | C32n? | 105.3 | 67.9 | 3.99E–03 | 1.3 | 2 | 150 | 150 | Org | Tied | | | | | | | | |
| 51R-4, 3 | 514.003 | 482.46 | N? | 1 | | 149.5 | 34.7 | 4.49E–03 | 4.9 | 2 | 150 | 150 | Org | Tied | | | | | | | | |
| 51R-5, 4 | 515.004 | 483.97 | N? | 1 | | 295.1 | 15.2 | 4.53E–03 | 1.5 | 2 | 150 | 150 | Org | Tied | | | | | | | | |
| 51R-6, 2 | 516.002 | 485.42 | RPP | –2 | ? | 341.6 | 10.4 | 5.76E–03 | 2.4 | 2 | 300 | 300 | Org | Tied | | | | | | | | |
| 51R-7, 3 | 517.003 | 486.93 | R? | –1 | | 267.8 | 38.7 | 5.53E–03 | 2.7 | 2 | 150 | 150 | Org | Tied | | | | | | | | |
| 51R-CC, 3 | 519.003 | 487.73 | RP | –3 | ? | 248.2 | –19.7 | 3.54E–03 | 5.0 | 4 | 270 | 270 | 300 | 300 | Org | Tied | | | | | | |
| 207-1259B- | | | | | | | | | | | | | | | | | | | | | | |
| 2R-1, 63 | 21.063 | 305.03 | N | 4 | C22n | 74.3 | 0.8 | 1.07E+00 | 1.3 | 7 | 200 | 240 | 270 | 300 | 330 | 360 | 400 | Org | Tied | | | |
| 2R-3, 61 | 23.061 | 308.01 | RPP | –2 | C22r | 351.7 | –32.2 | 6.80E–02 | 7.6 | 3 | 300 | 350 | 400 | Org | Tied | | | | | | | |
| 2R-5, 84 | 25.084 | 311.24 | RP | –3 | | 271.2 | 9.5 | 2.24E–02 | 2.4 | 4 | 250 | 300 | 350 | 400 | Org | Tied | | | | | | |
| 2R-7, 7 | 27.007 | 313.47 | N | 4 | C23n | 303.7 | 14.6 | 7.48E–02 | 2.9 | 5 | 270 | 300 | 330 | 360 | 400 | Org | Tied | | | | | |
| 4R-1, 64 | 41.064 | 315.34 | NP | 3 | | 80.8 | 10.4 | 3.96E–02 | 2.7 | 4 | 200 | 250 | 300 | 350 | Org | Tied | | | | | | |
| 4R-3, 14 | 43.014 | 317.84 | NP | 3 | | 53.7 | 0.3 | 7.52E–01 | 1.4 | 3 | 300 | 350 | 400 | Org | Tied | | | | | | | |
| 4R-5, 71 | 45.071 | 321.01 | N | 4 | | 41.5 | 2.5 | 1.63E+00 | 1.1 | 7 | 200 | 240 | 270 | 300 | 330 | 360 | 400 | Org | Tied | | | |
| | | | | | Hiatus? | | | | | | | | | | | | | | | | | |
| 5R-1, 5 | 51.005 | 335.30 | RP | –3 | C24r | 80.3 | 4.7 | 2.71E–02 | 3.4 | 5 | 200 | 250 | 300 | 350 | 400 | Org | Tied | | | | | |
| 5R-3, 7 | 53.007 | 338.32 | R | –4 | | 162.0 | –1.6 | 2.38E–02 | 2.4 | 5 | 270 | 300 | 330 | 360 | 400 | Org | Tied | | | | | |
| 5R-5, 4 | 55.004 | 341.29 | R | –4 | | 303.1 | –2.6 | 2.04E–02 | 4.5 | 4 | 250 | 300 | 350 | 400 | Org | Tied | | | | | | |
| 5R-7, 41 | 57.041 | 344.66 | R | –4 | | 299.7 | –0.9 | 1.46E–02 | 3.6 | 5 | 200 | 250 | 300 | 350 | 400 | Org | Tied | | | | | |

**Table T10 (continued).**

| Core, section, interval (cm) | PMAG code | Depth (mcd) | Polarity Label | Polarity Code | Chron/ subchron | Declination (°) | Inclination (°) | Intensity (mA/m) | MAD (°) | N | Temperature steps used in least-square analysis (°C) 1 | 2 | 3 | 4 | 5 | 6 | 7 | 8 | 9 | 10 | 11 | 12 |
|---|---|---|---|---|---|---|---|---|---|---|---|---|---|---|---|---|---|---|---|---|---|---|
| 6R-1, 22 | 61.022 | 346.75 | N? | 1 | | 29.9 | 0.4 | 9.26E–03 | 4.0 | 3 | 270 | 300 | 300 | Org | Tied | | | | | | | |
| 6R-2, 5 | 62.005 | 348.08 | NP | 3 | N within | 305.6 | –6.9 | 7.90E–03 | 4.0 | 3 | 350 | 400 | 400 | Org | Tied | | | | | | | |
| 6R-CC, 2 | 69.002 | 349.50 | NP | 3 | C24r? | 258.6 | 0.0 | 1.57E–02 | 3.6 | 5 | 200 | 250 | 300 | 350 | 400 | Org | Tied | | | | | |
| 7R-1, 37 | 71.037 | 355.20 | RP | –3 | | 280.7 | 6.3 | 2.39E–02 | 2.7 | 4 | 200 | 240 | 270 | 300 | Org | Tied | | | | | | |
| 7R-3, 8 | 73.008 | 357.91 | RP | –3 | C24r | 73.8 | –1.2 | 1.36E–02 | 3.7 | 4 | 250 | 300 | 350 | 400 | Org | Tied | | | | | | |
| 7R-5, 30 | 75.030 | 361.13 | R | –4 | | 217.8 | 11.3 | 1.46E–02 | 4.4 | 5 | 200 | 250 | 300 | 350 | 400 | Org | Tied | | | | | |
| 7R-7, 37 | 77.037 | 364.00 | RP | –3 | | 102.0 | 6.6 | 3.37E–02 | 3.2 | 6 | 150 | 200 | 240 | 270 | 300 | 330 | Org | Tied | | | | |
| 8R-1, 8 | 81.008 | 364.61 | R | –4 | | 190.4 | 15.9 | 2.77E–02 | 2.4 | 4 | 200 | 250 | 300 | 350 | Org | Tied | | | | | | |
| 8R-3, 5 | 83.005 | 367.58 | RPP | –2 | | 32.8 | 12.2 | 6.26E–03 | 2.7 | 2 | 350 | 350 | Org | Tied | | | | | | | | |
| 8R-CC, 3 | 89.003 | 371.94 | RP | –3 | | 248.8 | 5.5 | 1.41E–02 | 5.2 | 4 | 300 | 330 | 360 | 360 | Org | Tied | | | | | | |
| 9R-1, 33 | 91.033 | 374.46 | R | –4 | | 331.7 | –3.5 | 1.15E–02 | 6.4 | 9 | 200 | 225 | 250 | 250 | 300 | 300 | 350 | 400 | 400 | Org | Tied | |
| 10R-1, 6 | 101.006 | 418.76 | NP | 3 | C26n? | 53.7 | 12.3 | 1.13E–01 | 2.4 | 5 | 200 | 250 | 300 | 350 | 400 | Org | Tied | | | | | |
| 10R-3, 39 | 103.039 | 422.10 | INT | 0 | | 92.5 | 68.5 | 5.06E–03 | 3.7 | 2 | 150 | 150 | Org | Tied | | | | | | | | |
| 10R-5, 33 | 105.033 | 425.04 | R | –4 | C26r? | 93.3 | 9.4 | 7.57E–01 | 2.3 | 7 | 200 | 240 | 270 | 300 | 330 | 360 | 400 | Org | Tied | | | |
| 10R-7, 46 | 107.046 | 427.87 | RP | –3 | | 96.6 | –14.2 | 7.51E–03 | 3.2 | 4 | 300 | 350 | 350 | 400 | Org | Tied | | | | | | |
| 11R-1, 53 | 111.053 | 429.95 | R | –4 | | 127.4 | 3.7 | 4.17E–02 | 1.6 | 6 | 150 | 200 | 250 | 300 | 350 | 400 | Org | Tied | | | | |
| 11R-3, 2 | 113.002 | 432.14 | R | –4 | | 318.0 | 3.1 | 2.84E–02 | 1.8 | 6 | 150 | 200 | 250 | 300 | 350 | 400 | Org | Tied | | | | |
| 12R-1, 45 | 121.045 | 438.70 | R | –4 | | 304.8 | 8.0 | 6.05E–01 | 2.0 | 6 | 240 | 270 | 300 | 330 | 360 | 400 | Org | Tied | | | | |
| 13R-1, 3 | 131.003 | 443.27 | RP | –3 | C29r | 295.0 | –5.1 | 5.11E–02 | 2.2 | 8 | 200 | 240 | 270 | 270 | 300 | 330 | 360 | 400 | Org | Tied | | |
| 13R-2, 2 | 132.002 | 444.77 | RP | –3 | | 301.3 | –17.7 | 8.08E–03 | 2.5 | 3 | 300 | 350 | 350 | Org | Tied | | | | | | | |
| 13R-2, 100 | 132.100 | 445.75 | RPP | –2 | | 264.4 | –14.5 | 5.77E–03 | 5.4 | 4 | 300 | 300 | 350 | 350 | Org | Tied | | | | | | |
| 13R-5, 3 | 135.003 | 449.28 | NP | 3 | C30n | 45.8 | 0.2 | 4.47E–03 | 9.3 | 4 | 200 | 200 | 225 | 225 | Org | Tied | | | | | | |
| 13R-7, 3 | 137.003 | 452.29 | N? | 1 | to | 70.8 | 14.1 | 7.51E–03 | 2.5 | 2 | 150 | 150 | Org | Tied | | | | | | | | |
| 14R-1, 4 | 141.004 | 453.10 | NP | 3 | C31n | 66.0 | 24.3 | 8.31E–03 | 2.6 | 3 | 150 | 200 | 200 | Org | Tied | | | | | | | |
| 14R-3, 8 | 143.008 | 456.14 | NPP | 2 | | 164.7 | –2.1 | 6.23E–03 | 3.6 | 4 | 225 | 225 | 250 | 250 | Org | Tied | | | | | | |
| 14R-5, 5 | 145.005 | 459.11 | NPP | 2 | | 204.6 | 21.9 | 4.75E–03 | 3.1 | 2 | 200 | 200 | Org | Tied | | | | | | | | |
| 15R-1, 61 | 151.061 | 460.97 | NP | 3 | | 292.7 | –0.8 | 5.22E–03 | 2.8 | 4 | 200 | 200 | 240 | 240 | Org | Tied | | | | | | |
| 15R-3, 52 | 153.052 | 463.88 | NP | 3 | | 180.6 | 62.3 | 9.57E–03 | 1.1 | 3 | 150 | 200 | 200 | | | | | | | | | |
| 15R-5, 27 | 155.027 | 466.63 | R? | –1 | | 212.8 | –12.2 | 3.52E–03 | 6.5 | 2 | 200 | 200 | Org | Tied | | | | | | | | |
| 15R-7, 55 | 157.055 | 469.91 | NP | 3 | | 50.6 | 17.0 | 1.16E–02 | 5.4 | 6 | 50 | 150 | 200 | 200 | 225 | 225 | Org | Tied | | | | |
| 16R-1, 49 | 161.049 | 471.70 | RP | –3 | C31r | 80.1 | –18.5 | 5.98E–03 | 10.3 | 6 | 300 | 300 | 330 | 330 | 360 | 360 | Org | Tied | | | | |
| 16R-3, 53 | 163.053 | 474.74 | INT | 0 | | 73.6 | 48.5 | 3.15E–03 | 0.0 | 2 | 200 | 200 | | | | | | | | | | |
| 17R-1, 11 | 171.011 | 475.67 | RP | –3 | | 321.4 | 51.8 | 5.29E–03 | 6.2 | 7 | 200 | 225 | 225 | 250 | 250 | 300 | 300 | Org | Tied | | | |
| 17R-3, 6 | 173.006 | 478.62 | RPP | –2 | | 145.2 | –42.7 | 1.51E–02 | 5.7 | 10 | 150 | 200 | 200 | 240 | 270 | 300 | 330 | 330 | 360 | 400 | Org | Tied |
| 17R-5, 77 | 175.077 | 482.33 | NP | 3 | C32n? | 32.4 | 44.9 | 2.49E–03 | 9.2 | 6 | 225 | 225 | 250 | 250 | 300 | 300 | Org | Tied | | | | |
| 17R-7, 10 | 177.010 | 484.66 | NP | 3 | | 115.2 | 35.4 | 5.21E–03 | 7.2 | 6 | 200 | 200 | 225 | 225 | 250 | 250 | Org | Tied | | | | |
| 18R-1, 9 | 181.009 | 485.94 | RP | –3 | ? | 109.7 | 54.1 | 4.41E–03 | 5.7 | 4 | 240 | 240 | 270 | 270 | Org | Tied | | | | | | |
| 18R-2, 7 | 182.007 | 487.41 | NPP | 2 | ? | 352.2 | 21.8 | 5.44E–03 | 7.8 | 8 | 150 | 200 | 200 | 225 | 225 | 250 | 300 | 300 | Org | Tied | | |

Note: PMAG = paleomagnetism, MAD = maximum angular deviation. R = reversed polarity, N = normal polarity. RP and NP = less precise reversed and normal polarity assignments, respectively. RPP and NPP = sample did not achieve adequate cleaning during demagnetization but polarity was obviously reversed or normal, respectively. Orig. = origin. Black = normal polarity, white = reversed polarity, gray = intermediate or questionable polarity, yellow = gap in coverage or hiatus. Examples of interpretation of progressive demagnetization plots and methods of computation of the characteristic directions are given in **"Paleomagnetism,"** p. 16, in the "Explanatory Notes" chapter.

**Table T11.** Composite depths, Site 1259.

| Core | Depth (mbsf) | Offset (m) | Depth (mcd) | Depth shifted |
|---|---|---|---|---|
| 207-1259A- | | | | |
| 1R | 0.0 | 0.00 | 0.00 | N |
| 2R | 8.8 | 0.00 | 8.80 | N |
| 3R | 18.3 | 0.00 | 18.30 | N |
| 4R | 27.3 | 0.00 | 27.30 | N |
| 5R | 36.4 | 0.00 | 36.40 | N |
| 6R | 45.5 | 0.00 | 45.50 | N |
| 7R | 54.6 | 0.00 | 54.60 | N |
| 8R | 63.8 | 0.00 | 63.80 | N |
| 9R | 72.9 | 0.00 | 72.90 | N |
| 10R | 82.6 | 0.00 | 82.60 | N |
| 11R | 92.3 | 0.00 | 92.30 | N |
| 12R | 102.0 | 0.00 | 102.00 | N |
| 13R | 111.7 | 0.00 | 111.70 | N |
| 14R | 121.3 | 0.00 | 121.30 | N |
| 15R | 130.9 | 0.00 | 130.90 | N |
| 16R | 140.6 | 0.00 | 140.60 | N |
| 17R | 150.2 | 0.00 | 150.20 | N |
| 18R | 159.8 | 0.00 | 159.80 | N |
| 19R | 169.5 | 0.00 | 169.50 | N |
| 20R | 179.2 | 0.00 | 179.20 | N |
| 21R | 188.8 | 0.00 | 188.80 | N |
| 22R | 198.5 | 0.00 | 198.50 | N |
| 23R | 208.1 | 0.00 | 208.10 | N |
| 24R | 217.8 | 0.00 | 217.80 | N |
| 25R | 227.2 | 0.00 | 227.20 | N |
| 26R | 236.9 | 0.00 | 236.90 | N |
| 27R | 246.5 | 0.00 | 246.50 | N |
| 28R | 256.2 | 0.00 | 256.20 | N |
| 29R | 265.8 | 0.00 | 265.80 | N |
| 30R | 275.5 | 0.00 | 275.50 | N |
| 31R | 285.1 | 0.00 | 285.10 | N |
| 32R | 294.7 | 0.00 | 294.70 | N |
| 33R | 304.4 | 0.00 | 304.40 | N |
| 34R | 314.0 | –0.15 | 313.85 | Y |
| 35R | 323.7 | 0.21 | 323.91 | Y |
| 36R | 333.3 | 0.60 | 333.90 | Y |
| 37R | 343.0 | 0.68 | 343.68 | Y |
| 38R | 352.6 | 0.83 | 353.43 | Y |
| 39R | 362.2 | 1.18 | 363.38 | Y |
| 40R | 371.8 | –0.85 | 370.95 | Y |
| 41R | 381.4 | 1.17 | 382.57 | N |
| 42R | 391.1 | 1.17 | 392.27 | N |
| 43R | 400.7 | 1.17 | 401.87 | N |
| 44R | 410.4 | 1.17 | 411.57 | N |
| 45R | 420.0 | 1.48 | 421.48 | Y |
| 46R | 429.6 | 1.48 | 431.08 | N |
| 47R | 439.2 | 1.48 | 440.68 | N |
| 48R | 448.8 | 0.01 | 448.81 | Y |
| 49R | 458.4 | 0.86 | 459.26 | Y |
| 50R | 468.0 | 0.53 | 468.53 | Y |
| 51R | 477.6 | 0.33 | 477.93 | Y |
| 52R | 487.3 | 1.75 | 489.05 | Y |
| 53R | 497.0 | 1.75 | 498.75 | N |
| 54R | 506.6 | 1.75 | 508.35 | N |
| 55R | 510.6 | 1.75 | 512.35 | N |
| 56R | 515.8 | 1.75 | 517.55 | N |
| 57R | 520.3 | 1.75 | 522.05 | N |
| 58R | 529.9 | 1.43 | 531.33 | Y |
| 59R | 539.5 | 1.84 | 541.34 | Y |
| 60R | 549.1 | 1.00 | 550.10 | Y |
| 207-1259B- | | | | |
| 1R | 0.0 | 0.00 | 0.00 | N |
| 2R | 305.0 | –0.60 | 304.40 | Y |
| 3R | 314.6 | –0.60 | 314.00 | Y |
| 4R | 324.2 | –9.50 | 314.70 | Y |
| 5R | 333.8 | 1.45 | 335.25 | Y |
| 6R | 343.4 | 3.13 | 346.53 | Y |
| 7R | 353.1 | 1.73 | 354.83 | Y |
| 8R | 362.7 | 1.83 | 364.53 | Y |
| 9R | 372.3 | 1.83 | 374.13 | N |
| 10R | 420.5 | –1.79 | 418.71 | Y |
| 11R | 430.1 | –0.68 | 429.42 | Y |
| 12R | 439.7 | –1.45 | 438.25 | Y |
| 13R | 444.7 | –1.45 | 443.25 | Y |
| 14R | 454.3 | –1.24 | 453.06 | Y |
| 15R | 461.9 | –1.54 | 460.36 | Y |
| 16R | 471.5 | –0.29 | 471.21 | Y |
| 17R | 476.5 | –0.94 | 475.56 | Y |
| 18R | 485.9 | –0.05 | 485.85 | Y |
| 19R | 495.5 | 1.00 | 496.50 | Y |
| 20R | 505.1 | 3.68 | 508.78 | Y |
| 21R | 514.8 | 1.47 | 516.27 | Y |
| 22R | 524.4 | 0.43 | 524.83 | Y |
| 23R | 534.0 | 0.48 | 534.48 | Y |
| 24R | 543.6 | 0.89 | 544.49 | Y |
| 25R | 553.2 | 1.09 | 554.29 | N |
| 207-1259C- | | | | |
| 1R | 308.0 | 2.65 | 310.65 | Y |
| 2R | 317.6 | 3.81 | 321.41 | Y |
| 3R | 327.2 | 3.57 | 330.77 | Y |
| 4R | 335.2 | 3.38 | 338.58 | Y |
| 5R | 344.8 | 2.53 | 347.33 | Y |
| 6R | 354.4 | 3.76 | 358.16 | Y |
| 7R | 364.0 | 3.49 | 367.49 | Y |
| 8R | 436.0 | 1.25 | 437.25 | Y |
| 9R | 480.0 | 1.25 | 481.25 | Y |
| 10R | 485.0 | 1.43 | 486.43 | Y |
| 11R | 489.4 | 2.24 | 491.64 | Y |
| 12R | 495.4 | 4.25 | 499.65 | Y |
| 13R | 501.6 | 4.66 | 506.26 | Y |
| 14R | 508.6 | 4.22 | 512.82 | N |
| 15R | 513.8 | 4.82 | 518.62 | Y |
| 16R | 518.3 | 3.53 | 521.83 | Y |
| 17R | 527.9 | 3.12 | 531.02 | Y |
| 18R | 537.5 | 4.33 | 541.83 | Y |
| 19R | 547.1 | 2.35 | 549.45 | Y |

Note: N = no, Y = yes.

**Table T12.** Splice tie points, Site 1259.

| Hole, core, section, interval (cm) | Depth (mbsf) | Depth (mcd) | | Hole, core, section, interval (cm) | Depth (mbsf) | Depth (mcd) |
|---|---|---|---|---|---|---|
| 207- | | | | 207- | | |
| 1259A-33R-6, 80 | 312.70 | 312.70 | Tie to | 1259C-1R-2, 53 | 310.05 | 312.70 |
| 1259C-1R-3, 90 | 311.90 | 314.55 | Tie to | 1259A-34R-1, 70 | 314.70 | 314.55 |
| 1259A-34R-6, 115 | 322.67 | 322.52 | Tie to | 1259C-2R-1, 109.5 | 318.71 | 322.52 |
| 1259C-2R-2, 132.5 | 320.43 | 324.24 | Tie to | 1259A-35R-1, 32.5 | 324.03 | 324.24 |
| 1259A-35R-6, 105 | 332.21 | 332.42 | Tie to | 1259C-3R-2, 15 | 328.85 | 332.42 |
| 1259C-3R-3, 95 | 331.15 | 334.72 | Tie to | 1259A-36R-1, 81 | 334.12 | 334.72 |
| 1259A-36R-6, 45 | 341.25 | 341.85 | Tie to | 1259C-4R-3, 26 | 338.47 | 341.85 |
| 1259C-4R-5, 5 | 341.25 | 344.63 | Tie to | 1259A-37R-1, 95 | 343.95 | 344.63 |
| 1259A-37R-7, 25 | 352.25 | 352.93 | Tie to | 1259C-5R-4, 110 | 350.40 | 352.93 |
| 1259C-5R-7, 32.5 | 354.13 | 356.66 | Tie to | 1259B-7R-2, 32 | 354.93 | 356.66 |
| 1259B-7R-5, 7.5 | 359.18 | 360.91 | Tie to | 1259C-6R-2, 125 | 357.15 | 360.91 |
| 1259C-6R-6, 110 | 363.00 | 366.76 | Tie to | 1259B-8R-2, 72 | 364.93 | 366.76 |
| 1259B-8R-5, 107.5 | 369.78 | 371.61 | Tie to | 1259A-40R-1, 64.5 | 372.46 | 371.61 |
| 1259A-40R-4, 50 | 376.30 | 375.45 | | | | |
| 207- | | | | 207- | | |
| 1259A-47R-4, 122.5 | 444.31 | 445.79 | Tie to | 1259B-13R-2, 103.5 | 447.24 | 445.79 |
| 1259B-13R-5, 125 | 451.95 | 450.50 | Tie to | 1259A-48R-2, 18.5 | 450.49 | 450.50 |
| 1259A-48R-6, 130 | 457.60 | 457.61 | Tie to | 1259B-14R-4, 5 | 458.85 | 457.61 |
| 1259B-14R-5, 80 | 461.10 | 459.86 | Tie to | 1259A-49R-1, 60 | 459.00 | 459.86 |
| 1259A-49R-6, 22.5 | 465.88 | 466.74 | Tie to | 1259B-15R-5, 37.5 | 468.28 | 466.74 |
| 1259B-15R-6, 112.5 | 470.53 | 468.99 | Tie to | 1259A-50R-1, 44.5 | 468.46 | 468.99 |
| 1259A-50R-7, 37.5 | 476.41 | 476.94 | Tie to | 1259B-17R-1, 137.5 | 477.88 | 476.94 |
| 1259B-17R-2, 120 | 479.20 | 478.26 | Tie to | 1259A-51R-1, 32 | 477.93 | 478.26 |
| 1259A-51R-6, 122.5 | 486.30 | 486.63 | Tie to | 1259B-18R-1, 77.5 | 486.68 | 486.63 |
| 1259B-18R-5, 130 | 493.20 | 493.15 | Tie to | 1259C-11R-1, 151 | 490.91 | 493.15 |
| 1259C-11R-5, 60 | 495.53 | 497.77 | Tie to | 1259B-19R-1, 126 | 496.77 | 497.77 |
| 1259B-19R-3, 40 | 498.90 | 499.90 | Tie to | 1259C-12R-1, 25 | 495.65 | 499.90 |
| 1259C-12R-CC, 17.5 | 501.88 | 506.13 | | | | |
| 207- | | | | 207- | | |
| 1259A-56R-3, 140 | 520.01 | 521.76 | Append to | 1259A-57R-1, 0 | 520.30 | 522.05 |
| 1259A-57R-5, 125 | 527.55 | 529.30 | Tie to | 1259B-22R-3, 147 | 528.87 | 529.30 |
| 1259B-22R-5, 97.5 | 531.38 | 531.81 | Tie to | 1259A-58R-1, 47.5 | 530.38 | 531.81 |
| 1259A-58R-7, 65 | 537.78 | 539.21 | Tie to | 1259B-23R-4, 22 | 538.73 | 539.21 |
| 1259B-23R-6, 27.5 | 541.42 | 541.90 | Tie to | 1259A-59R-1, 54.5 | 540.06 | 541.90 |
| 1259A-59R-5, 95 | 546.09 | 547.93 | Tie to | 1259B-24R-3, 43.5 | 547.04 | 547.93 |
| 1259B-24R-4, 72.5 | 548.83 | 549.72 | Tie to | 1259C-19R-1, 26 | 547.37 | 549.72 |
| 1259C-19R-4, 80 | 551.34 | 553.69 | | | | |

**Table T13.** Calcareous nannofossil and planktonic foraminiferal datums used in the preliminary age-depth model, Hole 1259A.

| Core, section, interval (cm) | Depth (mbsf) | Foraminifer age (Ma) | | Foraminifer zone | Nannofossil age (Ma) | | Nannofossil zone | Epoch |
|---|---|---|---|---|---|---|---|---|
| | Base | Minimum | Maximum | | Minimum | Maximum | | |
| 207-1259A- | | | | | | | | |
| 4R-CC, 0–8 | 28.29 | | | | 19.6 | 19.6 | NN2 | early Miocene |
| 5R-CC, 5–13 | 50.06 | | | | 18.9 | 18.9 | NN2 | early Miocene |
| 6R-CC, 8–16 | 50.06 | | | | 23.2 | 23.2 | NN2 | early Miocene |
| 7R-3, 50–54 | 58.10 | 21.5 | 21.5 | M1b | | | | early Miocene |
| 8R-CC, 11–17 | 72.20 | | | | 22.9 | 22.9 | NN2 | early Miocene |
| 9R-7, 50–54 | 82.33 | 23.2 | 23.2 | M1b | | | | early Miocene |
| 9R-CC, 18–23 | 91.95 | | | | 23.5 | 23.5 | NN1 | early Miocene |
| 10R-5, 50–54 | 90.60 | 23.8 | 23.8 | M1a | | | | early Miocene |
| 10R-CC, 6–12 | 99.95 | | | | 30.4 | 30.4 | NP23 | late Oligocene |
| 11R-5, 50–54 | 99.95 | 29.4 | 29.4 | P21a | | | | early Oligocene |
| 13R-4, 50–54 | 116.70 | 32.0 | 32.0 | P18 | | | | early Oligocene |
| 14R-4, 50–54 | 126.30 | 33.7 | 33.7 | P16 | | | | late Eocene |
| 14R-CC, 17–22 | 127.00 | | | | 33.9 | 33.9 | NP20 | late Eocene |
| 15R-2, 50–54 | 132.90 | | | P14 | | | | middle Eocene |
| 16R-CC, 10–15 | 145.61 | | | | 37.1 | 37.1 | NP19 | middle Eocene |
| 19R-3, 50–53 | 172.70 | 40.1 | 40.1 | P13 | | | | middle Eocene |
| 20R-4, 50–53 | 185.60 | 40.5 | 40.5 | P13 | | | | middle Eocene |
| 20R-CC, 8–13 | 185.77 | | | | 40.4 | 40.4 | NP16 | middle Eocene |
| 24R-1, 50–54 | 218.30 | 43.6 | 43.6 | P11 | | | | middle Eocene |
| 24R-CC, 21–24 | 231.79 | | | | 42.5 | 42.5 | NP16 | middle Eocene |
| 24R-CC, 14–19 | 245.28 | | | | 44 | 44 | NP15 | middle Eocene |
| 27R-1, 50–54 | 248.50 | 45.8 | 45.8 | P11 | | | | middle Eocene |
| 30R-CC, 9–12 | 285.60 | 49.0 | 49.0 | P10 | | | | middle Eocene |
| 30R-CC, 15–19 | 287.81 | | | | 47.2 | 47.2 | NP14 | middle Eocene |
| 31R-CC, 15–19 | 298.12 | | | | 49.3 | 49.3 | NP14 | middle Eocene |
| 33R-1, 50–54 | 306.40 | 50.4 | 50.4 | P9 | | | | early Eocene |
| 34R-CC, 0–5 | 323.00 | 52.3 | 52.3 | P8 | | | | early Eocene |
| 34R-CC, 0–5 | 323.00 | | | | 51 | 51 | NP12 | early Eocene |
| 35R-CC, 21–26 | 334.70 | | | | 53.7 | 53.7 | NP10 | early Eocene |
| 36R-CC, 0–5 | 352.68 | | | | 53.9 | 53.9 | NP9 | early Eocene |
| 38R-4, 49–52 | 357.59 | 54.7 | 54.7 | P5 | | | | early Eocene |
| 43R-CC, 13–18 | 406.80 | 55.9 | 55.9 | P4 | | | | late Paleocene |
| 43R-CC, 13–18 | 406.80 | | | | 56.2 | 56.2 | NP9 | late Paleocene |
| 45R-1, 50–54 | 422.00 | 59.2 | 59.2 | P4 | | | | late Paleocene |
| 45R-CC, 5–11 | 436.43 | 60.0 | 60.0 | P3b | | | | late Paleocene |
| 46R-CC, 29–34 | 446.48 | 61.2 | 61.2 | P2 | | | | early Paleocene |
| 47R-CC, 38–43 | 446.48 | 65.0 | 65.0 | KS31 | | | | Maastrichtian |
| 47R-CC, 38–43 | 448.80 | | | | 65 | 65 | CC26 | late Maastrichtian |
| 48R-7, 50–54 | 458.67 | 68.6 | 68.6 | KS31 | | | | Maastrichtian |
| 49R-CC, 11–17 | 472.75 | 69.6 | 69.6 | KS30a | | | | Maastrichtian |
| 49R-CC, 11–17 | 477.12 | | | | 66.2 | 66.2 | CC25 | late Maastrichtian |
| 51R-CC, 14–16 | 490.37 | 73.8 | 73.8 | KS29 | | | | late Campanian |
| 51R-CC, 14–16 | 487.37 | 68.6 | 72.8 | KS29–30 | | | | Campanian–Maastrichtian |
| 51R-CC, 14–16 | 487.51 | | | | 71.3 | 71.3 | CC23 | Campanian–Maastrichtian |
| 52R-CC, 23–26 | 495.01 | 85.4 | 89.5 | KS23 | | | | Coniacian |
| 52R-3, 3–3 | 489.91 | | | | 75.3 | 76 | CC22 | late Campanian |
| 52R-4, 115–115 | 492.47 | | | | 75.3 | 76 | CC22 | late Campanian |
| 52R-5, 5–5 | 492.88 | | | | 80 | 83.4 | CC18 | early Campanian |
| 52R-6, 7–7 | 493.67 | | | | 80 | 83.4 | CC18 | early Campanian |
| 52R-6, 47–47 | 494.07 | | | | 80 | 83.4 | CC18 | early Campanian |
| 52R-6, 60–60 | 494.20 | | | | 80 | 84 | NA | Santonian–early Campanian |
| 52R-6, 103–103 | 494.63 | | | | 83.5 | 87.2 | NA | late Coniacian–Santonian |
| 52R-6, 115–115 | 494.80 | | | | 87.2 | 89 | NA | early Coniacian |
| 53R-CC, 20–22 | 501.70 | 85.4 | 89.5 | KS23 | | | | Coniacian |
| 54R-CC, 10–15 | 510.31 | 89.0 | 93.5 | NA | | | | Turonian |
| 55R-CC, 0–3 | 513.82 | 89.0 | 93.5 | NA | | | | Turonian |
| 56R-CC, 14–19 | 520.22 | 89.0 | 93.5 | NA | | | | Turonian |
| 57R-CC, 10–15 | 529.29 | 89.0 | 93.5 | NA | | | | Turonian |
| 58R-CC, 11–16 | 538.17 | 89.0 | 93.5 | NA | | | | Turonian |

Notes: Both minimal and maximal assigned ages (Ma) are given for each sample analyzed. NA = not applicable.

**Table T14.** Magnetostratigraphic datums used in the preliminary age-depth model, Hole 1259A.

| Core, section, interval (cm) | Depth (mbsf) | Age (Ma) | Polarity chron | Epoch |
|---|---|---|---|---|
| 207-1259A- | | | | |
| 21R-2, 105 | 191.35 | 41.25 | C18r (base) | middle Eocene |
| 22R-1, 50 | 199.00 | 41.52 | C19n (base) | middle Eocene |
| 35R-5, 13 | 329.79 | 52.66 | C24n (base) | early Eocene |
| 45R-2, 52 | 422.02 | 57.91 | C26n (base) | late Paleocene |
| 48R-3, 109 | 452.89 | 68.73 | C31n (base) | Maastrichtian |
| 51R-1, 10 | 477.70 | 71.07 | C31r (base) | Maastrichtian |
| 51R-6, 23 | 485.30 | 71.34 | C32n (base) | late Campanian |
| 53R-1, 59 | 497.59 | 73.40 | C32r (base) | late Campanian |

**Table T15.** Linear sedimentation rates and mass accumulation rates, Hole 1259A.

| Epoch | Core, section, interval (cm) | Top | | Bottom | | Thickness (m) | Duration (m.y.) | LSR | | DBD ($g/cm^3$) | MAR ($g/cm^2/k.y.$) |
|---|---|---|---|---|---|---|---|---|---|---|---|
| | | Depth (mbsf) | Age (Ma) | Depth (mbsf) | Age (Ma) | | | (m/m.y.) | (m/m.y.) | | |
| | 207-1259A- | | | | | | | | | | |
| early Miocene | 4R-CC, 0 to 10R-5, 54 | 28.29 | 19.6 | 89.14 | 23.8 | 60.85 | 4.2 | 13 | 1.3 | 1.14 | 1.1 |
| early Oligocene–late Eocene | 10R-CC, 6 to 14R-CC, 22 | 99.95 | 30.4 | 126.55 | 33.7 | 26.60 | 3.3 | 6 | 0.6 | 0.59 | 0.6 |
| middle Eocene–early Paleocene | 15R-2, 50 to 46R-CC, 34 | 132.90 | 37.1 | 436.48 | 61.2 | 303.58 | 24.1 | 12 | 1.2 | 1.41 | 1.4 |
| early Paleocene–late Campanian | 47R-CC, 38 to 52R-4, 115 | 446.48 | 65 | 492.47 | 75.3 | 45.99 | 10.3 | 4.5 | 0.45 | 0.79 | 0.8 |
| early Campanian–early Coniancian | 52R-5, 5 to 52R-6, 115 | 492.88 | 83.4 | 494.75 | 89 | 1.87 | 5.6 | 0.4 | 0.04 | — | — |
| Coniancian–Turonian | 53R-CC, 20 to 58R-CC, 16 | 501.70 | 85.4 | 538.22 | 93.5 | 36.52 | 8.1 | 5 | 0.5 | — | — |

Notes: Averaged dry bulk densities (DBD) of major lithologies per studied interval were used (see "Physical Properties," p. 33) to calculate mass accumulation rate (MAR) values. LSR = linear sedimentation rate. — = not assigned.

**Table T16.** Total carbon, inorganic carbon, carbonate, total organic carbon, and total nitrogen concentrations and carbon/nitrogen ratios, Site 1259. (See table notes. Continued on next two pages.)

| Hole, core, section, interval (cm) | Depth (mbsf) | TC (wt%) | IC (wt%) | $CaCO_3$ (wt%) | TOC (wt%) | N (wt%) | C/N (atomic) |
|---|---|---|---|---|---|---|---|
| 207- | | | | | | | |
| Unit I (foraminifer-bearing nannofossil ooze): | | | | | | | |
| 1259A-1R-1, 90–91 | 0.90 | 10.04 | 9.74 | 81.16 | 0.30 | | |
| 1259A-1R-3, 40–41 | 3.00 | | 10.03 | 83.57 | | | |
| 1259A-2R-2, 90–91 | 11.20 | | 9.77 | 81.39 | | | |
| 1259A-2R-3, 40–41 | 12.20 | 9.94 | 9.98 | 83.11 | 0.00 | | |
| 1259A-3R-1, 39–40 | 18.69 | | 10.04 | 83.60 | | | |
| 1259A-3R-3, 40–41 | 21.70 | 9.46 | 9.35 | 77.89 | 0.11 | | |
| 1259A-3R-5, 40–41 | 24.70 | | 9.04 | 75.29 | | | |
| 1259A-5R-1, 39–40 | 36.79 | | 9.98 | 83.16 | | | |
| Unit II (foraminifer-bearing nannofossil chalk): | | | | | | | |
| 1259A-5R-2, 39–40 | 38.29 | | 9.53 | 79.38 | | | |
| 1259A-5R-4, 40–41 | 41.00 | 10.15 | 9.97 | 83.07 | 0.18 | | |
| 1259A-6R-1, 31–32 | 45.81 | | 10.27 | 85.57 | | | |
| 1259A-6R-3, 30–31 | 48.80 | 9.88 | 9.67 | 80.55 | 0.21 | | |
| 1259A-7R-1, 40–41 | 55.00 | | 9.74 | 81.17 | | | |
| 1259A-7R-3, 39–40 | 57.99 | 9.08 | 8.85 | 73.69 | 0.23 | | |
| 1259A-7R-5, 39–40 | 60.99 | | 9.74 | 81.15 | | | |
| 1259A-8R-1, 40–41 | 64.20 | | 9.01 | 75.01 | | | |
| 1259A-8R-3, 40–41 | 67.20 | 9.37 | 9.20 | 76.67 | 0.17 | | |
| 1259A-8R-5, 20–21 | 70.00 | | 9.29 | 77.41 | | | |
| 1259A-9R-1, 18–19 | 73.08 | | 8.95 | 74.59 | | | |
| 1259A-9R-3, 123–124 | 77.13 | 8.66 | 8.43 | 70.23 | 0.23 | | |
| 1259A-9R-5, 108–109 | 79.98 | | 8.61 | 71.73 | | | |
| 1259A-9R-7, 43–44 | 81.93 | | 8.48 | 70.61 | | | |
| 1259A-10R-2, 96–97 | 85.06 | | 8.80 | 73.27 | | | |
| 1259A-10R-4, 47–48 | 87.57 | 9.27 | 9.06 | 75.48 | 0.21 | | |
| 1259A-10R-6, 53–54 | 90.63 | | 9.45 | 78.69 | | | |
| 1259A-11R-1, 78–79 | 93.08 | | 9.48 | 78.98 | | | |
| 1259A-11R-3, 97–98 | 96.27 | 9.69 | 9.56 | 79.62 | 0.13 | | |
| 1259A-11R-5, 59–60 | 98.89 | | 9.43 | 78.56 | | | |
| 1259A-12R-1, 80–81 | 102.80 | | 9.86 | 82.14 | | | |
| 1259A-12R-3, 65–66 | 105.65 | 9.65 | 9.41 | 78.41 | 0.24 | | |
| 1259A-12R-5, 78–79 | 108.78 | | 9.94 | 82.80 | | | |
| 1259A-14R-1, 95–96 | 122.25 | | 9.86 | 82.15 | | | |
| 1259A-14R-3, 76–77 | 125.06 | 9.73 | 9.17 | 76.39 | 0.56 | | |
| 1259A-15R-1, 72–73 | 131.62 | | 9.94 | 82.78 | | | |
| 1259A-15R-3, 82–83 | 134.72 | 9.80 | 9.97 | 83.06 | 0.00 | | |
| 1259A-16R-1, 79–80 | 141.39 | | 10.11 | 84.19 | | | |
| 1259A-16R-4, 66–67 | 145.46 | 9.84 | 9.72 | 80.93 | 0.12 | | |
| 1259A-17R-1, 5–6 | 150.25 | | 9.25 | 77.02 | | | |
| 1259A-17R-2, 37–38 | 152.07 | 8.91 | 8.70 | 72.45 | 0.21 | | |
| 1259A-18R-1, 120–121 | 161.00 | | 9.52 | 79.30 | | | |
| 1259A-18R-2, 95–96 | 162.20 | 8.07 | 8.13 | 67.74 | 0.00 | | |
| 1259A-20R-1, 86–87 | 180.06 | | 9.85 | 82.03 | | | |
| 1259A-20R-3, 67–68 | 182.87 | 9.84 | 9.68 | 80.62 | 0.16 | | |
| 1259A-20R-4, 115–116 | 184.85 | | 9.61 | 80.04 | | | |
| 1259A-21R-1, 88–89 | 189.68 | | 10.26 | 85.45 | | | |
| 1259A-21R-4, 39–40 | 193.19 | 9.34 | 9.31 | 77.53 | 0.03 | | |
| 1259A-22R-1, 87–88 | 199.37 | | 9.52 | 79.30 | | | |
| 1259A-22R-3, 89–90 | 202.39 | 10.14 | 9.39 | 78.24 | 0.75 | | |
| 1259A-22R-5, 65–66 | 205.15 | | 9.96 | 82.94 | | | |
| 1259A-23R-1, 90–91 | 209.00 | | 9.06 | 75.47 | | | |
| 1259A-23R-3, 78–79 | 211.88 | 9.84 | 9.75 | 81.24 | 0.09 | | |
| 1259A-23R-5, 14–15 | 213.74 | | 8.23 | 68.55 | | | |
| 1259A-24R-1, 61–62 | 218.41 | | 9.49 | 79.03 | | | |
| 1259A-24R-2, 61–62 | 219.83 | | 8.92 | 74.29 | | | |
| 1259A-25R-1, 62–63 | 227.82 | | 9.28 | 77.31 | | | |
| 1259A-25R-3, 69–70 | 230.89 | 9.18 | 9.19 | 76.54 | 0.00 | 0.01 | |
| 1259A-26R-1, 62–63 | 237.52 | | 9.37 | 78.04 | | | |
| 1259A-26R-3, 62–63 | 240.52 | 9.70 | 9.78 | 81.51 | 0.00 | 0.01 | |
| 1259A-26R-5, 65–66 | 243.55 | | 10.00 | 83.26 | | | |
| 1259A-26R-CC, 11–12 | 245.25 | | 9.84 | 81.95 | | | |
| 1259A-27R-1, 60–61 | 247.10 | | 9.79 | 81.53 | | | |
| 1259A-27R-3, 66–67 | 250.16 | 9.10 | 9.27 | 77.19 | 0.00 | 0.00 | |

Table T16 (continued).

| Hole, core, section, interval (cm) | Depth (mbsf) | TC (wt%) | IC (wt%) | $CaCO_3$ (wt%) | TOC (wt%) | N (wt%) | C/N (atomic) |
|---|---|---|---|---|---|---|---|
| 1259A-27R-5, 77–78 | 253.27 | | 7.97 | 66.36 | | | |
| 1259A-28R-2, 43–44 | 257.57 | 8.52 | 8.65 | 72.02 | 0.00 | 0.00 | |
| 1259A-29R-1, 48–49 | 266.28 | | 9.25 | 77.08 | | | |
| 1259A-29R-3, 49–50 | 269.29 | 8.70 | 8.84 | 73.67 | 0.00 | 0.01 | |
| 1259A-29R-5, 72–73 | 272.52 | | 8.72 | 72.63 | | | |
| 1259A-30R-1, 61–62 | 276.11 | | 9.24 | 77.01 | | | |
| 1259A-30R-3, 49–50 | 278.99 | 9.02 | 9.27 | 77.24 | 0.00 | 0.01 | |
| 1259A-30R-3, 73–74 | 279.23 | | 9.26 | 77.17 | | | |
| 1259A-32R-1, 76–77 | 295.46 | 8.52 | 8.52 | 71.01 | 0.00 | 0.01 | 0.31 |
| 1259A-33R-2, 86–87 | 306.76 | | 6.24 | 51.99 | | | |
| 1259A-33R-4, 86–87 | 309.76 | 6.54 | 6.73 | 56.05 | 0.00 | 0.01 | |
| 1259A-33R-6, 86–87 | 312.76 | | 7.73 | 64.39 | | | |
| 1259A-34R-1, 63–64 | 314.63 | | 5.72 | 47.64 | | | |
| 1259A-34R-3, 77–78 | 317.79 | | 6.04 | 50.35 | | | |
| 1259A-34R-5, 84–85 | 320.86 | 7.62 | 8.01 | 66.71 | 0.00 | 0.02 | |
| 1259A-35R-2, 92–93 | 326.12 | | 6.67 | 55.56 | | | |
| 1259A-35R-5, 92–93 | 330.58 | 7.08 | 7.13 | 59.37 | 0.00 | 0.01 | |
| 1259A-36R-3, 60–61 | 336.90 | | 7.12 | 59.30 | | | |
| 1259A-36R-5, 60–61 | 339.90 | 7.36 | 7.50 | 62.50 | 0.00 | 0.01 | |
| 1259A-37R-1, 86–87 | 343.86 | | 8.27 | 68.93 | | | |
| 1259A-37R-3, 8–9 | 346.08 | 7.99 | 7.98 | 66.46 | 0.01 | 0.01 | 1.79 |
| 1259A-37R-6, 91–92 | 351.41 | | 5.94 | 49.47 | | | |
| 1259A-38R-1, 34–35 | 352.94 | | 6.17 | 51.39 | | | |
| 1259A-38R-4, 81–82 | 357.91 | 7.58 | 7.68 | 63.95 | 0.00 | 0.03 | |
| 1259A-39R-1, 86–87 | 363.06 | | 4.52 | 37.69 | | | |
| 1259A-39R-4, 74–75 | 366.09 | | 5.90 | 49.15 | | | |
| 1259A-39R-5, 99–100 | 367.84 | 4.05 | 4.07 | 33.86 | 0.00 | 0.04 | |
| 1259A-40R-1, 24–25 | 372.04 | | 6.04 | 50.34 | | | |
| 1259A-40R-4, 24–25 | 376.04 | 5.08 | 5.08 | 42.28 | 0.00 | 0.03 | |
| Unit III (clayey nannofossil chalk): | | | | | | | |
| 1259A-43R-1, 104–105 | 401.74 | | 5.59 | 46.59 | | | |
| 1259A-43R-3, 130–131 | 405.00 | 6.42 | 6.68 | 55.62 | 0.00 | 0.04 | |
| 1259A-44R-4, 77–78 | 415.67 | | 5.25 | 43.75 | | | |
| 1259A-44R-6, 60–61 | 418.50 | 5.19 | 5.04 | 41.99 | 0.15 | 0.04 | 4.56 |
| 1259A-45R-2, 68–69 | 422.18 | | 6.58 | 54.79 | | | |
| 1259A-45R-4, 21–22 | 424.11 | 4.98 | 4.95 | 41.20 | 0.03 | 0.04 | 0.91 |
| 1259A-46R-2, 72–73 | 431.13 | | 7.94 | 66.15 | | | |
| 1259A-46R-3, 140–141 | 433.31 | 9.15 | 9.20 | 76.67 | 0.00 | 0.01 | |
| 1259A-46R-5, 73–74 | 435.64 | | 10.45 | 87.01 | | | |
| 1259A-47R-1, 66–67 | 439.86 | | 5.92 | 49.35 | | | |
| 1259A-47R-3, 58–59 | 442.16 | | 2.49 | 20.78 | | | |
| 1259A-47R-3, 72–73 | 442.30 | | 7.67 | 63.91 | | | |
| 1259B-12R-4, 40–40 | 444.10 | 2.97 | 2.88 | 23.95 | 0.09 | 0.03 | 3.79 |
| 1259A-47R-5, 47–48 | 445.05 | 8.35 | 8.15 | 67.87 | 0.20 | 0.01 | |
| 1259A-48R-1, 70–71 | 449.50 | | 8.73 | 72.72 | | | |
| 1259A-48R-3, 70–71 | 452.50 | | 8.16 | 67.95 | | | |
| 1259B-13R-6, 65–66 | 452.86 | 7.64 | 7.62 | 63.48 | 0.02 | 0.02 | 1.77 |
| 1259A-48R-5, 57–58 | 455.37 | 9.90 | 9.78 | 81.48 | 0.12 | 0.10 | 1.46 |
| 1259A-49R-1, 72–73 | 459.12 | | 9.98 | 83.12 | | | |
| 1259A-49R-3, 80–81 | 462.03 | | 7.33 | 61.09 | | | |
| 1259A-49R-4, 139–144 | 464.12 | 7.89 | 7.93 | 66.06 | | 0.01 | |
| 1259A-49R-5, 83–84 | 465.00 | 9.50 | 9.42 | 78.47 | 0.08 | 0.01 | 9.54 |
| 1259A-50R-1, 66–67 | 468.66 | | 9.68 | 80.65 | | | |
| 1259A-50R-4, 132–137 | 473.64 | 8.60 | 8.53 | 71.08 | 0.01 | 0.02 | 4.50 |
| 1259A-50R-6, 67–68 | 475.85 | 8.62 | 8.56 | 71.27 | 0.06 | 0.01 | 4.50 |
| 1259A-51R-1, 80–81 | 478.40 | | 7.72 | 64.34 | 0.03 | | |
| 1259A-51R-5, 77–79 | 484.37 | 4.32 | 4.77 | 39.75 | 0.00 | 0.04 | |
| 1259A-51R-6, 0–5 | 485.07 | 4.76 | 4.68 | 39.00 | 0.08 | 0.03 | 3.10 |
| 1259A-51R-7, 62–63 | 487.19 | 4.36 | 4.24 | 35.31 | 0.12 | 0.03 | 5.17 |
| 1259A-52R-1, 80–81 | 488.10 | 5.15 | 5.05 | 42.04 | 0.10 | 0.03 | 4.43 |
| 1259C-11R-1, 141–142 | 490.81 | 3.03 | 2.97 | 24.73 | 0.06 | 0.00 | |
| 1259C-11R-2, 75–76 | 491.65 | 2.68 | 2.51 | 20.89 | 0.17 | 0.02 | 12.90 |
| 1259A-52R-4, 80–81 | 492.12 | 2.89 | 2.74 | 22.82 | 0.15 | 0.03 | 5.44 |
| Unit IV (black shales and sandstones): | | | | | | | |
| 1259C-11R-3, 93–94 | 492.86 | 5.64 | 3.90 | 32.51 | 1.74 | 0.13 | 15.06 |
| 1259A-52R-6, 0–5 | 493.60 | 6.87 | 4.75 | 39.55 | 2.12 | 0.11 | 22.70 |
| 1259C-11R-4, 19–29 | 493.62 | 4.82 | 3.49 | 29.07 | 1.33 | 0.06 | 24.37 |
| 1259A-52R-6, 45–46 | 494.05 | 8.02 | 5.90 | 49.14 | 2.12 | 0.10 | 23.84 |

Table T16 (continued).

| Hole, core, section, interval (cm) | Depth (mbsf) | TC (wt%) | IC (wt%) | $CaCO_3$ (wt%) | TOC (wt%) | N (wt%) | C/N (atomic) |
|---|---|---|---|---|---|---|---|
| 1259A-52R-CC, 5–6 | 495.06 | 14.49 | 8.26 | 68.81 | 6.23 | 0.32 | 22.89 |
| 1259C-11R-5, 106–107 | 495.99 | 15.85 | 6.60 | 55.01 | 9.25 | 0.40 | 27.18 |
| 1259C-12R-2, 61–63 | 497.51 | 15.66 | 6.84 | 56.96 | 8.82 | 0.32 | 32.32 |
| 1259A-53R-2, 20–21 | 498.70 | 12.77 | 11.27 | 93.89 | 1.50 | 0.05 | 36.47 |
| 1259C-12R-3, 55–57 | 498.95 | 15.12 | 5.51 | 45.92 | 9.61 | 0.37 | 29.94 |
| 1259A-53R-2, 145–150 | 499.95 | 15.98 | 8.16 | 67.97 | 7.82 | 0.30 | 30.30 |
| 1259C-12R-4, 6–7 | 499.96 | 13.60 | 4.79 | 39.92 | 8.81 | 0.36 | 28.77 |
| 1259A-53R-3, 148–149 | 501.48 | 14.69 | 7.54 | 62.82 | 7.15 | 0.26 | 32.60 |
| 1259C-13R-3, 21–23 | 504.81 | 15.39 | 5.82 | 48.45 | 9.57 | 0.41 | 26.91 |
| 1259A-54R-1, 1–2 | 506.61 | 20.03 | 6.48 | 54.00 | 13.55 | 0.43 | 36.71 |
| 1259A-54R-1, 62–63 | 507.22 | 21.11 | 5.14 | 42.79 | 15.97 | 0.50 | 37.26 |
| 1259A-54R-2, 0–5 | 508.10 | 15.09 | 6.11 | 50.90 | 8.98 | 0.33 | 32.00 |
| 1259C-14R-2, 62–63 | 510.72 | 16.03 | 5.88 | 49.01 | 10.15 | 0.39 | 30.20 |
| 1259A-55R-1, 97–98 | 511.57 | 16.73 | 5.23 | 43.54 | 11.50 | 0.41 | 32.97 |
| 1259A-55R-2, 91–96 | 512.96 | 16.14 | 8.38 | 69.77 | 7.76 | 0.28 | 32.30 |
| 1259C-15R-2, 75–76 | 516.05 | 18.03 | 6.62 | 55.14 | 11.41 | 0.47 | 28.58 |
| 1259A-56R-2, 3–4 | 517.19 | 15.84 | 4.38 | 36.51 | 11.46 | 0.42 | 32.16 |
| 1259A-56R-2, 140–145 | 518.56 | 14.09 | 10.31 | 85.88 | 3.78 | 0.23 | 18.90 |
| 1259A-57R-2, 0–5 | 521.80 | 16.38 | 7.47 | 62.25 | 8.91 | 0.34 | 30.75 |
| 1259A-57R-3, 0–1 | 523.30 | 16.33 | 7.54 | 62.81 | 8.79 | 0.31 | 32.70 |
| 1259A-57R-6, 10–11 | 527.90 | 14.03 | 10.01 | 83.38 | 4.02 | 0.22 | 21.65 |
| 1259A-57R-6, 72–73 | 528.52 | 14.20 | 5.37 | 44.70 | 8.83 | 0.36 | 28.95 |
| 1259A-58R-2, 112–113 | 532.40 | 11.48 | 5.42 | 45.19 | 6.06 | 0.22 | 31.73 |
| 1259A-58R-4, 0–1 | 533.81 | 17.03 | 2.03 | 16.94 | 15.00 | 0.60 | 28.94 |
| 1259A-58R-4, 0–2 | 533.81 | 15.91 | 2.00 | 16.64 | 13.91 | 0.55 | 29.30 |
| 1259A-58R-6, 46–47 | 536.91 | 12.31 | 10.97 | 91.38 | 1.34 | 0.06 | 25.34 |
| 1259A-58R-7, 92–93 | 538.05 | 13.67 | 2.28 | 18.96 | 11.39 | 0.47 | 28.02 |
| 1259A-59R-1, 5–6 | 539.55 | 15.08 | 0.36 | 3.01 | 14.72 | 0.60 | 28.46 |
| 1259A-59R-2, 23–24 | 541.19 | 14.73 | 1.08 | 8.96 | 13.65 | 0.54 | 29.46 |
| 1259A-59R-4, 129–130 | 545.12 | 20.29 | 3.77 | 31.38 | 16.52 | 0.58 | 33.40 |
| 1259A-59R-5, 126–127 | 546.40 | 15.64 | 2.77 | 23.11 | 12.87 | 0.43 | 35.18 |
| 1259B-24R-3, 141–142 | 548.01 | 30.53 | 1.53 | 12.71 | 29.00 | 0.81 | 41.65 |
| Unit V (quartz sandstone): | | | | | | | |
| 1259A-60R-1, 9–13 | 549.19 | 0.02 | 0.02 | 0.15 | 0.00 | 0.01 | |
| 1259C-19R-3, 83–84 | 550.37 | 6.34 | 0.37 | 3.07 | 5.97 | 0.11 | 61.03 |
| 1259B-25R-2, 110–111 | 555.80 | 0.60 | 0.16 | 1.36 | 0.44 | 0.04 | 12.43 |

Notes: TC = total carbon, IC = inorganic carbon, TOC = total organic carbon. Atomic C/N ratios are calculated from concentrations of organic carbon and total nitrogen.

**Table T17.** Rock-Eval pyrolysis analyses of sediment samples, Site 1259.

| Hole, core, section, interval (cm) | Depth (mbsf) | TOC (wt%) | $T_{max}$ (°C) | $S_1$ | $S_2$ | $S_3$ | HI | OI |
|---|---|---|---|---|---|---|---|---|
| 207- | | | | | | | | |
| 1259C-11R-3, 93–94 | 492.86 | 1.74 | 420 | 0.27 | 4.87 | 2.86 | 279 | 164 |
| 1259A-52R-6, 45–46 | 494.05 | 2.12 | 417 | 0.23 | 9.32 | 1.66 | 439 | 78 |
| 1259A-52R-CC, 5–6 | 495.06 | 6.23 | 401 | 1.13 | 40.96 | 3.08 | 657 | 49 |
| 1259C-11R-5, 106–107 | 495.99 | 9.25 | 397 | 3.21 | 42.30 | 10.82 | 457 | 116 |
| 1259A-53R-2, 20–21 | 498.70 | 1.50 | 403 | 0.15 | 9.25 | 1.24 | 616 | 82 |
| 1259A-53R-3, 148–149 | 501.48 | 7.15 | 391 | 2.28 | 49.33 | 3.66 | 689 | 51 |
| 1259C-13R-3, 21–23 | 504.81 | 9.57 | 406 | 1.96 | 35.84 | 7.40 | 374 | 77 |
| 1259A-54R-1, 1–2 | 506.61 | 13.55 | 397 | 2.82 | 91.38 | 5.59 | 674 | 41 |
| 1259A-54R-1, 62–63 | 507.22 | 15.97 | 397 | 3.36 | 104.46 | 6.33 | 654 | 39 |
| 1259C-14R-2, 62–63 | 510.72 | 10.15 | 394 | 6.42 | 59.08 | 9.56 | 582 | 94 |
| 1259A-55R-1, 97–98 | 511.57 | 11.50 | 398 | 2.18 | 74.04 | 4.82 | 643 | 41 |
| 1259C-15R-2, 75–76 | 516.05 | 11.41 | 404 | 5.86 | 87.07 | 7.19 | 763 | 63 |
| 1259A-56R-2, 3–4 | 517.19 | 11.46 | 397 | 2.64 | 74.66 | 4.92 | 651 | 42 |
| 1259A-57R-3, 0–1 | 523.30 | 8.79 | 398 | 2.04 | 57.79 | 4.29 | 657 | 48 |
| 1259A-57R-6, 10–11 | 527.90 | 4.02 | 387 | 0.94 | 28.70 | 2.21 | 713 | 54 |
| 1259A-57R-6, 72–73 | 528.52 | 8.83 | 400 | 1.67 | 56.78 | 4.55 | 643 | 51 |
| 1259A-58R-2, 112–113 | 532.40 | 6.06 | 401 | 1.15 | 39.16 | 3.28 | 646 | 54 |
| 1259A-58R-4, 0–1 | 533.81 | 15.00 | 402 | 2.19 | 87.51 | 4.99 | 583 | 33 |
| 1259A-58R-6, 46–47 | 536.91 | 1.34 | 403 | 0.20 | 7.92 | 1.01 | 591 | 75 |
| 1259A-58R-7, 92–93 | 538.05 | 11.39 | 399 | 1.55 | 66.40 | 4.70 | 582 | 41 |
| 1259A-59R-1, 5–6 | 539.55 | 14.72 | 400 | 2.15 | 80.32 | 4.46 | 545 | 30 |
| 1259A-59R-2, 23–24 | 541.19 | 13.65 | 403 | 1.95 | 79.95 | 4.83 | 585 | 35 |
| 1259A-59R-5, 126–127 | 546.40 | 12.87 | 391 | 2.64 | 80.47 | 4.59 | 625 | 35 |
| 1259B-24R-3, 141–142 | 548.01 | 29.00 | 403 | 12.64 | 164.08 | 21.14 | 565 | 72 |
| 1259C-19R-3, 83–84 | 550.37 | 5.97 | 432 | 4.99 | 28.22 | 0.01 | 472 | 0 |

Note: TOC = total organic carbon. HI = milligrams of hydrocarbon-like material per gram of organic carbon (HI = $S_2 \times 100$/TOC), OI = milligrams of $CO_2$ ($S_3$) per gram of organic carbon. See **"Organic Geochemistry,"** p. 27, in the "Explanatory Notes" chapter for definitions of $T_{max}$, $S_1$, $S_2$, and $S_3$.

**Table T18.** Headspace analyses of interstitial and microbial gases, Hole 1259A.

| Core, section, interval (cm) | Depth (mbsf) | Routine safety monitoring | | | | Microbial study | | | | |
|---|---|---|---|---|---|---|---|---|---|---|
| | | $C_1$ (ppmv) | $C_2$ (ppmv) | $C_3$ (ppmv) | $C_1/C_2$ | $C_1$ (ppmv) | $C_2$ (ppmv) | $C_{2=}$ (ppmv) | $C_3$ (ppmv) | $C_1/C_2$ |
| 207-1259A- | | | | | | | | | | |
| Unit I (foraminifer-bearing nannofossil ooze): | | | | | | | | | | |
| 1R-2, 100–105 | 2.50 | 2 | | | | 114 | | | | |
| 2R-2, 140–145 | 11.70 | 2 | | | | 3 | | | | |
| 3R-4, 140–145 | 24.20 | 2 | | | | 2 | | | | |
| 4R-1, 94–99 | 28.24 | 2 | | | | | | | | |
| Unit II (foraminifer-bearing nannofossil chalk): | | | | | | | | | | |
| 5R-2, 140–145 | 39.30 | 2 | | | | 7 | | | | |
| 6R-2, 140–145 | 48.40 | 2 | | | | 5 | | | | |
| 7R-4, 140–145 | 60.50 | 2 | | | | 3 | | | | |
| 8R-4, 140–145 | 69.70 | 3 | | | | 3 | | | | |
| 9R-5, 140–145 | 80.30 | 3 | | | | 7 | | | | |
| 10R-5, 135–140 | 89.95 | 3 | | | | 4 | | | | |
| 11R-4, 0–5 | 96.80 | 4 | | | | 4 | | | | |
| 12R-5, 135–140 | 109.35 | 4 | | | | 15 | | | | |
| 13R-4, 145–150 | 117.65 | 4 | | | | 6 | | | | |
| 14R-3, 0–5 | 124.30 | 4 | | | | 6 | | | | |
| 15R-3, 0–5 | 133.90 | 5 | | | | 7 | | | | |
| 16R-2, 145–150 | 143.55 | 4 | | | | 51 | 1 | | | 51 |
| 17R-1, 145–150 | 151.65 | 4 | | | | 9 | 1 | | | 8 |
| 18R-2, 0–5 | 161.25 | 3 | | | | 6 | 1 | | | 7 |
| 19R-1, 145–150 | 170.95 | 3 | | | | 12 | 2 | | | 8 |
| 20R-3, 0–5 | 182.20 | 4 | | | | 8 | | | | |
| 21R-2, 0–5 | 190.30 | 4 | | | | 12 | 2 | | | 7 |
| 22R-3, 135–140 | 202.85 | 3 | | | | 11 | 1 | | | 10 |
| 23R-3, 0–5 | 211.10 | 3 | | | | 8 | 1 | | | 7 |
| 24R-1, 127–132 | 219.07 | 3 | | | | 9 | 2 | | | 5 |
| 25R-2, 0–5 | 228.70 | 4 | | | | 11 | 1 | | | 10 |
| 26R-4, 0–5 | 241.40 | 4 | | | | 6 | | | | |
| 27R-5, 0–5 | 252.50 | 3 | | | | 9 | 1 | | | 7 |
| 28R-2, 0–5 | 257.14 | 4 | | | | 9 | 2 | | | 5 |
| 29R-4, 0–5 | 270.30 | 3 | | | | 7 | 2 | | | 4 |
| 30R-2, 0–5 | 277.00 | 3 | | | | 7 | 1 | | | 7 |
| 31R-2, 0–5 | 286.60 | 3 | | | | | | | | |
| 32R-2, 0–5 | 296.13 | 3 | | | | | | | | |
| 33R-5, 0–5 | 310.40 | 3 | | | | 4 | | | | |
| 34R-5, 0–5 | 320.02 | 4 | | | | 3 | | | | |
| 35R-4, 0–5 | 328.16 | 4 | | | | 4 | | | | |
| 36R-5, 0–5 | 339.30 | 3 | | | | 3 | | | | |
| 37R-6, 0–5 | 350.50 | 15 | | | | | | | | |
| 38R-3, 0–5 | 355.60 | 24 | | | | 20 | | | | |
| 39R-3, 0–5 | 364.73 | 46 | | | | 403 | 1 | | | 630 |
| 40R-2, 0–5 | 373.30 | 579 | | | 1447 | 421 | | | | |
| 41R-1, 27–28 | 381.67 | 248 | | | | | | | | |
| Unit III (clayey nannofossil chalk): | | | | | | | | | | |
| 43R-4, 0–5 | 405.20 | 1,484 | 1 | | 1,484 | 1,837 | 2 | | | 1,141 |
| 44R-4, 0–5 | 414.90 | 2,134 | 2 | | 1,255 | 1,162 | 1 | | | 1,056 |
| 45R-4, 0–5 | 423.90 | 2,660 | 2 | | 1,330 | 2,263 | 2 | | | 1,067 |
| 46R-3, 145–150 | 433.36 | 2,235 | 2 | | 1,490 | 2,902 | 2 | | | 1,262 |
| 48R-4, 0–5 | 453.30 | 1,586 | 1 | | 1,442 | 1,819 | 2 | | | 1,083 |
| 49R-4, 139–144 | 464.12 | 2,854 | 2 | | 1,427 | 756 | 1 | | | 922 |
| 50R-4, 132–137 | 473.64 | 1,159 | 1 | | 1,449 | 2,238 | 2 | | | 1,264 |
| 51R-6, 0–5 | 485.07 | 3,368 | 2 | | 1,604 | 2,852 | 3 | | | 1,064 |
| Unit IV (black shales and sandstones): | | | | | | | | | | |
| 52R-6, 0–5 | 493.60 | 6,602 | 10 | | 681 | 7,173 | 10 | | | 701 |
| 53R-2, 145–150 | 499.95 | 24,936 | 46 | | 544 | 8,237 | 21 | | | 395 |
| 54R-2, 0–5 | 508.10 | 7,218 | 14 | | 505 | 16,108 | 27 | | | 603 |
| 55R-2, 91–96 | 512.96 | 37,762 | 65 | | 581 | 23,401 | 34 | | | 686 |
| 56R-2, 140–145 | 518.56 | 9,530 | 19 | | 491 | 7,454 | 12 | | | 626 |
| 57R-2, 0–5 | 521.80 | 12,900 | 20 | | 662 | 23,878 | 26 | | | 920 |
| 58R-4, 0–2 | 533.81 | 62,252 | 101 | 5 | 615 | 40,330 | 66 | | | 616 |
| 59R-4, 129–130 | 545.12 | 76,398 | 91 | 4 | 844 | 56,416 | 51 | | | 1,109 |
| Unit V (quartz sandstone): | | | | | | | | | | |
| 60R-1, 9–13 | 549.19 | 2,308 | | | | | | | | |

Note: $C_1$ = methane, $C_2$ = ethane, $C_{2=}$ = ethylene, $C_3$ = propane.

**Table T19.** Interstitial water analyses, Holes 1259A and 1259C.

| Core, section, interval (cm) | Depth (mbsf) | Depth (mcd) | Salinity | Alkalinity (mM) | pH | $Cl^-$ (mM) | $*SO_4^{2-}$ (mM) | $NH_4^+$ (μM) | $*H_4SiO_4$ (μM) | B (mM) | $Li^+$ (μM) | $Sr^{2+}$ (μM) | $Ca^{2+}$ (mM) | $K^+$ (mM) | $Mg^{2+}$ (mM) | $Ba^{2+}$ (μM) | $Fe^{2+}$ (μM) | $Mn^{2+}$ (μM) | $Na^+$ (mM) | $Na^+$ diff |
|---|---|---|---|---|---|---|---|---|---|---|---|---|---|---|---|---|---|---|---|---|
| 207-1259A- | | | | | | | | | | | | | | | | | | | | |
| 1R-2, 105–110 | 2.55 | 2.55 | 35.3 | 3.21 | 7.47 | 560 | 28.5 | 25 | 199 | 0.45 | 30 | 100 | 11.1 | 11.0 | 54.1 | 7 | 1 | 0.5 | 482 | 479 |
| 2R-2, 145–150 | 11.75 | 11.75 | 35.5 | 4.01 | 7.45 | 559 | 28.0 | 25 | 220 | 0.47 | 42 | 126 | 12.3 | 11.0 | 51.0 | 8 | 2 | 0.7 | 467 | 481 |
| 3R-4, 145–150 | 24.25 | 24.25 | 35.7 | 3.86 | 7.32 | 570 | 25.4 | 30 | 273 | 0.49 | 61 | 174 | 14.3 | 10.9 | 50.5 | 8 | 1 | 0.6 | 489 | 484 |
| 5R-2, 145–150 | 39.35 | 39.35 | 35.8 | 4.86 | 7.33 | 578 | 24.1 | 50 | 314 | 0.48 | 78 | 212 | 16.7 | 10.7 | 50.3 | 8 | 2 | 1.1 | 486 | 486 |
| 6R-2, 145–150 | 48.45 | 48.45 | 36.0 | 5.00 | 7.21 | 584 | 24.6 | 75 | 376 | 0.49 | 86 | 232 | 17.9 | 10.8 | 49.1 | 7 | 10 | 3.7 | 493 | 493 |
| 7R-4, 145–150 | 60.55 | 60.55 | 36.3 | 6.00 | 7.11 | 583 | 23.9 | 90 | 420 | 0.50 | 97 | 257 | 18.8 | 10.7 | 47.9 | 7 | 33 | 1.2 | 494 | 492 |
| 8R-4, 145–150 | 69.75 | 69.75 | 36.7 | 5.89 | 7.57 | 585 | 22.8 | 130 | 615 | 0.52 | 106 | 275 | 18.6 | 10.6 | 48.1 | 7 | 49 | 1.7 | 485 | 492 |
| 9R-5, 145–150 | 80.35 | 80.35 | 36.7 | 6.55 | 6.89 | 592 | 22.7 | 150 | 665 | 0.50 | 116 | 300 | 19.7 | 10.5 | 48.2 | 7 | 45 | 1.5 | 494 | 497 |
| 10R-5, 140–150 | 90.00 | 90.00 | 36.7 | 5.95 | 6.92 | 596 | 21.1 | 195 | 585 | 0.55 | 126 | 303 | 20.5 | 10.9 | 46.6 | 8 | 42 | 1.9 | 510 | 499 |
| 12R-5, 140–150 | 109.40 | 109.40 | 36.7 | 7.07 | 6.94 | 606 | 20.4 | 230 | 532 | 0.56 | 143 | 345 | 22.8 | 10.1 | 48.8 | 7 | 35 | 1.0 | 513 | 500 |
| 14R-3, 140–150 | 125.70 | 125.70 | 36.7 | 7.33 | 6.77 | 617 | 19.6 | 255 | 535 | 0.57 | 155 | 375 | 23.4 | 9.7 | 45.5 | 7 | 80 | 1.2 | 508 | 515 |
| 16R-1, 140–150 | 142.00 | 142.00 | 37.5 | 8.07 | 6.73 | 615 | 20.2 | 280 | 747 | 0.54 | 170 | 415 | 22.9 | 9.6 | 45.1 | 7 | 110 | 1.2 | 514 | 516 |
| 18R-1, 135–145 | 161.15 | 161.15 | 37.7 | 8.25 | 6.85 | 615 | 19.4 | 285 | 785 | 0.58 | 177 | 436 | 26.4 | 8.9 | 46.2 | 7 | 115 | 1.1 | 500 | 506 |
| 20R-4, 130–140 | 185.00 | 185.00 | 38.0 | 7.12 | 6.86 | 624 | 17.5 | 355 | 763 | 0.58 | 187 | 451 | 27.2 | 9.3 | 45.9 | 7 | 75 | 1.6 | 518 | 509 |
| 22R-3, 140–150 | 202.90 | 202.90 | 38.0 | 7.80 | 6.89 | 624 | 18.2 | 390 | 752 | 0.58 | 199 | 480 | 27.6 | 9.0 | 44.1 | 7 | 97 | 1.2 | 511 | 514 |
| 24R-1, 132–142 | 219.12 | 219.12 | 38.3 | 8.86 | 6.77 | 627 | 17.6 | 400 | 805 | 0.58 | 200 | 504 | 29.2 | 8.4 | 45.5 | 7 | 144 | 1.2 | 519 | 511 |
| 26R-5, 140–150 | 244.30 | 244.30 | 38.7 | 8.25 | 6.82 | 629 | 15.9 | 420 | 800 | 0.58 | 213 | 539 | 28.6 | 8.2 | 45.0 | 7 | 104 | 1.3 | 531 | 512 |
| 29R-4, 140–150 | 271.70 | 271.70 | 39.0 | 8.50 | 6.86 | 650 | 15.0 | 465 | 814 | 0.59 | 226 | 568 | 28.5 | 8.2 | 44.1 | 7 | 60 | 1.5 | 537 | 533 |
| 32R-1, 133–143 | 296.03 | 296.03 | 39.5 | 6.19 | 7.03 | 654 | 13.8 | 550 | 424 | 0.55 | 230 | 622 | 28.3 | 8.1 | 43.6 | 7 | 59 | 1.9 | 536 | 534 |
| 34R-2, 140–150 | 316.92 | 316.77 | 39.7 | 4.16 | 7.10 | 664 | 12.5 | 635 | 394 | 0.49 | 234 | 640 | 26.1 | 8.2 | 43.0 | 8 | 31 | 1.7 | 537 | 545 |
| 36R-1, 140–150 | 334.70 | 335.30 | 40.0 | 3.46 | 7.13 | 663 | 10.8 | 635 | 538 | 0.49 | 238 | 701 | 26.8 | 7.9 | 42.6 | 8 | 15 | 1.7 | 556 | 539 |
| 38R-1, 140–150 | 354.00 | 354.83 | 40.3 | 4.01 | 7.17 | 678 | 8.2 | 675 | 595 | 0.52 | 239 | 739 | 28.6 | 7.6 | 41.7 | 8 | 7 | 1.9 | 535 | 548 |
| 40R-3, 90–100 | 375.70 | 374.85 | 40.7 | 3.25 | 7.37 | 698 | 6.8 | 655 | 577 | 0.50 | 242 | 753 | 29.0 | 7.3 | 42.5 | 8 | 2 | 2.4 | 550 | 562 |
| 43R-1, 140–150 | 402.10 | 403.27 | 41.5 | 2.21 | 7.06 | 714 | 5.7 | 740 | 428 | 0.42 | 244 | 860 | 28.8 | 7.3 | 42.5 | 8 | 2 | 2.3 | 570 | 575 |
| 45R-2, 140–150 | 422.90 | 424.38 | 43.5 | 3.95 | 7.07 | 743 | 3.9 | 910 | 500 | 0.50 | 263 | 946 | 31.6 | 7.4 | 44.3 | 9 | 9 | 3.6 | 594 | 592 |
| 48R-3, 138–150 | 453.18 | 453.19 | 45.7 | 1.81 | 7.34 | 788 | 1.7 | 920 | 274 | 0.33 | 270 | 992 | 30.9 | 7.4 | 43.2 | 11 | 1 | 1.5 | 609 | 634 |
| 50R-5, 137–149 | 475.06 | 475.59 | 46.5 | ND | ND | 812 | 0.6 | 940 | 449 | 0.42 | 291 | 1223 | 34.2 | 7.2 | 43.2 | 22 | 2 | 1.1 | 649 | ND |
| 52R-1, 103–117 | 488.33 | 490.08 | 50.0 | ND | ND | 832 | 0.1 | 1015 | 725 | 0.55 | 298 | 1280 | 35.9 | 7.3 | 45.3 | 50 | 0 | 0.7 | 646 | ND |
| 207-1259C- | | | | | | | | | | | | | | | | | | | | |
| 16R-5, 137–150 | 525.65 | 529.18 | 50.7 | 4.52 | 7.06 | 883 | 0.0 | 1100 | 645 | 0.57 | 310 | 1546 | 35.9 | 7.3 | 45.8 | 247 | 1 | 0.2 | 656 | 712 |
| 17R-1, 136–146 | 529.26 | 532.38 | 51.7 | 4.89 | 6.83 | 896 | 0.0 | 1210 | 611 | 0.58 | 316 | 1559 | 38.0 | 7.1 | 42.1 | 262 | 1 | 0.3 | 707 | 729 |
| 18R-4, 140–150 | 543.40 | 547.73 | 52.0 | 3.94 | 7.06 | 903 | 0.0 | 1295 | 358 | 0.54 | 315 | 1545 | 38.0 | 7.3 | 40.0 | 323 | 6 | 1.2 | 724 | 739 |
| 19R-2, 78–88 | 549.22 | 551.57 | 54.7 | ND | ND | 907 | 0.6 | 955 | 99 | 0.23 | 302 | 1667 | 38.6 | 7.3 | 39.5 | 228 | 0 | 0.8 | 732 | 740 |

Notes: * = ICP-AES. ND = not determined.

**Table T20.** Moisture and density of discrete samples, Site 1259. (See table note. Continued on next three pages.)

| Core, section, interval (cm) | Depth (mbsf) | Depth (mcd) | Water content (%) Wet | Water content (%) Dry | Density (g/cm$^3$) Bulk | Density (g/cm$^3$) Dry | Density (g/cm$^3$) Grain | Porosity (%) | Void ratio |
|---|---|---|---|---|---|---|---|---|---|
| 207-1259A- | | | | | | | | | |
| 1R-1, 59–61 | 0.59 | 0.59 | 36.0 | 56.3 | 1.623 | 1.039 | 2.419 | 57.1 | 1.329 |
| 1R-2, 54–56 | 2.04 | 2.04 | 41.2 | 70.2 | 1.544 | 0.907 | 2.398 | 62.2 | 1.643 |
| 1R-3, 43–45 | 3.03 | 3.03 | 36.9 | 58.6 | 1.606 | 1.013 | 2.407 | 57.9 | 1.376 |
| 2R-1, 16–18 | 8.96 | 8.96 | 42.1 | 72.7 | 1.598 | 0.925 | 2.697 | 65.7 | 1.915 |
| 2R-2, 76–78 | 11.06 | 11.06 | 37.7 | 60.6 | 1.617 | 1.007 | 2.493 | 59.6 | 1.476 |
| 2R-3, 34–36 | 12.14 | 12.14 | 39.9 | 66.5 | 1.623 | 0.975 | 2.654 | 63.3 | 1.723 |
| 3R-1, 70–72 | 19.00 | 19.00 | 47.0 | 88.7 | 1.533 | 0.812 | 2.741 | 70.4 | 2.374 |
| 3R-2, 80–82 | 20.60 | 20.60 | 41.7 | 71.6 | 1.618 | 0.943 | 2.766 | 65.9 | 1.934 |
| 3R-3, 64–66 | 21.94 | 21.94 | 44.9 | 81.4 | 1.572 | 0.867 | 2.785 | 68.9 | 2.213 |
| 3R-4, 115–117 | 23.95 | 23.95 | 42.2 | 73.0 | 1.592 | 0.920 | 2.676 | 65.6 | 1.907 |
| 3R-5, 117–119 | 25.47 | 25.47 | 41.2 | 70.2 | 1.623 | 0.954 | 2.752 | 65.3 | 1.885 |
| 4R-1, 46–48 | 27.76 | 27.76 | 45.5 | 83.5 | 1.547 | 0.843 | 2.695 | 68.7 | 2.199 |
| 5R-1, 97–99 | 37.37 | 37.37 | 44.7 | 80.9 | 1.563 | 0.864 | 2.722 | 68.2 | 2.149 |
| 5R-2, 57–59 | 38.47 | 38.47 | 45.4 | 83.2 | 1.512 | 0.825 | 2.504 | 67.1 | 2.035 |
| 5R-3, 57–59 | 39.97 | 39.97 | 44.8 | 81.2 | 1.546 | 0.853 | 2.638 | 67.7 | 2.093 |
| 5R-4, 22–24 | 40.82 | 40.82 | 44.5 | 80.3 | 1.582 | 0.878 | 2.811 | 68.8 | 2.203 |
| 6R-1, 96–98 | 46.46 | 46.46 | 45.2 | 82.4 | 1.551 | 0.850 | 2.694 | 68.4 | 2.168 |
| 6R-2, 86–88 | 47.86 | 47.86 | 45.3 | 83.0 | 1.565 | 0.855 | 2.785 | 69.3 | 2.257 |
| 6R-3, 101–103 | 49.51 | 49.51 | 46.3 | 86.4 | 1.549 | 0.831 | 2.777 | 70.1 | 2.342 |
| 7R-1, 97–99 | 55.57 | 55.57 | 47.5 | 90.6 | 1.534 | 0.805 | 2.798 | 71.2 | 2.475 |
| 7R-2, 82–84 | 56.92 | 56.92 | 47.1 | 89.1 | 1.528 | 0.808 | 2.719 | 70.3 | 2.365 |
| 7R-3, 72–74 | 58.32 | 58.32 | 42.7 | 74.7 | 1.587 | 0.909 | 2.694 | 66.3 | 1.964 |
| 7R-4, 68–70 | 59.78 | 59.78 | 44.5 | 80.1 | 1.545 | 0.858 | 2.610 | 67.1 | 2.042 |
| 7R-5, 75–77 | 61.35 | 61.35 | 43.3 | 76.2 | 1.549 | 0.879 | 2.544 | 65.4 | 1.894 |
| 8R-1, 87–89 | 64.67 | 64.67 | 44.5 | 80.2 | 1.550 | 0.860 | 2.635 | 67.3 | 2.063 |
| 8R-2, 94–96 | 66.24 | 66.24 | 47.8 | 91.4 | 1.523 | 0.796 | 2.747 | 71.0 | 2.452 |
| 8R-3, 85–87 | 67.65 | 67.65 | 45.2 | 82.6 | 1.591 | 0.871 | 2.933 | 70.3 | 2.367 |
| 8R-4, 79–81 | 69.09 | 69.09 | 45.2 | 82.4 | 1.556 | 0.853 | 2.723 | 68.7 | 2.192 |
| 8R-5, 76–78 | 70.56 | 70.56 | 46.8 | 88.1 | 1.543 | 0.820 | 2.784 | 70.5 | 2.395 |
| 8R-6, 64–66 | 71.94 | 71.94 | 41.5 | 71.0 | 1.565 | 0.915 | 2.504 | 63.5 | 1.737 |
| 9R-1, 87–89 | 73.77 | 73.77 | 49.3 | 97.2 | 1.504 | 0.763 | 2.763 | 72.4 | 2.624 |
| 9R-2, 81–83 | 75.21 | 75.21 | 45.6 | 83.9 | 1.555 | 0.846 | 2.755 | 69.3 | 2.258 |
| 9R-3, 89–91 | 76.79 | 76.79 | 41.6 | 71.3 | 1.578 | 0.921 | 2.569 | 64.1 | 1.788 |
| 9R-4, 67–69 | 78.07 | 78.07 | 42.0 | 72.3 | 1.604 | 0.931 | 2.716 | 65.7 | 1.918 |
| 9R-5, 59–61 | 79.49 | 79.49 | 48.3 | 93.5 | 1.524 | 0.788 | 2.804 | 71.9 | 2.560 |
| 9R-6, 77–79 | 81.17 | 81.17 | 44.3 | 79.5 | 1.560 | 0.869 | 2.672 | 67.5 | 2.074 |
| 9R-7, 45–47 | 81.95 | 81.95 | 40.3 | 67.6 | 1.649 | 0.984 | 2.810 | 65.0 | 1.856 |
| 10R-1, 63–65 | 83.23 | 83.23 | 44.0 | 78.7 | 1.572 | 0.880 | 2.714 | 67.6 | 2.086 |
| 10R-2, 82–84 | 84.92 | 84.92 | 43.8 | 78.0 | 1.580 | 0.888 | 2.741 | 67.6 | 2.088 |
| 10R-3, 54–56 | 86.14 | 86.14 | 42.5 | 73.9 | 1.594 | 0.917 | 2.708 | 66.2 | 1.955 |
| 10R-4, 92–94 | 88.02 | 88.02 | 40.6 | 68.4 | 1.621 | 0.963 | 2.695 | 64.3 | 1.799 |
| 10R-5, 61–63 | 89.21 | 89.21 | 33.9 | 51.2 | 1.732 | 1.146 | 2.682 | 57.3 | 1.341 |
| 10R-6, 55–57 | 90.65 | 90.65 | 37.1 | 58.9 | 1.668 | 1.050 | 2.648 | 60.4 | 1.522 |
| 10R-7, 8–10 | 91.38 | 91.38 | 32.5 | 48.1 | 1.674 | 1.130 | 2.408 | 53.1 | 1.130 |
| 11R-1, 78–80 | 93.08 | 93.08 | 30.0 | 42.8 | 1.693 | 1.185 | 2.351 | 49.6 | 0.983 |
| 11R-2, 58–60 | 94.38 | 94.38 | 29.8 | 42.5 | 1.729 | 1.213 | 2.444 | 50.4 | 1.014 |
| 11R-3, 96–98 | 96.26 | 96.26 | 32.8 | 48.8 | 1.675 | 1.126 | 2.428 | 53.6 | 1.156 |
| 11R-4, 87–89 | 97.67 | 97.67 | 30.5 | 43.8 | 1.694 | 1.178 | 2.376 | 50.4 | 1.017 |
| 11R-5, 52–54 | 98.82 | 98.82 | 30.9 | 44.7 | 1.716 | 1.187 | 2.459 | 51.7 | 1.072 |
| 12R-1, 81–83 | 102.81 | 102.81 | 38.6 | 62.9 | 1.642 | 1.008 | 2.649 | 61.9 | 1.628 |
| 12R-2, 97–99 | 104.47 | 104.47 | 39.8 | 66.1 | 1.620 | 0.975 | 2.631 | 62.9 | 1.698 |
| 12R-3, 65–67 | 105.65 | 105.65 | 41.7 | 71.4 | 1.623 | 0.947 | 2.787 | 66.0 | 1.943 |
| 12R-4, 65–67 | 107.15 | 107.15 | 44.3 | 79.4 | 1.570 | 0.875 | 2.725 | 67.9 | 2.114 |
| 12R-5, 79–81 | 108.79 | 108.79 | 45.6 | 83.9 | 1.556 | 0.846 | 2.756 | 69.3 | 2.259 |
| 12R-6, 53–55 | 110.03 | 110.03 | 47.7 | 91.3 | 1.526 | 0.798 | 2.766 | 71.2 | 2.468 |
| 13R-1, 77–79 | 112.47 | 112.47 | 46.4 | 86.6 | 1.549 | 0.830 | 2.785 | 70.2 | 2.356 |
| 13R-2, 66–68 | 113.86 | 113.86 | 41.9 | 72.1 | 1.608 | 0.934 | 2.729 | 65.8 | 1.922 |
| 13R-3, 85–87 | 115.55 | 115.55 | 43.5 | 77.1 | 1.578 | 0.891 | 2.704 | 67.0 | 2.035 |
| 13R-4, 24–26 | 116.44 | 116.44 | 43.4 | 76.8 | 1.601 | 0.906 | 2.822 | 67.9 | 2.116 |
| 13R-5, 28–31 | 117.98 | 117.98 | 45.2 | 82.5 | 1.584 | 0.868 | 2.885 | 69.9 | 2.324 |
| 13R-6, 22–24 | 119.42 | 119.42 | 45.9 | 85.0 | 1.559 | 0.843 | 2.805 | 69.9 | 2.328 |
| 14R-1, 73–75 | 122.03 | 122.03 | 45.2 | 82.6 | 1.556 | 0.852 | 2.726 | 68.7 | 2.200 |
| 14R-2, 67–69 | 123.47 | 123.47 | 43.1 | 75.8 | 1.594 | 0.907 | 2.759 | 67.1 | 2.042 |
| 14R-3, 69–71 | 124.99 | 124.99 | 44.3 | 79.4 | 1.584 | 0.883 | 2.803 | 68.5 | 2.175 |
| 14R-4, 43–45 | 126.23 | 126.23 | 36.6 | 57.7 | 1.687 | 1.070 | 2.693 | 60.3 | 1.518 |
| 15R-1, 74–76 | 131.64 | 131.64 | 35.3 | 54.6 | 1.676 | 1.084 | 2.568 | 57.8 | 1.370 |
| 15R-2, 74–76 | 133.14 | 133.14 | 39.8 | 66.1 | 1.621 | 0.976 | 2.638 | 63.0 | 1.702 |

Table T20 (continued).

| Core, section, interval (cm) | Depth (mbsf) | Depth (mcd) | Water content (%) Wet | Water content (%) Dry | Density (g/cm³) Bulk | Density (g/cm³) Dry | Density (g/cm³) Grain | Porosity (%) | Void ratio |
|---|---|---|---|---|---|---|---|---|---|
| 15R-3, 76–78 | 134.66 | 134.66 | 41.2 | 70.0 | 1.615 | 0.950 | 2.711 | 65.0 | 1.854 |
| 15R-4, 49–51 | 135.89 | 135.89 | 42.6 | 74.4 | 1.607 | 0.922 | 2.786 | 66.9 | 2.023 |
| 16R-1, 64–66 | 141.24 | 141.24 | 43.2 | 76.0 | 1.582 | 0.899 | 2.700 | 66.7 | 2.004 |
| 16R-2, 74–76 | 142.84 | 142.84 | 41.1 | 69.9 | 1.598 | 0.941 | 2.630 | 64.2 | 1.795 |
| 16R-3, 50–52 | 144.10 | 144.10 | 46.8 | 87.8 | 1.516 | 0.807 | 2.625 | 69.2 | 2.252 |
| 16R-4, 48–50 | 145.28 | 145.28 | 43.1 | 75.6 | 1.580 | 0.900 | 2.681 | 66.4 | 1.979 |
| 17R-1, 72–74 | 150.92 | 150.92 | 41.6 | 71.2 | 1.601 | 0.935 | 2.671 | 65.0 | 1.856 |
| 17R-2, 64–66 | 152.34 | 152.34 | 46.4 | 86.4 | 1.540 | 0.826 | 2.731 | 69.7 | 2.306 |
| 18R-1, 66–68 | 160.46 | 160.46 | 47.2 | 89.3 | 1.521 | 0.803 | 2.685 | 70.1 | 2.342 |
| 18R-2, 74–76 | 161.99 | 161.99 | 44.0 | 78.6 | 1.558 | 0.872 | 2.639 | 67.0 | 2.026 |
| 19R-1, 66–68 | 170.16 | 170.16 | 41.6 | 71.1 | 1.620 | 0.947 | 2.763 | 65.7 | 1.919 |
| 19R-2, 65–67 | 171.65 | 171.65 | 44.8 | 81.2 | 1.553 | 0.857 | 2.676 | 68.0 | 2.123 |
| 20R-1, 72–74 | 179.92 | 179.92 | 38.9 | 63.8 | 1.661 | 1.014 | 2.753 | 63.2 | 1.714 |
| 20R-2, 69–71 | 181.39 | 181.39 | 38.6 | 62.9 | 1.676 | 1.029 | 2.794 | 63.2 | 1.716 |
| 20R-3, 66–68 | 182.86 | 182.86 | 35.3 | 54.5 | 1.711 | 1.107 | 2.697 | 59.0 | 1.437 |
| 20R-4, 74–76 | 184.44 | 184.44 | 36.1 | 56.5 | 1.684 | 1.076 | 2.647 | 59.4 | 1.461 |
| 21R-1, 70–72 | 189.50 | 189.50 | 40.3 | 67.4 | 1.621 | 0.968 | 2.669 | 63.7 | 1.756 |
| 21R-2, 75–77 | 191.05 | 191.05 | 36.1 | 56.5 | 1.703 | 1.088 | 2.722 | 60.0 | 1.501 |
| 21R-4, 46–48 | 193.26 | 193.26 | 36.6 | 57.7 | 1.668 | 1.058 | 2.616 | 59.6 | 1.473 |
| 22R-1, 71–73 | 199.21 | 199.21 | 41.3 | 70.4 | 1.609 | 0.945 | 2.691 | 64.9 | 1.849 |
| 22R-2, 80–82 | 200.80 | 200.80 | 39.6 | 65.5 | 1.635 | 0.988 | 2.684 | 63.2 | 1.717 |
| 22R-3, 27–29 | 201.77 | 201.77 | 36.9 | 58.4 | 1.715 | 1.083 | 2.831 | 61.8 | 1.615 |
| 22R-4, 20–22 | 203.20 | 203.20 | 37.4 | 59.8 | 1.681 | 1.052 | 2.727 | 61.4 | 1.592 |
| 22R-5, 21–23 | 204.71 | 204.71 | 37.2 | 59.2 | 1.693 | 1.063 | 2.762 | 61.5 | 1.598 |
| 23R-1, 78–80 | 208.88 | 208.88 | 39.1 | 64.2 | 1.641 | 1.000 | 2.677 | 62.7 | 1.678 |
| 23R-3, 79–81 | 211.89 | 211.89 | 40.9 | 69.2 | 1.626 | 0.961 | 2.740 | 64.9 | 1.852 |
| 23R-4, 53–55 | 213.13 | 213.13 | 43.9 | 78.4 | 1.584 | 0.888 | 2.774 | 68.0 | 2.124 |
| 24R-1, 80–82 | 218.60 | 218.60 | 42.3 | 73.2 | 1.597 | 0.922 | 2.708 | 66.0 | 1.937 |
| 24R-2, 48–50 | 219.70 | 219.70 | 39.3 | 64.7 | 1.619 | 0.983 | 2.595 | 62.1 | 1.640 |
| 25R-1, 60–62 | 227.80 | 227.80 | 37.1 | 59.0 | 1.671 | 1.050 | 2.663 | 60.6 | 1.535 |
| 25R-2, 54–56 | 229.24 | 229.24 | 39.1 | 64.2 | 1.633 | 0.994 | 2.642 | 62.4 | 1.657 |
| 25R-3, 54–56 | 230.74 | 230.74 | 40.3 | 67.4 | 1.622 | 0.969 | 2.677 | 63.8 | 1.761 |
| 26R-1, 62–64 | 237.52 | 237.52 | 37.4 | 59.8 | 1.671 | 1.046 | 2.686 | 61.1 | 1.569 |
| 26R-2, 61–63 | 239.01 | 239.01 | 35.7 | 55.5 | 1.693 | 1.089 | 2.654 | 59.0 | 1.437 |
| 26R-3, 61–63 | 240.51 | 240.51 | 35.5 | 55.1 | 1.715 | 1.106 | 2.732 | 59.5 | 1.471 |
| 26R-4, 80–82 | 242.20 | 242.20 | 34.1 | 51.7 | 1.728 | 1.139 | 2.683 | 57.5 | 1.355 |
| 26R-5, 52–54 | 243.42 | 243.42 | 31.2 | 45.3 | 1.772 | 1.220 | 2.648 | 53.9 | 1.171 |
| 26R-6, 17–19 | 244.57 | 244.57 | 34.6 | 52.8 | 1.729 | 1.131 | 2.717 | 58.4 | 1.402 |
| 27R-1, 59–61 | 247.09 | 247.09 | 36.4 | 57.2 | 1.679 | 1.068 | 2.650 | 59.7 | 1.480 |
| 27R-2, 64–66 | 248.64 | 248.64 | 37.9 | 61.1 | 1.665 | 1.033 | 2.696 | 61.7 | 1.610 |
| 27R-3, 64–66 | 250.14 | 250.14 | 34.2 | 51.9 | 1.726 | 1.136 | 2.680 | 57.6 | 1.360 |
| 27R-4, 82–84 | 251.82 | 251.82 | 35.7 | 55.6 | 1.695 | 1.090 | 2.666 | 59.1 | 1.446 |
| 27R-5, 78–80 | 253.28 | 253.28 | 38.1 | 61.4 | 1.681 | 1.041 | 2.775 | 62.5 | 1.664 |
| 27R-6, 83–85 | 254.83 | 254.83 | 39.8 | 66.1 | 1.618 | 0.974 | 2.626 | 62.9 | 1.695 |
| 28R-1, 40–42 | 256.60 | 256.60 | 35.8 | 55.8 | 1.707 | 1.095 | 2.716 | 59.7 | 1.480 |
| 29R-1, 79–81 | 266.59 | 266.59 | 32.9 | 49.0 | 1.755 | 1.178 | 2.697 | 56.3 | 1.291 |
| 29R-2, 79–81 | 268.09 | 268.09 | 33.3 | 50.0 | 1.751 | 1.167 | 2.713 | 57.0 | 1.325 |
| 29R-3, 90–92 | 269.70 | 269.70 | 34.5 | 52.6 | 1.720 | 1.127 | 2.679 | 57.9 | 1.377 |
| 29R-4, 81–83 | 271.11 | 271.11 | 36.0 | 56.3 | 1.700 | 1.088 | 2.704 | 59.8 | 1.486 |
| 29R-5, 75–77 | 272.55 | 272.55 | 34.6 | 52.9 | 1.706 | 1.116 | 2.635 | 57.7 | 1.362 |
| 29R-6, 17–19 | 273.47 | 273.47 | 33.9 | 51.3 | 1.737 | 1.148 | 2.701 | 57.5 | 1.353 |
| 30R-1, 62–64 | 276.12 | 276.12 | 31.6 | 46.2 | 1.744 | 1.193 | 2.585 | 53.8 | 1.166 |
| 30R-2, 57–59 | 277.57 | 277.57 | 32.2 | 47.5 | 1.762 | 1.195 | 2.679 | 55.4 | 1.243 |
| 30R-3, 75–77 | 279.25 | 279.25 | 28.4 | 39.7 | 1.842 | 1.319 | 2.698 | 51.1 | 1.046 |
| 30R-4, 66–68 | 280.16 | 280.16 | 28.2 | 39.2 | 1.844 | 1.324 | 2.688 | 50.7 | 1.030 |
| 31R-2, 59–61 | 287.19 | 287.19 | 36.7 | 58.1 | 1.670 | 1.056 | 2.637 | 59.9 | 1.496 |
| 32R-1, 58–60 | 295.28 | 295.28 | 33.7 | 50.9 | 1.729 | 1.146 | 2.661 | 56.9 | 1.321 |
| 32R-2, 57–59 | 296.70 | 296.70 | 33.0 | 49.3 | 1.725 | 1.156 | 2.605 | 55.6 | 1.254 |
| 33R-1, 55–57 | 304.95 | 304.95 | 31.6 | 46.3 | 1.744 | 1.192 | 2.584 | 53.9 | 1.168 |
| 33R-2, 68–70 | 306.58 | 306.58 | 37.9 | 61.1 | 1.657 | 1.028 | 2.662 | 61.4 | 1.588 |
| 33R-3, 55–57 | 307.95 | 307.95 | 34.7 | 53.1 | 1.703 | 1.113 | 2.628 | 57.7 | 1.361 |
| 33R-4, 73–75 | 309.63 | 309.63 | 33.0 | 49.2 | 1.729 | 1.159 | 2.616 | 55.7 | 1.257 |
| 33R-4, 90–92 | 309.80 | 309.80 | 33.3 | 50.0 | 1.727 | 1.151 | 2.631 | 56.2 | 1.285 |
| 33R-5, 80–82 | 311.20 | 311.20 | 33.2 | 49.8 | 1.717 | 1.146 | 2.590 | 55.7 | 1.260 |
| 33R-6, 80–82 | 312.70 | 312.70 | 32.2 | 47.6 | 1.775 | 1.203 | 2.726 | 55.9 | 1.266 |
| 34R-1, 60–62 | 314.60 | 314.45 | 31.9 | 46.8 | 1.750 | 1.192 | 2.619 | 54.5 | 1.197 |
| 34R-2, 75–77 | 316.27 | 316.12 | 29.2 | 41.2 | 1.790 | 1.267 | 2.586 | 51.0 | 1.041 |
| 34R-3, 75–77 | 317.77 | 317.62 | 32.8 | 48.8 | 1.713 | 1.151 | 2.552 | 54.9 | 1.217 |
| 34R-4, 81–83 | 319.33 | 319.18 | 30.8 | 44.5 | 1.771 | 1.225 | 2.623 | 53.3 | 1.140 |

Table T20 (continued).

| Core, section, interval (cm) | Depth (mbsf) | Depth (mcd) | Water content (%) Wet | Water content (%) Dry | Density (g/cm³) Bulk | Density (g/cm³) Dry | Density (g/cm³) Grain | Porosity (%) | Void ratio |
|---|---|---|---|---|---|---|---|---|---|
| 34R-5, 85–87 | 320.87 | 320.72 | 30.6 | 44.1 | 1.769 | 1.227 | 2.605 | 52.9 | 1.123 |
| 34R-6, 87–89 | 322.39 | 322.24 | 27.8 | 38.6 | 1.818 | 1.312 | 2.595 | 49.4 | 0.978 |
| 35R-1, 80–82 | 324.50 | 324.71 | 27.7 | 38.3 | 1.822 | 1.318 | 2.598 | 49.3 | 0.972 |
| 35R-2, 89–91 | 326.09 | 326.30 | 26.7 | 36.3 | 1.840 | 1.350 | 2.591 | 47.9 | 0.920 |
| 35R-3, 89–91 | 327.59 | 327.80 | 25.9 | 35.0 | 1.860 | 1.378 | 2.602 | 47.0 | 0.888 |
| 35R-4, 89–91 | 329.05 | 329.26 | 28.9 | 40.6 | 1.782 | 1.267 | 2.550 | 50.3 | 1.012 |
| 35R-5, 91–93 | 330.57 | 330.78 | 29.4 | 41.7 | 1.780 | 1.256 | 2.572 | 51.2 | 1.049 |
| 35R-6, 91–93 | 332.07 | 332.28 | 29.0 | 40.9 | 1.777 | 1.261 | 2.542 | 50.4 | 1.016 |
| 36R-1, 73–75 | 334.03 | 334.63 | 27.6 | 38.1 | 1.841 | 1.334 | 2.645 | 49.6 | 0.983 |
| 36R-2, 67–69 | 335.47 | 336.07 | 27.1 | 37.1 | 1.840 | 1.342 | 2.612 | 48.6 | 0.947 |
| 36R-3, 79–81 | 337.09 | 337.69 | 27.7 | 38.2 | 1.839 | 1.330 | 2.644 | 49.7 | 0.988 |
| 36R-4, 69–71 | 338.49 | 339.09 | 27.2 | 37.4 | 1.849 | 1.345 | 2.646 | 49.2 | 0.967 |
| 36R-5, 64–66 | 339.94 | 340.54 | 26.9 | 36.7 | 1.863 | 1.363 | 2.665 | 48.9 | 0.956 |
| 36R-6, 60–62 | 341.40 | 342.00 | 27.6 | 38.1 | 1.838 | 1.330 | 2.637 | 49.6 | 0.982 |
| 37R-1, 57–59 | 343.57 | 344.25 | 26.3 | 35.8 | 1.864 | 1.373 | 2.639 | 48.0 | 0.922 |
| 37R-2, 42–44 | 344.92 | 345.60 | 27.0 | 37.0 | 1.836 | 1.340 | 2.598 | 48.4 | 0.939 |
| 37R-3, 48–50 | 346.48 | 347.16 | 27.7 | 38.2 | 1.847 | 1.336 | 2.668 | 49.9 | 0.996 |
| 37R-5, 47–49 | 349.47 | 350.15 | 25.4 | 34.1 | 1.865 | 1.391 | 2.593 | 46.4 | 0.864 |
| 37R-6, 44–46 | 350.94 | 351.62 | 28.7 | 40.2 | 1.786 | 1.274 | 2.546 | 50.0 | 0.999 |
| 38R-1, 49–51 | 353.09 | 353.92 | 27.7 | 38.3 | 1.843 | 1.333 | 2.655 | 49.8 | 0.992 |
| 38R-2, 55–57 | 354.65 | 355.48 | 26.9 | 36.8 | 1.847 | 1.350 | 2.623 | 48.5 | 0.943 |
| 38R-3, 49–51 | 356.09 | 356.92 | 26.2 | 35.5 | 1.838 | 1.356 | 2.559 | 47.0 | 0.887 |
| 38R-4, 51–53 | 357.61 | 358.44 | 27.7 | 38.2 | 1.802 | 1.304 | 2.539 | 48.7 | 0.948 |
| 39R-1, 54–56 | 362.74 | 363.92 | 27.6 | 38.1 | 1.806 | 1.308 | 2.549 | 48.7 | 0.949 |
| 39R-2, 47–49 | 364.17 | 365.35 | 27.0 | 37.0 | 1.817 | 1.327 | 2.547 | 47.9 | 0.920 |
| 40R-1, 37–39 | 372.17 | 371.32 | 18.3 | 22.4 | 1.921 | 1.570 | 2.389 | 34.3 | 0.522 |
| 40R-4, 42–44 | 376.22 | 375.37 | 25.1 | 33.5 | 1.859 | 1.393 | 2.557 | 45.5 | 0.835 |
| 43R-1, 67–69 | 401.37 | 402.54 | 23.4 | 30.5 | 1.916 | 1.468 | 2.611 | 43.8 | 0.779 |
| 43R-2, 39–41 | 402.59 | 403.76 | 25.1 | 33.6 | 1.852 | 1.387 | 2.542 | 45.4 | 0.833 |
| 43R-3, 15–17 | 403.85 | 405.02 | 25.9 | 34.9 | 1.845 | 1.368 | 2.562 | 46.6 | 0.874 |
| 44R-1, 58–60 | 410.98 | 412.15 | 26.1 | 35.3 | 1.843 | 1.362 | 2.567 | 46.9 | 0.885 |
| 44R-2, 74–76 | 412.64 | 413.81 | 24.7 | 32.9 | 1.875 | 1.411 | 2.578 | 45.3 | 0.827 |
| 44R-3, 74–76 | 414.14 | 415.31 | 25.9 | 35.0 | 1.845 | 1.367 | 2.563 | 46.7 | 0.875 |
| 44R-4, 47–49 | 415.37 | 416.54 | 24.9 | 33.2 | 1.888 | 1.417 | 2.622 | 46.0 | 0.850 |
| 44R-5, 59–61 | 416.99 | 418.16 | 25.4 | 34.1 | 1.866 | 1.391 | 2.592 | 46.3 | 0.863 |
| 45R-1, 53–55 | 420.53 | 422.01 | 25.1 | 33.5 | 1.881 | 1.409 | 2.613 | 46.1 | 0.855 |
| 45R-2, 78–80 | 422.28 | 423.76 | 22.7 | 29.3 | 1.942 | 1.502 | 2.632 | 42.9 | 0.753 |
| 45R-3, 44–46 | 423.44 | 424.92 | 21.9 | 28.0 | 1.942 | 1.517 | 2.592 | 41.5 | 0.709 |
| 46R-1, 42–44 | 430.02 | 431.50 | 22.4 | 28.8 | 1.969 | 1.528 | 2.682 | 43.0 | 0.755 |
| 46R-2, 70–72 | 431.11 | 432.59 | 24.8 | 33.0 | 1.951 | 1.466 | 2.782 | 47.3 | 0.897 |
| 46R-3, 84–86 | 432.75 | 434.23 | 20.3 | 25.4 | 2.013 | 1.605 | 2.668 | 39.8 | 0.662 |
| 46R-4, 88–90 | 434.29 | 435.77 | 19.8 | 24.7 | 2.025 | 1.623 | 2.671 | 39.2 | 0.645 |
| 46R-5, 89–91 | 435.80 | 437.28 | 21.8 | 27.9 | 1.996 | 1.561 | 2.717 | 42.6 | 0.741 |
| 48R-1, 59–61 | 449.39 | 449.40 | 14.4 | 16.8 | 2.176 | 1.863 | 2.682 | 30.5 | 0.440 |
| 48R-2, 57–59 | 450.87 | 450.88 | 13.9 | 16.1 | 2.200 | 1.895 | 2.701 | 29.8 | 0.425 |
| 48R-3, 78–80 | 452.58 | 452.59 | 12.5 | 14.3 | 2.258 | 1.976 | 2.726 | 27.5 | 0.379 |
| 48R-4, 87–89 | 454.17 | 454.18 | 22.4 | 28.9 | 1.965 | 1.525 | 2.674 | 43.0 | 0.754 |
| 48R-5, 47–49 | 455.27 | 455.28 | 20.5 | 25.7 | 1.982 | 1.577 | 2.610 | 39.6 | 0.655 |
| 48R-6, 53–55 | 456.83 | 456.84 | 15.1 | 17.7 | 2.150 | 1.826 | 2.671 | 31.6 | 0.463 |
| 48R-7, 53–55 | 458.33 | 458.34 | 19.7 | 24.6 | 2.022 | 1.622 | 2.659 | 39.0 | 0.639 |
| 49R-1, 73–75 | 459.13 | 459.99 | 11.3 | 12.7 | 2.254 | 2.001 | 2.660 | 24.8 | 0.329 |
| 49R-2, 73–75 | 460.63 | 461.49 | 13.7 | 15.9 | 2.200 | 1.898 | 2.692 | 29.5 | 0.419 |
| 49R-3, 81–83 | 462.04 | 462.90 | 21.9 | 28.1 | 1.979 | 1.545 | 2.680 | 42.3 | 0.734 |
| 49R-4, 74–76 | 463.47 | 464.33 | 10.4 | 11.6 | 2.341 | 2.098 | 2.749 | 23.7 | 0.310 |
| 49R-5, 85–87 | 465.02 | 465.88 | 12.3 | 14.1 | 2.229 | 1.954 | 2.671 | 26.9 | 0.367 |
| 49R-6, 73–75 | 466.38 | 467.24 | 19.1 | 23.6 | 2.061 | 1.668 | 2.709 | 38.4 | 0.624 |
| 50R-1, 66–68 | 468.66 | 469.19 | 11.0 | 12.3 | 2.302 | 2.050 | 2.719 | 24.6 | 0.327 |
| 50R-2, 87–89 | 470.37 | 470.90 | 17.6 | 21.3 | 2.101 | 1.732 | 2.709 | 36.1 | 0.564 |
| 50R-3, 92–94 | 471.74 | 472.27 | 10.6 | 11.9 | 2.305 | 2.061 | 2.707 | 23.9 | 0.314 |
| 50R-4, 81–83 | 473.13 | 473.66 | 22.0 | 28.3 | 1.977 | 1.541 | 2.682 | 42.5 | 0.740 |
| 51R-1, 79–81 | 478.39 | 478.72 | 15.8 | 18.7 | 2.153 | 1.813 | 2.714 | 33.2 | 0.497 |
| 51R-2, 78–80 | 479.88 | 480.21 | 15.8 | 18.8 | 2.106 | 1.773 | 2.629 | 32.6 | 0.483 |
| 51R-3, 63–65 | 481.23 | 481.56 | 17.3 | 20.9 | 2.070 | 1.712 | 2.632 | 35.0 | 0.538 |
| 51R-4, 86–88 | 482.96 | 483.29 | 16.7 | 20.1 | 2.103 | 1.751 | 2.666 | 34.3 | 0.522 |
| 51R-5, 77–79 | 484.37 | 484.70 | 23.0 | 29.9 | 1.904 | 1.466 | 2.562 | 42.8 | 0.747 |
| 51R-6, 88–90 | 485.95 | 486.28 | 20.0 | 25.0 | 1.973 | 1.579 | 2.567 | 38.5 | 0.626 |
| 52R-1, 93–95 | 488.23 | 489.98 | 25.3 | 33.8 | 1.826 | 1.364 | 2.485 | 45.1 | 0.821 |
| 207-1259B- | | | | | | | | | |
| 2R-3, 66–68 | 308.66 | 308.06 | 33.6 | 50.6 | 1.724 | 1.145 | 2.636 | 56.6 | 1.303 |

Table T20 (continued).

| Core, section, interval (cm) | Depth (mbsf) | Depth (mcd) | Water content (%) Wet | Water content (%) Dry | Density (g/cm³) Bulk | Density (g/cm³) Dry | Density (g/cm³) Grain | Porosity (%) | Void ratio |
|---|---|---|---|---|---|---|---|---|---|
| 2R-5, 90–92 | 311.90 | 311.30 | 34.7 | 53.2 | 1.717 | 1.121 | 2.683 | 58.2 | 1.393 |
| 4R-2, 79–81 | 326.49 | 316.99 | 32.9 | 49.1 | 1.727 | 1.158 | 2.606 | 55.5 | 1.250 |
| 4R-3, 30–32 | 327.50 | 318.00 | 33.1 | 49.5 | 1.733 | 1.159 | 2.634 | 56.0 | 1.272 |
| 4R-4, 57–59 | 329.27 | 319.77 | 26.6 | 36.2 | 1.849 | 1.357 | 2.610 | 48.0 | 0.923 |
| 5R-3, 3–5 | 336.83 | 338.28 | 27.1 | 37.1 | 1.853 | 1.352 | 2.647 | 48.9 | 0.959 |
| 7R-1, 9–11 | 353.19 | 354.92 | 30.2 | 43.3 | 1.757 | 1.226 | 2.546 | 51.9 | 1.077 |
| 7R-CC, 1–3 | 362.58 | 364.31 | 25.3 | 33.9 | 1.842 | 1.375 | 2.526 | 45.6 | 0.837 |
| 10R-1, 4–6 | 420.54 | 418.75 | 27.5 | 37.9 | 1.872 | 1.358 | 2.727 | 50.2 | 1.008 |
| 10R-3, 36–38 | 423.86 | 422.07 | 25.2 | 33.7 | 1.871 | 1.400 | 2.592 | 46.0 | 0.852 |
| 10R-5, 28–30 | 426.78 | 424.99 | 21.6 | 27.6 | 1.968 | 1.543 | 2.639 | 41.5 | 0.710 |
| 10R-7, 4–6 | 429.24 | 427.45 | 23.5 | 30.8 | 1.926 | 1.473 | 2.642 | 44.2 | 0.794 |
| 11R-3, 5–7 | 432.85 | 432.17 | 21.7 | 27.7 | 2.018 | 1.580 | 2.760 | 42.7 | 0.747 |
| 12R-1, 40–42 | 440.10 | 438.65 | 18.9 | 23.2 | 2.070 | 1.679 | 2.713 | 38.1 | 0.616 |
| 13R-3, 5–7 | 447.75 | 446.30 | 17.2 | 20.7 | 2.106 | 1.745 | 2.696 | 35.3 | 0.546 |
| 13R-5, 6–8 | 450.76 | 449.31 | 15.1 | 17.7 | 2.173 | 1.845 | 2.713 | 32.0 | 0.470 |
| 13R-7, 7–9 | 453.78 | 452.33 | 14.2 | 16.5 | 2.152 | 1.847 | 2.630 | 29.8 | 0.424 |
| 14R-1, 7–9 | 454.37 | 453.13 | 17.4 | 21.0 | 2.089 | 1.726 | 2.673 | 35.4 | 0.549 |
| 14R-3, 4–6 | 457.34 | 456.10 | 14.6 | 17.0 | 2.194 | 1.875 | 2.724 | 31.2 | 0.453 |
| 14R-5, 8–10 | 460.38 | 459.14 | 23.1 | 30.0 | 1.957 | 1.506 | 2.693 | 44.1 | 0.789 |
| 15R-1, 56–58 | 462.46 | 460.92 | 24.7 | 32.9 | 1.862 | 1.401 | 2.546 | 45.0 | 0.817 |
| 15R-5, 31–33 | 468.21 | 466.67 | 12.1 | 13.8 | 2.262 | 1.988 | 2.717 | 26.8 | 0.367 |
| 15R-7, 59–61 | 471.49 | 469.95 | 11.3 | 12.7 | 2.314 | 2.053 | 2.755 | 25.5 | 0.342 |
| 16R-1, 74–76 | 472.24 | 471.95 | 9.6 | 10.6 | 2.346 | 2.121 | 2.718 | 22.0 | 0.281 |
| 16R-3, 78–80 | 475.28 | 474.99 | 12.2 | 14.0 | 2.270 | 1.992 | 2.735 | 27.2 | 0.373 |
| 17R-1, 14–16 | 476.64 | 475.70 | 13.2 | 15.2 | 2.181 | 1.893 | 2.634 | 28.1 | 0.391 |
| 17R-3, 10–12 | 479.60 | 478.66 | 13.9 | 16.1 | 2.481 | 2.137 | 3.221 | 33.7 | 0.508 |
| 17R-5, 79–81 | 483.29 | 482.35 | 24.2 | 32.0 | 1.899 | 1.439 | 2.613 | 44.9 | 0.816 |
| 25R-1, 134–136 | 554.54 | 555.63 | 9.0 | 9.9 | 2.354 | 2.141 | 2.703 | 20.8 | 0.262 |
| 207-1259C- | | | | | | | | | |
| 2R-1, 91–93 | 318.51 | 322.32 | 31.0 | 45.0 | 1.767 | 1.219 | 2.625 | 53.6 | 1.154 |
| 2R-2, 142–144 | 320.52 | 324.33 | 28.1 | 39.1 | 1.815 | 1.304 | 2.600 | 49.8 | 0.994 |
| 4R-1, 16–18 | 335.36 | 338.74 | 29.9 | 42.7 | 1.798 | 1.260 | 2.655 | 52.5 | 1.107 |
| 4R-3, 81–83 | 339.01 | 342.39 | 28.2 | 39.3 | 1.842 | 1.323 | 2.686 | 50.8 | 1.031 |
| 4R-5, 76–78 | 341.96 | 345.34 | 28.5 | 39.9 | 1.802 | 1.288 | 2.587 | 50.2 | 1.009 |
| 5R-1, 75–77 | 345.55 | 348.08 | 26.7 | 36.5 | 1.864 | 1.366 | 2.661 | 48.7 | 0.948 |
| 5R-3, 70–72 | 348.50 | 351.03 | 27.7 | 38.3 | 1.827 | 1.321 | 2.610 | 49.4 | 0.976 |
| 5R-5, 18–20 | 350.98 | 353.51 | 26.3 | 35.7 | 1.858 | 1.369 | 2.621 | 47.8 | 0.915 |
| 6R-1, 74–76 | 355.14 | 358.90 | 28.2 | 39.2 | 1.802 | 1.294 | 2.566 | 49.6 | 0.983 |
| 6R-3, 79–81 | 358.19 | 361.95 | 28.4 | 39.7 | 1.828 | 1.308 | 2.655 | 50.7 | 1.029 |
| 6R-5, 76–78 | 361.16 | 364.92 | 27.1 | 37.2 | 1.850 | 1.348 | 2.643 | 49.0 | 0.961 |
| 7R-1, 125–127 | 365.25 | 368.74 | 29.3 | 41.4 | 1.794 | 1.269 | 2.603 | 51.3 | 1.052 |
| 7R-3, 64–66 | 367.49 | 370.98 | 27.2 | 37.4 | 1.830 | 1.332 | 2.592 | 48.6 | 0.945 |
| 8R-1, 90–92 | 436.90 | 438.15 | 18.9 | 23.3 | 2.064 | 1.674 | 2.703 | 38.1 | 0.615 |
| 8R-4, 24–26 | 440.74 | 441.99 | 21.9 | 28.0 | 1.990 | 1.555 | 2.704 | 42.5 | 0.739 |
| 8R-7, 64–66 | 445.13 | 446.38 | 19.1 | 23.6 | 2.063 | 1.669 | 2.713 | 38.5 | 0.625 |
| 10R-1, 49–51 | 485.49 | 486.92 | 18.7 | 23.0 | 2.021 | 1.642 | 2.605 | 36.9 | 0.586 |
| 10R-3, 20–22 | 487.85 | 489.28 | 23.7 | 31.1 | 1.895 | 1.445 | 2.575 | 43.9 | 0.782 |
| 11R-1, 39–41 | 489.79 | 492.03 | 21.2 | 26.9 | 1.920 | 1.513 | 2.511 | 39.7 | 0.660 |
| 11R-2, 93–95 | 491.83 | 494.07 | 17.4 | 21.1 | 2.117 | 1.748 | 2.732 | 36.0 | 0.562 |
| 11R-5, 24–26 | 495.17 | 497.41 | 30.9 | 44.7 | 1.701 | 1.175 | 2.416 | 51.4 | 1.056 |
| 12R-2, 71–73 | 497.61 | 501.86 | 29.9 | 42.6 | 1.681 | 1.179 | 2.312 | 49.0 | 0.961 |
| 12R-3, 55–57 | 498.95 | 503.20 | 31.7 | 46.4 | 1.642 | 1.121 | 2.280 | 50.8 | 1.034 |
| 12R-4, 6–7 | 499.96 | 504.21 | 29.7 | 42.3 | 1.742 | 1.224 | 2.476 | 50.5 | 1.022 |
| 13R-3, 21–23 | 504.81 | 509.47 | 32.3 | 47.7 | 1.754 | 1.187 | 2.659 | 55.4 | 1.240 |
| 14R-1, 49–50 | 509.09 | 513.31 | 10.1 | 11.2 | 2.090 | 1.879 | 2.366 | 20.6 | 0.259 |
| 15R-1, 1–3 | 513.81 | 518.63 | 34.0 | 51.6 | 1.579 | 1.041 | 2.191 | 52.5 | 1.104 |
| 15R-2, 3–5 | 515.33 | 520.15 | 18.7 | 23.0 | 1.903 | 1.547 | 2.369 | 34.7 | 0.531 |
| 16R-3, 69–71 | 521.97 | 525.50 | 33.2 | 49.8 | 1.645 | 1.098 | 2.357 | 53.4 | 1.146 |
| 16R-7, 44–46 | 527.22 | 530.75 | 33.1 | 49.6 | 1.596 | 1.067 | 2.206 | 51.6 | 1.068 |
| 17R-1, 23–25 | 528.13 | 531.25 | 29.8 | 42.5 | 1.655 | 1.161 | 2.241 | 48.2 | 0.930 |
| 17R-3, 35–36 | 531.21 | 534.33 | 29.7 | 42.2 | 1.684 | 1.184 | 2.312 | 48.8 | 0.952 |
| 17R-5, 12–14 | 533.98 | 537.10 | 29.7 | 42.3 | 1.601 | 1.125 | 2.103 | 46.5 | 0.869 |
| 18R-3, 94–96 | 541.44 | 545.77 | 29.2 | 41.2 | 1.636 | 1.159 | 2.170 | 46.6 | 0.873 |
| 19R-1, 93–95 | 548.03 | 550.38 | 10.0 | 11.1 | 2.488 | 2.240 | 2.957 | 24.2 | 0.320 |
| 19R-2, 47–49 | 548.91 | 551.26 | 10.1 | 11.3 | 2.368 | 2.128 | 2.779 | 23.4 | 0.306 |
| 19R-3, 66–68 | 550.20 | 552.55 | 9.8 | 10.8 | 2.365 | 2.135 | 2.756 | 22.5 | 0.291 |
| 19R-4, 2–4 | 550.56 | 552.91 | 9.1 | 10.0 | 2.334 | 2.121 | 2.676 | 20.7 | 0.262 |

Note: This table is also available in **ASCII.**

**Table T21.** Average difference between GRA bulk density and MAD measurements, Site 1259.

| Unit/ Subunit | Hole | Average difference ($g/cm^3$) | Number of samples |
|---|---|---|---|
| | 207- | | |
| I | 1259A | 0.084 | 13 |
| IIA | 1259A | 0.106 | 52 |
| IIB | 1259A | 0.136 | 57 |
| IIC | 1259A | 0.181 | 39 |
| | 1259B | 0.136 | 8 |
| | 1259C | 0.207 | 11 |
| IIIA | 1259A | 0.231 | 18 |
| | 1259B | 0.200 | 6 |
| | 1259C | 0.232 | 5 |
| IIIB | 1259A | 0.273 | 24 |
| | 1259B | 0.275 | 14 |
| | 1259C | 0.227 | 3 |
| IV | 1259B | 0.228 | 15 |
| V | 1259B | 1.143 | 1 |
| | 1259C | 0.314 | 4 |

Note: Differences are calculated for each hole and lithostratigraphic unit.

**Table T22.** Discrete measurements of *P*-wave velocity, Site 1259.

| Core, section, interval (cm) | Depth (mbsf) | Depth (mcd) | Velocity (m/s) x | y | z |
|---|---|---|---|---|---|
| 207-1259A- | | | | | |
| 1R-1, 10.9 | 0.11 | 0.11 | 1604.7 | | |
| 1R-1, 47.6 | 0.48 | 0.48 | 1585.9 | | |
| 1R-1, 88.5 | 0.88 | 0.88 | 1584.5 | | |
| 1R-1, 134.6 | 1.35 | 1.35 | 1586.4 | | |
| 1R-2, 13.2 | 1.63 | 1.63 | 1573.2 | | |
| 1R-2, 55.1 | 2.05 | 2.05 | 1554.2 | | |
| 1R-2, 95.4 | 2.45 | 2.45 | 1621.4 | | |
| 1R-3, 14.6 | 2.75 | 2.75 | 1621.9 | | |
| 1R-3, 43.7 | 3.04 | 3.04 | 1573.3 | | |
| 2R-1, 14.2 | 8.94 | 8.94 | 1644.2 | | |
| 2R-1, 59.1 | 9.39 | 9.39 | 1659.4 | | |
| 2R-1, 136.6 | 10.17 | 10.17 | 1628.9 | | |
| 2R-2, 36.4 | 10.66 | 10.66 | 1573.3 | | |
| 2R-2, 77.2 | 11.07 | 11.07 | 1573.1 | | |
| 2R-2, 125.2 | 11.55 | 11.55 | 1581.2 | | |
| 2R-3, 34.7 | 12.15 | 12.15 | 1596.6 | | |
| 2R-3, 71.1 | 12.51 | 12.51 | 1715.4 | | |
| 2R-3, 124.4 | 13.04 | 13.04 | 1716.4 | | |
| 3R-1, 40.9 | 18.71 | 18.71 | 1558.1 | | |
| 3R-1, 70.6 | 19.01 | 19.01 | 1548.4 | | |
| 3R-1, 103 | 19.33 | 19.33 | 1587.6 | | |
| 3R-2, 32.4 | 20.12 | 20.12 | 1624.4 | | |
| 3R-2, 81.2 | 20.61 | 20.61 | 1623.3 | | |
| 3R-3, 19.5 | 21.50 | 21.50 | 1585.8 | | |
| 3R-3, 63.6 | 21.94 | 21.94 | 1610.6 | | |
| 3R-3, 101.8 | 22.32 | 22.32 | 1645.1 | | |
| 3R-4, 13.3 | 22.93 | 22.93 | 1576.8 | | |
| 3R-4, 48.3 | 23.28 | 23.28 | 1564.3 | | |
| 3R-4, 115.2 | 23.95 | 23.95 | 1618.9 | | |
| 3R-5, 18.7 | 24.49 | 24.49 | 1635.1 | | |
| 3R-5, 59.3 | 24.89 | 24.89 | 1608.0 | | |
| 3R-5, 97.1 | 25.27 | 25.27 | 1646.1 | | |
| 3R-5, 117 | 25.47 | 25.47 | 1628.1 | | |
| 4R-1, 27.3 | 27.57 | 27.57 | 1544.9 | | |
| 4R-1, 74.4 | 28.04 | 28.04 | 1537.8 | | |
| 5R-1, 24.9 | 36.65 | 36.65 | 1560.7 | | |
| 5R-1, 68.2 | 37.08 | 37.08 | 1586.6 | | |
| 5R-1, 96.7 | 37.37 | 37.37 | 1613.5 | | |
| 5R-1, 130 | 37.70 | 37.70 | 1592.5 | | |
| 5R-2, 25.2 | 38.15 | 38.15 | 1601.5 | | |
| 5R-2, 56.6 | 38.47 | 38.47 | 1600.1 | | |
| 5R-2, 85.7 | 38.76 | 38.76 | 1571.7 | | |
| 5R-2, 111.8 | 39.02 | 39.02 | 1589.6 | | |
| 5R-3, 29.1 | 39.69 | 39.69 | 1557.6 | | |
| 5R-3, 57.3 | 39.97 | 39.97 | 1601.0 | | |
| 5R-3, 103.9 | 40.44 | 40.44 | 1574.4 | | |
| 5R-4, 22.2 | 40.82 | 40.82 | 1603.4 | | |
| 5R-4, 52.6 | 41.13 | 41.13 | 1607.0 | | |
| 6R-1, 10 | 45.60 | 45.60 | 1678.4 | | |
| 6R-1, 58.9 | 46.09 | 46.09 | 1626.6 | | |
| 6R-1, 95.8 | 46.46 | 46.46 | 1634.5 | | |
| 6R-1, 116.5 | 46.67 | 46.67 | 1625.4 | | |
| 6R-2, 11.8 | 47.12 | 47.12 | 1631.8 | | |
| 6R-2, 42.2 | 47.42 | 47.42 | 1615.3 | | |
| 6R-2, 86.4 | 47.86 | 47.86 | 1570.3 | | |
| 6R-2, 118.2 | 48.18 | 48.18 | 1628.0 | | |
| 6R-3, 15.4 | 48.65 | 48.65 | 1651.4 | | |
| 6R-3, 44.5 | 48.94 | 48.94 | 1608.8 | | |
| 6R-3, 101.4 | 49.51 | 49.51 | 1613.6 | | |
| 6R-3, 132.6 | 49.83 | 49.83 | 1611.4 | | |
| 7R-1, 9.9 | 54.70 | 54.70 | 1632.2 | | |
| 7R-1, 48.8 | 55.09 | 55.09 | 1612.1 | | |
| 7R-1, 96 | 55.56 | 55.56 | 1624.9 | | |
| 7R-1, 140.3 | 56.00 | 56.00 | 1638.1 | | |
| 7R-2, 26.6 | 56.37 | 56.37 | 1592.7 | | |
| 7R-2, 52.5 | 56.62 | 56.62 | 1606.6 | | |
| 7R-2, 81.9 | 56.92 | 56.92 | 1551.9 | | |
| 7R-2, 125 | 57.35 | 57.35 | 1503.5 | | |
| 7R-3, 46.1 | 58.06 | 58.06 | 1577.2 | | |
| 7R-3, 72.5 | 58.33 | 58.33 | 1573.8 | | |
| 7R-3, 121.5 | 58.81 | 58.81 | 1635.4 | | |
| 7R-4, 31.5 | 59.42 | 59.42 | 1588.0 | | |
| 7R-4, 67.7 | 59.78 | 59.78 | 1610.1 | | |
| 7R-4, 89.9 | 60.00 | 60.00 | 1605.2 | | |
| 7R-4, 121.3 | 60.31 | 60.31 | 1630.2 | | |
| 7R-5, 14.4 | 60.74 | 60.74 | 1691.1 | | |
| 7R-5, 42.4 | 61.02 | 61.02 | 1619.0 | | |
| 7R-5, 74.9 | 61.35 | 61.35 | 1626.1 | | |
| 7R-5, 88.3 | 61.48 | 61.48 | 1509.8 | | |
| 7R-5, 113 | 61.73 | 61.73 | 1587.4 | | |
| 8R-1, 12.6 | 63.93 | 63.93 | 1658.0 | | |
| 8R-1, 87.4 | 64.67 | 64.67 | 1632.9 | | |
| 8R-2, 33.5 | 65.64 | 65.64 | 1517.0 | | |
| 8R-2, 93.9 | 66.24 | 66.24 | 1560.7 | | |
| 8R-2, 127.1 | 66.57 | 66.57 | 1564.8 | | |
| 8R-3, 19.1 | 66.99 | 66.99 | 1642.2 | | |
| 8R-3, 49.8 | 67.30 | 67.30 | 1612.8 | | |
| 8R-3, 84.7 | 67.65 | 67.65 | 1556.2 | | |
| 8R-4, 15.5 | 68.46 | 68.46 | 1561.0 | | |
| 8R-4, 45.8 | 68.76 | 68.76 | 1573.5 | | |
| 8R-4, 79.4 | 69.09 | 69.09 | 1580.9 | | |
| 8R-4, 112.3 | 69.42 | 69.42 | 1563.4 | | |
| 8R-5, 9.3 | 69.89 | 69.89 | 1569.4 | | |
| 8R-5, 75.9 | 70.56 | 70.56 | 1562.8 | | |
| 8R-5, 108.3 | 70.88 | 70.88 | 1577.1 | | |
| 8R-6, 11.3 | 71.41 | 71.41 | 1512.8 | | |
| 8R-6, 63.6 | 71.94 | 71.94 | 1575.5 | | |
| 9R-1, 27.7 | 73.18 | 73.18 | 1590.8 | | |
| 9R-1, 74.9 | 73.65 | 73.65 | 1589.0 | | |
| 9R-1, 102.6 | 73.93 | 73.93 | 1536.4 | | |
| 9R-1, 138.6 | 74.29 | 74.29 | 1586.5 | | |
| 9R-2, 16.4 | 74.56 | 74.56 | 1545.2 | | |
| 9R-2, 46.9 | 74.87 | 74.87 | 1563.4 | | |
| 9R-2, 81.4 | 75.21 | 75.21 | 1613.2 | | |
| 9R-2, 138.2 | 75.78 | 75.78 | 1552.8 | | |
| 9R-3, 17.2 | 76.07 | 76.07 | 1560.6 | | |
| 9R-3, 50.7 | 76.41 | 76.41 | 1610.0 | | |
| 9R-3, 88.8 | 76.79 | 76.79 | 1561.2 | | |
| 9R-3, 133.5 | 77.24 | 77.24 | 1555.5 | | |
| 9R-4, 14.4 | 77.54 | 77.54 | 1596.6 | | |
| 9R-4, 67.1 | 78.07 | 78.07 | 1599.2 | | |
| 9R-4, 98.8 | 78.39 | 78.39 | 1635.9 | | |
| 9R-4, 124.4 | 78.64 | 78.64 | 1653.7 | | |
| 9R-5, 24.5 | 79.14 | 79.14 | 1539.9 | | |
| 9R-5, 59.7 | 79.50 | 79.50 | 1585.5 | | |
| 9R-5, 119.6 | 80.10 | 80.10 | 1547.9 | | |
| 9R-6, 20.6 | 80.61 | 80.61 | 1636.4 | | |
| 9R-6, 77.6 | 81.18 | 81.18 | 1535.8 | | |
| 9R-7, 11.3 | 81.61 | 81.61 | 1574.0 | | |
| 9R-7, 45.1 | 81.95 | 81.95 | 1555.3 | | |
| 10R-1, 22.4 | 82.82 | 82.82 | 1577.9 | | |
| 10R-1, 63.1 | 83.23 | 83.23 | 1582.8 | | |
| 10R-1, 92.7 | 83.53 | 83.53 | 1545.9 | | |
| 10R-1, 127.3 | 83.87 | 83.87 | 1530.4 | | |
| 10R-2, 14.9 | 84.25 | 84.25 | 1552.3 | | |
| 10R-2, 44.6 | 84.55 | 84.55 | 1569.8 | | |
| 10R-2, 82.2 | 84.92 | 84.92 | 1552.7 | | |
| 10R-2, 120.4 | 85.30 | 85.30 | 1598.7 | | |
| 10R-3, 13.7 | 85.74 | 85.74 | 1542.1 | | |

Notes: Multiple axis measurements were performed on 2-cm$^3$ samples. x-direction is perpendicular to the surface of a split core, y-direction is parallel to the surface of a split core, and z-direction is perpendicular to the top of the core. Only a portion of this table appears here. The complete table is available in **ASCII.**